Title

Beyond Standard Model Physics from Effective Field Theory Higgs Interactions

Author

Chen, Miranda

Publication Date

2023

Peer reviewed|Thesis/dissertation

Beyond Standard Model Physics
from Effective Field Theory Higgs Interactions

By

MIRANDA CHEN
DISSERTATION

Submitted in partial satisfaction of the requirements for the degree of

DOCTOR OF PHILOSOPHY

in

Physics

in the

OFFICE OF GRADUATE STUDIES

of the

UNIVERSITY OF CALIFORNIA

DAVIS

Approved:

Markus Luty, Chair

Hsin-Chia Cheng

John Terning

Committee in Charge

2023

Contents

Abstract

In this dissertation, we study the effects of new physics involving the Higgs boson. Where possible, we avoid making any effective field theory (EFT) power counting assumptions and instead parametrize the new physics using a bottom up approach. We identify the energy scales at which one might detect Beyond Standard Model (BSM) physics given deviations in the Higgs couplings. We also provide lists of linearly independent primary operators for 3 and 4 point functions involving the Higgs, as well as a rough estimate of the size of their coefficients. Finally, we examine measuring anomalous Higgs couplings at a muon collider and focus on the top Yukawa coupling.

Acknowledgements

I would like to thank my adviser Markus Luty as well as Spencer Chang, and Da Liu. Also thanks to my mom, dad, brother, Frodo, and Louis.

Chapter 1

Introduction

Before we discuss the details of Beyond Standard Model (BSM) physics, we begin with a brief description of what is within the Standard Model (SM). In simple terms, the Standard Model describes the strong and electroweak interactions between the fundamental particles, which consists of four gauge bosons, six quarks, six leptons, and the scalar Higgs boson. The SM Lagrangian has a $SU(3) \times SU(2) \times U(1)$ symmetry. The SU(3) invariant part describes Quantum Chromodynamics (QCD) and the SU(2)xU(1) part is concerned with the electroweak interactions, which we discuss in more detail in the following section.

The SM also has a history of reliably predicting experimental results. One of the more famous examples of its accuracy is the electron's anomalous magnetic moment, where there is strong agreement between the measurement and the SM prediction. The particle content in the SM has also been detected at colliders with the Higgs boson being the most recent.

However, there are compelling reasons for expecting physics beyond what is contained in the SM. Some of these reasons are theoretical, where some features appear unexplained. One of the most well known examples is the hierarchy problem, where the Higgs mass value seems artificial. There is also the strong CP problem where, like the hierarchy problem, the small value of the strong CP phase appears unnatural. In addition, the SM fails to explain some phenomena. One example is the existence of neutrino masses. The other

massive particles gain their mass through the vacuum expectation value of the Higgs, which is explained in the next section. However, the purely left handed neutrino cannot acquire mass by a similar process. We also have good motivation for the existence of dark matter, with many experimental efforts to detect it and yet the SM does not include dark matter at all.

In the work presented in this dissertation, we do not attempt to model build or directly explain the theoretical problems or phenomena. Instead, we acknowledge that there is good reason for assuming BSM physics and use effective field theory (EFT) to understand their effects. This chapter briefly discusses some concepts and background that are relevant to most, if not all, of the chapters in this dissertation.

1.1 Higgs Couplings

The Higgs boson is important to symmetry breaking in the Standard Model. The SM contains a doublet H, which in unitary gauge is

$$H = \frac{1}{\sqrt{2}} \begin{pmatrix} 0 \\ v + h \end{pmatrix}. \tag{1.1.1}$$

The v refers to the vacuum expectation value (vev) of 246 GeV, which spontaneously breaks the symmetry $SU(2) \times U(1)_Y$ to $U(1)_{EM}$ and the h is the Higgs boson. Goldstone's theorem states that we should expect one massless Goldstone boson for every broken symmetry generator. After symmetry breaking in the SM, we are left with one massless boson (the photon) and three massive bosons ($W^{\pm}$ and Z) whose longitudinal modes contain the "missing" Goldstone bosons in unitary gauge.

The symmetry breaking by the vev also gives mass to the gauge bosons and fermions. In

the SM Lagrangian, we find the terms

$$(D_\mu H)^\dagger D^\mu H, \quad -Y^3_{ij}\bar{L}^i H e^j_R + h.c., \quad -Y^d_{ij}\bar{Q}^i_L H d^j_R, \quad -Y^u_{ij}\bar{Q}^i_L \tilde{H} u^j_R \tag{1.1.2}$$

where $\tilde{H}$ is related to H by $\tilde{H} = i\sigma_2 H$ where σ_2 is the Pauli matrix. The Y's are 3×3 Yukawa coupling matrices. The second term involves leptons, where L is the left handed lepton doublet and e_R is the right handed lepton. u_R and $\bar{Q}_L$ are the quark fields where $u_R(d_R)$ is the right handed up (down) field and Q_L is the doublet containing the left handed fields. Since D_μ is the covariant derivative that contains the gauge bosons, it is easy to see that the vev of the Higgs doublet generates a mass term for the massive gauge bosons. By the same process, the vev also generates a mass term for the leptons and quarks, though in order to explicitly find the terms, we first must rotate into the mass basis.

In this work, we are particularly interested in the interactions between the Higgs boson and other Standard Model particles. From Eq. 1.1.2, the Standard Model predicts the following 3 and 4 point interactions involving the Higgs:

$$\frac{m_f}{v} h\bar{f}f, \frac{m_V^2}{v} hVV, \frac{m_V}{v} h^2 VV, -\frac{m_h^2}{2v} h^3, -\frac{m_h^2}{8v^2} h^4 \tag{1.1.3}$$

along with effective couplings with gluons and photons. The V refers to the massive vector bosons $W^\pm$ and Z, the h to the Higgs boson, f and $\bar{f}$ to the fermion fields, m_X to the mass of the relevant particle, and v to the vev of the Higgs.

We are interested in deviations from these predicted couplings and interactions, because they would indicate new heavy physics, which we discuss in more detail in the effective field theory section.

Measurements at the Large Hadron Collider (LHC) have constrained some of these couplings. In previous runs, the kappa framework was introduced to describe the Yukawa and gauge boson couplings. The κ's are defined by relating the cross sections of Higgs production

and decay to the predicted SM cross sections so that

$$\kappa_j^2 = \frac{\sigma_j}{\sigma_J^{SM}} \quad or \quad \kappa_j^2 = \frac{\Gamma_j}{\Gamma_j^{SM}}, \tag{1.1.4}$$

where the j denotes the production or decay and σ and Γ refer to the relevant cross section and partial decay width [1]. $\kappa = 1$ is the predicted Standard Model value. From the processes that involve tree level diagrams with fermions and massive vector bosons, we can infer that κ_f and κ_V modify the SM couplings by $\kappa_f \frac{m_f}{v} h\bar{f}f$ and $\kappa_V \frac{m_V^2}{v} hVV$. For these types of coupling modifications, we primarily use the quantity δ to discuss anomalous couplings in this dissertation. The δs and the κs are related to each other by

$$\kappa = 1 + \delta \tag{1.1.5}$$

so the δ purely involves BSM physics and is 0 in the SM. The κs that are related to processes that involve loops are related to κ_V, κ_t, and κ_b, where V refers to the W and Z bosons and t and b to the top and bottom quark respectively.

ATLAS results constrain the top Yukawa coupling and Higgs to vector boson couplings, which are extensively discussed in this dissertation, to be around 20% at the 95% confidence level [2]. There are also recent projections for kappa measurements at the High Luminosity LHC (HL-LHC) [3].

Lepton colliders, which have reduced QCD background compared to hadron colliders, can also be potentially interesting for measurements of Higgs couplings. There are analyses for $t\bar{t}H$ production and the top Yukawa coupling at CLIC [4]. The future muon collider is also a possibility for such studies and could compete with the LHC in terms of constraining couplings [5, 6].

In the runs at the LHC, the constraints on the Higgs couplings are extracted by examining Higgs decays [3]. Since these processes contain a Higgs decaying to other particles, they will

naturally be sensitive to the couplings of the Higgs.

However, we can also examine scattering processes that do not explicitly involve an on-shell Higgs and extract information about the Higgs couplings [7]. For example, if we were interested in probing the top Yukawa coupling, instead of Higgs decays, we can also examine vector boson fusion (VBF) production of a top and antitop. This process involves diagrams where the Higgs is a propagator and is therefore sensitive to the value of the Higgs and top coupling. As we see in [7,8], such processes benefit from increased cross sections particularly at high energy. In this dissertation, we primarily focus on these types of scattering processes when considering phenomenology.

1.2 Effective Field Theory

Effective field theories (EFT) are theories that describe physics at low energies. The particles with masses much greater than the low energy scale are integrated out and not explicitly present in the effective theory. However, they still affect probability amplitudes because the process of integrating them out introduces interaction terms involving the remaining fields. In other words, even at low energy, evidence of the heavy particles still be found even if the particles themselves are not directly produced.

One difference between EFTs and theories like the SM is that EFTs allow for irrelevant operators, which are terms in the Lagrangian where the coupling's mass dimension is negative. Renormalizability prevents irrelevant operators from appearing in the SM. The loop diagrams in general contain divergent terms and renormalizability ensures that not only can such terms be absorbed by counterterms, but that there are a finite number of these counterterms. In other words, it is essentially the quality of being a predictive theory where the calculations are finite. When irrelevant operators appear in a theory, attempting to renormalize becomes an infinite recursion. However in an EFT, such operators contain inverse powers of the cutoff energy scale and so we can truncate the infinite recursive process by

only working to some power of energy.

In this dissertation, we are primarily concerned with Standard Model Effective Field Theory (SMEFT) and a 'bottom up' EFT, where in both cases, our EFT consists of the SM plus additional operators. The existence of such operators would indicate that the SM is not valid for all energy scales, but is instead an EFT with heavy states that have been integrated out.

One possible way of parametrizing new physics is by using dimension 6 SMEFT. The mass dimension of all fields in each SM operator are at most dimension 4, implying that their couplings have either positive or no mass dimension. SMEFT consists of adding irrelevant operators that can be grouped by their dimension. We assume that higher dimension operators are more suppressed and the leading contribution to BSM physics occurs at dimension 6.

With the inclusion of these new operators, existing 3 and 4 point interactions deviate from their predicted SM coupling. As an example, suppose we consider adding a single SMEFT operator to the SM so that the Lagrangian of the theory is

$$\mathcal{L} = \mathcal{L}_{SM} + \frac{c_{\mathcal{O}}}{\Lambda^2} H^\dagger H \bar{Q}_L \tilde{H} u_R. \tag{1.2.1}$$

The $\mathcal{L}_{SM}$ denotes the Standard Model Lagrangian. $c_{\mathcal{O}}$ is the dimensionless coefficient of the SMEFT operator and Λ is the energy cutoff scale for the EFT. Q_L, u_R, H and $\tilde{H}$ are the quarks and doublets as described under Eq. 1.1.2.

The new term in Eq. 1.2.1 contains a piece proportional to $\bar{t}th$, so the new Higgs and top quark coupling contains a term proportional to $c_{\mathcal{O}}$ in addition to the original SM coupling.

We can also consider a completely bottom up approach, where instead of first identifying higher dimension operators and then finding the resulting 3 and 4 point interactions, we

simply add in additional interactions. Under this approach, we would have

$$\mathcal{L} = \mathcal{L}_{SM} + \delta y_1 \bar{t}th \tag{1.2.2}$$

as opposed to Eq. 1.2.1 where δy_1 is a coupling.

The difference between the two can be appreciated when we consider higher point interactions that are related to lower point ones through SMEFT operators. As a concrete example, we can consider the $\bar{t}th$ and $\bar{t}th^2$ couplings. Both terms are contained in the dimension 6 SMEFT operator and their couplings are not independent of each other. In the bottom up approach, we can simply add a $\delta y_2 \bar{t}th^2$ to Eq. 1.2.2, which implies that one can conduct a measurement of the quadratic coupling $\bar{t}th^2$ without considering the linear $\bar{t}th$.

This is not to say that it is impossible to consider this situation in the SMEFT framework. Measuring $\bar{t}th^2$ alone can be justified in SMEFT by including a dimension eight operator and assuming that some cancellation between the two operators occurs so that $\bar{t}th^2$ is the leading BSM effect. The difference is that the bottom up approach more explicitly illustrates the possibility of considering higher point interactions without including discussions about higher dimension operators. A more detailed discussion of the comparison between SMEFT and a bottom up approach can be found in Chapters 2 and 3 of this dissertation.

1.3 Outline

The remainder consists of three papers where the author of this dissertation was a co-author and some overall concluding remarks.

Chapter 2 is from [9] and uses the concept of tree level unitarity to predict the scale of new physics. Specifically, it considers deviations in the Higgs couplings to massive vector bosons and top quarks and identifies the energy scales where one might expect to detect BSM physics at colliders. Chapter 3 is from [10] and identifies the list of linearly independent 3

and 4 point primary operators that involve the Higgs in a framework that connects directly to phenomenological observables. Chapter 4 is from [6] and discusses the measurement of the Higgs and top quark coupling at a future muon collider. Chapter 5 presents some conclusions.

Chapter 2

Higgs Coupling Measurements and the Scale of New Physics

2.1 Introduction

As discussed in the introduction, despite the success of the Standard Model, there are compelling reasons for expecting new physics. In this chapter, we use tree level unitarity to determine the scale of new physics given a Higgs coupling deviation from the SM prediction. Essentially, we assume that our low energy effective theory consists of the SM and additional interactions between the SM particles. As discussed above, these additional interactions can indicate the presence of heavy BSM particles. We then show that the BSM couplings can indicate the energy scale where this EFT should break down. In our analysis, we focus on the Higgs couplings to itself and other SM particles.

Before we discuss the reasoning behind this chapter, we briefly revisit the arguments first made in the 1970s, where unitarity led to a spontaneously broken gauge theory [11–14] (see [15–17] for a modern approach). More specifically, one can determine the energy scale for the Higgs sector by imposing tree level unitarity on longitudinal vector boson scattering [18–23].

Our approach is similar to the argument originally proposed by Lee, Quigg, and Thacker

[18, 19]. As is, the SM respects tree level unitarity. If we introduce new physics in the form of anomalous Higgs couplings, we expect that the cancellations that remove energy growing terms from scattering amplitudes will no longer hold, thus leading to tree level unitarity violation. Recall from the introduction that given our effective field theory framework, these anomalous couplings are the result of integrating out heavy particles. In other words, tree level unitarity violation indicates the existence of non SM particles with masses above the EFT's cutoff scale. Furthermore, since the BSM terms introduce energy growing terms in the amplitudes, we can also use tree level unitarity to determine the energy scale that we should expect to detect the new physics.

We use a "bottom up" framework that is model independent, where the only assumption is that there are no light BSM particles. In theory, our approach can be applied to any SM coupling. However the Higgs anomalous couplings are constrained at the 20% level (for δ_{V1} and δ_{t1}) or worse (for δ_3, δ_{V2}, and c_{t2}) compared to the percent level of the SM parameters. Furthermore, we anticipate these measurements improving at the HL-LHC run and future colliders. For these reasons, we focus on the Higgs to top couplings, the Higgs to vector boson couplings, and the Higgs self couplings. Our effective Lagrangian is

$$\begin{aligned}\mathcal{L} = \mathcal{L}_{\rm SM} &- \delta_3 \frac{m_h^2}{2v} h^3 - \delta_4 \frac{m_h^2}{8v^2} h^4 - \sum_{n=5}^{\infty} \frac{c_n}{n!} \frac{m_h^2}{v^{n-2}} h^n + \cdots \\ &+ \delta_{Z1} \frac{m_Z^2}{v} h Z^\mu Z_\mu + \delta_{W1} \frac{2m_W^2}{v} h W^{\mu+} W_\mu^- + \delta_{Z2} \frac{m_Z^2}{2v^2} h^2 Z^\mu Z_\mu + \delta_{W2} \frac{m_W^2}{v^2} h^2 W^{\mu+} W_\mu^- \\ &+ \sum_{n=3}^{\infty} \left[\frac{c_{Zn}}{n!} \frac{m_Z^2}{v^n} h^n Z^\mu Z_\mu + \frac{c_{Wn}}{n!} \frac{2m_W^2}{v^n} h^n W^{\mu+} W_\mu^- \right] + \cdots \\ &- \delta_{t1} \frac{m_t}{v} h \bar{t} t - \sum_{n=2}^{\infty} \frac{c_{tn}}{n!} \frac{m_t}{v^n} h^n \bar{t} t + \cdots .\end{aligned} \tag{2.1.1}$$

where, as in the introduction, $\mathcal{L}_{\rm SM}$ refers to the SM Lagrangian, h is the physical Higgs boson, Z_μ and $W_\mu^\pm$ are the massive gauge bosons, and t is the top quark. The BSM couplings are parametrized by δ and c, where δ refers to deviations from SM couplings and c refers to new

interactions. The relationship between δ and the κs of the κ-framework can be found in Eq. 1.1.5.

While there has been some previous work in this area with using unitarity to contrain $2 \to 2$ partial wave amplitudes [18–21, 24, 25] and inclusive cross sections [22, 23, 26–28], our analysis contains some new features. The bounds that we find are model independent in the sense that the bound arising from one anomalous coupling is insensitive to the value of other couplings, which may be related by specific EFTs such as SMEFT. Furthermore, using the techniques outlined in Ref. [29], we use $n \to m$ amplitudes that not only result in stronger bounds, but also contain potential IR enhancements that can be the subject of future work. We also discuss the effect multiple nonzero anomalous couplings have on our bounds. Finally, despite our framework being completely bottom-up, we find that we are able to estimate the accuracy of SMEFT predictions for coupling deviations given the unitarity violation scale.

In this chapter we extend the work of Ref. [29]. We first examine the Higgs cubic coupling and elaborate more on the model-independent nature of our bounds. We also discuss obtaining an optimal bound by considering other couplings and show that it is not significantly better than our model-independent bound. Finally, we estimate the deviation of the quartic Higgs coupling from the SMEFT prediction given the scale of new physics. We then perform the same analysis for the hVV and $h\bar{t}t$ couplings, where we find that the scale of new physics could potentially be reached at the HL-LHC.We continue with the $hhVV$ and $hh\bar{t}t$ couplings and finish with a summary of our conclusions. The details of our calculations can be found in Appendix A.

2.2 New Physics from the Higgs Self-Coupling

In this section we discuss the model-independent bound on the scale of new physics from measurements of the cubic Higgs self-coupling. This section is based on Ref. [29], but goes beyond it in a number of respects. First, we include a more complete discussion of the

model-independence of the bound and the role of additional deviations from the SM that are poorly constrained. Specifically, we explain why couplings with additional derivatives and powers of gauge fields do not affect the bounds. We also show that marginalizing over the infinitely unmeasured couplings does not substantially improve the bound. Second, we show that if the scale of unitarity violation is large compared to 1 TeV, unitarity alone implies that the deviation in the Higgs quartic coupling is related to that of the Higgs cubic coupling as predicted by the dimension-6 operator $(H^\dagger H)^3$. We are able to give a quantitative estimate of the error purely from bottom-up considerations.

2.2.1 Model-Independent Bound on the Scale of New Physics

Suppose that the experimentally measured value of the Higgs cubic coupling differs from the prediction of the SM. Obviously, this implies that there is physics beyond the SM, but at what scale? One possibility is that this physics is near the electroweak scale, for example additional Higgs bosons that mix with the observed Higgs boson. In this case, the new states can be potentially produced and observed in direct searches. But it is also possible that the new physics responsible for the deviation is at higher energies that are not directly probed by current experiments. Because the SM is the unique UV complete theory with the observed particle content, the scale of this new physics cannot be arbitrarily high. One sign of this is that any effective theory that can explain this result without the addition of new light particles violates tree-level unitarity at high energies. This scale can be computed without any additional assumptions, and gives an upper bound on the scale of new physics.

In a theory without gauge interactions, a cubic scalar interaction is a relevant coupling whose effects are small at high energies. Nonetheless, a deviation of the Higgs cubic coupling from the SM prediction implies a breakdown of tree-level unitarity at high energies. For example, this can be seen in the process $V_L V_L V_L \to V_L V_L V_L$, where V_L is a longitudinally polarized W or Z. This has a tree-level contribution from the Higgs cubic coupling, as

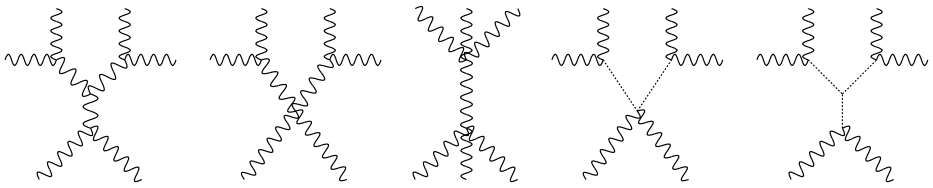

Fig. 2.1: Feynman diagrams contributing to scattering processes involving six electroweak gauge bosons.

shown in Fig. 2.1. By itself, this contributes to dimensionless amplitudes[1] with high-energy behavior $\sim E^2/v^2$, which would violate unitarity at high energy, but in the SM this diagram cancels with other diagrams to give high-energy behavior that respects unitarity. If the Higgs cubic coupling deviates from the SM prediction, this cancellation is destroyed, and the amplitude violates unitarity at high energies.

The scale of unitarity violation depends on the high-energy behavior of the amplitude. The calculation of this can be considerably simplified using the equivalence theorem, which tells us that the leading high-energy behavior of scattering amplitudes for longitudinally polarized gauge bosons is given by the amplitude for the corresponding 'eaten' Nambu-Goldstone bosons [14, 30]. We assume that experiments can be described by the effective Lagrangian Eq. (2.1.1), with no new degrees of freedom below some energy scale $E_{\text{max}} \gtrsim$ TeV. In this section, we focus on the couplings δ_3 and δ_4 in Eq. (2.1.1), which parameterize the deviations of the Higgs cubic and quartic couplings coupling from the SM values:

$$\delta_3 = \frac{g_{h^3} - g_{h^3}^{(\text{SM})}}{g_{h^3}^{(\text{SM})}}, \qquad \delta_4 = \frac{g_{h^4} - g_{h^4}^{(\text{SM})}}{g_{h^4}^{(\text{SM})}}, \tag{2.2.1}$$

while the c_n parameters in Eq. (2.1.1) are couplings that are not present in the SM.

The Lagrangian Eq. (2.1.1) is written in unitary gauge. To use the equivalence theorem to compute the leading high-energy behavior of amplitudes, we must restore the dependence on the Nambu-Goldstone fields. We do this by writing the Higgs doublet in a general gauge

[1] We use amplitudes that are many-particle generalizations of partial wave amplitudes normalized so that the unitarity bound is $|\hat{\mathcal{M}}| < 1$. See Appendix A for details.

as

$$H = \frac{1}{\sqrt{2}} \begin{pmatrix} G^1 + iG^2 \\ v + h + iG^3 \end{pmatrix}, \tag{2.2.2}$$

where $\boldsymbol{G} = (G^1, G^2, G^3)$ parameterizes the custodial $SU(2)$ triplet of 'eaten' Nambu-Goldstone bosons. We use a linear parameterization of the Nambu-Goldstone fields because the SM part of the Lagrangian has manifestly good high-energy behavior when written in terms of these fields. To use the equivalence theorem, we must restore the dependence on the Nambu-Goldstone of the non-SM couplings in Eq. (2.1.1). We do this by writing them in terms of the Higgs doublet Eq. (2.2.2):

$$X \equiv \sqrt{2H^\dagger H} - v = h + \frac{\boldsymbol{G}^2}{2(v+h)} - \frac{\boldsymbol{G}^4}{8(v+h)^3} + O\left(\frac{\boldsymbol{G}^6}{(v+h)^5}\right). \tag{2.2.3}$$

Because $X = h$ in unitary gauge, the generalization of Eq. (2.1.1) to a general gauge is obtained simply by the substitution $h \to X$ [28, 29]. Note that X is non-analytic at $H = 0$, but we are interested in the expansion around $\langle H \rangle \neq 0$.

The X^3 term contains interactions with arbitrarily high powers of the fields h and $\boldsymbol{G}$. However, such vertices also get contributions from terms of the form X^n with $n \geq 4$, and these terms are unconstrained experimentally. In order to obtain a bound we call our *model-independent bound*, we only consider processes that do not get corrections from the unmea-

sured couplings δ_n for $n \geq 4$. From Eq. (2.2.3) we have

$$\begin{aligned}
X^3 \sim\ & h^3 + \boldsymbol{G}^2(h^2 + h^3 + \cdots) + \boldsymbol{G}^4(h + h^2 + \cdots) + \boldsymbol{G}^6(1 + h + \cdots) \\
& + \boldsymbol{G}^8(1 + h + \cdots) + \boldsymbol{G}^{10}(1 + h + \cdots) + \cdots, \\
X^4 \sim\ & h^4 + \boldsymbol{G}^2(h^3 + h^4 + \cdots) + \boldsymbol{G}^4(h^2 + h^3 + \cdots) + \boldsymbol{G}^6(h + h^2 + \cdots) \\
& + \boldsymbol{G}^8(1 + h + \cdots) + \boldsymbol{G}^{10}(1 + h + \cdots) + \cdots, \\
X^5 \sim\ & h^5 + \boldsymbol{G}^2(h^4 + h^5 + \cdots) + \boldsymbol{G}^4(h^3 + h^4 + \cdots) + \boldsymbol{G}^6(h^2 + h^3 + \cdots) \\
& + \boldsymbol{G}^8(h + h^2 + \cdots) + \boldsymbol{G}^{10}(1 + h + \cdots) + \cdots.
\end{aligned} \tag{2.2.4}$$

where we have set $v = 1$ and ignored numerical factors. We note that the $h\boldsymbol{G}^4$ and $\boldsymbol{G}^6$ couplings violate unitarity at high energies, and are not affected by the unconstrained terms X^n for $n \geq 4$. We see that the unitarity-violating amplitudes that depend only on δ_3 are (restoring factors of v)

$$\hat{\mathcal{M}}(V_L V_L \to V_L V_L h) \sim \lambda \delta_3 \frac{E}{v}, \qquad \hat{\mathcal{M}}(V_L V_L V_L \to V_L V_L V_L) \sim \lambda \delta_3 \frac{E^2}{v^2}. \tag{2.2.5}$$

The strongest constraint comes from $W_L^+ W_L^+ W_L^- \to W_L^+ W_L^+ W_L^-$ and gives the bound

$$E_{\max} \simeq \frac{14 \text{ TeV}}{|\delta_3|^{1/2}}. \tag{2.2.6}$$

For details of the calculations, see Ref. [29] and the Appendix.

Experimental sensitivity to a deviation in the Higgs cubic coupling comes mainly from measurements of di-Higgs production.[2] However, a deviation in this process can also be explained by new physics contributions to the h^2V^2 or $h^2\bar{t}t$ couplings. This will be discussed in Sec. 2.5 below, where we show that a model-independent unitarity bound can be obtained by considering these couplings together.

[2] It is also possible to constrain a cubic deviation by looking for the hV^4 process in VBF production of hV^2 [7].

2.2.2 Model-Independence of the Bound

We claim that the bound Eq. (2.2.6) is valid independently of the infinitely many unconstrained couplings that parameterize possible deviations from the SM. In this subsection, we discuss this point in more detail.

The discussion above has assumed that a measured deviation in the Higgs trilinear coupling is explained by a h^3 coupling with no derivatives. (The same assumption is made by the experimental searches for this deviation.) However, there are infinitely many derivative couplings that can contribute to an observed deviation in the Higgs cubic coupling:

$$\Delta\mathcal{L} = \sum_{n=1}^{\infty} c_{3,n} \frac{m_h^2}{v^{2n+1}} \partial^{2n} h^3. \tag{2.2.7}$$

Here we have only shown the schematic dependence of the derivatives, but not the detailed Lorentz structure. If the experimentally measured h^3 coupling deviates from the Standard Model prediction, this is potentially due to some combination of the $c_{3,n}$ couplings above. If the deviation is dominated by a single coupling $c_{3,n}$, this requires

$$\frac{\delta g_{h^3}}{g_{h^3}^{(\mathrm{SM})}} \sim c_{3,n} \left(\frac{m_h}{v}\right)^{2n}, \tag{2.2.8}$$

since the Higgs coupling extraction is dominated at energies $\sim m_h$. The $V_L^3 \to V_L^3$ process leads to a unitarity violating scale (neglecting order one numerical factors)

$$E_{\max} \sim m_h \left(\frac{128\pi^3 v^4}{m_h^4} \frac{g_{h^3}^{(\mathrm{SM})}}{\delta g_{h^3}}\right)^{1/(2n+2)}. \tag{2.2.9}$$

If one takes $\delta g_{h^3}/g_{h^3}^{(\mathrm{SM})} \sim \delta_3$ to compare with the earlier bound Eq. (2.2.6), one finds the unitarity bound gets more stringent with increasing n and thus interpreting a Higgs trilinear deviation with the operator with the fewest derivatives leads to the most conservative new physics bound.

An important assumption in the argument above is that the number of derivatives in an operator determines its scaling with energy. In particular, we assume that each additional derivative give an additional factor of $\partial \sim E$ in scattering amplitudes at high energy. This is what is expected in general, but it can fail in certain choices of operator basis. This is because field redefinitions and integration by parts in the effective Lagrangian do not affect scattering amplitudes, so there are 'flat directions' in the space of effective Lagrangians. For example, the field redefinition $h \to h - (\delta_3/2v)h^2$ can be used to eliminate the deviation in the h^3 coupling, but will induce correlated couplings of the form $h^2\Box h, h^2V^2$ and $h^2\bar{t}t$. In this basis, the $h^2\Box h, h^2V^2$ couplings typically lead to E^4 growth in the V_L^6 amplitude as expected from counting derivatives, but with the correlated values induced by the field redefinition the leading growth is canceled, resulting in the same E^2 growth as the original h^3 deviation. Thus, a basis which eliminates h^3 is a poor basis for our purposes, since it obscures the energy scaling through non-trivial cancellations. To our knowledge, it has never been proven that there exists a basis where the naïve energy scaling holds, even though this assumption is commonly used in applications of effective field theory. In this chapter we will assume that such a basis exists, and leave further investigation of this point for future work.[3]

Since the unitarity bound Eq. (2.2.6) comes from scattering of gauge bosons, we must also consider effective couplings involving gauge fields. For example, from the unitary-gauge diagrams shown in Fig. 2.1 we can see that a deviation in the hV^2 and h^2V^2 couplings can also give rise to unitarity violation in the V_L^6 amplitude at high energy. The hV^2 and h^2V^2 couplings are phenomenologically interesting in their own right, and will be studied in detail in Sec. 2.3 and Sec. 2.5 respectively below. Here we preview some of the results of Sec. 2.3 to understand how modifications of the hV^2 and h^2V^2 couplings contribute to the V_L^6 amplitude. To use the equivalence theorem, we restore the Nambu-Goldstone bosons in the

[3] A natural guess is that this basis can be defined using amplitude methods [15, 31], where the connection between the number of derivatives and the energy scaling of amplitudes is manifest.

gauge boson fields in unitary gauge (see Eq. (2.3.3) below):

$$gV_\mu \to gV_\mu + \frac{\partial_\mu G}{v} + \frac{h\partial_\mu G}{v^2} + \cdots , \tag{2.2.10}$$

where g is the gauge coupling. This gives (temporarily setting $v = 1$)

$$\begin{aligned} X(gV)^2 &\sim \partial^2[\boldsymbol{G}^2(h + h^2 + \cdots) + \boldsymbol{G}^4(1 + h + \cdots) + \boldsymbol{G}^6(1 + h + \cdots) + \cdots], \\ X^2(gV)^2 &\sim \partial^2[\boldsymbol{G}^2(h^2 + h^3 + \cdots) + \boldsymbol{G}^4(h + h^2 + \cdots) + \boldsymbol{G}^6(1 + h + \cdots) + \cdots], \\ X^3(gV)^2 &\sim \partial^2[\boldsymbol{G}^2(h^3 + h^4 + \cdots) + \boldsymbol{G}^4(h^2 + h^3 + \cdots) + \boldsymbol{G}^6(h + h^2 + \cdots) + \cdots]. \end{aligned} \tag{2.2.11}$$

Here we have assumed custodial symmetry so that the Nambu-Goldstones appear in a custodial singlet $\boldsymbol{G}^2$. These give a contribution to the V_L^6 amplitude (restoring the factors of v)

$$\Delta\hat{\mathcal{M}}(V_L V_L V_L \to V_L V_L V_L) \sim (\delta_{V1} + \delta_{V2})\frac{E^4}{v^4}, \tag{2.2.12}$$

where δ_{V1} and δ_{V2} are defined in Eq. (2.1.1) and their coefficients in the above equation are only schematic. We see that deviations in the hV^2 and h^2V^2 couplings contribute to the amplitude the same way as higher-derivative couplings at high energy, and therefore they can only lower the scale of unitarity violation. Similar results hold for modifications of the V^3 and V^4 couplings, as well as terms with additional derivatives. These give contributions to the V_L^6 amplitude that grow even faster with energy, and therefore do not invalidate the bound Eq. (2.2.6).

To determine the unitarity bounds from a Higgs cubic coupling deviation, we conservatively assume that δ_{V1}, δ_{V2}, and higher-derivative couplings are zero and focus on the δ_3 coupling. Contributions to the amplitude that are higher order in δ_3 involve propagators that give additional $1/E^2$ suppression at high energies, so the leading unitarity violation is

given by a single insertion of δ_3 even for $\delta_3 \gtrsim 1$.[4]

2.2.3 The Optimal Bound

The bound Eq. (2.2.6) makes no assumption about the nature of the new physics other than that it is at high scales, and is valid independently of the values of the infinitely many unmeasured couplings δ_4, c_n in Eq. (2.1.1). However, it is not guaranteed this it is the best possible bound, because it does not take the effects of all possible unmeasured couplings into account. The reason is the following. If we allow additional unmeasured couplings to be nonzero, these predict additional higher-body processes that depend on δ_3 as well as the unmeasured couplings. Requiring that these additional processes do not violate unitarity below the scale Eq. (2.2.6) places additional constraints on these couplings.[5] It is possible that there is no choice of the new couplings that satisfies the unitarity bound Eq. (2.2.6), in which case we obtain a stronger unitarity bound. In other words, an optimal bound is obtained by marginalizing over the unmeasured couplings, while the bound Eq. (2.2.6) is independent of these couplings.

We have not found a general method to obtain the optimal bound. However, in the case of the V_L^6 amplitude we can constrain the optimal bound to show that it does not significantly improve the bound Eq. (2.2.6). To do this, we consider a theory consisting of the SM plus the dimension-6 interaction $(H^\dagger H)^3$. This corresponds to a particular choice of the higher dimension X^n operators that includes terms only up to six scalars (see Eq. (2.2.2)). Therefore, for this choice of couplings we can simply check all unitarity violating processes and put a bound on the scale of unitarity violation. The optimal bound will always be weaker than the unitarity violating scale obtained from the $(H^\dagger H)^3$ theory, since this corresponds to a particular choice for the infinitely many unconstrained couplings. If this scale is the

[4] For other processes, we will find that the leading contributions to the unitarity bound include diagrams with propagators, for example Eq. (2.4.5).

[5] In fact, we know that at least some of these couplings must be nonzero, because the theory with only $\delta_3 \neq 0$ violates unitarity at the TeV scale [28, 29].

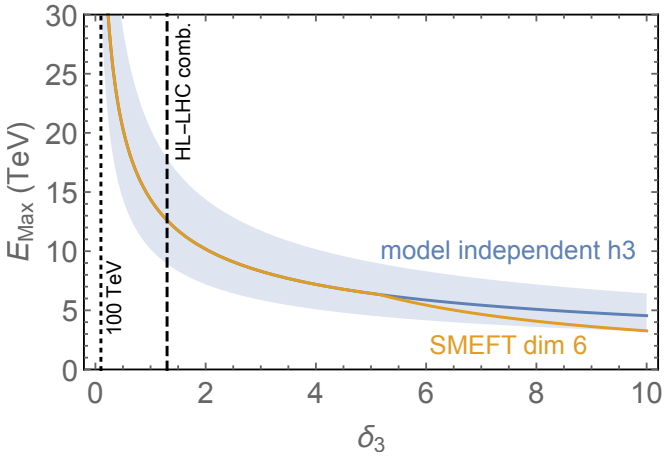

Fig. 2.2: The unitarity bound as a function of the deviation in the h^3 coupling. The optimal bound lies between the model-independent and SMEFT estimates. The band around the model-independent scale reflects the uncertainty of the bound from varying the unitarity constraint to $\frac{1}{2} \leq |\hat{\mathcal{M}}| \leq 2$. For comparison, we show projected 95% C.L. limits on δ_3 from a combination at HL-LHC and a 100 TeV pp collider from [3].

same as Eq. (2.2.6), we will know that this is the optimal bound; if not, we learn that the optimal bound is between the bound Eq. (2.2.6) and the one just described.

We find that the strongest bound in the $(H^\dagger H)^3$ theory comes from the V_L^6 amplitude for small values of δ_3, but for larger values the process $hh \to hhh$ dominates and gives

$$E_{\text{max}} \simeq \frac{32 \text{ TeV}}{|\delta_3|}. \tag{2.2.13}$$

The results are plotted in Fig. 2.2. The scale of tree-level unitarity violation is an estimate for the scale of strong coupling, and is therefore subject to theoretical uncertainty. As a rough parameterization of this uncertainty, we vary the constraint from $\frac{1}{2} < |\mathcal{M}| < 2$. Within this range, we see that there is no important difference between the model-independent bound and the optimal bound.

2.2.4 SMEFT Predictions from Unitarity

If the scale of new physics is high, we expect that the new physics must be of the decoupling type. This means that the effects of the new physics at low energies can be captured by adding to the SM a series of higher-dimension gauge-invariant operators. This is the SMEFT framework. If experiments reveal a deviation in one or more SM measurements, without any sign of new physics, it is most natural to interpret the results in terms of SMEFT.

SMEFT is predictive because the same SMEFT operator controls more than one observable. However, these predictions assume that we can neglect higher-dimension terms, and the size of these corrections is unknown without further theoretical input. We now show that we can make an interesting quantitative statement about this purely from unitarity considerations. Specifically, we show that if the scale of new physics is much larger than the TeV scale, we can bound the error of the SMEFT prediction, and this error bound gets better as the scale of new physics gets larger.

To be specific, we assume that $\delta_3 \neq 0$, and the energy scale of new physics is lower than some value E_{max}. In this case, we expect that the observed deviation in the Higgs cubic coupling can be explained by the dimension-6 SMEFT operator[6]

$$\delta\mathcal{L}_{\text{SMEFT}} = \frac{1}{M^2}\left(H^\dagger H - \frac{v^2}{2}\right)^3. \tag{2.2.14}$$

This form of the operator keeps the Higgs mass and electroweak VEV at their tree level values, but modifies the Higgs mass parameter and quartic coupling. If this operator dominates, it predicts

$$\delta_3 = \frac{2v^4}{M^2 m_h^2}, \qquad \delta_4 = 6\delta_3, \qquad c_5 = c_6 = 45\delta_3. \tag{2.2.15}$$

We expect these predictions to become more accurate if the scale of new physics is larger since

[6] Technically, this operator is a linear combination of dimension 0, 2, 4 and 6 operators, but we will refer to these linear combinations by their highest dimension.

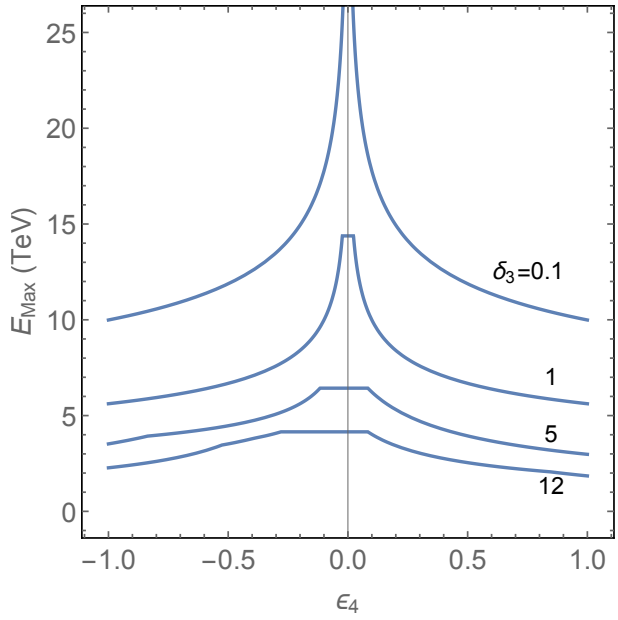

Fig. 2.3: Unitarity violating scales from processes that depend on δ_3 and δ_4 as a function of the fractional deviation ϵ_4 from the dimension-6 SMEFT prediction (see Eqs. (2.2.15) and (2.2.16)).

these additional couplings themselves generate new unitarity violating amplitudes which require coupling correlations to be canceled.

To make this quantitative, we simply require that any deviation in the quartic coupling does not give rise to tree-level unitarity violation below the scale E_{max}. This requirement not only bounds the quartic coupling from being too large, but it also predicts that its deviation must be close to the prediction of the dimension-6 SMEFT operator Eq. (2.2.14):

$$\epsilon_4 = \frac{\delta_4 - \delta_4^{\text{dim 6}}}{\delta_4^{\text{dim 6}}} \ll 1. \tag{2.2.16}$$

The reason for this is that adding a X^4 term to the effective Lagrangian means that there are now additional processes that violate unitarity, which are not affected by couplings of the form X^n with $n \geq 5$. The one that is most sensitive to new physics is the process

$W_L^+W_L^+W_L^-W_L^- \to W_L^+W_L^+W_L^-W_L^-$, which gives the bound

$$E_{\max} \simeq \frac{8.7 \text{ TeV}}{|\delta_4 - 6\delta_3|^{1/4}}. \tag{2.2.17}$$

The denominator vanishes for $\delta_4 = 6\delta_3$ because the SMEFT operator does not contain a $\boldsymbol{G}^8$ term. Requiring that the theory violates unitarity above some scale that is large compared to 1 TeV therefore requires that the deviations are close to the SMEFT prediction $\delta_4 = 6\delta_3$. Taking into account all of the processes predicted by the X^3 and X^4 couplings, the results are shown in Fig. 2.3. For example, we see that for $E_{\max} \sim 10$ TeV, the deviation in the quartic coupling is within $\sim 10\%$ of the value predicted by dimension-6 SMEFT. This shows that not finding new physics below some scale can be complementary to direct searches [32–34] in constraining the quartic coupling.

2.3 New Physics from hVV Couplings

The Higgs couplings to vector bosons $V = W^\pm, Z$ provides another sensitive probe for new physics. In this section, we work out the model-independent constraints on the scale of new physics from measurements of these couplings. Note that we will not consider Higgs coupling to massless gauge bosons, which can be probed by $h \to \gamma\gamma, Z\gamma, gg$. These lie outside the thrust of this chapter because they do not lead to high-energy growth in V_L scattering. Also, because these couplings are loop-induced in the Standard Model, we expect that deviations from the Standard Model predictions will give rather weak unitarity constraints.

2.3.1 Model-Independent Bound on the Scale of New Physics

It is well known that a deviation in the hVV couplings leads to unitarity violation in longitudinal W and Z scattering at high energies (see [18, 19] and more recently [35]). In the SM, the Higgs exchange contribution cancels the E^2 growth of other diagrams, so any modification of the hVV coupling will ruin this cancellation and lead to unitarity violation. We

can reproduce this result using the same model-independent bottom-up approach we used for the h^3 coupling. We write down the most general deviations from the SM involving the Higgs and vector bosons that are quadratic in the W and Z gauge boson fields:

$$\begin{aligned}\mathcal{L} = \mathcal{L}_{\rm SM} - \alpha\delta T\left(\tfrac{1}{2}m_Z^2 Z^\mu Z_\mu\right) + \delta_{Z1}\frac{m_Z^2}{v}hZ^\mu Z_\mu + \delta_{W1}\frac{2m_W^2}{v}hW^{\mu+}W_\mu^- \\ + \delta_{Z2}\frac{m_Z^2}{2v^2}h^2 Z^\mu Z_\mu + \delta_{W2}\frac{m_W^2}{v^2}h^2 W^{\mu+}W_\mu^- + c_{Z3}\frac{m_Z^2}{3!v^3}h^3 Z^\mu Z_\mu + \cdots,\end{aligned} \tag{2.3.1}$$

where h is the scalar field that parameterizes the physical Higgs boson (see Eq. (2.2.2)). As before, we do not assume any power counting for the higher terms, we only assume that their values are compatible with experimental constraints. Our bounds are obtained by marginalizing over the values of the infinitely many unmeasured couplings. For now, we do not assume that custodial symmetry is preserved by the deviations from the SM, and therefore we have included an additional contribution to the T parameter from shifting the Z mass.

To understand the implications of the couplings in Eq. (2.3.1) for processes involving longitudinally polarized vectors at high energy, we use the equivalence theorem. To do this, we write the new couplings in Eq. (2.3.1) in terms of gauge invariant operators using

$$\hat{H} = \frac{H}{\sqrt{H^\dagger H}} = \begin{pmatrix}0\\1\end{pmatrix} + O(\boldsymbol{G}). \tag{2.3.2}$$

This transforms under electroweak gauge symmetry just like a Higgs doublet. This allows us to write the vector fields in terms of gauge-invariant operators:

$$\begin{aligned}\hat{H}^\dagger i D_\mu \hat{H} &= -\frac{m_Z}{v}Z_\mu - \frac{1}{v}\partial_\mu G^0 + \cdots, \\ \tilde{\hat{H}}^\dagger i D_\mu \hat{H} &= \frac{\sqrt{2}m_W}{v}W_\mu^+ + \frac{i\sqrt{2}}{v}\partial_\mu G^+ + \cdots, \\ \hat{H}^\dagger i D_\mu \tilde{\hat{H}} &= \frac{\sqrt{2}m_W}{v}W_\mu^- - \frac{i\sqrt{2}}{v}\partial_\mu G^- + \cdots,\end{aligned} \tag{2.3.3}$$

where we have defined

$$\tilde{\hat{H}} = \epsilon \hat{H}^*, \qquad \epsilon = \begin{pmatrix} 0 & 1 \\ -1 & 0 \end{pmatrix}. \tag{2.3.4}$$

We then use Eq. (2.3.3) to write Eq. (2.3.1) as a sum of gauge invariant operators. We therefore have

$$\mathcal{L} = \mathcal{L}_{\rm SM} - \frac{\alpha v^2 \delta T}{2} |\hat{H}^\dagger D_\mu \hat{H}|^2 + \delta_{Z1} v X |\hat{H}^\dagger D_\mu \hat{H}|^2 + \delta_{W1} v X |\tilde{\hat{H}}^\dagger D_\mu \hat{H}|^2 + \cdots, \tag{2.3.5}$$

where X is defined in Eq. (2.2.3). We can now expand this expression in powers of the Nambu-Goldstone fields $\boldsymbol{G}$ and Higgs field h using

$$\begin{aligned} \hat{H} &= \left(1 + \frac{\boldsymbol{G}^2}{(v+h)^2}\right)^{-1/2} \begin{pmatrix} \dfrac{\sqrt{2}G^+}{v+h} \\ 1 + i\dfrac{G^0}{v+h} \end{pmatrix} \\ &= \begin{pmatrix} 0 \\ 1 \end{pmatrix} + \frac{1}{v+h} \begin{pmatrix} \sqrt{2}G^+ \\ iG^0 \end{pmatrix} - \frac{\boldsymbol{G}^2}{2(v+h)^2} \begin{pmatrix} 0 \\ 1 \end{pmatrix} + O(\boldsymbol{G}^3). \end{aligned} \tag{2.3.6}$$

The only model-independent couplings arising from $\delta T, \delta_{Z1}$ and δ_{W1} are then

$$\begin{aligned} \delta\mathcal{L} = {} & \frac{\alpha\delta T + \delta_{Z1}}{v} h \partial^\mu G^0 \partial_\mu G^0 + \frac{2\delta_{W1}}{v} h \partial^\mu G^+ \partial_\mu G^- + \frac{\alpha \delta T}{v} (\partial_\mu h \partial^\mu G^0) G^0 \\ & + \frac{i\alpha\delta T}{v} \partial_\mu G^0 (G^- \partial^\mu G^+ - G^+ \partial^\mu G^-) + \frac{\alpha \delta T}{2v^2} (G^+ \partial_\mu G^- - G^- \partial_\mu G^+)^2 \\ & + \frac{2\alpha\delta T + \delta_{Z1}}{2v^2} (\boldsymbol{G})^2 \partial^\mu G^0 \partial_\mu G^0 + \frac{\delta_{W1}}{v^2} (\boldsymbol{G})^2 \partial^\mu G^+ \partial_\mu G^- \\ & + \frac{i}{v^2} \left[(3\alpha\delta T - 2\delta_{W1} + 2\delta_{Z1}) h \partial^\mu G^0 + \alpha \delta T \, G^0 \partial^\mu h \right] (G^+ \partial_\mu G^- - G^- \partial_\mu G^+) \\ & + \frac{i}{v^3} (2\alpha\delta T - \delta_{W1} + \delta_{Z1}) (\boldsymbol{G})^2 \partial^\mu G^0 (G^+ \partial_\mu G^- - G^- \partial_\mu G^+). \end{aligned} \tag{2.3.7}$$

Interactions involving higher powers of Nambu-Goldstone or Higgs fields can be generated by next order couplings such as δ_{Z2} and δ_{W2}, which are much less constrained ex-

perimentally. Notice that the δT term contributes to these interactions at the same order as δ_{Z1}, δ_{W1}. However, given the stringent experimental constraints on the T parameter, $\alpha\delta T \lesssim 0.001$, these effects are subdominant because we are considering significantly larger deviations $\delta_{Z1}, \delta_{W1} \sim 0.1$, so we will often neglect δT in the following discussion.[7]

The unitarity constraints on δ_{Z1} and δ_{W1} come from the amplitudes $V_L V_L \to V_L h, V_L V_L \to V_L V_L$, and $V_L V_L V_L \to V_L V_L$. These get contributions from a contact term from Eq. (2.3.7) while the last two also have a contribution from a Higgs exchange giving the schematic form:

$$\begin{aligned} \hat{\mathcal{M}}(V_L V_L \to V_L h) &\sim (\delta_{V1}) \frac{E^2}{v^2}, \\ \hat{\mathcal{M}}(V_L V_L \to V_L V_L) &\sim (\delta_{V1} + \delta_{V1}^2) \frac{E^2}{v^2}, \\ \hat{\mathcal{M}}(V_L V_L V_L \to V_L V_L) &\sim (\delta_{V1} + \delta_{V1}^2) \frac{E^3}{v^3}. \end{aligned} \tag{2.3.8}$$

Because of the experimental constraint $|\delta_{V1}| \lesssim 0.2$, we neglect the quadratic terms. The processes that give the strongest constraints are:

$$\begin{aligned} W_L^+ W_L^+ \to W_L^+ W_L^+ &: E_{\max} \simeq \frac{1.2 \text{ TeV}}{|\delta_{W1}|^{1/2}}, \\ Z_L Z_L \to W_L^+ W_L^- &: E_{\max} \simeq \frac{1.5 \text{ TeV}}{|\delta_{Z1} + \delta_{W1}|^{1/2}}, \\ W_L^+ h \to W_L^+ Z_L &: E_{\max} \simeq \frac{1.0 \text{ TeV}}{|\delta_{Z1} - \delta_{W1}|^{1/2}}, \\ W_L^+ W_L^+ W_L^- \to W_L^+ Z_L &: E_{\max} \simeq \frac{1.5 \text{ TeV}}{|\delta_{Z1} - \delta_{W1}|^{1/3}}. \end{aligned} \tag{2.3.9}$$

There are no unitarity constraints depending on δ_{Z1} alone. This is because the $ZZ \to ZZ$ amplitude does not grow at high energies, since it is proportional to $s + t + u = 4m_Z^2$. Note that a measured deviation on one or both of these couplings of order of the current 2σ bounds $|\delta_{Z1}|, |\delta_{W1}| \sim 0.2$ would imply new physics below a few TeV, a scale that can be explored at the HL-LHC itself. We plot the strongest bounds from Eq. (2.3.9) in Fig. 2.4, together with

[7] Ref. [36] recently pointed out that the $W_L W_L Z_L h$ amplitude violates unitarity only if custodial symmetry is broken. This can be verified by the fourth line in Eq. (2.3.7). From the last line, we see that this also extends to the $Z_L W_L^4$ and $Z_L^3 W_L^2$ amplitudes.

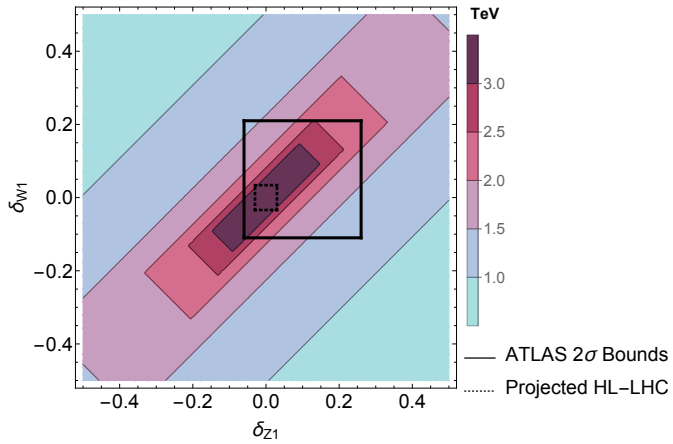

Fig. 2.4: The unitarity-violating scale that depends on δ_{Z1} and δ_{W1} assuming that custodial symmetry is not preserved. The solid black line represents the current ATLAS 95% C.L. constraints [2] while the dotted black line gives the HL-LHC projections [3].

the ATLAS limits on δ_{Z1} and δ_{W1} [2] and the HL-LHC projections [3]. Notice that $\delta_{Z1} = \delta_{W1}$ (the positive diagonal on the plot) corresponds to the custodial symmetry limit which has weaker unitarity bounds than the maximally custodial violating direction $\delta_{Z1} = -\delta_{W1}$, due to the last two processes in Eq. (2.3.9).

2.3.2 Optimal Bound with Custodial Symmetry

As emphasized in Sec. 2.2.1, bounds such as Eq. (2.3.9) make no assumptions about the nature of the new physics other than that it is at high scales, and are valid independently of the values of the infinitely many unmeasured couplings. However, as discussed in Sec. 2.2.3, marginalizing over these unmeasured couplings may give a stronger bound, which we call the optimal bound. In this section we show that if we assume that the new physics preserves custodial symmetry, the model-independent bound from Eq. (2.3.9) is in fact optimal. We will discuss the case without custodial symmetry in Sec. 2.3.4 below.

We focus on the custodial symmetry limit where $\delta T = 0$ and $\delta_{W1} = \delta_{Z1} \equiv \delta_{V1}$. This limit is well-motivated by the strong experimental bounds on the T parameter. We consider

the dimension-6 SMEFT operator

$$\delta\mathcal{L}_{\text{SMEFT}} = \frac{1}{M^2}\left(H^\dagger H - \frac{v^2}{2}\right)|D_\mu H|^2. \tag{2.3.10}$$

This does not contribute to the T parameter, and gives a custodial symmetry preserving deviation to the hVV couplings. Making a field redefinition to remove the momentum-dependent terms $h\partial h^2$ and $h^2\partial h^2$, we find that this operator predicts

$$\delta_{V1} = \frac{v^2}{2M^2}, \quad \delta_{V2} = 4\delta_{V1}, \quad c_{V3} = 8\delta_{V1}, \quad c_{V4} = 8\delta_{V1}, \tag{2.3.11}$$

where $\delta_{V2} = \delta_{Z2} = \delta_{W2}$, and $c_{Vn} = 0$ for $n \geq 5$. Using this, we can calculate the additional amplitudes predicted by Eq. (2.3.10) that violate unitarity, namely $h^2Z_L^2$ and $h^2W_L^2$ and check whether these give a lower scale of unitarity violation for a given value of δ_{V1}. We find that these new processes give weaker or equivalent bounds to the model-independent bound for $\delta_{Z1} = \delta_{W1}$,

$$E_{\text{max}} \simeq \frac{1.1\text{ TeV}}{|\delta_{V1}|^{1/2}}, \tag{2.3.12}$$

which is therefore also the optimal bound in this case. This is shown in Fig. 2.5 along with the constraints from ATLAS and a HL-LHC projection, showing the potential to constrain new physics below ~ 5 TeV.

2.3.3 SMEFT Predictions from Unitarity with Custodial Symmetry

If the scale of new physics is high, we expect that an observed deviation in the Higgs couplings can be described by the lowest-dimension SMEFT operator. In this section we assume that the new physics preserves custodial symmetry, and consider the question of the accuracy of the SMEFT prediction, following the logic explained in Sec. 2.2.4. The dimension-6 SMEFT

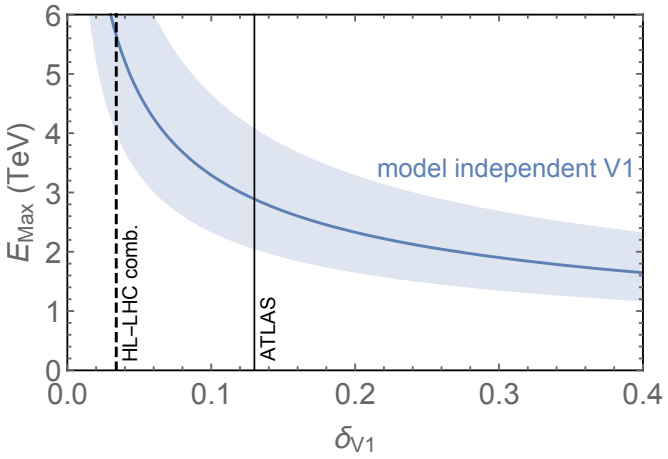

Fig. 2.5: The unitarity bound as a function of the deviation in the hVV coupling. The optimal bound lies between the model-independent and SMEFT estimate from the dimension-6 operator Eq. (2.3.10) and thus they are the same. The band around the model-independent scale results from varying the unitarity bound to $\frac{1}{2} \leq |\hat{\mathcal{M}}| \leq 2$. For comparison, we show the 95% C.L. limits on δ_{V1} from ATLAS [2] and a projected HL-LHC combination [3].

operator Eq. (2.3.10) predicts $\delta_{V2} = 4\delta_{V1}$, and we define

$$\epsilon_{V2} \equiv \frac{\delta_{V2} - \delta_{V2}^{\text{dim 6}}}{\delta_{V2}^{\text{dim 6}}}. \tag{2.3.13}$$

When we include both δ_{V1} and δ_{V2}, we have the additional model-independent processes $hh \to V_L V_L$, $hV_L V_L \to V_L V_L$ and $V_L V_L V_L \to V_L V_L V_L$. Requiring that these do not violate unitarity constrains E_{max} for a given value of ϵ_{V2}. The results are shown in Fig. 2.6. The results are qualitatively similar to the case of the Higgs self-interaction. The predictions of SMEFT become accurate for $E_{\text{max}} \gtrsim 10$ TeV, corresponding to values of δ_{V1} much smaller than what will be probed in upcoming experiments, and since the unitarity-violating scale is low even for δ_{V1} of $O(1\%)$, in this case a general value of δ_{V2} does not change the bound much.

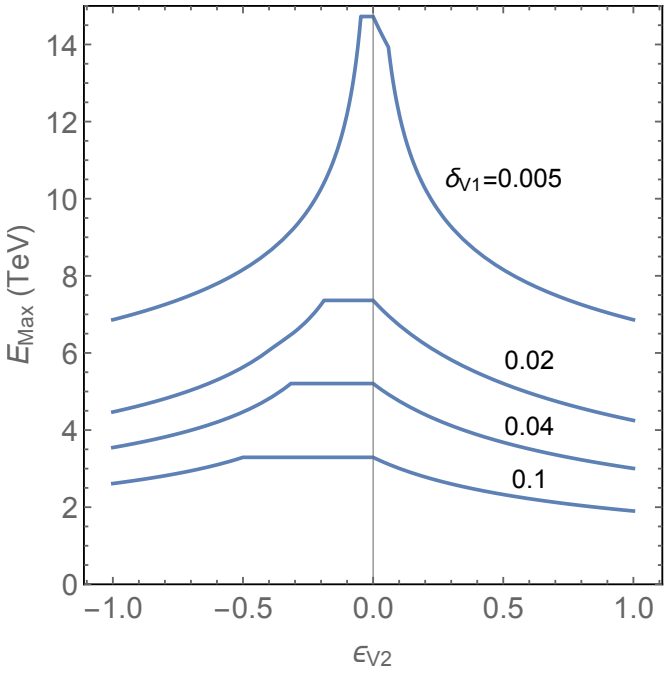

Fig. 2.6: Unitarity violating scales from processes that depend on δ_{V1} and δ_{V2} as a function of the fractional deviation of δ_{V2} from its SMEFT prediction, $\delta_{V2} = 4\delta_{V1}(1 + \epsilon_{V2})$.

2.3.4 Optimal Bound Without Custodial Symmetry

We now consider the unitarity bounds for the case $\delta_{Z1} \neq \delta_{W1}$. This case is somewhat unnatural, in the sense that for values of δ_{Z1} and δ_{W1} that violate custodial symmetry at a level that is observable in upcoming experiments, the small observed T parameter appears to require an unnatural cancellation. Nonetheless, δ_{Z1} and δ_{W1} will be independently measured, and it is interesting to explore the implications of $\delta_{Z1} \neq \delta_{W1}$.

For concreteness we consider the case $\delta_{Z1} \neq 0$, $\delta_{W1} \simeq 0$, $\alpha\delta T \simeq 0$. In order to explain this in SMEFT, we must introduce the dimension-8 operator

$$\frac{1}{M^4}\left(H^\dagger H - \frac{v^2}{2}\right)|H^\dagger D_\mu H|^2, \tag{2.3.14}$$

which has been chosen so that $\delta T = 0$. This operator predicts the following coupling

deviations:

$$\begin{aligned}
&\delta_{Z1} = \frac{v^4}{4M^4}, && \delta_{W1} = 0, && \delta_{Z2} = 8\delta_{Z1}, && \delta_{W2} = -\delta_{Z1}, \\
&c_{Z3} = 40\delta_{Z1}, && c_{W3} = -8\delta_{Z1}, && c_{Z4} = 136\delta_{Z1}, && c_{W4} = -32\delta_{Z1}, \\
&c_{Z5} = 288\delta_{Z1}, && c_{W5} = -72\delta_{Z1}, && c_{Z6} = 288\delta_{Z1}, && c_{W6} = -72\delta_{Z1}.
\end{aligned} \tag{2.3.15}$$

There are now many more unitarity-violating amplitudes, and the unitarity violating scale that we obtain assuming that the dimension-8 operator dominates is somewhat stronger than the model-independent bound. The results are shown in Fig. 2.7.

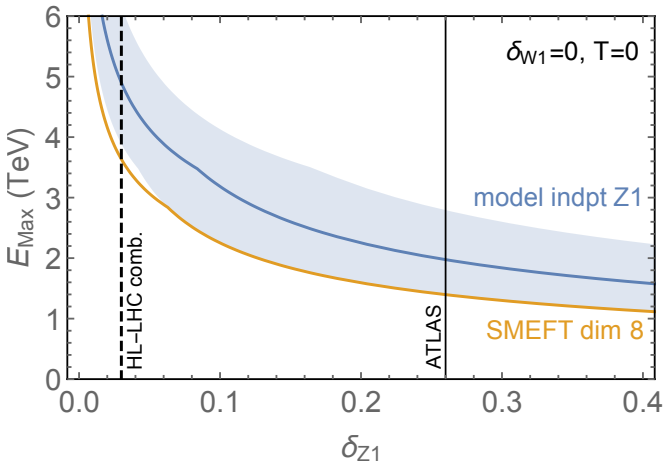

Fig. 2.7: The unitarity bound as a function of the deviation in the hZZ coupling, assuming $\delta_{W1} = 0$, $\delta T = 0$. The optimal bound lies between the model-independent and SMEFT estimate from the dimension-8 operator Eq. (2.3.14). The band around the model-independent scale results from varying the unitarity bound to $\frac{1}{2} \leq |\hat{\mathcal{M}}| \leq 2$. For comparison, we show the 95% C.L. limits on δ_{Z1} from ATLAS [2] and a projected HL-LHC combination [3].

2.4 New Physics from $h\bar{t}t$ Couplings

The Higgs couplings to top quarks $h\bar{t}t$ provides another sensitive probe of new physics. In this section we work out the model-independent constraints on the scale of new physics from measurements of this coupling.

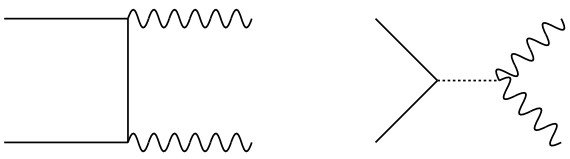

Fig. 2.8: Feynman diagrams contributing to $t\bar{t} \to W_L^+ W_L^-$ in unitary gauge.

2.4.1 Model-Independent Bound

If the $h\bar{t}t$ coupling deviates from the SM value, processes such as $t\bar{t} \to W_L^+ W_L^-$ will violate unitarity at high energy. This observation goes back to Ref. [20], which put a bound on the scale of fermion mass generation in a theory without a Higgs boson. The diagrams contributing to this process in unitary gauge are shown in Fig. 2.8. We see that they are sensitive to both the $\bar{t}th$ coupling and the hVV coupling, and we will see that the unitarity bound depends on both δ_{t1} and δ_{V1} in Eq. (2.1.1). Unitarity violation for more general top couplings in $2 \to 2$ processes has been recently studied in [37, 38].

As in the previous sections, we use the equivalence theorem to compute the high-energy behavior of amplitudes involving longitudinally polarized vector bosons and Higgs fields. We do this by writing the deviations from the SM in Eq. (2.1.1) that depend on the top quark in a general gauge:

$$\delta\mathcal{L} = -m_t(\bar{Q}_L \tilde{\hat{H}} t_R + \text{h.c.}) \left(\delta_{t1} \frac{X}{v} + c_{t2} \frac{X^2}{2! v^2} + \cdots \right), \tag{2.4.1}$$

where X is given by Eq. (2.2.3) and $\tilde{\hat{H}}$ is given by Eqs. (2.3.2) and (2.3.4). Expanding these terms in terms of the Higgs and Nambu-Goldstone bosons gives

$$\bar{Q}_L \tilde{\hat{H}} t_R + \text{h.c.} = \frac{1}{\sqrt{1 + \frac{\boldsymbol{G}^2}{(v+h)^2}}} \left(\bar{t}t - \frac{1}{v+h} \left[G^0 \bar{t} i\gamma_5 t + \sqrt{2} G^- \bar{b}_L t_R + \sqrt{2} G^+ \bar{t}_R b_L \right] \right). \tag{2.4.2}$$

This leads to the following interaction pattern (temporarily setting $v = 1$)

$$\begin{aligned}
\bar{t}tX &\sim tt^c[h + iG^0(h + \cdots) + \boldsymbol{G}^2(1 + \cdots) + iG^0\boldsymbol{G}^2(1 + \cdots) + \boldsymbol{G}^4(1 + \cdots) + \cdots] \\
&\quad + bt^cG^+[(h + \cdots) + \boldsymbol{G}^2(1 + \cdots) + \boldsymbol{G}^4(1 + \cdots) + \cdots] + \text{h.c.}, \\
\bar{t}tX^2 &\sim tt^c[h^2 + iG^0(h^2 + \cdots) + \boldsymbol{G}^2(h + \cdots) + iG^0\boldsymbol{G}^2(h + \cdots) + \boldsymbol{G}^4(1 + \cdots) + \cdots] \\
&\quad + bt^cG^+[(h^2 + \cdots) + \boldsymbol{G}^2(h + \cdots) + \boldsymbol{G}^4(1 + \cdots) + \cdots] + \text{h.c.}, \\
\bar{t}tX^3 &\sim tt^c[h^3 + iG^0(h^3 + \cdots) + \boldsymbol{G}^2(h^2 + \cdots) + iG^0\boldsymbol{G}^2(h^2 + \cdots) + \boldsymbol{G}^4(h + \cdots) + \cdots] \\
&\quad + bt^cG^+[(h^3 + \cdots) + \boldsymbol{G}^2(h^2 + \cdots) + \boldsymbol{G}^4(h + \cdots) + \cdots] + \text{h.c.},
\end{aligned} \tag{2.4.3}$$

where the parentheses allow arbitrary higher powers of h. Examining the structure of the interactions in Eq. (2.4.3), we see that the model-independent couplings that depend only on δ_{t1} are

$$\begin{aligned}
\delta\mathcal{L} \supset &- \delta_{t1}\frac{m_t}{v}\left[\left(h + \frac{1}{2v}\boldsymbol{G}^2\right)\bar{t}t - \left(h + \frac{1}{2v}\boldsymbol{G}^2\right)\frac{G^0}{v}\bar{t}i\gamma_5 t\right] \\
&+ \delta_{t1}\frac{\sqrt{2}m_t}{v^2}\left[\left(h + \frac{1}{2v}\boldsymbol{G}^2\right)G^-\bar{b}_L t_R + \text{h.c.}\right].
\end{aligned} \tag{2.4.4}$$

As discussed previously in Sec. 2.2.2, we can also consider tth interactions with additional derivatives, but again we expect these will give a parametrically lower scale of unitarity violation, and therefore in terms of new physics bounds, it is conservative to interpret a tth coupling deviation in terms of the coupling with no derivatives. We can then determine the schematic form for the following model-independent amplitudes:

$$\begin{aligned}
\hat{\mathcal{M}}(\bar{q}q \to V_L V_L) &\sim y_t\left(\delta_{t1} + \delta_{V1} + \delta_{t1}\delta_{V1}\right)\frac{E}{v}, \\
\hat{\mathcal{M}}(\bar{q}q \to V_L h) &\sim y_t\left(\delta_{t1} + \delta_{V1}\right)\frac{E}{v}, \\
\hat{\mathcal{M}}(\bar{q}q \to V_L V_L V_L) &\sim y_t\left(\delta_{t1} + \delta_{V1} + \delta_{t1}\delta_{V1} + \delta_{V1}^2\right)\frac{E^2}{v^2},
\end{aligned} \tag{2.4.5}$$

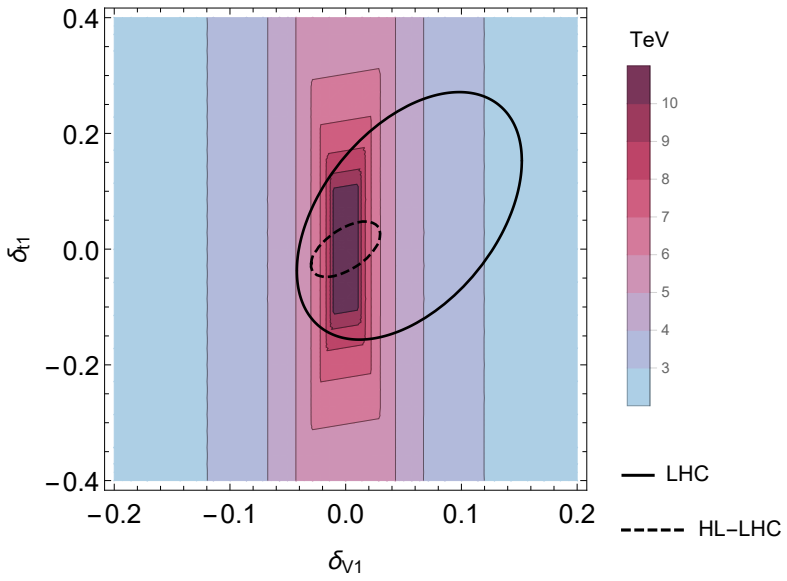

Fig. 2.9: Unitarity violating scales given values of δ_{t1} and δ_{V1}. The solid line represents the 95% C.L. at the LHC [2] and the dashed line is the HL-LHC projection for ATLAS [39].

where $q = t, b$. For the $\bar{b}t$ initial state processes, the first process vanishes. Amplitudes related to these by crossing have the same scaling. The terms depending on δ_{V1} arise from diagrams with propagators (see Eq. (2.3.7)). The 2 derivatives in vertices from δ_{V1} cancel the energy suppression of the extra propagators, so these contributions are the same order. For contributions with a propagator, there is a possibility of $\log(E/m)$ terms arising from the phase space integrals in the amplitudes. By direct calculation, we show that these are absent in all of the terms in Eq. (2.4.5), except possibly for the δ_{V1}^2 term in the last line. This contribution is numerically small even if a log is present, and so we will neglect all quadratic contributions.

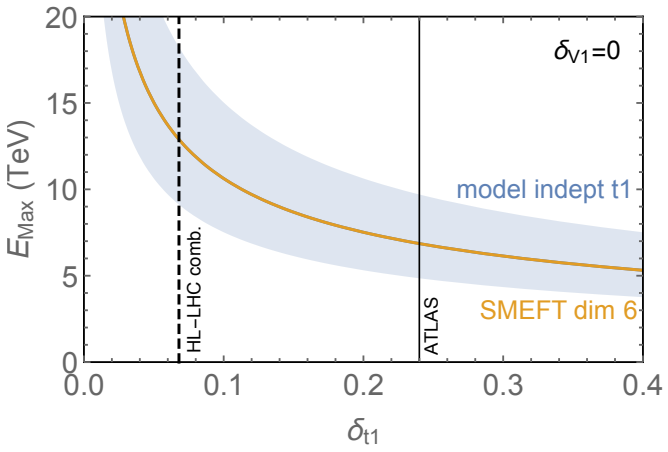

Fig. 2.10: The unitarity bound on δ_{t1} assuming $\delta_{W1}, \delta_{Z1} = 0$. The model-independent bound is equal to the optimal bound for all values of δ_{t1} shown. The band around the model-independent scale results from varying the unitarity bound to $\frac{1}{2} \leq |\hat{\mathcal{M}}| \leq 2$. For comparison, we show the 95% C.L. limits on the coupling from ATLAS [2] and a projected HL-LHC combination [3].

The best bounds on δ_{t1} from these processes are

$$\begin{aligned} t_R\bar{t}_R \to W_L^+W_L^- &: E_{\max} \simeq \frac{5.1 \text{ TeV}}{|\delta_{t1} + \delta_{V1}|}, \\ t_R\bar{b}_R \to W_L^+h &: E_{\max} \simeq \frac{3.6 \text{ TeV}}{|\delta_{t1} - \delta_{V1}|}, \\ t_R\bar{b}_R \to W_L^+W_L^+W_L^- &: E_{\max} \simeq \frac{3.3 \text{ TeV}}{\sqrt{|\delta_{t1} - \frac{1}{3}\delta_{V1}|}}, \end{aligned} \tag{2.4.6}$$

where we assume custodial symmetry $\delta_{Z1} = \delta_{W1} = \delta_{V1}$. As already mentioned above, these bounds are numerically stronger than previous bounds [20, 22, 23].

Fig. 2.9 shows the unitarity violating scale from these processes as a function of δ_{t1} and δ_{V1}, together with projected HL-LHC constraints on these couplings. From this graph, we see that upcoming measurements of δ_{V1} are sensitive to lower scales of new physics. However, if measurements of hVV agree with the SM, a deviation in the $h\bar{t}t$ coupling at HL-LHC that is compatible with current constraints can still point to a scale of new physics below 8 TeV.

2.4.2 Optimal Bound

To further discuss the implications of δ_{t1}, we consider a scenario where δ_{t1} is nonzero, but all the other Higgs couplings are compatible with the SM. To estimate the scale of new physics in this scenario, it is conservative to assume $\delta_{W1}, \delta_{Z1} = 0$, since unitarity bounds from Eq. (2.3.9) are stronger than Eq. (2.4.1). As in previous sections, we consider the optimal bound obtained by marginalizing over the infinitely many unmeasured couplings. The optimal bound can be constrained by considering the SMEFT operator

$$\delta\mathcal{L}_{\text{SMEFT}} = \frac{y_t}{M^2}\left(H^\dagger H - \frac{v^2}{2}\right)(\bar{Q}_L \tilde{H} t_R + \text{h.c.}), \tag{2.4.7}$$

which gives

$$\delta_{t1} = -\frac{v^2}{M^2}, \quad c_{t2} = c_{t3} = 3\delta_{t1}, \tag{2.4.8}$$

and $c_{tn} = 0$ for $n \geq 4$. This imposes additional unitarity bounds. We find that the bounds for the model-independent processes considered above give the most stringent bound for small δ_{t1}, but for larger values of δ_{t1} the strongest bound comes from $\bar{t}_R t_R \to hh$, which gives

$$E_{\text{max}} \simeq \frac{2.4 \text{ TeV}}{|\delta_{t1}|}. \tag{2.4.9}$$

However, this only dominates over the bounds in Eq. (2.4.1) for $\delta_{t1} \gtrsim 0.6$, which is larger than allowed by current constraints. In Fig. 2.10 we show the unitarity bounds on δ_{t1} along with the experimental bounds from ATLAS and the projected sensitivity of a HL-LHC combination.

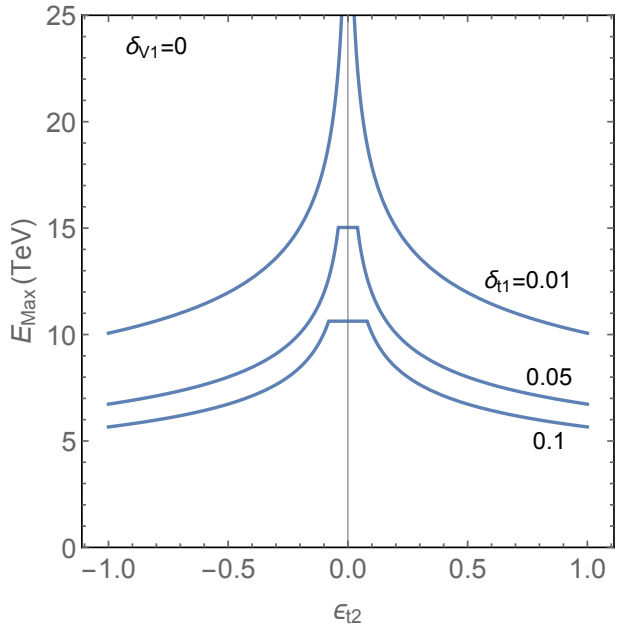

Fig. 2.11: The unitarity bound from processes that depend on δ_{t1}, $c_{t2} = 3\delta_{t1}(1+\epsilon_{t2})$ where $\epsilon_{t2} = 0$ is the prediction of the dimension-6 SMEFT operator. Due to these amplitudes depending on coupling δ_{V1}, it has been set to zero in this plot.

2.4.3 SMEFT Predictions from Unitarity

If the scale of new physics is high, we expect that an observed deviation in the Higgs couplings can be described by the lowest-dimension SMEFT operator. In the case of the $\bar{t}th$ coupling, this is the operator given in Eq. (2.4.7), which makes the predictions Eq. (2.4.8) for the higher-order deviations. We can constrain the accuracy of these predictions from unitarity, as outlined in previous sections. The results are shown in Fig. 2.11. As expected, the SMEFT predictions are accurate only if the scale of new physics is $\gtrsim 10$ TeV.

2.5 New Physics from $hhVV$ and $hh\bar{t}t$ Couplings

In this section we discuss the implications of a deviation in the $hhVV$ or $hh\bar{t}t$ coupling, parameterized respectively by δ_{V2} and c_{t2} in Eq. (2.1.1). Since there are no symmetries to prevent this, any new physics that contributes to these couplings should also contribute to a comparable deviation in δ_{V1} and δ_{t1}, which will be measured to greater precision. On the

other hand, it is possible that δ_{V1} and δ_{t1} are suppressed by an accidental cancellation. In any case, experimental constraints on δ_{V2} and c_{t2} will improve dramatically at the HL-LHC, and will give us additional information about possible new physics. Another motivation for studying these couplings is that they directly contribute to di-Higgs production. Therefore, an anomalous rate for di-Higgs production may be due to δ_{V2} (in vector boson fusion) or δ_{t2} (from gluon fusion). Therefore we should consider these couplings in order to determine the unitarity bounds from any future di-Higgs anomalies.

2.5.1 hhVV: Model-Independent Bound on the Scale of New Physics

We now work out the model-independent bound on the scale of new physics coming from an observation of $\delta_{V2} \neq 0$. This coupling can be measured from di-Higgs production via vector boson fusion [40]. Although this process in principle is sensitive to an anomaly in the h^3 coupling, this sensitivity is strongly reduced by requiring large di-Higgs invariant mass to suppress backgrounds. Because any new physics that contributes to δ_{V2} will also contribute to δ_{V1}, we assume that both couplings are nonzero in the present discussion.

The procedure we use to obtain the model-independent bound is an extension of the one used in Sec. 2.3 to include $\delta_{V2} \neq 0$. This adds the model-independent processes $h^2V_L^2$, hV_L^4, and V_L^6. Because the δ_{V1} and δ_{V2} couplings each contain 2 derivatives additional insertions of these vertices can cancel the $1/E^2$ from additional propagators. This means that the leading diagrams at high energy include diagrams with multiple propagators. We find

$$\begin{aligned}
\hat{\mathcal{M}}(V_LV_L \to hh) &\sim \left(\delta_{V1} + \delta_{V2} + \delta_{V1}^2\right)\frac{E^2}{v^2}, \\
\hat{\mathcal{M}}(V_LV_L \to V_LV_Lh) &\sim \left(\delta_{V1} + \delta_{V2} + \delta_{V1}^2 + \delta_{V1}\delta_{V2} + \delta_{V1}^3\right)\frac{E^3}{v^3}, \\
\hat{\mathcal{M}}(V_LV_LV_L \to V_LV_LV_L) &\sim \left(\delta_{V1} + \delta_{V2} + \delta_{V1}^2 + \delta_{V1}\delta_{V2} + \delta_{V1}^2\delta_{V2} + \delta_{V1}^3 + \delta_{V1}^4\right)\frac{E^4}{v^4}.
\end{aligned} \tag{2.5.1}$$

Amplitudes related to these by crossing have the same scaling. Current experimental constraints give $|\delta_{V1}| \lesssim 0.2$, while δ_{V2} has a weak constraint of $-1.8 \leq \delta_{V2} \leq 1.9$ at 95%

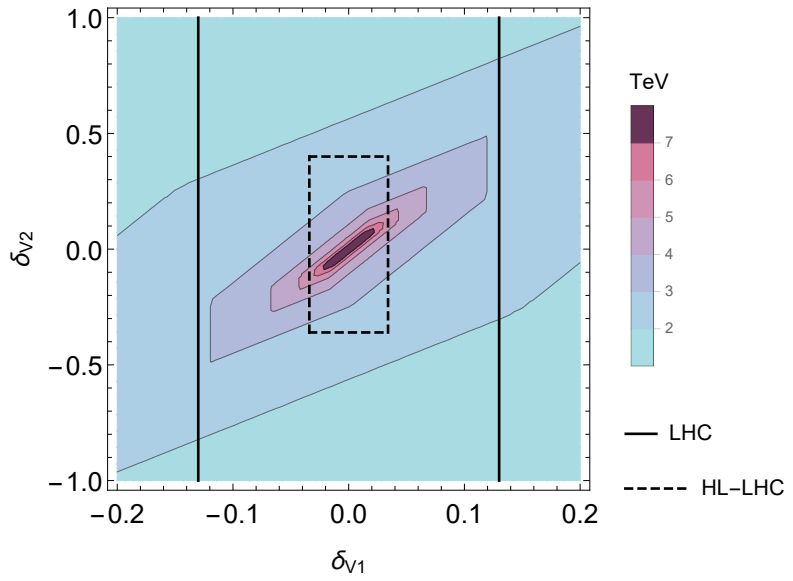

Fig. 2.12: Unitarity violating contours from δ_{V1} and δ_{V2}. The solid lines represent the ATLAS bound on δ_{V1} [2] while the δ_{V2} bound [41] is outside of the plot range. The dashed lines show the projected bounds for δ_{V1} [3] and δ_{V2} at HL-LHC, where the δ_{V2} bounds are the 95% C.L. bounds from doubling the 68% bounds from a projected vector boson fusion di-Higgs search [40].

C.L. [41]. We can therefore neglect the nonlinear terms in these amplitudes (which are also much more difficult to compute). Assuming custodial symmetry ($\delta_{Z1} = \delta_{W1}$, $\delta_{Z2} = \delta_{W2}$) the strongest bounds are

$$\begin{aligned} W_L^+W_L^- \to hh: \quad & E_{\max} \simeq \frac{1.5 \text{ TeV}}{|\delta_{V2} - 2\delta_{V1}|^{1/2}}, \\ Z_LZ_L \to hW_L^+W_L^-: \quad & E_{\max} \simeq \frac{1.9 \text{ TeV}}{|\delta_{V2} - 4\delta_{V1}|^{1/3}}, \\ W_L^+W_L^+Z_L \to W_L^+W_L^+Z_L: \quad & E_{\max} \simeq \frac{2.6 \text{ TeV}}{|\delta_{V2} - 4\delta_{V1}|^{1/4}}. \end{aligned} \tag{2.5.2}$$

In Fig. 2.12, we show the unitarity violating scale given values of δ_{V1} and δ_{V2} along with the bounds on both coupling deviations from standard searches and a search for vector boson fusion di-Higgs. The figure shows that HL-LHC searches for VBF di-Higgs could find coupling deviations with unitarity bounds below 3 TeV.

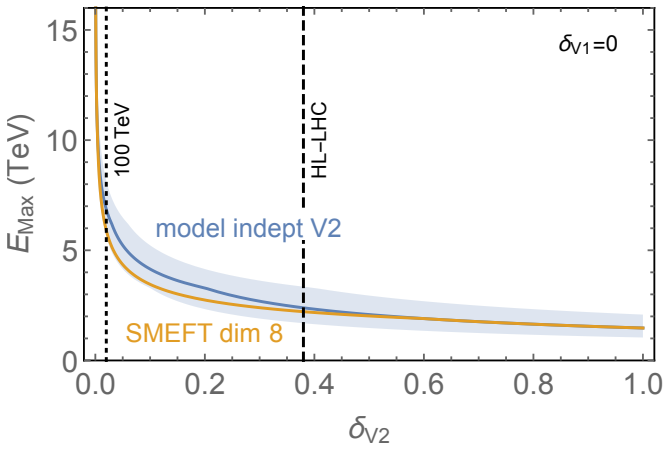

Fig. 2.13: The unitarity bound from as a function of δ_{V2} neglecting small terms proportional to δ_{V1}. The optimal bound lies between the model-independent and SMEFT estimates. The band around the model-independent bound results from varying the unitarity bound to $\frac{1}{2} \leq |\hat{\mathcal{M}}| \leq 2$. For comparison, we show 95% C.L. limits on the coupling from the vector boson fusion di-Higgs analysis projected for the HL-LHC and a 100 TeV pp collider [40].

2.5.2 hhVV: Optimal Bound and SMEFT Predictions

We now consider the optimal bound obtained by marginalizing over the infinitely many unmeasured couplings. As in previous sections, we do this by considering a scenario where these couplings are given by a single SMEFT operator. In the present case, we use the dimension-8 operator

$$\frac{1}{M^4}\left(H^\dagger H - \frac{v^2}{2}\right)^2 D^\mu H^\dagger D_\mu H, \tag{2.5.3}$$

which gives custodial symmetry preserving couplings. Performing field redefinitions to remove the Higgs self couplings at order $1/M^4$, we have find that the Higgs couplings to the vector bosons are given by

$$\delta_{V1} = 0, \quad \delta_{V2} = \frac{v^4}{M^4}, \quad c_{V3} = 8\delta_{V2}, \quad c_{V4} = 32\delta_{V2}, \quad c_{V5} = 72\delta_{V2}, \quad c_{V6} = 72\delta_{V2}, \tag{2.5.4}$$

and $c_{Vn} = 0$ for $n \geq 7$. The unitarity bound obtained from this operator is always stronger than the optimal bound, so the optimal bound lies between this bound and the model-

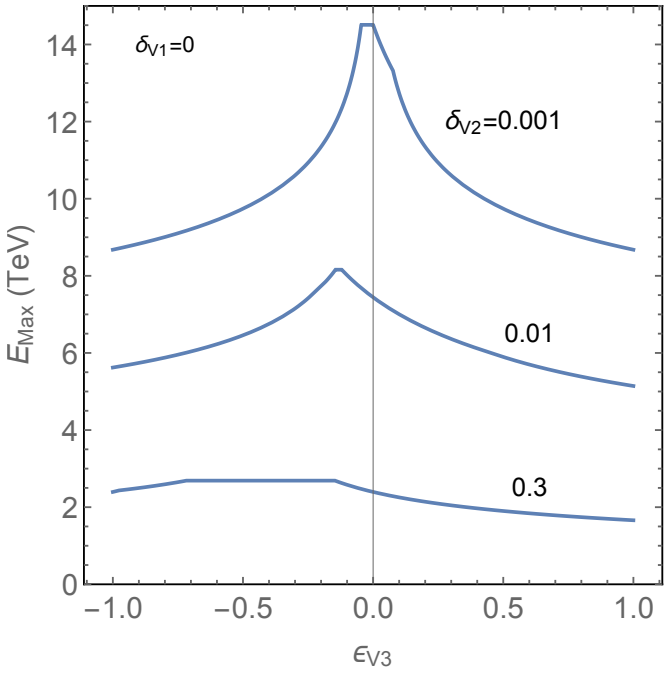

Fig. 2.14: The unitarity bound from processes that depend on δ_{V2} and $c_{V3} = 8\delta_{V2}(1+\epsilon_{V3})$ to linear order, where $\epsilon_{V3} = 0$ correspond to the SMEFT predictions, assuming $\delta_{V1} = 0$.

independent bound computed above. In Fig. 2.13, we plot both the model-independent and the SMEFT unitarity bound as a function of δ_{V2}, neglecting terms proportional to δ_{V1}, showing that the optimal bound is close to the model-independent one.

Next, we consider the accuracy of the SMEFT prediction for δ_{V2} from the operator Eq. (2.5.3). (We again consider the case where $\delta_{V1} = 0$). We expect the predictions of this operator to become more accurate as the scale of new physics becomes large. In Fig. 2.14 we plot the quantity

$$\epsilon_{V3} = \frac{c_{V3} - c_{V3}^{\text{dim 8}}}{c_{V3}^{\text{dim 8}}}, \tag{2.5.5}$$

where $c_{V3}^{\text{dim 8}} = 8\delta_{V2}$. As in previous cases, we find that the SMEFT prediction becomes accurate when the scale of new physics is larger than a TeV.

2.5.3 $hh\bar{t}t$: Model-Independent Bound on the Scale of New Physics

We now consider a deviation in the $hh\bar{t}t$ coupling c_{t2}. The study of this coupling is strongly motivated by the fact that di-Higgs production is sensitive to this coupling, and therefore di-Higgs production does not measure the h^3 coupling in a model-independent way [42]. However, measuring $ht\bar{t}$ and $hht\bar{t}$ production has been shown to break the degeneracies between the hhh, $h\bar{t}t$ and $hh\bar{t}t$ couplings [43–45].

In this subsection we focus on the unitarity bound on c_{t2}. We are interested in model-independent processes that do not depend on c_{tn} for $n \geq 3$. The relevant couplings are given in Eqs. (2.4.3) and (2.2.11). We can work out that the model-independent processes have the schematic form at leading order in the energy expansion:

$$\begin{aligned}
\hat{\mathcal{M}}(\bar{t}t \to hh) &\sim y_t c_{t2} \frac{E}{v}, \\
\hat{\mathcal{M}}(\bar{t}t \to V_L hh) &\sim y_t \big(\delta_{t1} + c_{t2} + \delta_{V1} + \delta_{V2} + \delta_{t1}\delta_{V1} + \delta_{V1}^2\big) \frac{E^2}{v^2}, \\
\hat{\mathcal{M}}(\bar{t}t \to V_L V_L h) &\sim y_t \big(\delta_{t1} + c_{t2} + \delta_{V1} + \delta_{V2} + \delta_{t1}\delta_{V1} + \delta_{t1}\delta_{V2} \\
&\qquad + c_{t2}\delta_{V1} + \delta_{V1}^2 + \delta_{t1}\delta_{V1}^2\big) \frac{E^2}{v^2}, \\
\hat{\mathcal{M}}(\bar{t}t \to V_L V_L V_L h) &\sim y_t \big(\delta_{t1} + c_{t2} + \delta_{V1} + \delta_{V2} + \delta_{t1}\delta_{V1} + \delta_{t1}\delta_{V2} \\
&\qquad + c_{t2}\delta_{V1} + \delta_{V1}^2 + \delta_{V1}\delta_{V2} + \delta_{t1}\delta_{V1}^2 + \delta_{V1}^3\big) \frac{E^3}{v^3}, \\
\hat{\mathcal{M}}(\bar{t}t \to V_L V_L V_L V_L V_L) &\sim y_t \big(\delta_{t1} + c_{t2} + \delta_{V1} + \delta_{V2} + \delta_{t1}\delta_{V1} + \delta_{t1}\delta_{V2} + c_{t2}\delta_{V1} \\
&\qquad + \delta_{V1}^2 + \delta_{V1}\delta_{V2} + \delta_{t1}\delta_{V1}^2 + \delta_{t1}\delta_{V1}\delta_{V2} + c_{t2}\delta_{V1}^2 \\
&\qquad + \delta_{V1}^3 + \delta_{V1}^2\delta_{V2} + \delta_{t1}\delta_{V1}^3 + \delta_{V1}^4\big) \frac{E^4}{v^4}.
\end{aligned} \tag{2.5.6}$$

For $\bar{t}b$ initial states, the first and third process vanish while the second process does not have a δ_{t1} term. Amplitudes related to these by crossing have the same scaling. Again, due to constraints on δ_{t1}, δ_{V1} we can neglect the nonlinear terms. At linear order, we see that only the $\bar{t}t \to hh$ amplitude is independent of δ_{V2}, which is poorly constrained experimentally and thus can substantially affect the constraints on c_{t2}. These linear contributions involving δ_{V1}

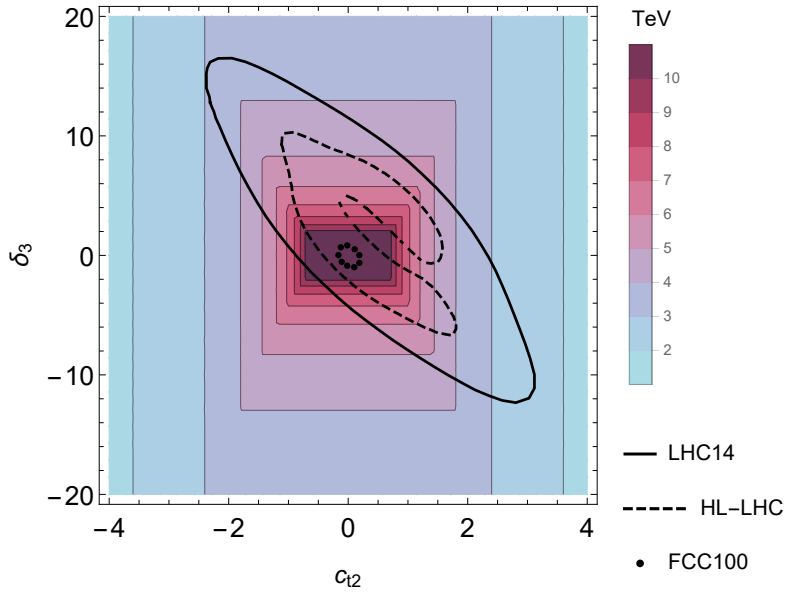

Fig. 2.15: Unitarity violating contours from δ_3 and c_{t2}. The 95% C.L. projections from gluon fusion di-Higgs searches are shown for the LHC (solid) and for the HL-LHC (dashed), which were obtained by expanding the 1σ contours of [42] by 1.6 to estimate the 95% C.L. sensitivity.

and δ_{V2} involve diagrams with propagators, which are significantly more difficult to compute so we have focused on the terms from δ_{V2}. Due to this contamination from δ_{V2}, we will use only $\bar{t}t \to hh$ to set unitarity bounds on c_{t2}. The bounds taking into account the dominant linear contributions are:

$$\begin{aligned}
t_R\bar{t}_R \to hh: &\quad E_{\max} \simeq \frac{7.2\ \text{TeV}}{|c_{t2}|}, \\
t_R\bar{t}_R \to W_L^+W_L^-h: &\quad E_{\max} \simeq \frac{4.7\ \text{TeV}}{|c_{t2} - 2\delta_{t1} + \frac{1}{3}\delta_{V2}|^{1/2}}, \\
t_R\bar{b}_R \to W_L^+h^2: &\quad E_{\max} \simeq \frac{4.7\ \text{TeV}}{|c_{t2} - 2\delta_{t1} - \frac{2}{3}\delta_{V2}|^{1/2}}, \\
t_R\bar{b}_RW_L^- \to hW_L^+W_L^-: &\quad E_{\max} \simeq \frac{3.9\ \text{TeV}}{|c_{t2} - 3\delta_{t1} + \frac{1}{2}\delta_{V2}|^{1/3}}, \\
t_R\bar{b}_RW_L^- \to W_L^+W_L^+W_L^-W_L^-: &\quad E_{\max} \simeq \frac{4.2\ \text{TeV}}{|c_{t2} - 3\delta_{t1} + \frac{1}{3}\delta_{V2}|^{1/4}}.
\end{aligned} \tag{2.5.7}$$

In Fig. 2.15, we plot the unitarity violating scale as a function of c_{t2} and δ_3. Superimposed

on the plot are estimates of the current bounds and sensitivity to these parameters from gluon fusion di-Higgs production [42]. We see that it is plausible that the HL-LHC could find deviations that point to a scale of new physics below 3 TeV, even allowing for the experimental degeneracy between c_{t2} and δ_3.

2.5.4 $hh\bar{t}t$: Optimal Bound and SMEFT Predictions

To obtain the relations between c_{2t} and higher order couplings, we use the dimension-8 SMEFT operator

$$\frac{y_t}{M^4}\left(H^\dagger H - \frac{v^2}{2}\right)^2 (\bar{Q}_L \tilde{H} t_R + \text{h.c.}), \tag{2.5.8}$$

which gives the predictions

$$\delta_{t1} = 0, \quad c_{t2} = -2\frac{v^4}{M^4}, \quad c_{t3} = 6c_{t2}, \quad c_{t4} = 15c_{t2}, \quad c_{t5} = 15c_{t2}, \tag{2.5.9}$$

and $c_{tn} = 0$ for $n \geq 6$. As in the previous cases, we can use Eq. (2.5.9) to obtain unitarity bounds from processes that we classified as model-independent. Fig 2.16 shows the unitarity bounds predicted by the model independent approach and the SMEFT operator, where we assume $\delta_{t1} = \delta_{V1} = \delta_{V2} = 0$ to focus on c_{t2}. Thus, the optimal bound is still within our estimated uncertainty of the model-independent bound.

Once again, we can see the effect that a high scale of unitarity violation (compared to 1 TeV) has on the SMEFT predictions in Eq. (2.5.9). Fig. 2.17 shows the unitarity scale dependence on ϵ_{t3} where $c_{t3} = 6c_{t2}(1 + \epsilon_{t3})$ and we assume $\delta_{t1} = \delta_{V1} = \delta_{V2} = 0$. As with the other couplings, at high scales of unitarity violation (e.g. 10 TeV), c_{t3} is close to its SMEFT value.

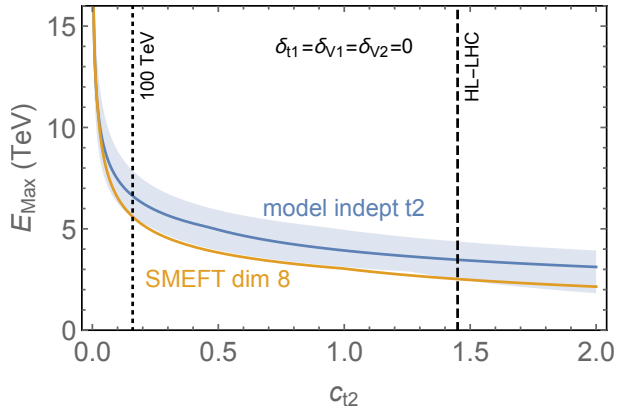

Fig. 2.16: The unitarity bounds from both the model-independent approach and the SMEFT dimension-8 prediction, the optimized bound from marginalizing over other couplings should be somewhere between these two lines. We assume $\delta_{t1} = \delta_{V1} = \delta_{V2} = 0$. We also plot the projected 95% C.L. limits on the coupling from the gluon fusion di-Higgs analysis at the HL-LHC and a 100 TeV pp collider [42]

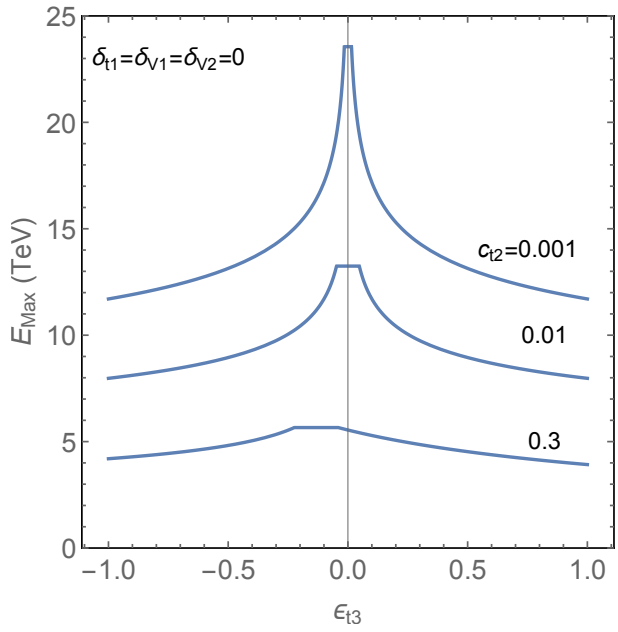

Fig. 2.17: The unitarity bound from processes that depend only on c_{t2} and $c_{t3} = 6c_{t2}(1+\epsilon_3)$ when $\delta_{t1} = \delta_{V1} = \delta_{V2} = 0$. Setting $\epsilon_{t3} = 0$ corresponds to the SMEFT prediction from the dimension-8 operator.

2.6 Conclusions

In this chapter, we have investigated the scale of unitarity violation due to nonstandard Higgs self-couplings, and Higgs couplings to W/Z bosons and top quarks. In the SM, good high

energy behavior for multiparticle scattering amplitudes relies on delicate cancellations among the various Higgs couplings. If these cancellations are upset by new physics contributions to the Higgs couplings, this leads to tree-level unitarity violation at high energies, signaling the breakdown of perturbation theory and the onset of new physics. In this way, we can give a model-independent bound on the scale of new physics directly from any observed deviation from the SM prediction for Higgs couplings.

In this work, we focused on the couplings h^3, h^4, hVV, h^2VV, $h\bar{t}t$, and $h^2\bar{t}t$ where $V = W$ or Z, which will be probed at the HL-LHC and future colliders. In the SM, these couplings are predicted at the percent level while current constraints are only at the 10%–100% level. Upcoming experiments will significantly improve these constraints, giving many opportunities to discover physics beyond the SM. Our work translates these searches into a direct probe of the scale of new physics.

For the $hVV, h\bar{t}t$ couplings, the current constraints allow coupling values that require new physics below 3 TeV for W/Z couplings, and below 8 TeV for the top coupling. The Higgs trilinear coupling is much more weakly constrained, allowing a scale of new physics as low as 4 TeV. The couplings $hh\bar{t}t$ and $hhVV$ are of particular interest for di-Higgs searches in gluon-fusion and vector boson fusion, and their constraints allow a scale of new physics as low as 2 TeV. These results show that measurements of Higgs couplings can point to a scale of new physics within the kinematic reach for HL-LHC and future colliders.

Unitarity bounds can also place indirect constraints on couplings that are difficult to measure directly, such as the h^4 coupling. For example if there is a nonstandard Higgs trilinear coupling, we show that to keep the new physics bound above 10 TeV, the quartic coupling must closely approximate the coupling correlation from the dimension-6 SMEFT operator $(H^\dagger H)^3$. We present similar results for the W/Z and top couplings as well. We emphasize that these predictions do not make any assumptions about the smallness of higher-dimension operators, and rely only on unitarity.

Our main conclusion is that, from a purely data-driven viewpoint, our current knowledge

of the Higgs couplings allows new physics at the few TeV scale. This scale will be extensively probed at the HL-LHC and future colliders, both through direct searches and Higgs coupling measurements, and there is a great deal of room for discovery in both types of analyses. In particular, the scales probed by the upcoming HL-LHC are not sufficiently large that we can confidently neglect higher-dimension operators in SMEFT. We have therefore adopted a completely bottom-up and model-independent approach to translating these measurements into direct statements about the scale of new physics. We hope that these results will be useful in interpreting and further motivating the precision study of the Higgs boson's properties.

Chapter 3

Primary Observables for Indirect Searches at Colliders

This chapter is taken from [10]

3.1 Introduction

In this chapter, we are interested in enumerating the 3 and 4 point operators that can appear in a BSM Lagrangian. We also make a few phenomenological comments and estimates. As discussed in the previous chapters, the motivation for considering SM coupling deviations and new interactions between SM particles is that under our EFT framework, they can be indicative of new heavy physics. Once again, we adopt a bottom up framework where we assume there are no new light particles and for the 4 point operators, we focus on the interactions involving the Higgs. We restrict our analysis to three and four point functions, since the motivation for our work is phenomenological. For this same reason, since we are interested in connecting our work to collider searches, for practical purposes, we assume that linearly independent operators are independent observables. We are also only interested in

the leading terms.

We introduce the distinction between primary and Mandelstam descendent operators. For example, we have

$$\delta\mathcal{M}(f_1\bar{f}_2 \to Z_3 h_4) = \frac{c_1^{hZ\bar{f}f}}{v}(\bar{u}_{\mathrm{L}2}\not{\epsilon}_3^* u_{\mathrm{L}1})\left[1 + \alpha_1\frac{s}{M^2} + \beta_1\frac{t}{M^2} + O(E^4/M^4)\right] + i\frac{c_9^{hZ\bar{f}f}}{2v^3}\epsilon_{\mu\nu\rho\sigma}(\bar{u}_{\mathrm{L}2}\gamma^\mu u_{\mathrm{L}1})(p_1-p_2)^\nu(p_3^\rho\epsilon_3^{\sigma\,*} - p_3^\sigma\epsilon_3^{\rho\,*})\left[1 + \alpha_9\frac{s}{M^2} + \beta_9\frac{t}{M^2} + O(E^4/M^4)\right] + \cdots \tag{3.1.1}$$

from Table 3.3. The prefactors are the primaries [1] and the terms that are proportional to the Mandelstams are the Mandelstam descendents. Our problem then essentially becomes finding a list of linearly independent primaries. To accomplish this, we use some brute force numerical techniques, a new analytical approach, and cross check against the Hilbert series prediction [47–53]. As stated before, we are interested in the leading terms, which we assume are the primaries. There exist cases where the primary operators are suppressed and the descendent becomes the leading term, such as in [42,54,55]. We do not consider these cases.

There is some ambiguity because the basis of operators is not unique, since we can always integrate by parts or perform field redefinitions [56–59]. We choose to use the fact that each local on-shell amplitude corresponds to an independent EFT operator [16,31,60–64], so that our operators are written in terms of the physical fields and each amplitude is simply the Feynman rule of its operator.

While the main focus of this chapter is presenting the techniques for determining the independent primaries and listing them for 3 and 4 point interactions, we also discuss some phenomological estimates. For each of the primary operators that we find, we provide a rough estimate of the size of their coefficients allowed by tree level unitarity. In order to identify the most phenomenologically interesting ones, we use these values to identify those that are most relevant to Higgs decays. We also examine the effects of precision electroweak

[1] We borrow the terminology of [46], where the leading contributions are referred to as "BSM primaries"

constraints.

There has been some previous work that also attempts to list the independent observables and operators, such as the "Higgs basis" [65] and the "BSM primaries" [46] which use dimension 6 SMEFT. Ref. [66] goes beyond dimension 6, but only examines 3 point functions. Refs [16, 63] performs similar work to us using the spinor helicity formalism. Our work differs from these papers in that we use a bottom up approach and do not make any model assumptions. In particular, we do not assume that all interactions arise from dimension 6 SMEFT. The advantage to this is that we are not limited to decoupling new physics, since dimension 6 SMEFT does not accurately capture the effects of non-decoupling physics [67–70]. Furthermore, as discussed in the previous chapter and [9], the SMEFT prediction is most accurate if the scale of new physics is high. We also analyze cases with massless and/or indistinguishable particles and list primary operators.

In this chapter, we begin by discussing the 3 and 4 point functions that we will consider. We then discuss our methods for determining linear independence amongst the operators, followed by our phenomenological estimates. Finally we list our operators and summarize our conclusions.

3.2 Scope of Paper

The aim of this chapter is to classify the primary operators that are relevant for Higgs signals at hadron and lepton colliders. Specifically, we focus on all 3- and 4-point couplings that are relevant for Higgs decays, di-Higgs production, and Higgs associated production. In this section, we specify the couplings that we will study in the remainder of the chapter. We will also define our notation and normalization conventions, and comment on ambiguities in the operator basis associated with off-shell 3-point couplings.

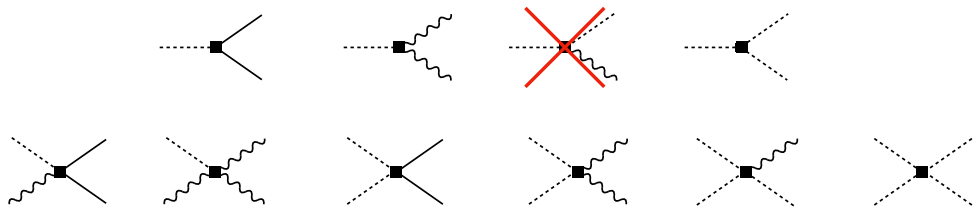

Fig. 3.1: Three and 4-point couplings relevant for Higgs decays and Higgs production. Dashed lines denote the Higgs particle, solid lines denote fermions, and wavy lines denote any of the SM gauge bosons γ, g, W, or Z. The crossed-out diagrams are not relevant because they vanish on shell (see text).

3.2.1 Topologies and Couplings

The 3-point and 4-point couplings that involve at least one Higgs boson are shown in Fig. 3.1. The most general couplings compatible with $SU(3)_{\rm C} \times U(1)_{\rm EM}$ gauge invariance are

$$\text{3-point} : h\bar{f}f, hZZ, hWW, hZ\gamma, h\gamma\gamma, hgg, \cancel{hhZ}, \cancel{hh\gamma}, hhh, \tag{3.2.1a}$$

$$\begin{aligned}\text{4-point} : & \; hZ\bar{f}f, hW\bar{f}f', h\gamma\bar{f}f, hg\bar{f}f, \\ & hWWZ, hZZZ, hWW\gamma, hZZ\gamma, hZ\gamma\gamma, hZgg, h\gamma\gamma\gamma, h\gamma gg, hggg, \\ & hh\bar{f}f, hhWW, hhZZ, hhZ\gamma, hh\gamma\gamma, hhgg, \\ & hhhZ, hhh\gamma, hhhh.\end{aligned} \tag{3.2.1b}$$

Some of these three-point couplings vanish on-shell, and we have crossed these out above.[2]

In addition, there are 3-point couplings that do not involve the Higgs which contribute to some of the 4-point processes that get contribution from the couplings in Eq. (3.2.1b). These are shown in Fig. 3.2. These couplings are given by

$$\begin{aligned}& Z\bar{f}f, W\bar{f}f', \gamma\bar{f}f, g\bar{f}f, \\ & WWZ, \cancel{ZZZ}, WW\gamma, \cancel{ZZ\gamma}, \cancel{Z\gamma\gamma}, \cancel{Zgg}, \cancel{\gamma\gamma\gamma}, \cancel{\gamma gg}, ggg,\end{aligned} \tag{3.2.2}$$

[2] These operators can be nonzero off-shell, but field redefinitions allows us to eliminate them in favor or redefining the 4-point functions, as explained in Sec. 3.2.2 below.

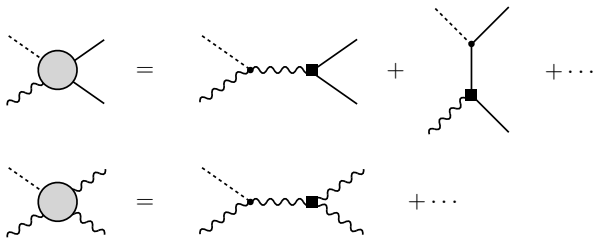

Fig. 3.2: Exchange contributions to 4-point amplitudes involving BSM 3-point couplings that do not contain the Higgs. The notation is the same as Fig. 3.1. We do not show diagrams involving Higgs exchange that involve 3-point functions already shown in Fig. 3.1. We also do not show diagrams involving two Higgses and a neutral gauge bosoon, since these vanish on shell (see text).

where we have again crossed out couplings that are not allowed on-shell.

These interactions parameterize the BSM contributions to general 2-body and 3-body decays of the the Higgs boson. They also parameterize the BSM contributions to the production of a single Higgs, a pair of Higgs, and Higgs associated production via the processes

$$\begin{aligned}
&(\bar{f}f, gg, W^+W^-, ZZ) \to (h, hh, hZ, h\gamma, hg)\\
&(\bar{f}f', ZW) \to hW,\\
&(fg, f\gamma, fZ) \to hf,\\
&fW \to f'h.
\end{aligned} \tag{3.2.3}$$

Note that the $hhhZ, hhh\gamma$ amplitudes can be used to calculate exchange diagrams for hhh production, *e.g.* $\bar{f}f \to (Z^*, \gamma^*) \to hhh$, but fully characterizing the 5-point amplitude would require us to classify the 5-point couplings $hhh\bar{f}f$.

Because of the large number of couplings that we are considering, we will use a uniform notation for their couplings. The operators contributing to a 3- or 4-point coupling $X = ABC$ or $ABCD$ will be denoted by $\mathcal{O}_i^X$, where i runs from 1 to the number of primary operators of type X. For a primary operator $\mathcal{O}$ with mass dimension $d(\mathcal{O})$, we write the

coupling as

$$\Delta\mathcal{L}_{\rm BSM} = \frac{c_{\mathcal{O}}}{v^{d(\mathcal{O})-4}}\mathcal{O}, \tag{3.2.4}$$

where $v = 246$ GeV is the Higgs VEV, and $c_{\mathcal{O}}$ is a dimensionless coefficient. Note that if $c_{\mathcal{O}} \sim 1$ we expect the effects of the inserting such an interaction into an electroweak process to be roughly of order the SM contribution, since in that case all couplings are order unity, and all mass scales are of order 100 GeV. For operators that are present in the SM Lagrangian, the coupling $c_{\mathcal{O}}$ is related to the associated 'κ parameter' by

$$\kappa_{\mathcal{O}} = \frac{c_{\mathcal{O}} + c_{\mathcal{O}}^{(\rm SM)}}{c_{\mathcal{O}}^{(\rm SM)}}, \tag{3.2.5}$$

where $c_{\mathcal{O}}^{(\rm SM)}$ is the coefficient of $\mathcal{O}$ in the SM Lagrangian.

3.2.2 Off-Shell Ambiguities

The correspondence between local on-shell amplitudes and EFT couplings completely removes any basis ambiguity as long as the EFT couplings are used at tree-level and on shell. However, some of our processes of interest involve 3-point couplings where particles are exchanged and thus potentially off-shell. In this case, there are residual ambiguities in the basis. These are straightforward to remove, but we discuss them here for completeness.

To explain the point, it will be sufficient to consider a simple example, the coupling $h\bar{f}f$. If all particles are on shell, then this interaction is equivalent to the higher-derivative couplings

$$(\Box h)\bar{f}f, \quad h\bar{f}(i\not{\partial}f), \quad \ldots \tag{3.2.6}$$

For off-shell kinematics, these operators parameterize 'form factor' corrections to the minimal on-shell coupling $h\bar{f}f$. They parameterize the ambiguity in continuing the coupling $h\bar{f}f$ off-

shell. We can use field redefinitions to reduce any linear combination of such couplings to the minimal three-point coupling $h\bar{f}f$ [58,59]. However, making such a field redefinition also shifts the values of some of the 4-point couplings so that amplitudes that involve both the 3-point and the 4-point couplings remain invariant. The conclusion is that the choice of basis for 3-point functions is part of the definition of the basis for the 4-point couplings. Said in another way, if we allow for the most general local and on-shell 3 and 4-point interactions, then using them in Feynman diagrams generate the most general 3 and 4-point on-shell amplitudes in an expansion in Mandelstam invariants.

3.3 Independence of Operators/Amplitudes

In this section, we explain the methods we used to determine a basis for the independent primary operators. This is done in 3 steps:

Enumerating an over-complete basis of amplitudes

Determining the independent primary amplitudes

Checking the result against the Hilbert series counting We will give a short summary of each of these steps before going into the details in the subsections below.

The first step is to find an over-complete basis of local amplitudes for a given process. These basis elements are scalar monomials in the momenta and wavefunctions of the particles involved. They are Lorentz invariant, so the indices are contracted using the metric and the Levi-Civita tensor. When there are no indistinguishable particles, we can omit monomials where the momenta are contracted with other momenta, since these can be written in terms of Mandelstam invariants and masses. Operators with indistinguishable particles can be treated by appropriately symmetrizing these amplitudes, as we will discuss below. In this way, we obtain a finite number of amplitudes such that any local amplitude is a linear combination of these amplitudes and their Mandelstam descendants. This step is done by hand, and in some cases we used `Mathematica` [71] to enumerate the index contractions.

The second step is to find the independent primary interactions. The fact that these are parameterized by on-shell amplitudes turns this into a problem about linearly independent functions. We proceed order by order in the number of powers of momenta. Note that the number of momenta determines the mass dimension of the amplitude (and the corresponding EFT operator), so we are also working order by order in the operator dimension. We first determine the linearly independent amplitudes of lowest dimension that do not contain inner products of momenta. We look for linear relations of the form

$$\sum_a C_a(m)\mathcal{M}_a(p,s,m) = 0, \tag{3.3.1}$$

where the basis amplitudes are denoted by $\mathcal{M}_a(p,s,m)$, where p denotes the momenta, s the spins, and m the masses of the particles. The notation reminds us that the coefficients in the linear relations can depend on the masses, but not the momenta and spins of the external particles. These amplitudes have no Mandelstam factors are thus are guaranteed to be primary amplitudes, since there is no operator that they can be descendants of. Then we consider operators of higher dimension, including Mandelstam descendants of primary operators found in earlier steps that have the same dimension. Eventually, we reach a dimension where all of the amplitudes at that dimension are linear combinations of the Mandelstam descendants of operators we already have.[3] At that point, we know that we have found all of the primary amplitudes. We used several methods to find the linearly independent amplitudes, including a new analytic method, and these are described below.

Finally, we compare the results to the Hilbert series counting of operators of different dimension [47–53]. The Hilbert series gives a direct counting of the primary operators up to certain redundancies, which we review below.

We now turn to a detailed description of each of these steps.

[3] For technical reasons, we have not been able to do this for operators involving 3 identical particles. In that case, we used the Hilbert series to tell us when to stop. The details are discussed below.

3.3.1 Enumerating the Local Amplitudes

The first step is to enumerate all possible local amplitudes of a given topology and symmetry that do not involve any Mandelstam invariants. We will explain the procedure using the example of the $hZ\bar{f}f$ coupling. The most general form of the corresponding amplitude is

$$\mathcal{M}(f_1\bar{f}_2 \to Z_3 h_4) = \bar{v}_2 \Gamma^\mu u_1 \epsilon^*_{3\mu}. \tag{3.3.2}$$

The choice of the channel is arbitrary, and does not affect the results.[4] We do not use massive spinor-helicity variables because momentum conservation is a quadratic constraint in terms of them, while if we work with 4-momenta we can simply write all possible functions of the 3 independent momenta. Also, the Mandelstam variables are manifest when the amplitude is written in terms of the 4-momenta.

For the amplitude Eq. (3.3.2), the problem reduces to enumerating all possible Γ^μ. This is obtained by forming all possible 4-vectors formed from $p^\mu_{1,2,3}$ and γ^μ with indices contracted with the spacetime metric and up to one power of the Levi-Civita tensor (since products of Levi-Civita tensor can be written in terms of Kronecker deltas). We omit terms where the momenta are contracted with other momenta, since these are Mandelstam descendants of other amplitudes. This gives a finite list of operators that includes all primary operators. In

[4] We can also choose the masses arbitrarily, as long as we do not take the massless limit.

this way, we find

$$
\begin{aligned}
\Gamma^\mu =& c_1 p_1^\mu + c_2 p_2^\mu + c_3 p_1^\mu \gamma_5 + c_4 p_2^\mu \gamma_5 + c_5 \gamma^\mu + c_6 p_1^\mu \not{p}_3 + c_7 p_2^\mu \not{p}_3 \\
&+ c_8 \gamma^\mu \gamma_5 + c_9 p_1^\mu \not{p}_3 \gamma_5 + c_{10} p_2^\mu \not{p}_3 \gamma_5 + c_{11} \gamma^{\mu\nu} p_{3\,\nu} \\
&+ \epsilon^{\mu\nu\rho\sigma} p_{1\,\nu} p_{2\,\rho} p_{3\,\sigma} \left(c_{12} + c_{13}\gamma_5 + c_{14} \not{p}_3 \right) + \epsilon^{\mu\nu\rho\sigma} \gamma_\nu \left(c_{15} p_{1\,\rho} p_{2\,\sigma} + c_{16} p_{1\,\rho} p_{3\,\sigma} + c_{17} p_{2\,\rho} p_{3\,\sigma} \right) \\
&+ \epsilon^{\mu\nu\rho\sigma} p_{1\,\nu} p_{2\,\rho} p_{3\,\sigma} \left(c_{18} \not{p}_3 \gamma_5 \right) + \epsilon^{\mu\nu\rho\sigma} \gamma_\nu \gamma_5 \left(c_{19} p_{1\,\rho} p_{2\,\sigma} + c_{20} p_{1\,\rho} p_{3\,\sigma} + c_{21} p_{2\,\rho} p_{3\,\sigma} \right) \\
&+ c_{22} \epsilon_{\nu\rho\sigma\gamma} \gamma^{\mu\nu} p_1^\rho p_2^\sigma p_3^\gamma + \epsilon^{\mu\nu\rho\sigma} \gamma_{\nu\gamma} p_3^\gamma (c_{23} p_{1\,\rho} p_{2\,\sigma} + c_{24} p_{1\,\rho} p_{3\,\sigma} + c_{25} p_{2\,\rho} p_{3\,\sigma}) \\
&+ \epsilon^{\mu\nu\rho\sigma} \gamma_{\nu\rho} (c_{26} p_{1\,\sigma} + c_{27} p_{2\,\sigma} + c_{28} p_{3\,\sigma}) \\
&+ \epsilon^{\alpha\beta\gamma\delta} \gamma_\alpha p_{1\,\beta} p_{2\,\gamma} p_{3\,\delta} \left(c_{29} p_1^\mu + c_{30} p_2^\mu + c_{31} p_1^\mu \gamma_5 + c_{32} p_2^\mu \gamma_5 \right).
\end{aligned}
\tag{3.3.3}
$$

Note that terms containing γ_5 and $\gamma^\mu\gamma_5$ implicitly contain one power of the Levi-Civita tensor since $\gamma_5 \propto \epsilon_{\mu\nu\rho\sigma}\gamma^\mu\gamma^\nu\gamma^\rho\gamma^\sigma$. We have omitted terms that can obviously be simplified by equations of motion, for example $\not{p}_1 u_1 = m_1 u_1$ and $p_3 \cdot \epsilon_3^* = 0$.

There are several complications that are not illustrated in the present example. The first involves amplitudes containing massless gauge bosons, which for us means photons and gluons. In operator language, there are local interactions involving massless gauge bosons that arise from expanding covariant derivatives. However, these do not give rise to gauge invariant local amplitudes because they are always accompanied by exchange diagrams involving the same interaction. For example, the WWZ BSM coupling $\epsilon^{\mu\nu\rho\sigma}(W_\mu^+ \overset{\leftrightarrow}{D}_\nu W_\nu^-)Z_\sigma$ contributes to the amplitude $WWZ\gamma$ both through a a direct 4-point coupling and an exchange diagram with a SM $WW\gamma$ vertex. In the amplitude approach, we find the WWZ local amplitude when characterizing the 3-point amplitudes, and the gauge invariant operator is parameterized by the usual replacement $\partial_\mu \to D_\mu$ acting on charged fields.

The gauge invariant local on-shell amplitudes involving massless gauge bosons must satisfy the Ward identity, and are therefore proportional to the combination $p_\mu\epsilon_\nu(p) - p_\nu\epsilon_\mu(p)$. In the operator language, these correspond to gauge invariant operators involving the field

strength tensor.

Another complication that is not illustrated in our example above occurs when we have identical particles. For 3-point functions, this is a simple matter of symmetrizing the amplitudes, but it is nontrivial for 4-point functions because they can depend on Mandelstam invariants. In this case, some of the primary amplitudes may contain powers of the Mandelstam invariants because the operators do not satisfy the appropriate Bose/Fermi symmetries without them. For the operators we consider, we only have identical bosons, and we discuss the relevant cases below.

Two identical bosons: We want to find a basis for the primary amplitudes $\mathcal{M}(1234)$ where 1 and 2 are identical bosons. We find these starting with the amplitudes where 1 and 2 are distinguishable and then symmetrizing $1 \leftrightarrow 2$. To do this, we first write a basis for the distinguishable amplitudes $\hat{\mathcal{M}}(1234)$ that do not contain any Mandelstam invariants. We then define the symmetric and antisymmetric combinations

$$\hat{\mathcal{M}}_{\pm}(12;34) = \tfrac{1}{2}\big[\hat{\mathcal{M}}(1234) \pm \hat{\mathcal{M}}(2134)\big]. \tag{3.3.4}$$

We then construct all Mandelstam descendants of these operators that are symmetric under $1 \leftrightarrow 2$. This exchange acts on the Mandelstam invariants as $t \leftrightarrow u$, so the most general such amplitude symmetric under $1 \leftrightarrow 2$ can be written as

$$\mathcal{M}(12;34) = F(s,(t-u)^2)\hat{\mathcal{M}}_{+}(12;34) + (t-u)G(s,(t-u)^2)\hat{\mathcal{M}}_{-}(12;34), \tag{3.3.5}$$

where F and G are polynomial functions of their arguments. We see that the amplitudes of the form $\hat{\mathcal{M}}_{+}(12;34)$ and $(t-u)\hat{\mathcal{M}}_{-}(12;34)$ are an over-complete basis for the primary operators in this case, and the higher order terms in F and G give the descendants.

Three identical bosons: Now we want to find a basis for the primary amplitudes $\mathcal{M}(1234)$ where 1, 2, and 3 are identical bosons. In this case, we proceed by first symmetrizing

with respect to $1 \leftrightarrow 2$ as above, and then symmetrize the results with respect to the remaining symmetries. This implies that the most general symmetric amplitude has the form

$$\mathcal{M}(123;4) = H(s,(t-u)^2)\mathcal{M}(12;34) + (2 \leftrightarrow 3) + (3 \leftrightarrow 1), \tag{3.3.6}$$

where $\mathcal{M}(12;34)$ is a symmetrized amplitude as in Eq. (3.3.5) and H is a polynomial. Noting that $2 \leftrightarrow 3$ implies $s \leftrightarrow t$ and $3 \leftrightarrow 1$ implies $s \leftrightarrow u$ this gives

$$\begin{aligned}\mathcal{M}(123;4) = {} & H(s,(t-u)^2)\mathcal{M}(12;34) \\ & + H(t,(s-u)^2)\mathcal{M}(13;24) + H(u,(t-s)^2)\mathcal{M}(32;14).\end{aligned} \tag{3.3.7}$$

We can therefore start with the primary operators invariant under the symmetry $1 \leftrightarrow 2$ and expand in powers of the Mandelstams:

$$\begin{aligned}\text{dimension } d \quad &: \quad \mathcal{M}(12;34) + \mathcal{M}(13;24) + \mathcal{M}(32;14), \\ d+2 \quad &: \quad s\mathcal{M}(12;34) + t\mathcal{M}(13;24) + u\mathcal{M}(32;14), \\ d+4 \quad &: \quad s^2\mathcal{M}(12;34) + t^2\mathcal{M}(13;24) + u^2\mathcal{M}(32;14), \\ & \qquad (t-u)^2\mathcal{M}(12;34) + (s-u)^2\mathcal{M}(13;24) + (t-s)^2\mathcal{M}(32;14), \\ \vdots \qquad & \qquad \vdots\end{aligned} \tag{3.3.8}$$

The amplitudes generated in this way are not guaranteed to be Mandelstam descendants of primary operators of 3 identical particles. Such descendants have the form

$$\text{descendants} \quad : \quad \mathcal{M}(123;4) = J(stu, s^2+t^2+u^2)\hat{\mathcal{M}}(123;4), \tag{3.3.9}$$

where $\hat{\mathcal{M}}$ is a primary amplitude and J is a polynomial. (Note that $s+t+u = 3m_1^2 + m_4^2$.)

Because of this issue, we cannot claim that we have rigorously enumerated all primaries to arbitrarily high mass dimension. The Hilbert series determines the maximum dimension of

the primaries if we assume that there are are no relations among operators at lower dimension (see discussion below). The results we obtain are compatible with the Hilbert series, so this would require a cancelation in the Hilbert series between the new primary operators and a constraint that appears at the same mass dimension. This appears to be unlikely, but we cannot rigorously rule it out. We emphasize that our methods correctly classify all the operators up to the highest dimension that we checked. For example, we have determined all operators of the form $h\gamma\gamma\gamma$ and $hggg$ up to dimension 15, and we will see that this is more than sufficient for the phenomenology of Higgs decays at the HL-LHC.

3.3.2 Independence of Amplitudes: Numerical Methods

We now describe the methods used to determine which of the amplitudes are independent. This means that we have to find all linear redundancies of the form Eq. (3.3.1). In this section we describe 'brute force' numerical methods similar to those used in previous works [72].

We start with a basis of amplitudes $\mathcal{M}_a$ with $a = 1, \ldots, n$. The first approach is to construct an $n \times N$ matrix X whose rows consist of the values of $\mathcal{M}_a$ for $N \gg n$ values of p and s and at fixed values for the masses. This matrix can be written as

$$X_{a(p,s)} = \mathcal{M}_a(p, s), \tag{3.3.10}$$

where the index (p, s) runs over N kinematic configurations p, including all possible choices of the helicities s for each configuration. For each linear redundancy Eq. (3.3.1), this matrix satisfies $C \cdot X = 0$, so the redundancies are associated with the singular values of X.

Equivalently, we can consider a rectangular matrix Y whose columns are given by derivatives of the amplitudes with respect to the independent kinematic variables, evaluated at a canonical kinematic point p_0:

$$Y_{(n,s)a} \sim \frac{\partial^n}{\partial p^n} \mathcal{M}_a(p, m)\Big|_{p=p_0}. \tag{3.3.11}$$

Here the notation $\partial^n/\partial p^n$ is schematic: it means that we consider a large number of mixed partial derivatives with respect to the independent kinematic variables (see below). We again include all possible choices of the spin variables s for each $\partial^n/\partial p^n$. We expect that this will work for any choice of kinematic point p_0, but we chose to expand the amplitudes around threshold in several channels.

We find that both of these methods work well for moderately large matrices, typically less than around 1000 columns. However, for sufficiently large matrices, the numerical methods will find more 'nonzero' singular values because of the effects of round-off errors in the numerical calculation. This can be addressed using a smaller numerical tolerance, and checking for robustness of the results by looking at different kinematic configurations.

3.3.3 Independence of Amplitudes: Analytical Method

The shortcomings of the numerical approaches described above motivated us to develop an analytical approach, which we now describe. To explain it, we will need to be specific about the kinematic variables involved. In the center of mass frame for a $12 \to 34$ process, we can write the momenta as

$$p_1^\mu = \begin{pmatrix} E_1 \\ 0 \\ 0 \\ p_i \end{pmatrix}, \quad p_2^\mu = \begin{pmatrix} E_2 \\ 0 \\ 0 \\ -p_i \end{pmatrix}, \quad p_3^\mu = \begin{pmatrix} E_3 \\ 0 \\ p_f \sin\theta \\ p_f \cos\theta \end{pmatrix}, \quad p_4^\mu = \begin{pmatrix} E_4 \\ 0 \\ -p_f \sin\theta \\ -p_f \cos\theta \end{pmatrix}, \tag{3.3.12}$$

where

$$E_1 + E_2 = E_3 + E_4 = E_{\text{cm}}, \tag{3.3.13a}$$

$$|\boldsymbol{p}_1| = |\boldsymbol{p}_2| = p_i, \quad |\boldsymbol{p}_3| = |\boldsymbol{p}_4| = p_f. \tag{3.3.13b}$$

and $E_k = \sqrt{|\boldsymbol{p}_k|^2 + m_k^2}$, $k = 1, 2, 3, 4$. There are 2 independent kinematic variables, which can be taken to be p_i and θ, for example.

For vector bosons, the polarization vectors can be taken to have the form

$$\epsilon^\mu_{1,2} = e_{x1,2} \begin{pmatrix} 0 \\ 1 \\ 0 \\ 0 \end{pmatrix} + e_{y1,2} \begin{pmatrix} 0 \\ 0 \\ 1 \\ 0 \end{pmatrix} + \frac{e_{z1,2}}{m_{1,2}} \begin{pmatrix} \pm p_i \\ 0 \\ 0 \\ E_{1,2} \end{pmatrix}, \tag{3.3.14a}$$

$$\epsilon^\mu_{3,4} = e_{x3,4} \begin{pmatrix} 0 \\ 1 \\ 0 \\ 0 \end{pmatrix} + e_{y3,4} \begin{pmatrix} 0 \\ 0 \\ \cos\theta \\ -\sin\theta \end{pmatrix} + e_{z3,4} \frac{1}{m_{3,4}} \begin{pmatrix} \pm p_f \\ 0 \\ E_{3,4} \sin\theta \\ E_{3,4} \cos\theta \end{pmatrix}. \tag{3.3.14b}$$

Here $e_{x,y}$ are the coefficients of the transverse polarizations (linear combinations of helicity ± 1), while e_z is the coefficient for the longitudinal polarizations (helicity 0). For massless vectors, only the transverse polarizations are present.

Let us first consider a 4-point amplitude involving only vector and scalar particles (no fermions). From Eqs. (3.3.12) and (3.3.14), we see that these are polynomials in the variables

$$p_i,\ p_f,\ E_{1,2,3,4},\ \sin\theta,\ \cos\theta. \tag{3.3.15}$$

If these variables were independent of each other, then finding the linear redundancies Eq. (3.3.1) would be a simple matter of requiring that the coefficient of each monomial vanishes. However, there are in fact only 2 independent variables. Nonetheless, we show that there is a sense in which we can in fact treat the amplitude as a polynomial in a set of independent variables.

To illustrate the idea, suppose that the amplitudes were polynomials in $\cos\theta$ and $\sin\theta$

only. These are not independent because of the relation $\cos^2\theta + \sin^2\theta = 1$. We consider the polyomial to be a function of the two complex variable $c = \cos\theta$, and $s = \sin\theta$. We can use the relation to eliminate all powers of s larger than one, so that we can write the redundancy condition as

$$0 \equiv \sum_a C_a \mathcal{M}_a = P(c) + Q(c)s, \tag{3.3.16}$$

where $P(c)$ and $Q(c)$ are polynomials in c and since we are working with an upper bound on the operator dimension, they are also finite polynomials. Even though s and c are not independent, we claim that the constraint that the function vanishes implies that the polynomials P and Q vanish identically, just as if s and c were independent variables. To see this, note that we can view the right-hand side of Eq. (3.3.16) as a function of c alone, with $s = \sqrt{1-c^2}$. For general coefficients C_a, there are singularities in the complex c plane that are branch cuts starting at $c = \pm 1$. In order for this function of c to vanish identically, the coefficient of this singularity must vanish, which implies that the polyomial Q vanishes identically:

$$Q(c) \equiv 0. \tag{3.3.17}$$

Once this condition imposed, Eq. (3.3.16) implies

$$P(c) \equiv 0. \tag{3.3.18}$$

We can extend this method to include the full set of kinematic variables in Eq. (3.3.15). We consider the remaining variables to be a function of $E_{\rm cm}$, which we think of as a complex

variable. Then $p_{i,f}$ are given by

$$p_i = \frac{1}{2E_{\rm cm}}\sqrt{\left[E_{\rm cm}^2-(m_1+m_2)^2\right]\left[E_{\rm cm}^2-(m_1-m_2)^2\right]}\,, \tag{3.3.19a}$$

$$p_f = \frac{1}{2E_{\rm cm}}\sqrt{\left[E_{\rm cm}^2-(m_3+m_4)^2\right]\left[E_{\rm cm}^2-(m_3-m_4)^2\right]}\,. \tag{3.3.19b}$$

These have branch point singularities at 4 points, $E_{\rm cm} = \pm(m_1 \pm m_2), \pm(m_3 \pm m_4)$. The energies E_k can be written in terms of $E_{\rm cm}$ using

$$E_1 = \frac{m_1^2-m_2^2+E_{\rm cm}^2}{2E_{\rm cm}}, \qquad E_2 = \frac{m_2^2-m_1^2+E_{\rm cm}^2}{2E_{\rm cm}}, \tag{3.3.20a}$$

$$E_3 = \frac{m_3^2-m_4^2+E_{\rm cm}^2}{2E_{\rm cm}}, \qquad E_4 = \frac{m_4^2-m_3^2+E_{\rm cm}^2}{2E_{\rm cm}}. \tag{3.3.20b}$$

We can use Eqs. (3.3.19) and (3.3.20) to eliminate the dependence on E_k and even powers of $p_{i,f}$. The resulting function of $E_{\rm cm}$ has $1/E_{\rm cm}^n$ singularities, which we eliminate by multiplying by $E_{\rm cm}^N$ for some sufficiently large N. The result has the form of a polynomial in $E_{\rm cm}$, s, c, p_i, p_f with at most linear powers of s, p_i, and p_f:

$$\begin{aligned} 0 &= E_{\rm cm}^N \sum_a C_a \mathcal{M}_a \\ &= P + Qs + Rp_i + Sp_f + Tsp_i + Usp_f + Vp_ip_f + Wsp_ip_f, \end{aligned} \tag{3.3.21}$$

where $P, \ldots, W$ are polynomials in $E_{\rm cm}$ and x. Because s, p_i, and p_f all have different singularity structure when written as functions of $E_{\rm cm}$ and c, we can treat all of the variables in Eq. (3.3.21) as independent when solving the constraints, which again requires that all of the polynomials separately vanish.

Extending these ideas to amplitudes involving fermions is nontrivial because the spinor wavefunctions contain factors of $\sqrt{E \pm p_{i,f}}$. We were able to extend the method to amplitudes involving 2 fermions, for special choices of the fermion masses. Taking the fermions to

be the incoming particles, the spinor wavefunctions are functions of $\sqrt{E_{1,2} \pm p_i}$, for example

$$(u_1)_s = \begin{pmatrix} \begin{pmatrix} \sqrt{E_1 - p_i} & 0 \\ 0 & \sqrt{E_1 + p_i} \end{pmatrix} \xi_s \\ \begin{pmatrix} \sqrt{E_1 + p_i} & 0 \\ 0 & \sqrt{E_1 - p_i} \end{pmatrix} \xi_s \end{pmatrix}. \tag{3.3.22}$$

where $s = 1, 2$ is the spin label and $\xi_{1,2}$ are a basis for 2-component spinors. The analytic method can be extended for the following special cases:

$m_1 = m_2$: In this case $E_1 = E_2 = E_i$. The amplitude is proportional to the product of spinor wavefunctions for particles 1 and 2, which contain the following square root structures:

$$\left(\sqrt{E_i \pm p_i}\right)^2 = E_i \pm p_i, \tag{3.3.23}$$

$$\sqrt{E_i + p_i}\sqrt{E_i - p_i} = m_1 = m_2. \tag{3.3.24}$$

The constraints therefore have the same form as Eq. (3.3.21).

$m_2 = 0$: In this case we have

$$p_i = E_2 = \frac{E_{\rm cm}^2 - m_1^2}{2E_{\rm cm}}, \tag{3.3.25}$$

so p_i no longer has a branch cut singularity as a function of $E_{\rm cm}$, but p_f does. The spinor wavefunctions contain the following square root structures:

$$\sqrt{E_1 + p_i} = \sqrt{E_{\rm cm}}, \qquad \sqrt{E_1 - p_i} = \frac{m_1\sqrt{E_{\rm cm}}}{E_{\rm cm}}, \tag{3.3.26a}$$

$$\sqrt{E_2 + p_i} = \sqrt{2p_i}, \qquad \sqrt{E_2 - p_i} = 0. \tag{3.3.26b}$$

The amplitudes are proportional to one factor from Eq. (3.3.26a) and one factor from Eq. (3.3.26b), so the nonzero amplitudes are all proportional to $\sqrt{E_{\rm cm}}\sqrt{p_i}$. By multiply-

ing by $\sqrt{E_{\rm cm}}\sqrt{p_i}E_{\rm cm}^N$ for some N, the constraints can therefore be written as a polynomial in $E_{\rm cm}$, s, c, p_f that is linear in s and p_f:

$$\begin{aligned} 0 &= \sqrt{E_{\rm cm}}\sqrt{p_i}E_{\rm cm}^N \sum_a C_a \mathcal{M}_a \\ &= P + Qs + Rp_f + Sp_f s, \end{aligned} \tag{3.3.27}$$

where $P, \ldots, S$ are again polynomials in $E_{\rm cm}$ and c. The same argument above therefore shows that we can treat all of the variables in Eq. (3.3.27) as independent when solving the constraints.

We find that both methods find the same sets of independent amplitudes with 2 fermions, and that these methods also agree with the numerical methods for generic masses. This is reassuring, since we do not expect the independent amplitudes to be different for special choices of the fermion masses.

To summarize, given that the redundancies require the polynomials to individually vanish, we can analyze the number of independent amplitudes by choosing the kinematic variables E_{cm}, p_i, p_f, c, s where we treat them independently, as long as we've replaced factors of s^2, p_i^2, p_f^2 in terms of c and E_{cm}. It would be interesting to generalize this analytic argument to general amplitudes, for example involving 4 fermions. The method relies on the fact that the singularities of the amplitudes are simple square root branch cuts. In comparison to the spinor helicity formalism, the local amplitudes are polynomials in spinor-helicity variables. These variables are also not independent, but the constraints they satisfy are quadratic polynomial equations. It is natural to speculate that this underlying structure allows us to generalize the results above beyond special kinematic points.

3.3.4 Hilbert Series

An important check of our results is the Hilbert series that counts the number of independent EFT operators, described in Refs. [47–50, 53]. The Hilbert series counts the number of operators at a given mass dimension, taking into account symmetry constraints as well redundancies due to integration by parts are field redefinitions.[5]

The Hilbert series for our trilinear interactions are the following:

$$
\begin{aligned}
&H_{h\bar{f}f} = 2q^4, \quad H_{h\gamma Z} = H_{h\gamma\gamma} = H_{hgg} = 2q^5, \quad H_{hZZ} = H_{hWW} = q^3 + 2q^5, \\
&H_{hhZ} = H_{hh\gamma} = 0, \quad H_{hhh} = q^3, \\
&H_{\gamma\bar{f}f} = 2q^5, \quad H_{Z\bar{f}f} = H_{W\bar{f}f'} = 2q^4 + 2q^5, \\
&H_{WWZ} = 5q^4 + 2q^6, \quad H_{WW\gamma} = 2q^4 + 2q^6, \quad H_{ggg} = 2q^6, \\
&H_{ZZZ} = H_{ZZ\gamma} = H_{Z\gamma\gamma} = H_{Zgg} = 0.
\end{aligned}
\tag{3.3.28}
$$

Here q is a parameter that counts the mass dimension of the operators. The power of q in each term is the mass dimension of the operator, and the coefficient gives the number of operators at that dimension. So for example, $H_{h\bar{f}f} = 2q^4$ implies that there are 2 operators with dimension 4.

[5] We thank X. Lu for patiently explaining Hilbert series to us.

The Hilbert series for our four-point interactions are the following:

$$
\begin{aligned}
&H_{hZ\bar{f}f} = H_{hW\bar{f}'f} = \frac{2q^5+6q^6+4q^7}{(1-q^2)^2}, \quad H_{h\gamma\bar{f}f} = H_{hg\bar{f}f} = \frac{2q^6+4q^7+2q^8}{(1-q^2)^2},\\
&H_{hZ\gamma\gamma} = H_{hZgg} = \frac{3q^7+7q^9+2q^{11}}{(1-q^2)(1-q^4)}, \quad H_{hggg} = \frac{2q^7+2q^9+4q^{11}+6q^{13}+2q^{15}}{(1-q^4)(1-q^6)},\\
&H_{h\gamma gg} = \frac{4q^9+4q^{11}}{(1-q^2)(1-q^4)}, \quad H_{h\gamma\gamma\gamma} = \frac{2q^{11}+4q^{13}+2q^{15}}{(1-q^4)(1-q^6)},\\
&H_{hWW\gamma} = \frac{2q^5+14q^7+2q^9}{(1-q^2)^2}, \quad H_{hZZ\gamma} = \frac{8q^7+8q^9+2q^{11}}{(1-q^2)(1-q^4)},\\
&H_{hWWZ} = \frac{9q^5+18q^7}{(1-q^2)^2}, \quad H_{hZZZ} = \frac{q^5+6q^7+8q^9+7q^{11}+5q^{13}}{(1-q^4)(1-q^6)},\\
&H_{hh\bar{f}f} = \frac{2q^5+2q^8}{(1-q^2)(1-q^4)},\\
&H_{hhWW} = \frac{q^4+3q^6+5q^8}{(1-q^2)(1-q^4)}, \quad H_{hhZZ} = \frac{q^4+3q^6+2q^8}{(1-q^2)(1-q^4)}\\
&H_{hhZ\gamma} = \frac{2q^6+4q^8}{(1-q^2)(1-q^4)}, \quad H_{hh\gamma\gamma} = H_{hhgg} = \frac{2q^6+q^8}{(1-q^2)(1-q^4)},\\
&H_{hhhZ} = \frac{q^7+q^9+q^{13}}{(1-q^4)(1-q^6)}, \quad H_{hhh\gamma} = \frac{2q^{13}}{(1-q^4)(1-q^6)},\\
&H_{hhhh} = \frac{1}{(1-q^4)(1-q^6)}.
\end{aligned}
\tag{3.3.29}
$$

The denominators represent the infinite series of Mandelstam descendants. For the couplings where all particles are distinguishable, this factor is given by

$$
\frac{1}{(1-q^2)^2} = (1+q^2+q^4+\cdots)^2, \tag{3.3.30}
$$

which counts the series of products of the two independent Mandelstam variables (s and t say). For couplings containing indistinguishable particles, the denominator factor is modified because the series of Mandelstam variables is constrained by symmetry. For example, for $hh\bar{f}f$ in the channel $hh \to \bar{f}f$, the independent symmetric Mandelstam invariants are s and

$(t-u)^2$. The denominator factor is given by

$$\frac{1}{(1-q^2)(1-q^4)} = (1+q^2+q^4+\cdots)(1+q^4+q^8+\cdots) \tag{3.3.31}$$

which counts the series of products of s and $(t-u)^2$. For $hZZZ$, the independent symmetric Mandelstam invariants are $s^2+t^2+u^2$ and stu, which is matched by the denominator factor

$$\frac{1}{(1-q^4)(1-q^6)} = (1+q^4+q^8+\cdots)(1+q^6+q^{12}+\cdots). \tag{3.3.32}$$

This suggests that the the numerator factors simply count the number of primary operators at each dimension. While this is the simplest interpretation, it is not necessarily correct. The reason is that there can be relations between Mandelstam descendants of independent primary operators. For example, two lower dimensional primaries may become redundant at higher mass dimension when one includes enough Mandelstam factors. If there are n such relations that arise at dimension d, this is parameterized in the Hilbert series by an infinite series

$$\frac{-nq^d}{(1-q^2)^2} = -nq^d(1+q^2+q^4+\cdots)^2, \tag{3.3.33}$$

which subtracts off the redundant terms in the Hilbert series. (The remaining positive terms in the Hilbert series must of course ensure that the coefficient of each power of q is positive.) In fact, negative terms in the numerator of the Hilbert series appear for 4-fermion couplings, which are not considered in this work. Although all of the coefficients in the numerators of the Hilbert series above are positive, it is possible that there are relations at the same mass dimension that we have new primaries. In other words, the coefficient of q^d in the numerator is equal to the number of independent primaries minus the number of relations between Mandeltam descendants that appear at dimension d. For all operators other than those that contain 3 identical particles, our methods determine all primary operators up to

arbitrary mass dimension independently of the Hilbert series. In these cases, the Hilbert series is used only as a check, and we find that the coefficients in the numerators do in fact count the number of primary operators in all cases.

For the case of 3 indistinguishable particles, as discussed in Sec. 3.3.1 , our methods do not guarantee that there are no additional primary operators at dimensions higher than we have explicitly checked. In these cases, the primary operators we find are equal to the coefficients of the numerators of the Hilbert series above, so we again have agreement with the Hilbert series. However, we cannot exclude the possibility that at higher dimensions there are additional primary operators with an equal number of additional constraints at that dimension. Even if this is the case, we have determined all primary operators up to dimension 13, and any additional operators are unlikely to be phenomenologically relevant.

3.4 Phenomenology from the Bottom Up

In this section, we discuss some of the basic phenomenology of the operators that we have found. We first show that unitarity bounds can give us an upper bound on the couplings of the SM deviations. As emphasized in [29], any new interaction that is not included in the SM implies that tree-level unitarity is violated at some energy scale, and this scale can be estimated without a complete EFT framework. Assuming an energy scale where unitarity is valid to, enables us to to give an upper bound on couplings of the interactions. In this section, we will describe the assumptions and methods that we use to obtain these bounds. We also give rough estimates of the size of physical effects of the new interactions for Higgs decays. Comparing these to the unitarity bounds gives an idea of which operators may be plausibly large enough to be observed in upcoming Higgs searches.

3.4.1 Perturbative Unitarity Bounds

We now describe how we place bounds on the coefficients of the primary operators from unitarity considerations. It is a classic result that the SM is the unique theory with the observed particle content that does not violate tree-level unitarity at high energies [14] (see [73] for a purely on-shell derivation). Therefore, any deviation from the SM will lead to a violation of tree-level unitarity at some scale, which can be used to bound the scale of new physics. We now turn this around to determine the allowed coefficients of the primary interactions such that the scale of unitarity violation is larger than some value, for example 1 TeV. This gives a theoretical upper bound on the deviations from the SM that can be used to decide which searches are sufficiently motivated to carry out.

As emphasized in [9, 29], the unitarity bounds can be obtained from a purely bottom-up perspective (without assuming any EFT power counting), but the unitarity bounds do depend on what assumptions we make about other couplings. To illustrate this, we consider the coupling $hh\bar{t}t$. We want to know whether this coupling could possibly be the first observed sign of new physics. In order for this to be the case, we must assume that the BSM contribution to the $h\bar{t}t$ coupling is suppressed, due to the greater sensitivity of experiments to this coupling. This assumption affects the unitarity bounds on the $hh\bar{t}t$ couplings, as we will now explain.

The strongest constraint on the $hh\bar{t}t$ coupling from unitarity violation at the highest energies comes not from the 4-particle amplitudes such as $hh \to \bar{t}t$, but from higher-point amplitudes involving longitudinally polarized W and Z bosons. This arises because the $hh\bar{t}t$ coupling ruins cancelations that otherwise ensure tree-level unitarity of these higher-point amplitudes. As shown in Refs. [9, 28, 29], these can be understood at the level of the Lagrangian using the Goldstone boson equivalence theorem [14, 21, 30]. The point is that gauge invariance implies that couplings like $hh\bar{t}t$ have associated dependence on the triplet of eaten Nambu-Goldstone fields $\boldsymbol{G}$, and the amplitudes for the Nambu-Goldstone bosons

are the same as the longitudinal W and Z bosons in the high-energy limit, which can be determined by replacing

$$h \to \sqrt{(v+h)^2 + \boldsymbol{G}^2} - v, \tag{3.4.1}$$

$$\bar{t}t \to \frac{1}{\sqrt{(v+h)^2 + \boldsymbol{G}^2}} \left((v+h)\bar{t}t + G^0 \bar{t} i\gamma_5 t - \sqrt{2} G^+ \bar{b}_R t_L - \sqrt{2} G^- \bar{b}_L t_R \right). \tag{3.4.2}$$

For simplicity, we only consider amplitudes of the form $\bar{t}tG^m$ from $h^n\bar{t}t$ couplings, so we can then expand the expressions above to give

$$\begin{aligned} &\sum_n c_{t,n} h^n \bar{t}t \\ &\quad \to \left(\frac{c_{t,1}}{2v} \boldsymbol{G}^2 - \frac{3c_{t,1} - 2c_{t,2}}{8v^3} \boldsymbol{G}^4 + \frac{5c_{t,1} - 4c_{t,2} + 2c_{3,t}}{16v^5} \boldsymbol{G}^6 + \cdots \right) \left(\bar{t}t + \frac{G^0}{v} \bar{t} i\gamma_5 t \right) + \cdots \end{aligned} \tag{3.4.3}$$

Note that $c_{t,2}$ gives rise to amplitudes of the form $\bar{t}tG^n$ for $n \geq 4$, but these can be canceled by other couplings. Because we are assuming that $c_{t,1}$ is small, its contribution cannot cancel the contribution to the $\bar{t}tG^4$ and $\bar{t}tG^5$ couplings, but the higher couplings can be canceled by the unconstrained couplings $c_{t,n}$ for $n \geq 3$. We can therefore use the $\bar{t}tG^4$ and $\bar{t}tG^5$ couplings to obtain a unitarity bound on $c_{t,2}$. We see that with the assumptions that we are making, the $hh\bar{t}t$ coupling effectively behaves like a dimension 8 operator at high energies. This can also be understood from the perspective of SMEFT, as we will discuss below.

In general, we compute the unitarity bounds for 4-point couplings under the assumption that the 3-point couplings are sufficiently small that their contribution to the unitarity bound can be neglected. If a deviation from the SM is observed in any channel, one would obviously want to perform a complete analysis including all experimental constraints, but we believe that the bound we are presenting is appropriate for the purpose at hand.

To calculate the unitarity bounds from higher-point processes such as $\bar{t}t \to G^5$, we use the results of Refs. [9, 29]. We will use a simplified version of these estimates that neglects

some numerical factors of order 1. A coupling of n distinguishable scalars can be written

$$\mathcal{L}_{\text{int}} = \frac{C_n}{v^{n-4}}\phi_1 \cdots \phi_n, \tag{3.4.4}$$

and the associated scattering amplitudes are

$$\mathcal{M}(\phi_1 \cdots \phi_k \to \phi_{k+1} \cdots \phi_n) \sim \frac{C_n}{v^{n-4}}. \tag{3.4.5}$$

The unitarity bound on this amplitude is [9]

$$\mathcal{M}(\phi_1 \cdots \phi_k \to \phi_{k+1} \cdots \phi_n) \lesssim \frac{1}{\sqrt{\Phi_k(E)\Phi_{n-k}(E)}}, \tag{3.4.6}$$

where

$$\Phi_k(E) \sim \frac{1}{8\pi}\left(\frac{E}{4\pi}\right)^{2k-4} \tag{3.4.7}$$

is the total massless phase space for k distinguishable massless particles with total energy E, where we have neglected a combinatoric factor $1/(k-1)!(k-2)!$. By ignoring those combinatorial factors, the combination $\Phi_k\Phi_{n-k}$ that appears in Eq. (3.4.6) is independent of k, and we do not have to optimize the number of incoming and outgoing particles. If we require that unitarity is satisfied up to some maximum energy E_{max}, we obtain the unitarity bound

$$C_n \lesssim 8\pi\left(\frac{4\pi v}{E_{\text{max}}}\right)^{4-n}. \tag{3.4.8}$$

For a fermion coupling

$$\Delta\mathcal{L} = \frac{C_{t,n}}{v^{n-1}}\bar{t}t\phi_1 \cdots \phi_n \tag{3.4.9}$$

we have

$$\mathcal{M}(\underbrace{\bar{t}t\phi_1\cdots\phi_k}_{k+2}\to\underbrace{\phi_{k+1}\cdots\phi_n}_{n-k})\sim\frac{C_{t,n}}{v^{n-1}}E, \tag{3.4.10}$$

and we obtain the bound

$$C_{t,n}\lesssim\left(\frac{4\pi v}{E_{\max}}\right)^{n-1}. \tag{3.4.11}$$

In this way, we obtain the approximate unitarity bounds

$$\bar{t}t\to G^2 \quad : \quad c_{t,2}\lesssim 6/E_{\rm TeV}, \tag{3.4.12a}$$

$$\bar{t}t\to G^3 \quad : \quad c_{t,2}\lesssim 20/E_{\rm TeV}^2 \tag{3.4.12b}$$

$$\bar{t}t\to G^4 \quad : \quad c_{t,2}\lesssim 60/E_{\rm TeV}^3 \tag{3.4.12c}$$

$$\bar{t}t\to G^5 \quad : \quad c_{t,2}\lesssim 200/E_{\rm TeV}^4, \tag{3.4.12d}$$

where $E_{\rm TeV}$ is $E_{\max}$ measured in TeV. Even though these estimates were obtained by ignoring combinatoric factors in the phase space and matrix elements, they agree well with the results of [9], where all such factors are included.

Which of the unitarity bounds in Eq. (3.4.12) is the strongest depends on the scale $E_{\max}$. For asymptotically large values of $E_{\max}$, the process with the most particles gives the strongest bound, but for low values of $E_{\max}$ the process with the smallest number of particles dominates. If we neglect combinatoric factors, these bounds cross at the NDA scale $E_{\max}\sim 4\pi v\sim 3$ TeV. In the tables, we will give the unitarity bounds in terms of $E_{\rm TeV}$, since 1 TeV is roughly the scale that has been probed by measurements at the LHC.

Although every Higgs interaction can be understood from the bottom-up approach described above, we find it convenient to use SMEFT operators as a proxy for calculating the unitarity bounds in our tables. Specifically, for 3-point functions, we use the lowest-dimension

SMEFT operator as a proxy, while for 4-point functions, we use a combination of SMEFT operators of lowest dimension that does not modify the 3-point functions. This is motivated by the fact that 3-point functions are generally more constrained by experiments. In the example of $hh\bar{t}t$, we use a combination of the $H^\dagger H\bar{Q}_L\widetilde{H}t_R$ and $(H^\dagger H)^2\bar{Q}_L\widetilde{H}t_R$ SMEFT operators, and assume that the deviation in $h\bar{t}t$ is suppressed by a cancelation between them. This could be viewed as an accidental cancelation, or it may be that the SMEFT power counting simply does not hold for new physics at low scales. The SMEFT approach predicts that interaction behaves as a dimension-8 operator with at most 7-particle interactions, just as we found from the bottom-up point of view. When we estimate the unitarity bounds for couplings such as $hZ\bar{t}t$ and $hW\bar{t}b$, we will assume that they come in combinations that preserve custodial symmetry, since this gives weaker unitarity constraints. The fact that custodial symmetry is straightforward to incorporate in SMEFT is another reason we make use of it.

Let us illustrate the use of SMEFT operators to obtain the unitarity bounds with the example of the coupling $hZ_\mu\bar{t}_L\gamma^\mu t_R$. We assume that the 3-point coupling $Z_\mu\bar{t}_L\gamma^\mu t_R$ is not modified, so this requires a cancelation between the SMEFT operators $(H^\dagger\overset{\leftrightarrow}{D}_\mu H)\bar{Q}_L\gamma^\mu Q_L$ and $H^\dagger H(H^\dagger\overset{\leftrightarrow}{D}_\mu H)\bar{Q}_L\gamma^\mu Q_L$. We have

$$\frac{c_1^{hZtt}}{v}hZ_\mu\bar{t}_L\gamma^\mu t_R \subset \frac{c_1^{hZtt}}{m_Z v^3}H^\dagger H(H^\dagger\overset{\leftrightarrow}{D}_\mu H)\bar{Q}_L\gamma^\mu Q_L, \tag{3.4.13}$$

where the additional factors of m_Z and v on the right-hand side come from expanding the Higgs doublets and covariant derivatives.[6] (We are ignoring order-1 numeric factors, since we are performing a rough calculation.) We see that at high energies, the unitarity growth is that of a dimension-8 operator, and that we can consider amplitudes with a maximum of

[6] From the bottom-up point of view, we can understand the factor of $1/m_Z$ from the equivalence theorem $Z_\mu \to \partial_\mu G^0/m_Z$ at high energies.

7 particles. The fastest energy growth at high energies can be read off from the amplitude

$$\mathcal{M}(\bar{t}t \to G^4) \sim \frac{c_1^{hZtt}}{m_Z v^3} E_{\rm max}^2 \lesssim \left[8\pi \frac{(8\pi)^5}{E_{\rm max}^4} \right]^{1/2} \qquad \Rightarrow \qquad c_1^{hZtt} \lesssim \frac{5}{E_{\rm TeV}^4}. \tag{3.4.14}$$

Processes with 7 particles such as $\bar{t}t \to ZG^4$ trade one derivative (power of energy) with an additional Z boson and give a slightly weaker bound at high energies. At lower energies, the bound comes from the processes such as

$$\mathcal{M}(\bar{t}t \to G^2) \sim \frac{c_1^{hZtt}}{m_Z v} E_{\rm max}^2 \lesssim 8\pi \qquad \Rightarrow \qquad c_1^{hZtt} \lesssim \frac{0.6}{E_{\rm TeV}^2}. \tag{3.4.15}$$

As mentioned above, with these approximations all of the unitarity bounds become degenerate at $E_{\rm max} \sim 4\pi v \sim 3$ TeV, so it is sufficient to compute the one with the bounds for the processes with the largest and smallest number of particles.

3.4.2 Precision Electroweak Constraints

Precision electroweak measurements also give stringent constraints on corrections to the SM. In our approach, primary operators that are not directly constrained by precision electroweak measurements are simply treated as independent. For example, μ decays constrain one linear combination of the $W\bar{\ell}\nu$ couplings, but allow large deviations in individual couplings if there is a cancelation in the combination that controls the μ decay rate. From a bottom-up perspective, precision electroweak constraints are similar to naturalness constraints, since they can be satisfied by fine-tuning different contributions to the same process.

However, the degree of cancelation required to obtain an observable signal is an important factor in deciding which observables are sufficiently well-motivated to merit further investigation. We therefore performed estimates of loop-induced precision electroweak corrections, even though we are not working in a complete EFT framework. That is, we treat the primary operators as interaction terms in an $SU(3)_{\rm C} \times U(1)_{\rm EM}$ invariant EFT, and estimate the size

of loop corrections with a UV cutoff Λ that we identify with the scale of new physics. We have not analyzed all of the primary operators, but we generally find that requiring the absence of cancelations in precision electroweak observables gives weaker constraints than the unitarity constraints as long as we assume that the new physics satisfies custodial symmetry.

As an example of a strong constraint in the absence of custodial symmetry, we consider the operator $hhZ^\mu Z_\mu$. Closing the Higgs loop gives a quadratically divergent contribution to the Z mass. If this is not canceled by a custodial preserving contribution to the W mass, we obtain the constraint on the coefficient

$$c_1^{hhZZ} \lesssim \frac{10^{-3}}{\Lambda_{\rm TeV}^2}, \tag{3.4.16}$$

where $\Lambda_{\rm TeV}$ is the cutoff in TeV units and we are using the operator numbering in Table 3.13. If we identify Λ with the unitarity violating scale $E_{\rm max}$, the precision electroweak constraint is stronger than the unitarity constraint for $\Lambda \lesssim 40$ TeV (see Table 3.13). Approximate custodial symmetry can significantly weaken this constraint, but its implementation in EFT is subtle (see [74]). Therefore, we will not attempt to estimate corrections to precision electroweak observables that are sensitive to custodial symmetry violation.

We now some examples of the precision electroweak constraints for some of the operators that are the most promising for Higgs decay phenomenology (see Sec. 3.5.3 below). For example, the CP-even operators $hZ^\mu Z_\mu$ and $hZ^{\mu\nu} Z_{\mu\nu}$ give a 1-loop contribution to the Z kinetic term, generating a correction equivalent to the S parameter. This gives the constraints

$$c_1^{hZZ} \lesssim 20\,\Lambda_{\rm TeV}^2, \qquad c_2^{hZZ} \lesssim \frac{0.5}{1 + 0.4 \cdot \log \Lambda_{\rm TeV}}. \tag{3.4.17}$$

where we have used the operator numbering in Table 3.1. These are weaker than the corresponding unitarity constraints.

Next, we consider the CP-even $hZff$ couplings in Table 3.3. At one loop these induce a

correction to Zff couplings, which are highly constrained by LEP. Operators 1 and 2 induce a correction to the vector and axial-vector Z couplings, and give

$$c_{1,2}^{hZff} \lesssim \frac{0.5}{1 + 0.4 \cdot \log \Lambda_{\text{TeV}}}, \tag{3.4.18}$$

which are comparable to the unitarity bounds for $\Lambda \sim$ TeV, but are otherwise weaker. Operator 5 corrects the coupling $iZ^\mu \bar{\psi} \overleftrightarrow{\partial^\mu} \psi$, which flips the fermion helicity. This has a weaker constraint at LEP because it does not interfere constructively with the SM Z coupling. Using the results of [75], we find the weak constraint

$$c_5^{hZff} \lesssim \frac{60}{1 + 0.4 \cdot \log \Lambda_{\text{TeV}}}. \tag{3.4.19}$$

Operator 7 corrects the coupling $\partial^\mu Z_\mu \bar{\psi}\psi$, which vanishes on shell. To get a nonzero correction, we must go to higher loop, and this will give weak constraints. Operators 9 and 11 correct the coupling $i\tilde{Z}_{\mu\nu} \bar{\psi} \gamma^\mu \overleftrightarrow{\partial^\nu} \psi$, which gives the constraint

$$c_{9,11}^{hZff} \lesssim \frac{3}{1 + 0.4 \cdot \log \Lambda_{\text{TeV}}}, \tag{3.4.20}$$

which is weaker than the unitarity bound.

The general pattern that we find is that the unitarity bounds are more sensitive to the UV scale than the precision electroweak observables, at least if we neglect the corrections to the W and Z masses that violate custodial symmetry. It would be interesting to give a more complete analysis, including constraints on CP-odd operators, but we leave this for further work.

3.4.3 Estimates for Higgs Decays

We now perform some crude estimates determine what ranges of BSM couplings can be probed in Higgs decays at the LHC. Specifically, we will estimate the corrections to the

branching ratios of Higgs decays to determine which operators can give an observable number of Higgs decays. These couplings can then be compared to the unitarity bounds discussed above to determine whether it is motivated to search for a particular coupling.

We will focus on operators that are not present in the SM. In the case where the BSM operator $\mathcal{O}$ modifies a Higgs coupling, the phenomenology can be studied in the so-called 'κ framework' [76]. The κ parameter associated to $\mathcal{O}$ is given by

$$\kappa_{\mathcal{O}} = \frac{c_{\mathcal{O}}^{(\mathrm{SM})} + c_{\mathcal{O}}}{c_{\mathcal{O}}^{(\mathrm{SM})}}. \tag{3.4.21}$$

Projections for the sensitivity of the HL-LHC to various κ parameters can be found in Ref. [3]. We will therefore focus on couplings that are not present in the SM.

We are interested in the sensitivity to Higgs decays at the HL-LHC, where we expect about $N_h \sim 10^8$ Higgses to be produced with 3 ab^{-1}. Estimating the SM Higgs branching ratios to the decays we consider, we find that they all have branching ratios larger than 10^{-8} so that all of these searches have a SM background. Thus, looking at total decay rates, we should compare the new contribution to the fluctuations in the SM Higgs background.

$$\frac{\delta\Gamma_{\mathcal{O}}}{\Gamma_h} N_h \gtrsim \left(\frac{\Gamma_{\mathrm{SM}}}{\Gamma_h} N_h\right)^{1/2}. \tag{3.4.22}$$

If this is satisfied, there is at least the possibility to distinguish the new contribution from the SM Higgs background.

We begin by considering the case where the interference between the BSM and the SM contribution is negligible. This may occur because the SM contribution is so small that the BSM contribution dominates. Another interesting case is where the BSM contribution is CP odd. If the measurement performed is sufficiently inclusive that it weights CP conjugate final states equally, the interference term between CP-even and CP-odd amplitudes cancels. This occurs for example in the total rate summed over final state spins. Measurements of

differential distributions may be sensitive to interference terms, but these are beyond the simple estimates performed here and should be studied on a case-by-case basis.

We will estimate the size of the BSM contribution assuming that the matrix element of the decay is constant, and that the decay is not phase space suppressed. The matrix elements for 2- and 3-body decays due to the insertion of a BSM operator $\mathcal{O}$ are then approximated by

$$\mathcal{M}_{\mathcal{O}}(h \to 2) \simeq \frac{c_{\mathcal{O}}}{v^{d_{\mathcal{O}}-4}} m_h^{d_{\mathcal{O}}-3}, \tag{3.4.23a}$$

$$\mathcal{M}_{\mathcal{O}}(h \to 3) \simeq \frac{c_{\mathcal{O}}}{v^{d_{\mathcal{O}}-4}} m_h^{d_{\mathcal{O}}-4}, \tag{3.4.23b}$$

where $d_{\mathcal{O}}$ is the dimension of the operator $\mathcal{O}$. The corresponding decay rates are approximated by

$$\delta\Gamma_{\mathcal{O}}(h \to 2) \simeq \frac{1}{16\pi m_h} \left|\mathcal{M}_{\mathcal{O}}(h \to 2)\right|^2 \simeq \frac{m_h}{16\pi} \left|c_{\mathcal{O}}\right|^2 \left(\frac{m_h^2}{v^2}\right)^{d_{\mathcal{O}}-4}, \tag{3.4.24a}$$

$$\delta\Gamma_{\mathcal{O}}(h \to 3) \simeq \frac{m_h}{512\pi^3} \left|\mathcal{M}_{\mathcal{O}}(h \to 3)\right|^2 \simeq \frac{m_h}{512\pi^3} \left|c_{\mathcal{O}}\right|^2 \left(\frac{m_h^2}{v^2}\right)^{d_{\mathcal{O}}-4} \tag{3.4.24b}$$

To be of interest, we need to compare this deviation to the fluctuations in the SM Higgs background Eq. (3.4.22), which is conservative since many of these will have additional backgrounds. This gives the bounds

$$\text{2-body, no interference: } |c_{\mathcal{O}}| \gtrsim \left(4 \times 10^{-4}\right) \left(\text{BR}_{\text{SM}}\right)^{1/4} 2^{d_{\mathcal{O}}-4} \left(\frac{N_h}{10^8}\right)^{-1/4}, \tag{3.4.25a}$$

$$\text{3-body, no interference: } |c_{\mathcal{O}}| \gtrsim \left(7 \times 10^{-3}\right) \left(\text{BR}_{\text{SM}}\right)^{1/4} 2^{d_{\mathcal{O}}-4} \left(\frac{N_h}{10^8}\right)^{-1/4}, \tag{3.4.25b}$$

where BR_{SM} is the branching ratio of the decay in the SM. The estimates for higher-dimension operators are more uncertain due to the high powers of ratios of scales involved.

Now we consider the case where there is significant interference with the SM. In this case, we obtain a rough estimate by also approximating the SM amplitude as a constant.

For example, for 2-body decays this gives

$$\Gamma_{\rm SM}(h \to 2) \simeq \frac{1}{16\pi m_h} \big|\mathcal{M}_{\rm SM}(h \to 2)\big|^2. \tag{3.4.26}$$

The correction to the decay rate due to the BSM operator $\mathcal{O}$ is then

$$\begin{aligned} \big|\delta\Gamma_{\mathcal{O}}(h \to 2)\big| &\simeq \frac{1}{16\pi m_h} \big|\mathcal{M}_{\rm SM}\big|\big|\mathcal{M}_{\mathcal{O}}\big| \\ &\simeq \frac{1}{16\pi}\Big[16\pi m_h \Gamma_{\rm SM}(h \to 2)\Big]^{1/2} |c_{\mathcal{O}}| \left(\frac{m_h}{v}\right)^{d_{\mathcal{O}}-4}. \end{aligned} \tag{3.4.27}$$

To be observable, the difference in the number of Higgs decays compared with the SM must be larger than the fluctuations in the SM background, as in Eq. (3.4.22). In this case, we find that the dependence on $\Gamma_{\rm SM}$ cancels out in the bound, and we obtain the bounds:

$$\text{2-body, interference: } |c_{\mathcal{O}}| \gtrsim \left(4 \times 10^{-6}\right) 2^{d_{\mathcal{O}}-4} \left(\frac{N_h}{10^8}\right)^{-1/2}, \tag{3.4.28a}$$

$$\text{3-body, interference: } |c_{\mathcal{O}}| \gtrsim \left(7 \times 10^{-5}\right) 2^{d_{\mathcal{O}}-4} \left(\frac{N_h}{10^8}\right)^{-1/2}. \tag{3.4.28b}$$

Note that comparing to the no interference case, we see that when there is interference it allows better coupling sensitivity since we've estimated that $\text{BR}_{\rm SM} \gtrsim 10^{-8}$.

These approximations made above are very crude, and are intended only as a rough guide. It will be interesting to compare them with detailed phenomenological studies, but we leave that for future work. In Sec. 3.5, we will combine these estimates with the unitarity bounds to identify some BSM operators that are worthy of further study.

3.5 Results

In this section, we present our results for the independent primary operators for the 3-point and 4-point amplitudes. We do not consider flavor-violating operators. Equivalently, our results are presented for a single generation of quarks and leptons. This section consists

mainly of the tables of operators, with some brief comments in the main text. We then use the results to discuss the most promising primary observables for Higgs decays.

3.5.1 3-Point Couplings

We begin with the 3-point couplings. These are equivalent to on-shell 3-point amplitudes (for complex momenta), which have no Mandelstam invariants. Therefore, all 3-point functions correspond to primary observables in our terminology. This problem has been previously studied by many authors, see for example Refs. [16,61,66]. Our main focus is the enumeration of the 4-particle observables, but we have taken a fresh look at the 3-point functions to check our approach.

The 3-point functions involving the Higgs boson are shown in Table 3.1, and the additional 3-point functions needed for Higgs processes that do not involve the Higgs boson are shown in Table 3.2. The table gives the CP of the operator, the lowest-dimension SMEFT operator that contains the interaction, and the unitarity bound for the coefficient of the operator, where the normalization for the couplings is defined by Eq. (3.2.4).[7]

For the triple gauge boson couplings, we note that our approach differs from the classic work Ref. [77] in that we are performing a systematic low-energy expansion of the kinematic dependence. As explained in Sec. 3.2.2 above, this necessarily involves an interplay between 3-point and higher-point couplings. We have put the effects of possible 'form factors' of our 3-point couplings into higher-point couplings. Ref. [77] instead defines this in terms of form factors whose momentum dependence must be specified to define a model for experimental searches. In particular, they include form factors for couplings of the form $\mathcal{O}_{4,5}^{WWZ}$ with Z_μ replaced by A_μ even though these couplings are not $U(1)_{\rm EM}$ gauge invariant. (They restore gauge invariance by using a specific non-local form factor for these couplings that contains massless poles.) We believe that our approach is more physically transparent and can be

[7] The SMEFT operator is included for comparison only; we are not claiming that using the SMEFT operators in our tables is a consistent EFT basis.

systematically matched to EFT frameworks such as SMEFT.

i	$\mathcal{O}_i^{h\bar{f}f}$	CP	$d_{\mathcal{O}_i}$	SMEFT Operator	c Unitarity Bound
1	$h\bar{\psi}_L\psi_R + \text{h.c.}$	+	4	$H^\dagger H\bar{Q}_L\tilde{H}u_R + \text{h.c.}$	$\frac{6}{E_{\text{TeV}}}, \frac{20}{E_{\text{TeV}}^2}$
2	$ih\bar{\psi}_L\psi_R + \text{h.c.}$	−		$iH^\dagger H\bar{Q}_L\tilde{H}u_R + \text{h.c.}$	

i	$\mathcal{O}_i^{hZZ}$	CP	$d_{\mathcal{O}_i}$	SMEFT Operator	c Unitarity Bound
1	$hZ_\mu Z^\mu$	+	3	$H^\dagger HD^\mu H^\dagger D_\mu H$	$\frac{0.2}{E_{\text{TeV}}^2}$
2	$hZ_{\mu\nu}Z^{\mu\nu}$	+	5	$H^\dagger HW^a_{\mu\nu}W^{a\mu\nu}$	$\frac{2}{E_{\text{TeV}}^2}$
3	$hZ_{\mu\nu}\widetilde{Z}^{\mu\nu}$	−		$H^\dagger HW^a_{\mu\nu}\widetilde{W}^{a\mu\nu}$	

i	$\mathcal{O}_i^{hWW}$	CP	$d_{\mathcal{O}_i}$	SMEFT Operator	c Unitarity Bound
1	$hW^+_\mu W^{-\mu}$	+	3	$H^\dagger HD^\mu H^\dagger D_\mu H$	$\frac{0.2}{E_{\text{TeV}}^2}$
2	$hW^+_{\mu\nu}W^{-\mu\nu}$	+	5	$H^\dagger HW^a_{\mu\nu}W^{a\mu\nu}$	$\frac{2}{E_{\text{TeV}}^2}$
3	$hW^+_{\mu\nu}\widetilde{W}^{\mu\nu}$	−		$H^\dagger HW^a_{\mu\nu}\widetilde{W}^{a\mu\nu}$	

i	$\mathcal{O}_i^{hZ\gamma}$	CP	$d_{\mathcal{O}_i}$	SMEFT Operator	c Unitarity Bound
1	$hF_{\mu\nu}Z^{\mu\nu}$	+	5	$H^\dagger\sigma^a HW^a_{\mu\nu}B^{\mu\nu}$	$\frac{2}{E_{\text{TeV}}^2}$
2	$hF_{\mu\nu}\widetilde{Z}^{\mu\nu}$	−		$H^\dagger\sigma^a HB_{\mu\nu}\widetilde{W}^{a\mu\nu}$	

i	$\mathcal{O}_i^{h\gamma\gamma}$	CP	$d_{\mathcal{O}_i}$	SMEFT Operator	c Unitarity Bound
1	$hF_{\mu\nu}F^{\mu\nu}$	+	5	$H^\dagger HB_{\mu\nu}B^{\mu\nu}$	$\frac{2}{E_{\text{TeV}}^2}$
2	$hF_{\mu\nu}\widetilde{F}^{\mu\nu}$	−		$H^\dagger HB_{\mu\nu}\widetilde{B}^{\mu\nu}$	

i	$\mathcal{O}_i^{hGG}$	CP	$d_{\mathcal{O}_i}$	SMEFT Operator	c Unitarity Bound
1	$hG_{\mu\nu}G^{\mu\nu}$	+	5	$H^\dagger HG_{\mu\nu}G^{\mu\nu}$	$\frac{2}{E_{\text{TeV}}^2}$
2	$hG_{\mu\nu}\widetilde{G}^{\mu\nu}$	−		$H^\dagger HG_{\mu\nu}\widetilde{G}^{\mu\nu}$	

	$\mathcal{O}^{hhh}$	CP	$d_{\mathcal{O}_i}$	SMEFT Operator	c Unitarity Bound
	hhh	+	3	$\lvert H\rvert^6$	$\frac{80}{E_{\text{TeV}}}, \frac{200}{E_{\text{TeV}}^2}$

Table 3.1: Three point functions that involve the Higgs boson. We write $V_{\mu\nu} = \partial_\mu V_\nu - \partial_\nu V_\mu$ and $\widetilde{V}_{\mu\nu} = \frac{1}{2}\epsilon_{\mu\nu\rho\sigma}V^{\rho\sigma}$ for $V = W, Z$, while $F_{\mu\nu}$ and $G_{\mu\nu}$ are the field strength tensors for the photon and gluon, respectively. We have omitted the color indices of the gluon fields. The last column gives the maximum allowed value for the coupling c defined in Eq. (3.2.4) allowed by tree-level unitarity, where E_{TeV} is the unitarity violating scale in units of TeV.

i	$\mathcal{O}_i^{\gamma \bar{f} f}$	CP	$d_{\mathcal{O}_i}$	SMEFT Operator	c Unitarity Bound
1	$F^{\mu\nu}\bar{\psi}_L\sigma_{\mu\nu}\psi_R + \text{h.c.}$	+	5	$B_{\mu\nu}\bar{Q}_L\sigma^{\mu\nu}\tilde{H}u_R + \text{h.c.}$	$\frac{2}{E^2_{\text{TeV}}}$
2	$iF^{\mu\nu}\bar{\psi}_L\sigma_{\mu\nu}\psi_R + \text{h.c.}$	−		$iB_{\mu\nu}\bar{Q}_L\sigma^{\mu\nu}\tilde{H}u_R + \text{h.c.}$	

i	$\mathcal{O}_i^{Z \bar{f} f}$ ($Z \to W$ gives $W\bar{f}f'$)	CP	$d_{\mathcal{O}_i}$	SMEFT Operator	c Unitarity Bound
1	$Z^\mu\bar{\psi}_L\gamma_\mu\psi_L$	+	4	$iH^\dagger \overleftrightarrow{D}_\mu H\bar{Q}_L\gamma^\mu Q_L$	$\frac{0.6}{E^2_{\text{TeV}}}$
2	$Z^\mu\bar{\psi}_R\gamma_\mu\psi_R$	+		$iH^\dagger \overleftrightarrow{D}_\mu H\bar{u}_R\gamma^\mu u_R$	
3	$Z^{\mu\nu}\bar{\psi}_L\sigma_{\mu\nu}\psi_R + \text{h.c.}$	+	5	$W^a_{\mu\nu}\bar{Q}_L\sigma^{\mu\nu}\sigma^a\tilde{H}u_R + \text{h.c.}$	$\frac{2}{E^2_{\text{TeV}}}$
4	$Z^{\mu\nu}i\bar{\psi}_L\sigma_{\mu\nu}\psi_R + \text{h.c.}$	−		$iW^a_{\mu\nu}\bar{Q}_L\sigma^{\mu\nu}\sigma^a\tilde{H}u_R + \text{h.c.}$	

i	$\mathcal{O}_i^{WWZ}$	CP	$d_{\mathcal{O}_i}$	SMEFT Operator	c Unitarity Bound
1	$iW^+_{\mu\nu}W^{-\,\mu}Z^\nu + \text{h.c.}$	+	4	$iH^\dagger\sigma^a \overleftrightarrow{D^\mu} HD^\nu W^a_{\mu\nu}$	$\frac{0.5}{E^2_{\text{TeV}}}$
2	$iW^+_\mu W^-_\nu Z^{\mu\nu}$	+		$i(D_\mu H)^\dagger\sigma^a D_\nu H W^{a\mu\nu}$	
3	$iW^+_\mu W^-_\nu \widetilde{Z}^{\mu\nu}$	−		$i(D_\mu H)^\dagger\sigma^a D_\nu H \widetilde{W}^{a\mu\nu}$	
4	$-W^+_\mu W^-_\nu(\partial^\mu Z^\nu + \partial^\nu Z^\mu)$	−	4	$iD_\mu H^\dagger D_\nu H H^\dagger D^{\mu\nu}H + \text{h.c.}$	$\frac{4\cdot 10^{-3}}{E^4_{\text{TeV}}}$
5	$\epsilon^{\mu\nu\rho\sigma}(W^+_\mu \overleftrightarrow{D}_\rho W^-_\nu)Z_\sigma$	+	4	$\epsilon^{\mu\nu\rho\sigma}(H^\dagger\sigma^a D_\mu H)W^a_{\rho\nu}H^\dagger D_\sigma H + \text{h.c.}$	$\frac{0.04}{E^3_{\text{TeV}}}$, $\frac{0.1}{E^4_{\text{TeV}}}$
6	$iW^+_{\lambda\mu}W^{-\,\mu}_{\quad\ \nu}Z^{\nu\lambda}$	+	6	$\epsilon_{abc}W^a_{\lambda\mu}W^{b\,\mu}_{\quad\ \nu}W^{c\nu\lambda}$	$\frac{5}{E^2_{\text{TeV}}}$
7	$iW^+_{\lambda\mu}W^{-\,\mu}_{\quad\ \nu}\widetilde{Z}^{\nu\lambda}$	−		$\epsilon_{abc}W^a_{\lambda\mu}W^{b\,\mu}_{\quad\ \nu}\widetilde{W}^{c\nu\lambda}$	

i	$\mathcal{O}_i^{WW\gamma}$	CP	$d_{\mathcal{O}_i}$	SMEFT Operator	c Unitarity Bound
1	$iW^+_\mu W^-_\nu F^{\mu\nu}$	+	4	$i(D_\mu H)^\dagger D_\nu H B^{\mu\nu}$	$\frac{0.5}{E^2_{\text{TeV}}}$
2	$iW^+_\mu W^-_\nu \widetilde{F}^{\mu\nu}$	−		$i(D_\mu H)^\dagger D_\nu H \widetilde{B}^{\mu\nu}$	
3	$iW^+_{\mu\nu}W^{-\,\nu\rho}F_\rho^{\ \mu}$	+	6	$\epsilon_{abc}W^a_{\mu\nu}W^{b\,\nu\rho}W^{c\,\mu}_\rho$	$\frac{5}{E^2_{\text{TeV}}}$
4	$iW^+_{\mu\nu}W^{-\,\nu\rho}\widetilde{F}_\rho^{\ \mu}$	−		$\epsilon_{abc}W^a_{\mu\nu}W^{b\,\nu\rho}\widetilde{W}^{c\,\mu}_\rho$	

i	$\mathcal{O}_i^{ggg}$	CP	$d_{\mathcal{O}_i}$	SMEFT Operator	c Unitarity Bound
1	$f_{ABC}G^A_{\mu\nu}G^{B\,\nu\rho}G^{C\,\mu}_\rho$	+	6	$f_{ABC}G^A_{\mu\nu}G^{B\nu\rho}G^{C\mu}_\rho$	$\frac{2}{E^2_{\text{TeV}}}$
2	$f_{ABC}G^A_{\mu\nu}G^{B\nu\rho}\widetilde{G}^{C\mu}_\rho$	−		$f_{ABC}G^A_{\mu\nu}G^{B\nu\rho}\widetilde{G}^{C\mu}_\rho$	

Table 3.2: Additional three point functions needed to calculate 4-point amplitudes involving the Higgs. The notation is the same as in Table 3.1. Here $\sigma^{\mu\nu} = \frac{i}{4}[\gamma^\mu, \gamma^\nu]$, σ^a are Pauli matrices, and $H^\dagger \overleftrightarrow{D}_\mu H = H^\dagger D_\mu H - (D_\mu H)^\dagger H$.

3.5.2 4-Point Couplings

Our results for 4-point operators are summarized in Tables 3.3–3.14. The notation is hopefully self-explanatory; to save space, we have used $\partial_{\mu\nu\rho} = \partial_\mu\partial_\nu\partial_\rho$, $D_{\mu\nu\rho} = D_\mu\partial_\nu\partial_\rho$, *etc*. There are several cases for which we do not provide separate tables, because the operators can be read off from other tables by simple substitutions:

$hW\bar{f}f'$ can be read off from $hZ\bar{f}f$ in Table 3.3 with the substitution $Z_\mu\bar{f}f \to W_\mu\bar{f}f'$ and $\partial_\mu \to D_\mu$.

$hg\bar{f}f$ can be obtained from $h\gamma\bar{f}f$ in Table 3.4 with the substitution $F_{\mu\nu} \to G^A_{\mu\nu}T_A$. The operators are $SU(3)_{\rm C}$ gauge invariant only if the fermions are quarks.

$hZgg$ can be obtained from $hZ\gamma\gamma$ in Table 3.5 with the substitution $F_{\mu\nu}F_{\rho\sigma} \to G^A_{\mu\nu}G^A_{\rho\sigma}$.

$hhZZ$ can be obtained from $hhWW$ in Table 3.13 by replacing $W_\mu \to Z_\mu$. When this is done, the operators numbered 5, 7 and 8 vanish by symmetry, so there are only 6 nonzero operators in this case.

For $hhhh$ the only primary operator is h^4, and we have not made a table for that.

There are other cases where the results are closely related, but additional corrections must be made. For example, we can take operators involving Z and convert them to operators with a photon, by taking $Z_\mu \to A_\mu$ and forming the field strength for the photon by using derivatives and anti-symmetrizing. This allows $hZ\bar{f}f, hZgg$ to be respectively converted to $h\gamma\bar{f}f$ and $h\gamma gg$.

The tables list the primary operators. In the on-shell amplitude language, the remaining amplitudes are obtained by multiplying each operator by a power series in the Mandelstam variables. In the operator language, these correspond to operators with additional derivatives with the Lorentz indices contracted between them. For operators where all particles are distinguishable, this is simply a series in the Mandelstam variables s, t, and u (with $s+t+u$ fixed). For operators with identical particles, these additional terms must be appropriately symmetrized. For $hZ\gamma\gamma$, $h\gamma gg$ (Table 3.5), $hZZ\gamma$ (Table 3.9), $hh\bar{f}f$ (Table 3.12), $hhWW$,

$hhZ\gamma$ and $hh\gamma\gamma$ (Table 3.13), we can add arbitrary powers of s and $(t-u)^2$. For $h\gamma\gamma\gamma$ (Table 3.6), $hggg$ (Table 3.7), $hZZZ$ (Table 3.11), $hhhZ$ and $hhh\gamma$ (Table 3.14), we can add arbitrary powers of $s^2+t^2+u^2$ and stu. As an example, adding a factor of $s^2+t^2+u^2$ to $h\partial^\mu Z^\nu Z_\mu Z_\nu$ can be done by adding four derivatives, *i.e.* $h\partial^\mu Z^\nu \partial^\alpha \partial^\beta Z_\mu \partial_\alpha \partial_\beta Z_\nu$.

The tables give unitarity bounds on the coefficients of the operators (see Sec. 3.4.1). As one might expect, the unitarity bounds become more stringent for operators of higher dimension. These bounds should be used only as a very rough guide, especially for the operators with high mass dimension.

Our final results are in full agreement with the Hilbert series counting in all cases (see Sec. 3.3.4). We also agree with the results of Ref. [63] in all cases where they overlap. We found a discrepancy in the results for $hWWZ$ (see Table 3.10) in an earlier version of their paper, but our results agree after they identified and corrected a mistake. Our results also include massless particles, the effects of symmetrization for identical particles, and we have found all primary operators to arbitrarily high dimension, at least in the cases where there are two or fewer identical particles (see Sec. 3.3.1).

3.5.3 Primary Observables for Higgs Decay

We now use the results in the tables to identify promising primary observables to search for new physics in Higgs decays. We limit ourselves to CP even operators, so that it is clear that there is interference with SM processes. (Also, CP-odd new physics effects may be suppressed by approximate CP symmetry.) In this case Eq. (3.4.28) gives an estimate for the minimal value of the coefficients in order for the new contribution to the decay to be observable at the HL-LHC. We compare this to the bound on the coefficient arising from the unitarity bounds in the tables.

In this way, we find that the following operators are potentially observable at the LHC

assuming a unitarity violating scale above 10 TeV:

$$\mathcal{O}_1^{h\bar{f}f}, \quad \mathcal{O}_{1,2}^{hVV}, \quad \mathcal{O}_1^{hZ\gamma}, \quad \mathcal{O}_1^{h\gamma\gamma}, \quad \mathcal{O}_1^{hGG}, \quad \mathcal{O}_{1,2,3}^{hZ\bar{f}f}, \quad \mathcal{O}_{1,2,3}^{hW\bar{f}f'}, \quad \mathcal{O}_1^{h\gamma\bar{f}f}, \tag{3.5.1}$$

where $V = W, Z$. The next class of operators are those that are potentially observable with a unitarity violating scale between 1 and 10 TeV:

$$\mathcal{O}_{5,7,9,11}^{hZ\bar{f}f}, \quad \mathcal{O}_{5,7,9,11}^{hW\bar{f}f'}, \quad \mathcal{O}_{3,5,7}^{h\gamma\bar{f}f}, \quad \mathcal{O}_{1,4,5,8,9}^{hZ\gamma\gamma}, \quad \mathcal{O}_{1,2}^{h\gamma gg}, \quad \mathcal{O}_{1,3}^{hggg,f}. \tag{3.5.2}$$

These are also interesting, but it may be that new physics models that can give these effects can be better probed by direct searches for new heavy particles. The remaining operators are observable only if the unitarity violating scale is below 1 TeV:

$$\mathcal{O}_{11}^{hZ\gamma\gamma}, \quad \mathcal{O}_{5,6}^{h\gamma gg}, \quad \mathcal{O}_{1,3,4,7}^{h\gamma\gamma\gamma}, \quad \mathcal{O}_{1,3,4,7}^{hggg,d}, \quad \mathcal{O}_{5,7}^{hggg,f}. \tag{3.5.3}$$

These are presumably already constrained, and not as theoretically motivated as the others.

We see that there are a large number of observables that worthy of further investigation. This motivates searches for BSM effects in Higgs 2-body decays, as well as 3-body decays to $Z\bar{f}f$, $W\bar{f}f'$, $\gamma\bar{f}f$, $g\bar{f}f$, $Z\gamma\gamma$, γgg, and ggg. The decays to strongly-interacting particles are likely very challenging due to QCD backgrounds that we have neglected. We note that some detailed phenomenological studies on the effects of higher-dimension operators on 3-body decays have already been performed. For example, [78] considers effects equivalent to some of the operators above in the decay $h \to e^- e^+ \mu^- \mu^+$, but not all of them. We leave further detailed study of these effects for future work.

i	$\mathcal{O}_i^{hZ\bar{f}f}$	CP	$d_{\mathcal{O}_i}$	SMEFT Operator	c Unitarity Bound
1	$hZ^\mu\bar{\psi}_L\gamma_\mu\psi_L$	$+$	5	$i\big(H^\dagger\overleftrightarrow{D}_\mu H\big)\bar{Q}_L\gamma^\mu Q_L$	$\frac{0.6}{E^2_{\rm TeV}}, \frac{5}{E^4_{\rm TeV}}$
2	$hZ^\mu\bar{\psi}_R\gamma_\mu\psi_R$	$+$		$i\big(H^\dagger\overleftrightarrow{D}_\mu H\big)\bar{u}_R\gamma^\mu u_R$	
3	$hZ^{\mu\nu}\bar{\psi}_L\sigma_{\mu\nu}\psi_R + \text{h.c.}$	$+$	6	$\bar{Q}_L\sigma^{\mu\nu}u_R\sigma^a\widetilde{H}W^a_{\mu\nu} + \text{h.c.}$	$\frac{2}{E^2_{\rm TeV}}, \frac{10}{E^4_{\rm TeV}}$
4	$ih\widetilde{Z}_{\mu\nu}\bar{\psi}_L\sigma^{\mu\nu}\psi_R + \text{h.c.}$	$-$		$i\bar{Q}_L\sigma^{\mu\nu}u_R\sigma^a\widetilde{H}\widetilde{W}^a_{\mu\nu} + \text{h.c.}$	
5	$ihZ^\mu\big(\bar{\psi}_L\overleftrightarrow{\partial}_\mu\psi_R\big) + \text{h.c.}$	$+$	6	$\big(H^\dagger\overleftrightarrow{D}_\mu H\big)\big(\bar{Q}_L\overleftrightarrow{D^\mu}u_R\big)\widetilde{H} + \text{h.c.}$	$\frac{0.1}{E^3_{\rm TeV}}, \frac{4}{E^6_{\rm TeV}}$
6	$hZ^\mu\partial_\mu\big(\bar{\psi}_L\psi_R\big) + \text{h.c.}$	$-$		$i\big(H^\dagger\overleftrightarrow{D}_\mu H\big)D^\mu\big(\bar{Q}_L u_R\big)\widetilde{H} + \text{h.c.}$	
7	$ihZ^\mu\partial_\mu\big(\bar{\psi}_L\psi_R\big) + \text{h.c.}$	$+$		$\big(H^\dagger\overleftrightarrow{D}_\mu H\big)D^\mu(\bar{Q}_L u_R)\widetilde{H} + \text{h.c.}$	
8	$hZ^\mu\big(\bar{\psi}_L\overleftrightarrow{\partial}_\mu\psi_R\big) + \text{h.c.}$	$-$		$i\big(H^\dagger\overleftrightarrow{D}_\mu H\big)\big(\bar{Q}_L\overleftrightarrow{D^\mu}u_R\big)\widetilde{H} + \text{h.c.}$	
9	$ih\widetilde{Z}_{\mu\nu}\big(\bar{\psi}_L\gamma^\mu\overleftrightarrow{\partial^\nu}\psi_L\big)$	$+$	7	$i\lvert H\rvert^2\widetilde{W}^{a\mu\nu}\big(\bar{Q}_L\gamma_\mu\sigma^a\overleftrightarrow{D}_\nu Q_L\big)$	$\frac{0.4}{E^3_{\rm TeV}}, \frac{1}{E^4_{\rm TeV}}$
10	$h\widetilde{Z}_{\mu\nu}\partial^\mu\big(\bar{\psi}_L\gamma^\nu\psi_L\big)$	$-$		$\lvert H\rvert^2\widetilde{W}^{a\mu\nu}D_\mu(\bar{Q}_L\gamma_\nu\sigma^a Q_L)$	
11	$ih\widetilde{Z}_{\mu\nu}\big(\bar{\psi}_R\gamma^\mu\overleftrightarrow{\partial^\nu}\psi_R\big)$	$+$		$i\lvert H\rvert^2\widetilde{B}^{\mu\nu}\big(\bar{u}_R\gamma_\mu\overleftrightarrow{D}_\nu u_R\big)$	
12	$h\widetilde{Z}_{\mu\nu}\partial^\mu\big(\bar{\psi}_R\gamma^\nu\psi_R\big)$	$-$		$\lvert H\rvert^2\widetilde{B}^{\mu\nu}D_\mu\big(\bar{u}_R\gamma_\nu u_R\big)$	

Table 3.3: Primary operators for couplings of the form $hZ\bar{f}f$. As noted in the text, the $hW\bar{f}f'$ operators can be obtained from the $hZ\bar{f}f$ operators by the replacement $Z\bar{f}f \to W\bar{f}f'$.

i	$\mathcal{O}_i^{h\gamma\bar{f}f}$	CP	$d_{\mathcal{O}_i}$	SMEFT Operator	c Unitarity Bound
1	$hF^{\mu\nu}\bar{\psi}_L\sigma_{\mu\nu}\psi_R + \text{h.c.}$	$+$	6	$\bar{Q}_L\sigma^{\mu\nu}u_R\widetilde{H}B_{\mu\nu} + \text{h.c.}$	$\frac{2}{E^2_{\text{TeV}}}, \frac{20}{E^4_{\text{TeV}}}$
2	$ih\widetilde{F}_{\mu\nu}\bar{\psi}_L\sigma^{\mu\nu}\psi_R + \text{h.c.}$	$-$		$i\bar{Q}_L\sigma^{\mu\nu}u_R\widetilde{H}\widetilde{B}_{\mu\nu} + \text{h.c.}$	
3	$ih\widetilde{F}_{\mu\nu}\big(\bar{\psi}_L\gamma^\mu\overset{\leftrightarrow}{\partial}{}^\nu\psi_L\big)$	$+$	7	$i\lvert H\rvert^2\widetilde{B}^{\mu\nu}\bar{Q}_L\gamma_\mu\overset{\leftrightarrow}{D}_\nu Q_L$	$\frac{0.4}{E^3_{\text{TeV}}}, \frac{1}{E^4_{\text{TeV}}}$
4	$h\widetilde{F}_{\mu\nu}\partial^\mu\left(\bar{\psi}_L\gamma^\nu\psi_L\right)$	$-$		$\lvert H\rvert^2\widetilde{B}^{\mu\nu}D_\mu\big(\bar{Q}_L\gamma_\nu Q_L\big)$	
5	$ih\widetilde{F}_{\mu\nu}\big(\bar{\psi}_R\gamma^\mu\overset{\leftrightarrow}{\partial}{}^\nu\psi_R\big)$	$+$		$i\lvert H\rvert^2\widetilde{B}^{\mu\nu}\big(\bar{u}_R\gamma_\mu\overset{\leftrightarrow}{D}_\nu u_R\big)$	
6	$h\widetilde{F}_{\mu\nu}\partial^\mu\left(\bar{\psi}_R\gamma^\nu\psi_R\right)$	$-$		$\lvert H\rvert^2\widetilde{B}^{\mu\nu}D_\mu\big(\bar{u}_R\gamma_\nu u_R\big)$	
7	$ihF^{\mu\nu}\partial_\mu\bar{\psi}_L\partial_\nu\psi_R + \text{h.c.}$	$+$	8	$iB^{\mu\nu}D_\mu\bar{Q}_L D_\nu u_R\widetilde{H} + \text{h.c.}$	$\frac{0.09}{E^4_{\text{TeV}}}, \frac{0.9}{E^6_{\text{TeV}}}$
8	$hF^{\mu\nu}\partial_\mu\bar{\psi}_L\partial_\nu\psi_R + \text{h.c.}$	$-$		$B^{\mu\nu}D_\mu\bar{Q}_L D_\nu u_R\widetilde{H} + \text{h.c.}$	

Table 3.4: Primary operators for couplings of the form $h\gamma f\bar{f}$. As noted in the text, the $hg\bar{f}f$ operators can be obtained from the $h\gamma\bar{f}f$ operators by the replacement $F_{\mu\nu} \to G_{\mu\nu}$.

i	$\mathcal{O}_i^{hZ\gamma\gamma}$	CP	$d_{\mathcal{O}_i}$	SMEFT Operator	c Unitarity Bound
1	$h\partial^\mu F^{\alpha\beta}\widetilde{F}_{\alpha\beta}Z_\mu$	+	7	$iH^\dagger \overleftrightarrow{D}_\mu H\partial^\mu B^{\alpha\beta}\widetilde{B}_{\alpha\beta}$	$\frac{0.1}{E^3_{\rm TeV}}$
2	$h\partial^\mu F^{\nu\rho}F_{\mu\nu}Z_\rho$	−		$iH^\dagger \overleftrightarrow{D}_\rho H\partial^\mu B^{\nu\rho}B_{\mu\nu}$	
3	$hF^{\mu\nu}F_{\mu\rho}\partial_\nu Z^\rho$	−	7	$iH^\dagger D_\nu D^\rho H B^{\mu\nu}B_{\mu\rho}+\text{h.c.}$	$\frac{0.1}{E^3_{\rm TeV}}, \frac{1}{E^5_{\rm TeV}}$
4	$h\partial_\mu F^{\alpha\nu}F^{\mu\delta}\partial_\nu\widetilde{Z}^{\alpha\delta}$	+	9	$H^\dagger\sigma^a H\partial_\mu B^{\alpha\nu}B^{\mu\delta}D_\nu\widetilde{W}^{a\alpha\delta}$	$\frac{0.02}{E^5_{\rm TeV}}, \frac{0.07}{E^6_{\rm TeV}}$
5	$hF^{\alpha\mu}\overleftrightarrow{\partial}^\nu\widetilde{F}_{\alpha\beta}\partial_\nu Z_\mu{}^\beta$	+		$H^\dagger\sigma^a HB^{\alpha\mu}\overleftrightarrow{\partial}^\nu\widetilde{B}_{\alpha\beta}D_\nu W_\mu^{a\beta}$	
6	$hF^{\mu\nu}\overleftrightarrow{\partial}^\sigma F_{\mu\rho}\partial_\sigma\partial_\nu Z^\rho$	−	9	$iH^\dagger D_{\sigma\nu\rho}HB^{\mu\nu}\overleftrightarrow{\partial}^\sigma B_{\mu\rho}+\text{h.c.}$	$\frac{2\cdot10^{-3}}{E^6_{\rm TeV}}, \frac{0.02}{E^8_{\rm TeV}}$
7	$h\partial^\mu F^{\nu\rho}F_{\mu\sigma}\partial_\rho\partial^\sigma Z_\nu$	−		$iH^\dagger D_\rho D^\sigma D_\nu H\partial^\mu B^{\nu\rho}B_{\mu\sigma}+\text{h.c.}$	
8	$hF^{\alpha\mu}\overleftrightarrow{\partial}^\nu\tilde{F}_{\alpha\beta}\partial_\nu(\partial_\mu Z^\beta+\partial^\beta Z_\mu)$	+	9	$iH^\dagger D_\nu(D_\mu{}^\beta+D^\beta{}_\mu)HB^{\alpha\mu}\overleftrightarrow{\partial}^\nu\widetilde{B}_{\alpha\beta}+\text{h.c.}$	$\frac{2\cdot10^{-3}}{E^6_{\rm TeV}}, \frac{0.02}{E^8_{\rm TeV}}$
9	$h\partial^\mu F^{\alpha\beta}\overleftrightarrow{\partial}^\nu\widetilde{F}_{\alpha\beta}\partial_\nu Z_\mu$	+		$iH^\dagger D_{\nu\mu}H\partial^\mu B^{\alpha\beta}\overleftrightarrow{\partial}^\nu\widetilde{B}_{\alpha\beta}+\text{h.c.}$	
10	$h\partial^\mu F^{\nu\rho}\overleftrightarrow{\partial}^\sigma F_{\mu\nu}\partial_\sigma Z_\rho$	−		$iH^\dagger D_{\sigma\rho}H\partial^\mu B^{\nu\rho}\overleftrightarrow{\partial}^\sigma B_{\mu\nu}+\text{h.c.}$	
11	$h\partial_\mu F^{\alpha\nu}\overleftrightarrow{\partial}^\rho F^{\mu\delta}\partial_\rho\partial_\nu\widetilde{Z}_{\alpha\delta}$	+	11	$H^\dagger\sigma^a HD_{\rho\nu}\widetilde{W}^a_{\alpha\delta}\partial_\mu B^{\alpha\nu}\overleftrightarrow{\partial}^\rho B^{\mu\delta}+\text{h.c.}$	$\frac{1\cdot10^{-3}}{E^7_{\rm TeV}}, \frac{4\cdot10^{-3}}{E^8_{\rm TeV}}$
12	$h\partial^\mu F^{\nu\rho}\overleftrightarrow{\partial}^\gamma F_{\mu\sigma}\partial_\gamma\partial_\rho\partial^\sigma Z_\nu$	−	11	$iH^\dagger D_\gamma{}^{\rho\sigma\nu}H\partial^\mu B_{\nu\rho}\overleftrightarrow{\partial}^\gamma B_{\mu\sigma}+\text{h.c.}$	$\frac{1\cdot10^{-4}}{E^8_{\rm TeV}}, \frac{1\cdot10^{-3}}{E^{10}_{\rm TeV}}$

Table 3.5: Primary operators for $hZ\gamma\gamma$. As noted in the text, the $hZgg$ operators can be obtained from these by the replacement $F_{\mu\nu}\to G_{\mu\nu}$.

i	$\mathcal{O}_i^{h\gamma gg}$	CP	$d_{\mathcal{O}_i}$	SMEFT Operator	c Unitarity Bound
1	$hD_\mu G^{\alpha\nu} G^{\mu\delta} \partial_\nu \widetilde{F}_{\alpha\delta}$	+	9	$H^\dagger H \partial_\mu G^{\alpha\nu} G^{\mu\delta} \partial_\nu \widetilde{B}_{\alpha\delta}$	$\frac{0.02}{E_{\rm TeV}^5}, \frac{0.07}{E_{\rm TeV}^6}$
2	$hG^{\alpha\mu} \overleftrightarrow{D}_\nu \widetilde{G}_{\alpha\beta} \partial^\nu F_\mu{}^\beta$	+		$H^\dagger H G^{\alpha\mu} \overleftrightarrow{D}_\nu \widetilde{G}_{\alpha\beta} \partial^\nu B_\mu{}^\beta$	
3	$hD_\sigma G^{\mu\nu} G_{\mu\rho} \partial_\nu F^{\sigma\rho}$	−		$H^\dagger H D_\sigma G^{\mu\nu} G_{\mu\rho} \partial_\nu B^{\sigma\rho}$	
4	$hG^{\mu\nu} D_\sigma G_{\mu\rho} \partial_\nu F^{\sigma\rho}$	−		$H^\dagger H G^{\mu\nu} D_\sigma G_{\mu\rho} \partial_\nu B^{\sigma\rho}$	
5	$hD_\sigma G^{\alpha\mu} \overleftrightarrow{D}_\nu \widetilde{G}_{\alpha\beta} \partial^\nu{}_\mu F^{\sigma\beta}$	+	11	$H^\dagger H D_\sigma G^{\alpha\mu} \overleftrightarrow{D}_\nu \widetilde{G}_{\alpha\beta} \partial^\nu{}_\mu B^{\sigma\beta}$	$\frac{1\cdot 10^{-3}}{E_{\rm TeV}^7}, \frac{4\cdot 10^{-3}}{E_{\rm TeV}^8}$
6	$hD_\mu G^{\alpha\beta} \overleftrightarrow{D}_\nu D_\sigma \widetilde{G}_{\alpha\beta} \partial^\nu F^{\sigma\mu}$	+		$H^\dagger H D_\mu G^{\alpha\beta} \overleftrightarrow{D}_\nu D_\sigma \widetilde{G}_{\alpha\beta} \partial^\nu B^{\sigma\mu}$	
7	$hD_\gamma G^{\mu\nu} \overleftrightarrow{D}_\sigma G_{\mu\rho} \partial^\sigma{}_\nu F^{\gamma\rho}$	−		$H^\dagger H D_\gamma G^{\mu\nu} \overleftrightarrow{D}_\sigma G_{\mu\rho} \partial^\sigma{}_\nu B^{\gamma\rho}$	
8	$hD^\mu G^{\nu\rho} \overleftrightarrow{D}_\sigma D_\gamma G_{\mu\nu} \partial^\sigma F^\gamma{}_\rho$	−		$H^\dagger H D^\mu G^{\nu\rho} \overleftrightarrow{D}_\sigma D_\gamma G_{\mu\nu} \partial^\sigma B^\gamma{}_\rho$	

i	$\mathcal{O}_i^{h\gamma\gamma\gamma}$	CP	$d_{\mathcal{O}_i}$	SMEFT Operator	c Unitarity Bound
1	$h\partial_\sigma F^{\alpha\mu} \overleftrightarrow{\partial}_\nu \widetilde{F}_{\alpha\beta} \partial^\nu{}_\mu F^{\sigma\beta}$	+	11	$H^\dagger H \partial_\sigma B^{\alpha\mu} \overleftrightarrow{\partial}_\nu \widetilde{B}_{\alpha\beta} \partial^\nu{}_\mu B^{\sigma\beta}$	$\frac{0.001}{E_{\rm TeV}^7}, \frac{0.004}{E_{\rm TeV}^8}$
2	$h\partial_\gamma F^{\mu\nu} \overleftrightarrow{\partial}_\sigma F_{\mu\rho} \partial^\sigma{}_\nu F^{\gamma\rho}$	−		$H^\dagger H \partial_\gamma B^{\mu\nu} \overleftrightarrow{\partial}_\sigma B_{\mu\rho} \partial^\sigma{}_\nu B^{\gamma\rho}$	
3	$h\partial_{\mu\rho\sigma} F^{\alpha\nu} \partial^{\rho\sigma} F^{\mu\delta} \partial_\nu \widetilde{F}_{\alpha\delta}$	+	13	$H^\dagger H \partial_{\mu\rho\sigma} B^{\alpha\nu} \partial^{\rho\sigma} B^{\mu\delta} \partial_\nu \widetilde{B}_{\alpha\delta}$	$\frac{8\cdot 10^{-5}}{E_{\rm TeV}^9}, \frac{3\cdot 10^{-4}}{E_{\rm TeV}^{10}}$
4	$h\partial_{\rho\sigma} F^{\alpha\mu} \overleftrightarrow{\partial}_\nu \partial^{\rho\sigma} \widetilde{F}_{\alpha\beta} \partial^\nu F_\mu{}^\beta$	+		$\partial_{\rho\sigma} B^{\alpha\mu} \overleftrightarrow{\partial}_\nu \partial^{\rho\sigma} \widetilde{B}_{\alpha\beta} \partial^\nu B_\mu{}^\beta$	
5	$h\partial_{\sigma\alpha\beta} F^{\mu\nu} \partial_{\alpha\beta} F_{\mu\rho} \partial_\nu F^{\sigma\rho}$	−		$H^\dagger H \partial_{\sigma\alpha\beta} B^{\mu\nu} \partial_{\alpha\beta} B_{\mu\rho} \partial_\nu B^{\sigma\rho}$	
6	$h\partial^{\alpha\beta} F^{\mu\nu} \partial_{\sigma\alpha\beta} F_{\mu\rho} \partial_\nu F^{\sigma\rho}$	−		$H^\dagger H \partial^{\alpha\beta} B^{\mu\nu} \partial_{\sigma\alpha\beta} B_{\mu\rho} \partial_\nu B^{\sigma\rho}$	
7	$h\partial_{\eta\rho\sigma} F^{\alpha\mu} \overleftrightarrow{\partial}_\nu \partial^{\eta\rho\sigma} \widetilde{F}_{\alpha\beta} \partial^\nu F_\mu{}^\beta$	+	15	$H^\dagger H \partial_{\eta\rho\sigma} B^{\alpha\mu} \overleftrightarrow{\partial}_\nu \partial^{\eta\rho\sigma} \widetilde{B}_{\alpha\beta} \partial^\nu B_\mu{}^\beta$	$\frac{5\cdot 10^{-6}}{E_{\rm TeV}^{11}}, \frac{2\cdot 10^{-5}}{E_{\rm TeV}^{12}}$
8	$h\partial^{\eta\alpha\beta} F^{\mu\nu} \partial_{\sigma\eta\alpha\beta} F_{\mu\rho} \partial_\nu F^{\sigma\rho}$	−		$H^\dagger H \partial^{\eta\alpha\beta} B^{\mu\nu} \partial_{\sigma\eta\alpha\beta} B_{\mu\rho} \partial_\nu B^{\sigma\rho}$	

Table 3.6: Primary operators for $h\gamma gg$ and $h\gamma\gamma\gamma$.

i	$\mathcal{O}_i^{hggg,d}$ Color indices contracted with d_{ABC}	CP	$d_{\mathcal{O}_i}$	SMEFT Operator	c Unitarity Bound
1	$hD_\sigma G^{\alpha\mu}\overleftrightarrow{D}_\nu\widetilde{G}_{\alpha\beta}D^\nu{}_\mu G^{\sigma\beta}$	+	11	$H^\dagger HD_\sigma G^{\alpha\mu}\overleftrightarrow{D}_\nu\widetilde{G}_{\alpha\beta}D^\nu{}_\mu G^{\sigma\beta}$	$\frac{1\cdot10^{-3}}{E^7_{\rm TeV}}, \frac{4\cdot10^{-3}}{E^8_{\rm TeV}}$
2	$hD_\gamma G^{\mu\nu}\overleftrightarrow{D}_\sigma G_{\mu\rho}D^\sigma{}_\nu G^{\gamma\rho}$	−		$H^\dagger HD_\gamma G^{\mu\nu}\overleftrightarrow{D}_\sigma G_{\mu\rho}D^\sigma{}_\nu G^{\gamma\rho}$	
3	$hD_{\mu\rho\sigma}G^{\alpha\nu}D^{\rho\sigma}G^{\mu\delta}D_\nu\widetilde{G}_{\alpha\delta}$	+	13	$H^\dagger HD_{\mu\rho\sigma}G^{\alpha\nu}D^{\rho\sigma}G^{\mu\delta}D_\nu\widetilde{G}_{\alpha\delta}$	$\frac{8\cdot10^{-5}}{E^9_{\rm TeV}}, \frac{3\cdot10^{-4}}{E^{10}_{\rm TeV}}$
4	$hD_{\rho\sigma}G^{\alpha\mu}\overleftrightarrow{D}_\nu D^{\rho\sigma}\widetilde{G}_{\alpha\beta}D^\nu G_\mu{}^\beta$	+		$H^\dagger HD_{\rho\sigma}G^{\alpha\mu}\overleftrightarrow{D}_\nu D^{\rho\sigma}\widetilde{G}_{\alpha\beta}D^\nu G_\mu{}^\beta$	
5	$hD_\sigma^{\alpha\beta}G^{\mu\nu}D_{\alpha\beta}G_{\mu\rho}D_\nu G^{\sigma\rho}$	−		$H^\dagger HD_\sigma{}^{\alpha\beta}G^{\mu\nu}D_{\alpha\beta}G_{\mu\rho}D_\nu G^{\sigma\rho}$	
6	$hD^{\alpha\beta}G^{\mu\nu}D_{\sigma\alpha\beta}G_{\mu\rho}D_\nu G^{\sigma\rho}$	−		$H^\dagger HD^{\alpha\beta}G^{\mu\nu}D_{\sigma\alpha\beta}G_{\mu\rho}D_\nu G^{\sigma\rho}$	
7	$hD_{\eta\rho\sigma}G^{\alpha\mu}\overleftrightarrow{D}_\nu D^{\eta\rho\sigma}\widetilde{G}_{\alpha\beta}\partial^\nu G_\mu^\beta$	+	15	$H^\dagger HD_{\eta\rho\sigma}G^{\alpha\mu}\overleftrightarrow{D}_\nu D^{\eta\rho\sigma}\widetilde{G}_{\alpha\beta}D^\nu G_\mu^\beta$	$\frac{5\cdot10^{-6}}{E^{11}_{\rm TeV}}, \frac{2\cdot10^{-5}}{E^{12}_{\rm TeV}}$
8	$hD^{\eta\alpha\beta}G^{\mu\nu}D_{\sigma\eta\alpha\beta}G_{\mu\rho}D_\nu G^{\sigma\rho}$	−		$H^\dagger HD^{\eta\alpha\beta}G^{\mu\nu}D_{\sigma\eta\alpha\beta}G_{\mu\rho}D_\nu G^{\sigma\rho}$	

i	$\mathcal{O}_i^{hggg,f}$ Color indices contracted with f_{ABC}	CP	$d_{\mathcal{O}_i}$	SMEFT Operator	c Unitarity Bound
1	$hG^{\mu\nu}G_{\nu\gamma}G^\gamma{}_\mu$	+	7	$H^\dagger HG^{\mu\nu}G_{\nu\gamma}G^\gamma{}_\mu$	$\frac{0.4}{E^3_{\rm TeV}}, \frac{1}{E^4_{\rm TeV}}$
2	$hG^{\alpha\rho}G^\beta{}_\rho\widetilde{G}_{\alpha\beta}$	−		$H^\dagger HG^{\alpha\rho}G^\beta{}_\rho\widetilde{G}_{\alpha\beta}$	
3	$hD^\mu G^{\nu\gamma}G_{\nu\rho}D^\rho G_{\ \gamma\mu}$	+	9	$H^\dagger HD^\mu G^{\nu\gamma}G_{\nu\rho}D^\rho G_{\gamma\mu}$	$\frac{0.02}{E^5_{\rm TeV}}, \frac{0.3}{E^6_{\rm TeV}}$
4	$hD^\alpha G^{\rho\sigma}\widetilde{G}_{\alpha\beta}D^\beta G_{\rho\sigma}$	−		$H^\dagger HD^\alpha G^{\rho\sigma}\widetilde{G}_{\alpha\beta}D^\beta G_{\rho\sigma}$	
5	$hD^\mu G^{\nu\gamma}\overleftrightarrow{D}_\eta G_{\nu\rho}D^{\eta\rho}G_{\gamma\mu}$	+	11	$H^\dagger HD^\mu G^{\nu\gamma}\overleftrightarrow{D}_\eta G_{\nu\rho}D^{\eta\rho}G_{\gamma\mu}$	$\frac{1\cdot10^{-3}}{E^7_{\rm TeV}}, \frac{0.02}{E^8_{\rm TeV}}$
6	$hD^\alpha G^{\rho\sigma}\overleftrightarrow{D}_\eta\widetilde{G}_{\alpha\beta}D^{\eta\beta}G_{\rho\sigma}$	−		$H^\dagger HD^\alpha G^{\rho\sigma}\overleftrightarrow{D}_\eta\widetilde{G}_{\alpha\beta}D^{\eta\beta}G_{\rho\sigma}$	
7	$hD^{\sigma\mu}G^{\nu\gamma}D_\sigma\overleftrightarrow{D}_\eta G_{\nu\rho}D^{\eta\rho}G_{\gamma\mu}$	+	13	$H^\dagger HD^{\sigma\mu}G^{\nu\gamma}D_\sigma\overleftrightarrow{D}_\eta G_{\nu\rho}D^{\eta\rho}G_{\gamma\mu}$	$\frac{8\cdot10^{-5}}{E^9_{\rm TeV}}, \frac{1\cdot10^{-3}}{E^{10}_{\rm TeV}}$
8	$hD^{\chi\alpha}G^{\rho\sigma}D_\chi\overleftrightarrow{D}_\eta\widetilde{G}_{\alpha\beta}D^{\eta\beta}G_{\rho\sigma}$	−		$H^\dagger HD^{\chi\alpha}G^{\rho\sigma}D_\chi\overleftrightarrow{D}_\eta\widetilde{G}_{\alpha\beta}D^{\eta\beta}G_{\rho\sigma}$	

Table 3.7: Primary operators for $hggg$. Gluon color indices are omitted.

i	$\mathcal{O}_i^{hWW\gamma}$	CP	$d_{\mathcal{O}_i}$	SMEFT Operator	c Unitarity Bound
1	$ihW_\mu^+ W_\nu^- F^{\mu\nu}$ + h.c.	+	5	$iD_\nu H^\dagger D_\mu H B^{\mu\nu}$ + h.c.	$\frac{0.04}{E^3_{\text{TeV}}}, \frac{0.1}{E^4_{\text{TeV}}}$
2	$ihW^{+\alpha} W^{-\beta} \widetilde{F}_{\alpha\beta}$ + h.c.	−		$iD^\beta H^\dagger D^\alpha H \widetilde{B}_{\alpha\beta}$ + h.c.	
3	$ihD^\mu W_\nu^+ \overleftrightarrow{D}_\gamma W_\mu^- F^{\nu\gamma}$ + h.c.	+	7	$iD^\mu{}_\nu H^\dagger \overleftrightarrow{D}_\gamma D_\mu H B^{\nu\gamma}$ + h.c.	$\frac{2\cdot10^{-3}}{E^5_{\text{TeV}}}, \frac{7\cdot10^{-3}}{E^6_{\text{TeV}}}$
4	$hD^\mu W_\nu^+ \overleftrightarrow{D}_\gamma W_\mu^- F^{\nu\gamma}$ + h.c.	−		$D^\mu{}_\nu H^\dagger \overleftrightarrow{D}_\gamma D_\mu H B^{\nu\gamma}$ + h.c.	
5	$ihD_\mu W^{+\nu} \overleftrightarrow{D}_\gamma W_\nu^- F^{\mu\gamma}$ + h.c.	+		$iD^\mu{}_\nu H^\dagger \overleftrightarrow{D}_\gamma D_\nu H B^{\mu\gamma}$ + h.c.	
6	$ihW_\mu^+ \overleftrightarrow{D}_\gamma W_\nu^- \partial^\mu F^{\nu\gamma}$ + h.c.	+		$iD_\mu H^\dagger \overleftrightarrow{D}_\gamma D_\nu H \partial^\mu B^{\nu\gamma}$ + h.c.	
7	$ihD^\nu W^+_{\mu\gamma} W_\nu^- F^{\gamma\mu}$ + h.c.	+	7	$D^\nu W^a_{\mu\gamma} H^\dagger \sigma^a D_\nu H B^{\gamma\mu}$ + h.c.	$\frac{7\cdot10^{-3}}{E^5_{\text{TeV}}}, \frac{0.07}{E^7_{\text{TeV}}}$
8	$hD^\nu W^+_{\mu\gamma} W_\nu^- F^{\gamma\mu}$ + h.c.	−		$iD^\nu W^a_{\mu\gamma} H^\dagger \sigma^a D_\nu H B^{\gamma\mu}$ + h.c.	
9	$hW^+_{\gamma\mu} W_\nu^- \partial^\nu F^{\mu\gamma}$ + h.c.	−		$iW^a_{\gamma\mu} H^\dagger \sigma^a D_\nu H \partial^\nu B^{\mu\gamma}$ + h.c.	
10	$h\widetilde{W}^+_{\gamma\delta} \overleftrightarrow{D}_\rho W^{-\gamma} F^{\delta\rho}$ + h.c.	+		$i\widetilde{W}^a_{\gamma\delta} \overleftrightarrow{D}_\rho (H^\dagger \sigma^a D^\gamma H) B^{\delta\rho}$ + h.c.	
11	$ih\widetilde{W}^+_{\gamma\delta} \overleftrightarrow{D}_\rho W^{-\gamma} F^{\delta\rho}$ + h.c.	−		$\widetilde{W}^a_{\gamma\delta} \overleftrightarrow{D}_\rho (H^\dagger \sigma^a D^\gamma H) B^{\delta\rho}$ + h.c.	
12	$hD^\rho \widetilde{W}^+_{\gamma\delta} W_\rho^- F^{\delta\gamma}$ + h.c.	+		$iD^\rho \widetilde{W}^a_{\gamma\delta} H^\dagger \sigma^a D_\rho H B^{\delta\gamma}$ + h.c.	
13	$ihD^\rho \widetilde{W}^+_{\gamma\delta} W_\rho^- F^{\delta\gamma}$ + h.c.	−		$D^\rho \widetilde{W}^a_{\gamma\delta} H^\dagger \sigma^a D_\rho H B^{\delta\gamma}$ + h.c.	
14	$h\widetilde{W}^+_{\alpha\beta} W_\rho^- \partial^\rho F^{\alpha\beta}$ + h.c.	+		$i\widetilde{W}^a_{\alpha\beta} H^\dagger \sigma^a D_\rho H \partial^\rho B^{\alpha\beta}$ + h.c.	
15	$ih\widetilde{W}^+_{\alpha\beta} W_\rho^- \partial^\rho F^{\alpha\beta}$ + h.c.	−		$\widetilde{W}^a_{\alpha\beta} H^\dagger \sigma^a D_\rho H \partial^\rho B^{\alpha\beta}$ + h.c.	
16	$ih\widetilde{W}^+_{\alpha\beta} D^\alpha W_\rho^- F^{\rho\beta}$ + h.c.	−		$\widetilde{W}^a_{\alpha\beta} H^\dagger \sigma^a D^\alpha{}_\rho H B^{\rho\beta}$ + h.c.	
17	$ihD^\mu{}_\nu W_\gamma^+ \overleftrightarrow{D}_\rho D^\gamma W_\mu^- F^{\nu\rho}$ + h.c.	+	9	$iD^\mu{}_{\nu\gamma} H^\dagger \overleftrightarrow{D}_\rho D^\gamma D_\mu H B^{\nu\rho}$ + h.c.	$\frac{1\cdot10^{-4}}{E^7_{\text{TeV}}}, \frac{4\cdot10^{-4}}{E^8_{\text{TeV}}}$
18	$ihD_\rho \widetilde{W}^+_{\gamma\delta} \overleftrightarrow{\partial}_\sigma W^{-\delta\gamma} F^{\rho\sigma}$ + h.c.	−	9	$i\epsilon^{abc} H^\dagger H D_\rho \widetilde{W}^a_{\gamma\delta} \overleftrightarrow{D}_\sigma W^{b\delta\gamma} W^{c\rho\sigma}$ + h.c.	$\frac{0.02}{E^5_{\text{TeV}}}, \frac{0.7}{E^8_{\text{TeV}}}$

Table 3.8: Primary operators for $hWW\gamma$.

i	$\mathcal{O}_i^{hZZ\gamma}$	CP	$d_{\mathcal{O}_i}$	SMEFT Operator	c Unitarity Bound
1	$hZ_\mu \overset{\leftrightarrow}{\partial}_\gamma Z_\nu \partial^\gamma F^{\mu\nu}$	$-$	7	$D_\mu H^\dagger \overset{\leftrightarrow}{D}_\gamma D_\nu H \partial^\gamma B^{\mu\nu}$	$\frac{3\cdot 10^{-3}}{E^5_{\rm TeV}}, \frac{0.01}{E^6_{\rm TeV}}$
2	$hZ^\alpha \overset{\leftrightarrow}{\partial}_\rho Z^\beta \partial^\rho \widetilde{F}_{\alpha\beta}$	$+$		$D^\alpha H^\dagger \overset{\leftrightarrow}{D}_\rho D^\beta H \partial^\rho \widetilde{B}_{\alpha\beta}$ + h.c.	
3	$h\partial^\mu Z_\nu \overset{\leftrightarrow}{\partial}_\gamma Z_\mu F^{\nu\gamma}$	$-$		$D^\mu{}_\nu H^\dagger \overset{\leftrightarrow}{D}_\gamma D_\mu H B^{\nu\gamma}$ + h.c.	
4	$h\partial^\nu Z_{\mu\gamma} Z_\nu F^{\gamma\mu}$	$-$	7	$iD^\nu W^a_{\mu\gamma} H^\dagger \sigma^a D_\nu H B^{\gamma\mu} + h.c.$	$\frac{0.03}{E^4_{\rm TeV}}, \frac{0.3}{E^6_{\rm TeV}}$
5	$hZ_{\gamma\mu} Z_\nu \partial^\nu F^{\mu\gamma}$	$-$		$iW^a_{\gamma\mu} H^\dagger \sigma^a D_\nu H \partial^\nu B^{\mu\gamma} + h.c.$	
6	$h\widetilde{Z}_{\gamma\delta} \overset{\leftrightarrow}{\partial}_\rho Z^\gamma F^{\delta\rho}$	$+$	7	$i\widetilde{W}^a_{\gamma\delta} \overset{\leftrightarrow}{D}_\rho (H^\dagger \sigma^a D^\gamma H) B^{\delta\rho}$ + h.c.	$\frac{0.03}{E^4_{\rm TeV}}, \frac{0.3}{E^6_{\rm TeV}}$
7	$h\partial^\rho \widetilde{Z}_{\gamma\delta} Z_\rho F^{\delta\gamma}$	$+$		$iD^\rho \widetilde{W}^a_{\gamma\delta} H^\dagger \sigma^a D_\rho H B^{\delta\gamma}$ + h.c.	
8	$h\widetilde{Z}_{\alpha\beta} Z_\rho \partial^\rho F^{\alpha\beta}$	$+$		$i\widetilde{W}^a_{\alpha\beta} H^\dagger \sigma^a D_\rho H \partial^\rho B^{\alpha\beta}$ + h.c.	
9	$h\widetilde{Z}_{\alpha\beta} \overset{\leftrightarrow}{\partial}_\sigma Z_\rho \partial^{\sigma\rho} F^{\alpha\beta}$	$+$	9	$\widetilde{W}^a_{\alpha\beta} \overset{\leftrightarrow}{D}_\sigma (H^\dagger \sigma^a D_\rho H) \partial^{\sigma\rho} B^{\alpha\beta}$ + h.c.	$\frac{2\cdot 10^{-3}}{E^6_{\rm TeV}}, \frac{0.02}{E^8_{\rm TeV}}$
10	$h\partial^\mu Z_\nu \overset{\leftrightarrow}{\partial}_\rho \overset{\leftrightarrow}{\partial}_\gamma Z_\mu \partial^\rho F^{\nu\gamma}$	$-$	9	$D^\mu{}_\nu H^\dagger \overset{\leftrightarrow}{D}_\rho \overset{\leftrightarrow}{D}_\gamma D_\mu H \partial^\rho B^{\nu\gamma}$ + h.c.	$\frac{2\cdot 10^{-4}}{E^7_{\rm TeV}}, \frac{6\cdot 10^{-4}}{E^8_{\rm TeV}}$
11	$h\partial_\mu Z^\nu \overset{\leftrightarrow}{\partial}_\rho \overset{\leftrightarrow}{\partial}_\gamma Z_\nu \partial^\rho F^{\mu\gamma}$	$-$		$D_\mu{}^\nu H^\dagger \overset{\leftrightarrow}{D}_\rho \overset{\leftrightarrow}{D}_\gamma D_\nu H \partial^\rho B^{\mu\gamma}$ + h.c.	
12	$hZ^\mu \overset{\leftrightarrow}{\partial}_\rho \overset{\leftrightarrow}{\partial}_\gamma Z_\nu \partial^\rho{}_\mu F^{\nu\gamma}$	$-$		$D^\mu H^\dagger \overset{\leftrightarrow}{D}_\rho \overset{\leftrightarrow}{D}_\gamma D_\nu H \partial^\rho{}_\mu B^{\nu\gamma}$ + h.c.	
13	$h\partial^\nu Z_{\mu\gamma} \overset{\leftrightarrow}{\partial}_\rho Z_\nu \partial^\rho F^{\gamma\mu}$	$-$	9	$iD^\nu W^a_{\mu\gamma} \overset{\leftrightarrow}{D}_\rho (H^\dagger \sigma^a D_\nu H) \partial^\rho B^{\gamma\mu}$ + h.c.	$\frac{2\cdot 10^{-3}}{E^6_{\rm TeV}}, \frac{0.08}{E^8_{\rm TeV}}$
14	$h\widetilde{Z}_{\gamma\delta} \overset{\leftrightarrow}{\partial}_\sigma \overset{\leftrightarrow}{\partial}_\rho Z^\gamma \partial^\sigma F^{\delta\rho}$	$+$	9	$\widetilde{W}^a_{\gamma\delta} \overset{\leftrightarrow}{D}_\sigma \overset{\leftrightarrow}{D}_\rho (H^\dagger \sigma^a D^\gamma H) \partial^\sigma B^{\delta\rho}$ + h.c.	$\frac{2\cdot 10^{-3}}{E^6_{\rm TeV}}, \frac{0.02}{E^8_{\rm TeV}}$
15	$h\partial^\rho \widetilde{Z}_{\gamma\delta} \overset{\leftrightarrow}{\partial}_\sigma Z_\rho \partial^\sigma F^{\delta\gamma}$	$+$		$D^\rho \widetilde{W}^a_{\gamma\delta} \overset{\leftrightarrow}{D}_\sigma (H^\dagger \sigma^a D_\rho H) \partial^\sigma B^{\delta\gamma}$ + h.c.	
16	$h\partial^\alpha Z^\rho \overset{\leftrightarrow}{\partial}_\sigma \widetilde{Z}_{\alpha\beta} \partial^\sigma F^{\rho\beta}$	$+$		$(H^\dagger \sigma^a D^{\alpha\rho} H) \overset{\leftrightarrow}{D}_\sigma \widetilde{W}^a_{\alpha\beta} \partial^\sigma B^{\rho\beta}$ + h.c.	
17	$h\partial^\mu{}_\nu Z_\gamma \overset{\leftrightarrow}{\partial}_\sigma \overset{\leftrightarrow}{\partial}_\rho \partial^\gamma Z_\mu \partial^\sigma F^{\nu\rho}$	$-$	11	$D^\mu{}_{\nu\gamma} H^\dagger \overset{\leftrightarrow}{D}_\sigma \overset{\leftrightarrow}{D}_\rho D^\gamma D_\mu H \partial^\sigma B^{\nu\rho}$ + h.c.	$\frac{1\cdot 10^{-5}}{E^9_{\rm TeV}}, \frac{4\cdot 10^{-5}}{E^{10}_{\rm TeV}}$
18	$h\partial_\rho \widetilde{Z}_{\gamma\delta} \overset{\leftrightarrow}{\partial}_\eta \overset{\leftrightarrow}{\partial}_\sigma Z^{\delta\gamma} \partial^\eta F^{\rho\sigma}$	$+$	11	$H^\dagger H D_\rho \widetilde{W}^a_{\gamma\delta} \overset{\leftrightarrow}{D}_\eta \overset{\leftrightarrow}{D}_\sigma W^{a\delta\gamma} \partial^\eta B^{\rho\sigma}$ + h.c.	$\frac{1\cdot 10^{-3}}{E^7_{\rm TeV}}, \frac{4\cdot 10^{-3}}{E^8_{\rm TeV}}$

Table 3.9: Primary operators for $hZZ\gamma$.

i	$\mathcal{O}_i^{hWWZ}$	CP	$d_{\mathcal{O}_i}$	SMEFT Operator	c Unitarity Bound
1	$h\widetilde{W}^+_{\mu\nu}W^{-\mu}Z^\nu + \text{h.c.}$	+	5	$H^\dagger\sigma^a D^\mu H\widetilde{W}^a_{\mu\nu}H^\dagger D^\nu H + \text{h.c.}$	$\frac{0.04}{E^3_{\text{TeV}}}, \frac{1}{E^6_{\text{TeV}}}$
2	$ih\widetilde{W}^+_{\mu\nu}W^{-\mu}Z^\nu + \text{h.c.}$	−		$iD^\mu H^\dagger\sigma^a D^\nu H\widetilde{W}^a_{\mu\nu}$	
3	$ih\widetilde{Z}_{\mu\nu}W^{+\mu}W^{-\nu} + \text{h.c.}$	−		$iD^\mu H^\dagger\sigma^a D^\nu H\widetilde{W}^a_{\mu\nu}$	
4	$ihD^\mu W^{+\nu}W^-_\mu Z_\nu + \text{h.c.}$	+	5	$iH^\dagger\overleftrightarrow{D}_\nu H\left(D_\mu H^\dagger D_{\mu\nu}H + \text{h.c.}\right)$	$\frac{4\cdot10^{-3}}{E^4_{\text{TeV}}}, \frac{0.03}{E^6_{\text{TeV}}}$
5	$hD^\mu W^{+\nu}W^-_\mu Z_\nu + \text{h.c.}$	−		$iH^\dagger\overleftrightarrow{D}_\nu H\left(D_\mu H^\dagger D_{\mu\nu}H + \text{h.c.}\right)$	
6	$ihD^\mu W^{+\nu}W^-_\nu Z_\mu + \text{h.c.}$	+		$iH^\dagger\overleftrightarrow{D}_\mu H\left(D_\nu H^\dagger D_{\mu\nu}H + \text{h.c.}\right)$	
7	$hD^\mu W^{+\nu}W^-_\nu Z_\mu + \text{h.c.}$	−		$iH^\dagger\overleftrightarrow{D}_\mu H\left(D_\nu H^\dagger D_{\mu\nu}H + \text{h.c.}\right)$	
8	$ihZ^{\mu\nu}W^+_\mu W^-_\nu$	+	5	$iD_\mu H^\dagger\sigma^a D_\nu HW^{a\mu\nu}$	$\frac{0.04}{E^3_{\text{TeV}}}, \frac{0.1}{E^4_{\text{TeV}}}$
9	$h\partial^\mu Z^\nu W^+_\mu W^-_\nu + \text{h.c.}$	−	5	$iH^\dagger D^{\mu\nu}HD_\nu H^\dagger D_\mu H + \text{h.c.}$	$\frac{4\cdot10^{-3}}{E^4_{\text{TeV}}}, \frac{0.03}{E^6_{\text{TeV}}}$
10	$h\partial_\mu W^+_{\alpha\beta}\widetilde{W}^{-\alpha\beta}Z^\mu + h.c.$	+	7	$iH^\dagger\overleftrightarrow{D}_\mu HD^\mu W^{a\alpha\beta}\widetilde{W}^a_{\alpha\beta}$	$\frac{0.03}{E^4_{\text{TeV}}}, \frac{0.3}{E^6_{\text{TeV}}}$
11	$ih\partial_\mu W^+_{\alpha\beta}\widetilde{W}^{-\alpha\beta}Z^\mu + \text{h.c.}$	−		$i\epsilon^{abc}H^\dagger\sigma^a\overleftrightarrow{D}_\mu HD^\mu W^{b\alpha\beta}\widetilde{W}^c_{\alpha\beta}$	
12	$h\partial^\mu W^+_{\alpha\beta}\widetilde{Z}^{\alpha\beta}W^-_\mu + h.c.$	+		$\epsilon^{abc}H^\dagger\sigma^a\overleftrightarrow{D}_\mu HD^\mu W^{b\alpha\beta}\widetilde{W}^c_{\alpha\beta} + h.c.$	
13	$ih\partial^\mu W^+_{\alpha\beta}\widetilde{Z}^{\alpha\beta}W^-_\mu + \text{h.c.}$	−		$i\epsilon^{abc}H^\dagger\sigma^a\overleftrightarrow{D}_\mu HD^\mu W^{b\alpha\beta}\widetilde{W}^c_{\alpha\beta}$	
14	$h\partial^\mu Z_{\alpha\beta}\widetilde{W}^{+\alpha\beta}W^-_\mu + h.c.$	+		$\epsilon^{abc}H^\dagger\sigma^a\overleftrightarrow{D}_\mu HD^\mu W^{b\alpha\beta}\widetilde{W}^c_{\alpha\beta} + h.c.$	
15	$ih\partial^\mu Z_{\alpha\beta}\widetilde{W}^{+\alpha\beta}W^-_\mu + \text{h.c.}$	−		$i\epsilon^{abc}H^\dagger\sigma^a\overleftrightarrow{D}_\mu HD^\mu W^{b\alpha\beta}\widetilde{W}^c_{\alpha\beta}$	
16	$h\partial^\mu W^{+\alpha}\widetilde{W}^-_{\alpha\beta}\partial^\beta Z_\mu + \text{h.c.}$	+	7	$D^{\mu\alpha}H^\dagger\sigma^a D^\beta{}_\mu H\widetilde{W}^a_{\alpha\beta} + \text{h.c.}$	$\frac{0.01}{E^5}, \frac{0.03}{E^6}$
17	$ih\partial^\mu W^{+\alpha}\widetilde{W}^-_{\alpha\beta}\partial^\beta Z_\mu + \text{h.c.}$	−		$iD^{\mu\alpha}H^\dagger\sigma^a D^\beta{}_\mu H\widetilde{W}^a_{\alpha\beta} + \text{h.c.}$	
18	$ih\partial^\alpha W^+_\mu\widetilde{W}^-_{\alpha\beta}\partial^\mu Z^\beta + \text{h.c.}$	−		$iD^\alpha{}_\mu H^\dagger\sigma^a D^{\mu\beta}H\widetilde{W}^a_{\alpha\beta} + \text{h.c.}$	
19	$ih\partial^\delta W^+_\mu\widetilde{W}^-_{\beta\delta}\partial^\beta Z^\mu + \text{h.c.}$	−		$iD^\delta{}_\mu H^\dagger\sigma^a D^{\beta\mu}H\widetilde{W}^-_{\beta\delta} + \text{h.c.}$	
20	$ih\partial^{\mu\nu}W^+_\rho\partial^\rho W^-_\mu Z_\nu + \text{h.c.}$	+	7	$D^{\mu\nu}{}_\rho H^\dagger D^\rho{}_\mu HH^\dagger D_\nu H + \text{h.c.}$	$\frac{2\cdot10^{-4}}{E^6_{\text{TeV}}}, \frac{2\cdot10^{-3}}{E^8_{\text{TeV}}}$
21	$h\partial^{\mu\nu}W^+_\rho\partial^\rho W^-_\mu Z_\nu + \text{h.c.}$	−		$iD^{\mu\nu}{}_\rho H^\dagger D^\rho{}_\mu HH^\dagger D_\nu H + \text{h.c.}$	
22	$ih\partial^{\mu\nu}W^+_\rho\partial^\rho Z_\mu W^-_\nu + \text{h.c.}$	+		$D^{\mu\nu}{}_\rho H^\dagger D_\nu HH^\dagger D^\rho{}_\mu H + \text{h.c.}$	
23	$h\partial^{\mu\nu}W^+_\rho\partial^\rho Z_\mu W^-_\nu + \text{h.c.}$	−		$iD^{\mu\nu}{}_\rho H^\dagger D_\nu HH^\dagger D^\rho{}_\mu H + \text{h.c.}$	
24	$ih\partial^{\mu\nu}Z_\rho\partial^\rho W^+_\mu W^-_\nu + \text{h.c.}$	+		$D^\rho{}_\mu H^\dagger D_\nu HH^\dagger D^{\mu\nu}{}_\rho H + \text{h.c.}$	
25	$h\partial^{\mu\nu}Z_\rho\partial^\rho W^+_\mu W^-_\nu + \text{h.c.}$	−		$iD^\rho{}_\mu H^\dagger D_\nu HH^\dagger D^{\mu\nu}{}_\rho H + \text{h.c.}$	
26	$ih\partial^\mu W^+_\nu\partial^\nu W^-_\rho\partial^\rho Z_\mu + \text{h.c.}$	+		$D^\mu{}_\nu H^\dagger D^\nu{}_\rho HH^\dagger D^\rho{}_\mu H + \text{h.c.}$	
27	$h\partial^\mu W^+_\nu\partial^\nu W^-_\rho\partial^\rho Z_\mu + \text{h.c.}$	−		$iD^\mu{}_\nu H^\dagger D^\nu{}_\rho HH^\dagger D^\rho{}_\mu H + \text{h.c.}$	

Table 3.10: Primary operators for $hWWZ$.

i	$\mathcal{O}_i^{hZZZ}$	CP	$d_{\mathcal{O}_i}$	SMEFT Operator	c Unitarity Bound
1	$h\partial^\mu Z^\nu Z_\mu Z_\nu$	$-$	5	$iH^\dagger D^{\mu\nu} H H^\dagger D_{\mu\nu} H + h.c.$	$\frac{5\cdot10^{-3}}{E^4_{\rm TeV}}, \frac{0.04}{E^6_{\rm TeV}}$
2	$h\partial^\mu Z^{\alpha\beta} \widetilde{Z}_{\alpha\beta} Z_\mu$	$+$	7	$iD^\mu W^{a\alpha\beta} \widetilde{W}^a_{\alpha\beta} H^\dagger D_\mu H + h.c.$	$\frac{0.03}{E^4_{\rm TeV}}, \frac{0.3}{E^6_{\rm TeV}}$
3	$h(\widetilde{Z}_{\alpha\beta} \overleftrightarrow{\partial}_\mu Z^\alpha)\partial^\mu Z^\beta$	$+$	7	$\widetilde{W}^a_{\alpha\beta} \overleftrightarrow{D}_\mu (D^\alpha H^\dagger \sigma^a D^{\mu\beta} H) + h.c.$	$\frac{3\cdot10^{-3}}{E^5_{\rm TeV}}, \frac{0.01}{E^6_{\rm TeV}}$
4	$h\partial^{\mu\nu} Z^\rho \partial_\rho Z_\mu Z_\nu$	$-$	7	$iH^\dagger D^{\mu\nu\rho} H H^\dagger D_{\rho\mu\nu} H + h.c.$	$\frac{3\cdot10^{-4}}{E^6_{\rm TeV}}, \frac{3\cdot10^{-3}}{E^8_{\rm TeV}}$
5	$h\partial^\mu Z^\nu \partial_\nu Z^\rho \partial_\rho Z_\mu$	$-$		$iH^\dagger D^{\mu\nu} H D_\nu{}^\rho H^\dagger D_{\rho\mu} H + h.c.$	
6	$h(\partial^\mu Z^\nu \overleftrightarrow{\partial}_\rho Z_\mu)\partial^\rho Z_\nu$	$-$		$i(H^\dagger D^{\mu\nu} H) \overleftrightarrow{\partial}_\rho (D_\mu H^\dagger D^\rho{}_\nu H) + h.c.$	
7	$h(\partial^\mu Z^\nu \overleftrightarrow{\partial}_\rho Z_\nu)\partial^\rho Z_\mu$	$-$		$i(H^\dagger D^{\mu\nu} H) \overleftrightarrow{\partial}_\rho (D_\nu H^\dagger D^\rho{}_\mu H) + h.c.$	
8	$h(\partial^\mu Z^{\alpha\beta} \overleftrightarrow{\partial}_\rho \widetilde{Z}_{\alpha\beta})\partial^\rho Z_\mu$	$+$	9	$i(D^\mu W^{a\alpha\beta}) \overleftrightarrow{D}_\rho \widetilde{W}^a_{\alpha\beta}) H^\dagger D^\rho{}_\mu H + h.c.$	$\frac{2\cdot10^{-3}}{E^6_{\rm TeV}}, \frac{0.02}{E^8_{\rm TeV}}$
9	$h(\partial^\mu Z^{\alpha\beta} \overleftrightarrow{\partial}_\rho Z_\mu)\partial^\rho \widetilde{Z}_{\alpha\beta}$	$+$		$i(D^\mu W^{a\alpha\beta}) \overleftrightarrow{D}_\rho (H^\dagger D_\mu H) D^\rho \widetilde{W}^a_{\alpha\beta} + h.c.$	
10	$h(\partial^\mu Z^\alpha \overleftrightarrow{\partial}_\rho \widetilde{Z}_{\alpha\beta})\partial^{\rho\beta} Z_\mu$	$+$	9	$\widetilde{W}^a_{\alpha\beta} \overleftrightarrow{D}_\rho (D^{\mu\alpha} H^\dagger \sigma^a D^{\rho\beta}{}_\mu H) + h.c.$	$\frac{2\cdot10^{-4}}{E^7_{\rm TeV}}, \frac{6\cdot10^{-4}}{E^8_{\rm TeV}}$
11	$h(\partial^\alpha Z^\mu \overleftrightarrow{\partial}_\rho \widetilde{Z}_{\alpha\beta})\partial^\rho{}_\mu Z^\beta$	$+$		$\widetilde{W}^a_{\alpha\beta} \overleftrightarrow{D}_\rho (D^{\alpha\mu} H^\dagger \sigma^a D^\rho{}_\mu{}^\beta H) + h.c.$	
12	$h(\partial^{\mu\nu} Z^\rho \overleftrightarrow{\partial}_\sigma \partial_\rho Z_\mu)\partial^\sigma Z_\nu$	$-$	9	$i(H^\dagger D^{\mu\nu\rho} H) \overleftrightarrow{\partial}_\sigma (D_{\rho\mu} H^\dagger D^\sigma{}_\nu H) + h.c.$	$\frac{2\cdot10^{-5}}{E^8_{\rm TeV}}, \frac{2\cdot10^{-4}}{E^{10}_{\rm TeV}}$
13	$h(\partial^{\mu\nu} Z^\rho \overleftrightarrow{\partial}_\sigma Z_\nu)\partial^\sigma{}_\rho Z_\mu$	$-$		$i(H^\dagger D^{\mu\nu\rho} H) \overleftrightarrow{\partial}_\sigma (D_\nu H^\dagger D^\sigma{}_{\rho\mu} H) + h.c.$	
14	$h(\partial^{\rho\mu} Z^\nu \overleftrightarrow{\partial}_\sigma \partial_\rho Z_\mu)\partial^\sigma Z_\nu$	$-$		$i(H^\dagger D^{\rho\mu\nu} H) \overleftrightarrow{\partial}_\sigma D_{\rho\mu} H^\dagger D^\sigma{}_\nu H + h.c.$	
15	$h(\partial^{\rho\mu} Z^\nu \overleftrightarrow{\partial}_\sigma \partial_\rho Z_\nu)\partial^\sigma Z_\mu$	$-$		$i(H^\dagger D^{\rho\mu\nu} H) \overleftrightarrow{\partial}_\sigma (D_{\rho\nu} H^\dagger D^\sigma{}_\mu H) + h.c.$	
16	$h(\partial^{\sigma\mu} Z^{\alpha\beta} \overleftrightarrow{\partial}_\rho \partial_\sigma \widetilde{Z}_{\alpha\beta})\partial^\rho Z_\mu$	$+$	11	$i(D^{\sigma\mu} W^{a\alpha\beta}) \overleftrightarrow{D}_\rho (D_\sigma \widetilde{W}^a_{\alpha\beta}) H^\dagger D^\rho{}_\mu H + h.c.$	$\frac{1\cdot10^{-4}}{E^8_{\rm TeV}}, \frac{1\cdot10^{-3}}{E^{10}_{\rm TeV}}$
17	$h(\partial^{\sigma\mu} Z^{\alpha\beta} \overleftrightarrow{\partial}_\rho \partial_\sigma Z_\mu)\partial^\rho \widetilde{Z}_{\alpha\beta}$	$+$		$i(D^{\sigma\mu} W^{a\alpha\beta}) \overleftrightarrow{D}_\rho (H^\dagger \sigma^a D_{\sigma\mu} H) D^\rho \widetilde{W}^a_{\alpha\beta} + h.c.$	
18	$h(\partial^{\sigma\mu} Z^\alpha \overleftrightarrow{\partial}_\rho \partial_\sigma \widetilde{Z}_{\alpha\beta})\partial^{\rho\beta} Z_\mu$	$+$	11	$(D_\sigma \widetilde{W}^a_{\alpha\beta}) \overleftrightarrow{D}_\rho (D^{\sigma\mu\alpha} H^\dagger \sigma^a D^{\rho\beta}{}_\mu H) + h.c.$	$\frac{1\cdot10^{-5}}{E^9_{\rm TeV}}, \frac{4\cdot10^{-5}}{E^{10}_{\rm TeV}}$
19	$h(\partial^{\sigma\alpha} Z^\mu \overleftrightarrow{\partial}_\rho \partial_\sigma \widetilde{Z}_{\alpha\beta})\partial^\rho{}_\mu Z^\beta$	$+$		$(D_\sigma \widetilde{W}^a_{\alpha\beta}) \overleftrightarrow{D}_\rho (D^{\sigma\alpha\mu} H^\dagger \sigma^a D^\rho{}_\mu{}^\beta H) + h.c.$	
20	$h(\partial^{\gamma\mu\nu} Z^\rho \overleftrightarrow{\partial}_\sigma \partial_\gamma{}_\rho Z_\mu)\partial^\sigma Z_\nu$	$-$	11	$i(H^\dagger D^{\gamma\mu\nu\rho} H) \overleftrightarrow{\partial}_\sigma (D_{\gamma\rho\mu} H^\dagger D^\sigma{}_\nu H) + h.c.$	$\frac{1\cdot10^{-6}}{E^{10}_{\rm TeV}}, \frac{1\cdot10^{-5}}{E^{12}_{\rm TeV}}$
21	$h(\partial^{\gamma\mu\nu} Z^\rho \overleftrightarrow{\partial}_\sigma \partial_\gamma Z_\nu)\partial^\sigma{}_\rho Z_\mu$	$-$		$i(H^\dagger D^{\gamma\mu\nu\rho} H) \overleftrightarrow{\partial}_\sigma (D_{\gamma\nu} H^\dagger D^\sigma{}_{\rho\mu} H) + h.c.$	
22	$h(\partial^{\gamma\rho\mu} Z^\nu \overleftrightarrow{\partial}_\sigma \partial_\gamma{}_\rho Z_\mu)\partial^\sigma Z_\nu$	$-$		$i(H^\dagger D^{\gamma\rho\mu\nu} H) \overleftrightarrow{\partial}_\sigma (D_{\gamma\rho\mu} H^\dagger D^\sigma{}_\nu H) + h.c.$	
23	$h(\partial^{\eta\sigma\mu} Z^{\alpha\beta} \overleftrightarrow{\partial}_\rho \partial_{\eta\sigma} \widetilde{Z}_{\alpha\beta})\partial^\rho Z_\mu$	$+$	13	$i(D^{\eta\sigma\mu} W^{a\alpha\beta}) \overleftrightarrow{D}_\rho (D_{\eta\sigma} \widetilde{W}^a_{\alpha\beta}) H^\dagger D^\rho{}_\mu H + h.c.$	$\frac{8\cdot10^{-6}}{E^{10}_{\rm TeV}}, \frac{7\cdot10^{-5}}{E^{12}_{\rm TeV}}$
24	$h(\partial^{\eta\sigma\mu} Z^\alpha \overleftrightarrow{\partial}_\rho \partial_{\eta\sigma} \widetilde{Z}_{\alpha\beta})\partial^{\rho\beta} Z_\mu$	$+$	13	$(D_{\eta\sigma} \widetilde{W}^a_{\alpha\beta}) \overleftrightarrow{D}_\rho (D^{\eta\sigma\mu\alpha} H^\dagger \sigma^a D^{\rho\beta}{}_\mu H) + h.c.$	$\frac{7\cdot10^{-7}}{E^{11}_{\rm TeV}}, \frac{2\cdot10^{-6}}{E^{12}_{\rm TeV}}$
25	$h(\partial^{\eta\sigma} \widetilde{Z}_{\beta\delta} \overleftrightarrow{\partial}_\rho \partial_{\eta\sigma}{}^\delta Z^\mu)\partial^{\rho\beta} Z_\mu$	$+$		$(D^{\eta\sigma} \widetilde{W}^a_{\beta\delta}) \overleftrightarrow{D}_\rho (D_{\eta\sigma}{}^{\delta\mu} H^\dagger \sigma^a D^{\rho\beta}{}_\mu H) + h.c.$	
26	$h(\partial^{\eta\gamma\mu\nu} Z^\rho \overleftrightarrow{\partial}_\sigma \partial_{\eta\gamma\rho} Z_\mu)\partial^\sigma Z_\nu$	$-$	13	$i(H^\dagger D^{\eta\gamma\mu\nu} D^\rho H) \overleftrightarrow{\partial}_\sigma (D_{\eta\gamma\rho\mu} H^\dagger D^\sigma{}_\nu H) + h.c.$	$\frac{6\cdot10^{-8}}{E^{12}_{\rm TeV}}, \frac{6\cdot10^{-7}}{E^{14}_{\rm TeV}}$
27	$h(\partial^{\eta\gamma\mu} Z^\nu \overleftrightarrow{\partial}_\sigma \partial_{\eta\gamma\nu} Z_\rho)\partial^{\sigma\rho} Z_\mu$	$-$		$i(H^\dagger D^{\eta\gamma\mu\nu} H) \overleftrightarrow{\partial}_\sigma (D_{\eta\gamma\nu\rho} H^\dagger D^{\sigma\rho}{}_\mu H) + h.c.$	

Table 3.11: Primary operators for $hZZZ$.

i	$\mathcal{O}_i^{hh\bar{f}f}$	CP	$d_{\mathcal{O}_i}$	SMEFT Operator	c Unitarity Bound
1	$h^2\bar{\psi}_L\psi_R + \text{h.c.}$	$+$	5	$H^\dagger H\bar{Q}_L\tilde{H}u_R + \text{h.c.}$	$\frac{6}{E_{\text{TeV}}}, \frac{200}{E^4_{\text{TeV}}}$
2	$ih^2\bar{\psi}_L\psi_R + \text{h.c.}$	$-$		$iH^\dagger H\bar{Q}_L\tilde{H}u_R + \text{h.c.}$	
3	$i\partial^\mu h\partial^\nu h\bar{\psi}_L\gamma_\mu \overset{\leftrightarrow}{\partial}_\nu \psi_L$	$+$	8	$iD^\mu H^\dagger D^\nu H\bar{Q}_L\gamma_\mu \overset{\leftrightarrow}{D}_\nu Q_L$	$\frac{0.09}{E^4_{\text{TeV}}}$
4	$i\partial^\mu h\partial^\nu h\bar{\psi}_R\gamma_\mu \overset{\leftrightarrow}{\partial}_\nu \psi_R$	$+$		$iD^\mu H^\dagger D^\nu H\bar{u}_R\gamma_\mu \overset{\leftrightarrow}{D}_\nu u_R$	

Table 3.12: Primary operators for $hh\bar{f}f$.

i	$\mathcal{O}_i^{hhWW}$	CP	$d_{\mathcal{O}_i}$	SMEFT Operator	c Unitarity Bound
1	$h^2 W_\mu^+ W^{-\mu}$	+	4	$H^\dagger H D_\mu H^\dagger D^\mu H$	$\frac{0.2}{E_{\rm TeV}^2}, \frac{2}{E_{\rm TeV}^4}$
2	$h^2 W_{\mu\nu}^+ W^{-\mu\nu}$	+	6	$H^\dagger H W_{\mu\nu}^a W^{a\mu\nu}$	$\frac{2}{E_{\rm TeV}^2}, \frac{10}{E_{\rm TeV}^4}$
3	$h^2 W_{\mu\nu}^+ \widetilde{W}^{-\mu\nu}$	−		$H^\dagger H W_{\mu\nu}^a \widetilde{W}^{a\mu\nu}$	
4	$h\partial^{\mu\nu} h W_\mu^+ W_\nu^-$	+	6	$H^\dagger D^{\mu\nu} H D_\mu H^\dagger D_\nu H + \text{h.c.}$	$\frac{0.01}{E_{\rm TeV}^4}, \frac{0.09}{E_{\rm TeV}^6}$
5	$ih\partial^{\mu\nu} h \widetilde{W}_{\mu\beta}^+ W_\nu^{-\,\beta} + \text{h.c.}$	+	8	$\epsilon^{abc} H^\dagger \sigma^a D^{\mu\nu} H \widetilde{W}_{\mu\beta}^b W_\nu^{c\beta} + \text{h.c.}$	$\frac{0.09}{E_{\rm TeV}^4}, \frac{0.9}{E_{\rm TeV}^6}$
6	$h\partial^{\mu\nu} h D_\mu W_\beta^+ W_\nu^{-\,\beta} + \text{h.c.}$	+	8	$H^\dagger D^{\mu\nu} H H^\dagger \sigma^a D_{\mu\beta} H W_\nu^{a\beta} + \text{h.c.}$	$\frac{7\cdot 10^{-3}}{E_{\rm TeV}^5}, \frac{0.2}{E_{\rm TeV}^8}$
7	$ih\partial^{\mu\nu} h D_\mu W_\beta^+ \widetilde{W}_\nu^{-\,\beta} + \text{h.c.}$	+		$\epsilon^{abc} H^\dagger \sigma^a D^{\mu\nu} H H^\dagger \sigma^b D_{\mu\beta} H \widetilde{W}_\nu^{c\beta} + \text{h.c.}$	
8	$ih\partial^{\mu\nu} h D_\mu W_\beta^+ W_\nu^{-\,\beta} + \text{h.c.}$	−		$\epsilon^{abc} H^\dagger \sigma^a D^{\mu\nu} H H^\dagger \sigma^b D_{\mu\beta} H W_\nu^{c\beta} + \text{h.c.}$	
9	$h\partial^{\mu\nu} h D_\mu W_\beta^+ \widetilde{W}_\nu^{-\,\beta} + \text{h.c.}$	−		$H^\dagger D^{\mu\nu} H H^\dagger \sigma^a D_{\mu\beta} H \widetilde{W}_\nu^{a\beta} + \text{h.c.}$	

i	$\mathcal{O}_i^{hhZ\gamma}$	CP	$d_{\mathcal{O}_i}$	SMEFT Operator	c Unitarity Bound
1	$h^2 F^{\mu\nu} Z_{\mu\nu}$	+	6	$H^\dagger \sigma^a H W^{a\mu\nu} B_{\mu\nu}$	$\frac{2}{E_{\rm TeV}^2}, \frac{10}{E_{\rm TeV}^4}$
2	$h^2 F_{\mu\nu} \widetilde{Z}^{\mu\nu}$	−		$H^\dagger \sigma^a H \widetilde{W}^{a\mu\nu} B_{\mu\nu}$	
3	$h\partial_\nu{}^\rho h F^{\mu\nu} Z_{\mu\rho}$	+	8	$H^\dagger \sigma^a D_\nu{}^\rho H W_{a\mu\rho} B^{\mu\nu} + \text{h.c.}$	$\frac{0.09}{E_{\rm TeV}^4}, \frac{0.9}{E_{\rm TeV}^6}$
4	$h \overleftrightarrow{\partial}_\rho \overleftrightarrow{\partial}_\mu h F^{\mu\nu} \partial^\rho Z_\nu$	+		$H^\dagger \overleftrightarrow{D}_\rho \overleftrightarrow{D}_\mu H H^\dagger D^\rho{}_\nu H B^{\mu\nu} + \text{h.c.}$	$\frac{8\cdot 10^{-3}}{E_{\rm TeV}^5}, \frac{0.2}{E_{\rm TeV}^8}$
5	$h\partial_\nu{}^\rho h F^{\mu\nu} \widetilde{Z}_{\mu\rho}$	−		$H^\dagger \sigma^a D_\nu{}^\rho H \widetilde{W}_{a\mu\rho} B^{\mu\nu} + \text{h.c.}$	$\frac{0.09}{E_{\rm TeV}^4}, \frac{0.9}{E_{\rm TeV}^6}$
6	$h \overleftrightarrow{\partial}_\rho \overleftrightarrow{\partial}_\mu h \widetilde{F}^{\mu\nu} \partial^\rho Z_\nu$	−		$H^\dagger \overleftrightarrow{D}_\rho \overleftrightarrow{D}_\mu H H^\dagger D^\rho{}_\nu H \tilde{B}^{\mu\nu} + \text{h.c.}$	$\frac{8\cdot 10^{-3}}{E_{\rm TeV}^5}, \frac{0.2}{E_{\rm TeV}^8}$

i	$\mathcal{O}_i^{hh\gamma\gamma}$	CP	$d_{\mathcal{O}_i}$	SMEFT Operator	c Unitarity Bound
1	$h^2 F_{\mu\nu} F^{\mu\nu}$	+	6	$H^\dagger H B_{\mu\nu} B^{\mu\nu}$	$\frac{2}{E_{\rm TeV}^2}, \frac{10}{E_{\rm TeV}^4}$
2	$h^2 F_{\mu\nu} \widetilde{F}^{\mu\nu}$	−		$H^\dagger H B_{\mu\nu} \widetilde{B}^{\mu\nu}$	
3	$h\partial^\mu{}_\nu h F_{\mu\alpha} F^{\nu\alpha}$	+	8	$H^\dagger D^\mu{}_\nu H B_{\mu\alpha} B^{\nu\alpha} + \text{h.c.}$	$\frac{0.09}{E_{\rm TeV}^4}, \frac{0.9}{E_{\rm TeV}^6}$

Table 3.13: Primary operators for $hhWW$, $hhZ\gamma$, and $hh\gamma\gamma$. As noted in the text, the $hhZZ$ primary operators can be obtained from the $hhWW$ operators by the replacement $W_\mu \to Z_\mu$ and the $hhgg$ primary operators can be obtained from the $hh\gamma\gamma$ operators by the replacement $F_{\mu\nu} \to G_{\mu\nu}$.

i	$\mathcal{O}_i^{hhhZ}$	CP	$d_{\mathcal{O}_i}$	SMEFT Operator	c Unitarity Bound
1	$\left(h\overset{\leftrightarrow}{\partial}_\nu\overset{\leftrightarrow}{\partial}_\mu h\right)\partial^\nu hZ^\mu$	$-$	7	$iH^\dagger\overset{\leftrightarrow}{D}_\nu\overset{\leftrightarrow}{D}_\mu HH^\dagger D^{\mu\nu}H+\text{h.c.}$	$\frac{0.03}{E_{\text{TeV}}^4}$, $\frac{0.3}{E_{\text{TeV}}^6}$
2	$\left(\partial^\gamma h\partial_\gamma\overset{\leftrightarrow}{\partial}_\nu\overset{\leftrightarrow}{\partial}_\mu h\right)\partial^\nu hZ^\mu$	$-$	9	$iD^\gamma H^\dagger D_\gamma\overset{\leftrightarrow}{D}_\nu\overset{\leftrightarrow}{D}_\mu HH^\dagger D^{\mu\nu}H+\text{h.c.}$	$\frac{2\cdot10^{-3}}{E_{\text{TeV}}^6}$, $\frac{0.02}{E_{\text{TeV}}^8}$
3	$\epsilon_{\alpha\beta\gamma\delta}\partial^{\eta\sigma\alpha}h\partial_{\eta\sigma}\overset{\leftrightarrow}{\partial}_\rho\partial^\beta h\partial^\rho\partial^\gamma hZ^\delta$	$+$	13	$\epsilon_{\alpha\beta\gamma\delta}D^{\eta\sigma\alpha}H^\dagger D_{\eta\sigma}\overset{\leftrightarrow}{D}_\rho D^\beta H\ D^\delta H^\dagger D^{\rho\gamma}H+\text{h.c.}$	$\frac{8\cdot10^{-6}}{E_{\text{TeV}}^{10}}$

i	$\mathcal{O}_i^{hhh\gamma}$	CP	$d_{\mathcal{O}_i}$	SMEFT Operator	c Unitarity Bound
1	$\partial^{\eta\sigma\alpha}h\partial_{\eta\sigma}\overset{\leftrightarrow}{\partial}_\rho\partial^\beta h\partial^\rho\widetilde{F}_{\alpha\beta}$	$+$	13	$D^{\eta\sigma\alpha}H^\dagger D_{\eta\sigma}\overset{\leftrightarrow}{D}_\rho D^\beta HH^\dagger D^\rho H\widetilde{B}_{\alpha\beta}+\text{h.c.}$	$\frac{8\cdot10^{-5}}{E_{\text{TeV}}^9}$, $\frac{8\cdot10^{-4}}{E_{\text{TeV}}^{11}}$
2	$\partial^{\rho\sigma\mu}h\partial_{\rho\sigma}\overset{\leftrightarrow}{\partial}_\gamma\partial^\nu h\partial^\gamma hF_{\mu\nu}$	$-$		$D^{\rho\sigma\mu}H^\dagger D_{\rho\sigma}\overset{\leftrightarrow}{D}_\gamma D^\nu HH^\dagger D^\gamma HB_{\mu\nu}+\text{h.c.}$	

Table 3.14: Primary operators for $hhhZ$ and $hhh\gamma$.

3.6 Conclusions

This chapter has analyzed the most general observables that parameterize the indirect effect of new heavy physics at colliders. An important conceptual point is that the space of these observables is finite, with a finite basis that can be enumerated. This can be most easily seen in the language of on-shell amplitudes: any local amplitude can be written as a linear combination of a finitely many 'primary' amplitudes, each of which is multiplied by an infinite series in Mandelstam invariants. Under very general physical assumptions, the additional Mandelstam invariants are suppressed by powers of a heavy mass scale M, and the leading approximation is given by the first nonzero term in this expansion. Each primary amplitude can be associated with a local operator, up to the usual ambiguities from integration by parts and integration by parts. However, these ambiguities do not change the on-shell amplitude, so we can make the simplest choice when defining the operator basis.

The major results of this chapter are a systematic method for determining all primary operators, and an explicit determination of the 3-point and 4-point primary operators relevant for Higgs signals at colliders. The 3-point on-shell amplitudes have no Mandelstam

invariants, so there is a finite list of 3-point operators, which has previously been found in the literature Refs. [16, 61, 66]. Partial results for primary 4-point functions have been given in [16, 63], and our results agree where they overlap.

The correspondence between local on-shell amplitudes and EFT operators has been invaluable in this work. For example, we found that if the on-shell amplitudes are expressed in a specific set of kinematic variables, the amplitudes can be treated as polynomials in the kinematic variables for purposes of determining the linearly independent amplitudes. This allows us to efficiently and reliably determine the independent amplitudes. The Hilbert series that counts independent operators is also an invaluable check on these methods.

The primary operators are a natural set of observables for searches for new physics at colliders, and they can be matched onto theoretical models or EFT frameworks (such as SMEFT or HEFT). We have considered the unitarity and precision electroweak constraints on these observables, and made a first pass at determining which may be promising for searches for new physics in Higgs decays. In particular, the three-body decays into $Z\bar{f}f$, $W\bar{f}f'$, $\gamma\bar{f}f$, and $Z\gamma\gamma$ are estimated to be of interest at the HL-LHC. Investigating the phenomenology of these observables is an obvious direction for future work.

It is our hope that this framework will prove useful for the LHC program of constraining (or discovering!) the indirect effects of new particles too heavy to be produced. Under the general assumptions made here, the primary observables are independent of each other, and experiments can measure them without worrying about correlations with other observables. These results can then be compared with predictive theoretical frameworks. In subsequent work, we plan to study experimental strategies for carrying out such searches and reporting the results in a way that can be compared with searches in other channels, or in future colliders.

Chapter 4

Top Yukawa Coupling at the Muon Collider

This chapter is taken from [6].

As explained in the introduction, we are interested in deviations in the predicted SM Higgs couplings because they may indicate the existence of new physics. In constructing effective field theories, we integrate out particles with masses above a certain scale, which introduces new interactions among the light particles and SM coupling deviations could be indicative of such interactions. In this chapter, we discuss a few of these anomalous couplings in the context of a high energy muon collider and provide a detailed analysis on the measurement of the top Yukawa coupling.

There are two common experimental methods for detecting new physics. The first, precision measurement, involves measuring parameters at particle pole masses [79, 80] to search for deviations from the SM predictions. The second, direct resonance searches, uses the kinematic variables of the decay products to detect evidence of new particles. Specifically, peaks in the distribution of such variables (particularly invariant mass) could indicate new particles.

In searches for anomalous Higgs couplings, we benefit from energy growing behavior [14] (see [73] recently for the on-shell derivation). We also discuss this feature in detail in Chapter 2. Experimentalists have used this fact in combination with the high energy bins at the LHC to conduct precision measurements [81–84].

In addition to hadron colliders, high energy muon colliders also seem promising for new physics searches [5, 8, 85–112]. The muon collider is able to reach energies $\gtrsim 10$ TeV and maintain low systematic uncertainty with a potential high integrated luminosity of

$$L = \left(\frac{\sqrt{s_\mu}}{10\,\text{TeV}}\right)^2 \times 10\,\text{ab}^{-1}, \tag{4.0.1}$$

which allows us to better constrain measurements. For example, muon annihilation electroweak processes with di-fermion and di-boson final states can achieve percent-level precision in the $\gtrsim 10$ TeV bins [107], effectively probing the 100 TeV scale.[1] Furthermore, because the electroweak gauge boson parton distribution functions grow logarithmically, we can consider a high energy muon collider as a gauge boson collider [5, 8, 89].

In this chapter, we are concerned with the prospects of measuring the top Yukawa coupling at a high energy muon collider. We begin with a general analysis of signal significance for vector boson fusion processes given anomalous couplings, followed by a more detailed analysis of $W^+W^- \to t\bar{t}$. We then examine the sensitivity to the top Yukawa coupling in VBF production of $t\bar{t}$ and briefly present results for $t\bar{t}h$. Finally we summarize our conclusions.

4.1 General Analysis of Weak Boson Fusion Processes

In this section, we will study the energy scaling behavior of $S/\sqrt{B}$ and S/B in the presence of anomalous couplings for the weak boson fusion processes in the two particle final states at the high energy muon collider. We will focus on the hard scattering regime where the

[1] This is higher than the flavor physics scale in composite Higgs scenarios. [113, 114]

scattering angle is in the central region, i.e. $-\hat{t} \sim \hat{s} = \hat{E}^2$. We start from the analysis of the partonic processes $VV \to XY$ and then employ the Effective W-boson Approximation (EWA) [115–117] to analyze the energy scaling at the $\mu^+\mu^-$ collider.

4.1.1 Energy Scaling Behavior in $W^+W^- \to XX, ZZ \to XX, WZ \to XY$

As a preliminary step to understanding the energy scaling behavior of processes at a muon collider, we consider the simpler problem of $VV \to XY$ where the V stands for a W or Z boson and X, Y can be any SM particles with electroweak charges such that the processes have non-zero tree-level contributions. We can later relate the results from this analysis to $\mu^+\mu^-$ cross sections by the Effective W Approximation [115–117]. Restricting to $2 \to 2$ processes where the initial state contains two massive bosons, we can express our cross sections schematically in terms of amplitudes as:

$$\sigma_{int} \sim \frac{\mathcal{M}_{\rm SM}\mathcal{M}_{\delta_i}}{\hat{E}^2}; \quad \sigma_{\rm SM} \sim \frac{\mathcal{M}^2_{\rm SM}}{\hat{E}^2}, \tag{4.1.1}$$

where $\mathcal{M}_{\rm SM}$ refers to the SM amplitude and $\mathcal{M}_{\delta_i}$ refers to amplitudes containing BSM physics. As only the energy scaling is concerned here, we also neglect the possible phase of the amplitudes. Note that we also study the hard scattering regime which is away from the possible scattering angle singularities (mainly from t-channel or u-channel). Then given our processes, $\mathcal{M}_{\delta_i}$ is linear in the anomalous couplings δ_i and we see that σ_{int} is the interference term. We start from the analysis by assuming that we can exactly measure the helicities of the initial bosons and final state particles, so we are really considering:

$$\frac{S^{h_1 \ldots h_4}}{\sqrt{B^{h_1 \ldots h_4}}}. \tag{4.1.2}$$

where the signal in the helicity configuration $S^{h_1 \ldots h_4}$ is linear in the coupling modifier δ_i. In what follows, we only consider the SM process $VV \to XY$ as our dominant background. It is straightforward to see that under our simplified assumption, for the case where statistical

error dominates, the dependence on the SM amplitude of the statistical significance cancels out:

$$\frac{S^{h_1\ldots h_4}}{\sqrt{B^{h_1\ldots h_4}}} \sim \frac{\sigma_{int}^{h_1\cdots h_4}}{\sqrt{\sigma_{\rm SM}^{h_1\cdots h_4}}} \sim \frac{\mathcal{M}_{\delta_i}^{h_1\cdots h_4}}{\hat{E}} \tag{4.1.3}$$

Note that we have neglected all the constant factors, like the integrated luminosity. Then we can see that in order for the significance to grow with energy, $\mathcal{M}_{\delta_i}$ must be at least quadratic in $\hat{E}$. This is certainly true for the Higgs gauge boson coupling modification in the vector boson scattering processes $V_LV_L \to V_LV_L$ and for the anomalous gauge boson fermion coupling in the $V_LV_L \to f\bar{f}$ processes. However for the top Yukawa coupling, we only have linear energy growing behavior and we expect that the significance stays constant as the bin energy increases. This does not mean the high energy bins are completely irrelevant, as one can still improve the significance by combing all the energy bins.

In reality, we cannot measure the helicities of the final states exactly and there is always contamination from other helicity categories. At the muon collider, it will likely be difficult to determine the initial gauge boson helicities, especially for the $W^\pm$ bosons. We now consider the inclusive case, where we sum over the cross sections from all the helicity configurations for the initial and final states. In this fully inclusive case, the statistical significance scales like:

$$\frac{S}{\sqrt{B}} \sim \frac{\sum_{h_1\ldots h_4}\sigma_{int}^{h_1\ldots h_4}}{\sqrt{\sum_{h_1\ldots h_4}\sigma_{SM}^{h_1\ldots h_4}}} \sim \frac{1}{\hat{E}}\sum_{h_1\cdots h_4}\mathcal{M}_{\rm SM}^{h_1\cdots h_4}\mathcal{M}_{\delta_i}^{h_1\cdots h_4} \tag{4.1.4}$$

where we have used the fact the inclusive SM cross section has the following energy scaling:

$$\sum_{h_1\ldots h_4}\sigma_{\rm SM}^{h_1\ldots h_4} \sim \frac{1}{\hat{E}^2} \tag{4.1.5}$$

We can see that in order for the significance to increase with energy, not only should the BSM helicity amplitude $\mathcal{M}_{\delta_i}^{h_1\cdots h_4}$ grow as $\hat{E}^2$, but the corresponding linearly mixing term $\mathcal{M}_{\rm SM}^{h_1\cdots h_4}$ should also stay constant as the energy increases [2]. Before studying the energy scaling of

[2] When taking into account the angular distributions of the decayed products of final particles, the require-

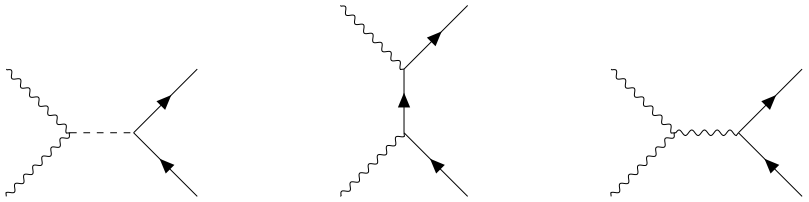

Fig. 4.1: Tree-level diagrams for $W^+W^- \to t\bar{t}$. The gauge boson propagator in the last diagrams can be either Z or γ.

the weak boson parton luminosity in detail, we comment on the systematic uncertainty. If the systematic error dominates, the signal significance becomes:

$$\frac{S^{h_1 \ldots h_4}}{B^{h_1 \ldots h_4}} \sim \frac{\sigma_{int}^{h_1 \cdots h_4}}{\sigma_{\rm SM}^{h_1 \cdots h_4}} \sim \frac{\mathcal{M}_{\delta_i}^{h_1 \cdots h_4}}{\mathcal{M}_{\rm SM}^{h_1 \cdots h_4}}. \tag{4.1.6}$$

while for the inclusive case, it reads:

$$\frac{S}{B} = \frac{\sum_{h1 \ldots h4} \sigma_{int}^{h_1 \ldots h_4}}{\sum_{h_1 \cdots h_4} \sigma_{\rm SM}^{h_1 \ldots h_4}} \sim \sum_{h_1 \cdots h_4} \mathcal{M}_{\rm SM}^{h_1 \cdots h_4} \mathcal{M}_{\delta_i}^{h_1 \cdots h_4} \tag{4.1.7}$$

In the exclusive case, since the SM helicity amplitudes $\mathcal{M}_{\rm SM}^{h_1 \cdots h_4}$ are at most a constant for the $2 \to 2$ processes, any energy growing behavior in the BSM amplitude $\mathcal{M}_{\delta_i}^{h_1 \cdots h_4}$ will lead to enhancement of the signal significance at high energy bins. This is especially the case at the hadron colliders like the LHC, as one generally has large systematic errors ranging from a few percent to tens of percents. For the inclusive case, similar to the statistical uncertainty dominance, we need both $\mathcal{M}_{\delta_i}^{h_1 \cdots h_4}$ to increase with energy and $\mathcal{M}_{\rm SM}^{h_1 \cdots h_4}$ to not decrease too quickly.

4.1.2 Anatomy of $W^+W^- \to t\bar{t}$

In this subsection, we focus on the VBF production of the top pair and study in detail the helicity amplitudes of the subprocess $W^+W^- \to t\bar{t}$ in the presence of anomalous couplings. The relevant Feynman diagrams are shown in Fig. 4.1. For completeness and also for future

ment may be relaxed as different helicity configurations of XY can interfere with each other [118, 119].

Table 4.1: High energy limit of the Helicity amplitude for $W^+W^- \to t\bar{t}$ with $h_t - h_{\bar{t}} = \mp 1$. Here $m_{\rm SM}$ denotes m_W, m_t, m_h.

$(h_t\, h_{\bar{t}})$	$(h_{W^+} h_{W^-})$	$\widetilde{\mathcal{M}}^{\rm SM}_{h_{W^+}h_{W^-};h_t\,h_{\bar{t}}}$	$\widetilde{\mathcal{M}}^{\rm BSM}_{h_{W^+}h_{W^-};h_t\,h_{\bar{t}}}$
$(-\frac{1}{2}\ \frac{1}{2})$	(+1 -1),(-1 +1)	$i\frac{g^2}{-1+\cos\theta}$	$\mathcal{O}(\delta_{Wtb})$
	(+1 +1),(-1 -1)	$\mathcal{O}(\frac{m^2_{\rm SM}}{\hat{E}^2})$	$i\frac{g^2\hat{E}^2(3\lambda_Z+4s^2_W(\lambda_\gamma-\lambda_Z))}{6\sqrt{2}m^2_W}$
	(+1 0),(0 -1)	$\mathcal{O}(\frac{m_{\rm SM}}{\hat{E}})$	$\mathcal{O}\left(\frac{\hat{E}}{m_{\rm SM}}(\delta g^Z_1, \delta\kappa_{Z,\gamma}, \delta_{Wtb}, \delta_{Zt_L}, \lambda_{Z,\gamma})\right)$
	(-1 0),(0 +1)	$\mathcal{O}(\frac{m_{\rm SM}}{\hat{E}})$	$\mathcal{O}\left(\frac{\hat{E}}{m_{\rm SM}}(\delta g^Z_1, \delta\kappa_{Z,\gamma}, \delta_{Wtb}, \delta_{Zt_L}, \lambda_{Z,\gamma})\right)$
	(0 0)	$i\frac{3g^2+g'^2}{6\sqrt{2}}$	$i\frac{g^2\hat{E}^2}{6\sqrt{2}m^2_W}\left((-3+4s^2_W)(\delta\kappa_Z+\delta_{Zt_L})+6\delta_{Wtb}-4s^2_W\delta\kappa_\gamma\right))$

$(h_t\, h_{\bar{t}})$	$(h_{W^+} h_{W^-})$	$\widetilde{\mathcal{M}}^{\rm SM}_{h_{W^+}h_{W^-};h_t\,h_{\bar{t}}}$	$\widetilde{\mathcal{M}}^{\rm BSM}_{h_{W^+}h_{W^-};h_t\,h_{\bar{t}}}$
$(\frac{1}{2}\ -\frac{1}{2})$	(+1 -1),(-1 +1)	$\mathcal{O}(\frac{m^2_{\rm SM}}{\hat{E}^2})$	$\mathcal{O}(\frac{m^2_{\rm SM}}{\hat{E}^2})$
	(+1 +1),(-1 -1)	$\mathcal{O}(\frac{m^2_{\rm SM}}{\hat{E}^2})$	$i\frac{\sqrt{2}g^2s^2_W\hat{E}^2(\lambda_\gamma-\lambda_Z)}{3m^2_W}$
	(+1 0),(0 -1)	$\mathcal{O}(\frac{m_{\rm SM}}{\hat{E}})$	$\mathcal{O}\left(\frac{\hat{E}}{m_{\rm SM}}(\delta g^Z_1, \delta\kappa_{Z,\gamma}, \delta_{Zt_R}, \lambda_{Z,\gamma})\right)$
	(-1 0),(0 +1)	$\mathcal{O}(\frac{m_{\rm SM}}{\hat{E}})$	$\mathcal{O}\left(\frac{\hat{E}}{m_{\rm SM}}(\delta g^Z_1, \delta\kappa_{Z,\gamma}, \delta_{Zt_R}, \lambda_{Z,\gamma})\right)$
	(0 0)	$i\frac{\sqrt{2}g'^2}{3}+i\frac{2\sqrt{2}m^2_t}{v^2(-1+\cos\theta)}$	$i\frac{\sqrt{2}g^2s^2_W\hat{E}^2}{3m^2_W}\left(\delta\kappa_Z-\delta\kappa_\gamma+\delta_{Zt_R}\right)$

possible studies, we also include the anomalous triple gauge boson couplings (aTGCs), the gauge boson fermion couplings and Higgs gauge boson coupling. The full formulae and the conventions are presented in the Appendix C (see Ref. [37, 120] for $tW \to tW$ helicity amplitudes). Here we discuss their high energy and threshold behaviors. We start from the high energy hard scattering limit and consider the central region, where $1 \pm \cos\theta$ is large enough to justify our expansion. As before, we denote $\hat{E} = \sqrt{\hat{s}}$. The results for the helicity-conserving configurations of the top quarks, i.e. $(h_t, h_{\bar{t}} = (\pm\frac{1}{2}, \mp\frac{1}{2}))$ are listed in Table 4.1, while the results for the helicity-violating configurations i.e. $(h_t, h_{\bar{t}} = (\pm\frac{1}{2}, \pm\frac{1}{2}))$ are presented in Table 4.2. The energy scaling for the helicity partonic cross section and the exclusive statistical significance is given in Table 4.3. Several comments are in order. First, for the SM helicity amplitudes, only the following helicity configurations survive in the high

Table 4.2: High energy limit of the Helicity amplitude for $W^+W^- \to t\bar{t}$ with $h_t - h_{\bar{t}} = 0$. Here $m_{\rm SM}$ denotes m_W, m_t, m_h.

$(h_t\, h_{\bar{t}})$	$(h_{W^+} h_{W^-})$	$\widetilde{\mathcal{M}}^{\rm SM}_{h_{W^+}h_{W^-};h_t\,h_{\bar{t}}}$	$\widetilde{\mathcal{M}}^{\rm BSM}_{h_{W^+}h_{W^-};h_t\,h_{\bar{t}}}$
$(-\frac{1}{2}\ \ -\frac{1}{2})$	(+1 -1),(-1 +1)	$\mathcal{O}(\frac{m_{\rm SM}}{\hat{E}})$	$\mathcal{O}(\frac{m_{\rm SM}}{\hat{E}}\delta_{Wtb})$
	(+1 +1)	$\mathcal{O}(\frac{m^3_{\rm SM}}{\hat{E}^3})$	$\mathcal{O}\left(\frac{\hat{E}}{m_{\rm SM}}\lambda_{Z,\gamma}\right)$
	(-1 -1)	$\mathcal{O}(\frac{m_{\rm SM}}{\hat{E}})$	$\mathcal{O}\left(\frac{\hat{E}}{m_{\rm SM}}\lambda_{Z,\gamma}\right)$
	(+1 0),(0 -1)	$\mathcal{O}(\frac{m^2_{\rm SM}}{\hat{E}^2})$	$\mathcal{O}\left(\delta g_1^Z, \delta\kappa_{Z,\gamma}, \delta_{Wtb}, \lambda_{Z,\gamma}, \delta_{Zt_L}, \delta_{Zt_R}\right)$
	(-1 0)	$ig^2\frac{m_t}{m_W(-1+\cos\theta)}$	$\mathcal{O}\left(\delta g_1^Z, \delta\kappa_{Z,\gamma}, \delta_{Wtb}, \lambda_{Z,\gamma}, \delta_{Zt_L}, \delta_{Zt_R}\right)$
	(0 +1)	$\mathcal{O}(\frac{m^2_{\rm SM}}{\hat{E}^2})$	$\mathcal{O}\left(\delta g_1^Z, \delta\kappa_{Z,\gamma}, \delta_{Wtb}, \lambda_{Z,\gamma}, \delta_{Zt_L}, \delta_{Zt_R}\right)$
	(0 0)	$\mathcal{O}(\frac{m_{\rm SM}}{\hat{E}})$	$-i\frac{g^2 m_t \hat{E}}{4m_W^2}\left(\delta_{hWW} + \delta_{tth} + \mathcal{O}(\delta\kappa_{Z,\gamma}, \delta_{Zt_L}, \delta_{Zt_R})\right)$

$(h_t\, h_{\bar{t}})$	$(h_{W^+} h_{W^-})$	$\widetilde{\mathcal{M}}^{\rm SM}_{h_{W^+}h_{W^-};h_t\,h_{\bar{t}}}$	$\widetilde{\mathcal{M}}^{\rm BSM}_{h_{W^+}h_{W^-};h_t\,h_{\bar{t}}}$
$(\frac{1}{2}\ \ \frac{1}{2})$	(+1 -1),(-1 +1)	$\mathcal{O}(\frac{m_{\rm SM}}{\hat{E}})$	$\mathcal{O}(\frac{m_{\rm SM}}{\hat{E}}\delta_{Wtb})$
	(+1 +1)	$\mathcal{O}(\frac{m_{\rm SM}}{\hat{E}})$	$\mathcal{O}(\frac{\hat{E}}{m_{\rm SM}}\lambda_{Z,\gamma})$
	(-1 -1)	$\mathcal{O}(\frac{m^3_{\rm SM}}{\hat{E}^3})$	$\mathcal{O}(\frac{\hat{E}}{m_{\rm SM}}\lambda_{Z,\gamma})$
	(+1 0),(0 -1)	$\mathcal{O}(\frac{m^2_{\rm SM}}{\hat{E}^2})$	$\mathcal{O}\left(\delta g_1^Z, \delta\kappa_{Z,\gamma}, \delta_{Wtb}, \lambda_{Z,\gamma}, \delta_{Zt_L}, \delta_{Zt_R}\right)$
	(-1 0)	$\mathcal{O}(\frac{m^2_{\rm SM}}{\hat{E}^2})$	$\mathcal{O}\left(\delta g_1^Z, \delta\kappa_{Z,\gamma}, \delta_{Wtb}, \lambda_{Z,\gamma}, \delta_{Zt_L}, \delta_{Zt_R}\right)$
	(0 +1)	$ig^2\frac{m_t}{m_W(1-\cos\theta)}$	$\mathcal{O}\left(\delta g_1^Z, \delta\kappa_{Z,\gamma}, \delta_{Wtb}, \lambda_{Z,\gamma}, \delta_{Zt_L}, \delta_{Zt_R}\right)$
	(0 0)	$\mathcal{O}(\frac{m_{\rm SM}}{\hat{E}})$	$i\frac{g^2 m_t \hat{E}}{4m_W^2}\left(\delta_{hWW} + \delta_{tth} + \mathcal{O}(\delta\kappa_{Z,\gamma}, \delta_{Zt_L}, \delta_{Zt_R})\right)$

energy limit:

$$(h_{W^+}, h_{W^-}, h_t, h_{\bar{t}}) = (\pm1, \mp1, -\frac{1}{2}, \frac{1}{2}), \quad (0, 0, \mp\frac{1}{2}, \pm\frac{1}{2}), \quad (-1, 0, -\frac{1}{2}, -\frac{1}{2}), \qquad (0, 1, \frac{1}{2}, \frac{1}{2}) \tag{4.1.8}$$

The results can be understood by using the Goldstone equivalence theorem and by working in the electroweak-symmetry-unbroken phase of the SM where the Goldstone scalars $\phi_\pm$ appear as external states and the SM gauge bosons and top quarks are massless particles. For the longitudinal $W^\pm$ bosons processes, we can see that the $SU(2)_L \times U(1)_Y$ quantum

numbers of the top quarks appear in the helicity amplitudes:

$$T_3^L(t_{L,R})g^2 + Y(t_{L,R})g'^2 \tag{4.1.9}$$

where T_3^L is the third weak isospin generator and Y is the hypercharge. The presence of the SM top Yukawa coupling squared term m_t^2/v^2 associated with t-channel pole in the $(0, 0, \frac{1}{2}, -\frac{1}{2})$ configuration is due to left-handed bottom quark exchange diagram in the $\phi^+\phi^- \to t\bar{t}$ process. Note that if the bottom quark mass were not set to zero in our calculation, there would be a similar term with m_b^2/v^2 in the $(0, 0, -\frac{1}{2}, \frac{1}{2})$ configuration. Following this reasoning, we can understand the processes involving only one longitudinal gauge bosons $W^\pm\phi^\mp \to t\bar{t}$.

Table 4.3: Energy scaling for cross sections and statistical signal significance of $W^+W^- \to t\bar{t}$ in different helicity categories with different anomalous couplings. The results for δ_{hWW} has the same behavior as δ_{tth} and therefore are not shown here.

$(h_{W^+}, h_{W^-}, h_t, h_{\bar{t}})$	$\hat{\sigma}_{\rm SM}$	$\hat{\sigma}_{\delta_{tth}}$	$\hat{\sigma}_{\lambda_{Z,\gamma}}$	$\hat{\sigma}_{\delta\kappa_{Z,\gamma}}$	$\hat{\sigma}_{\delta_{Wtb}}$	$\hat{\sigma}_{Zt_L}$	$\hat{\sigma}_{Zt_R}$	$\hat{\sigma}_{\delta g_1^Z}$	$\frac{S_{\delta_{tth}}}{\sqrt{B}}$	$\frac{S_{\lambda_{Z,\gamma}}}{\sqrt{B}}$	$\frac{S_{\delta\kappa_{Z,\gamma}}}{\sqrt{B}}$	$\frac{S_{\delta_{Wtb}}}{\sqrt{B}}$	$\frac{S_{\delta_{Zt_L}}}{\sqrt{B}}$	$\frac{S_{\delta_{Zt_R}}}{\sqrt{B}}$	$\frac{S_{\delta g_1^Z}}{\sqrt{B}}$
$(0, 0, -, +)$	$\frac{1}{\hat{E}^2}$	$\times$	$\times$	$\hat{E}^0$	$\hat{E}^0$	$\hat{E}^0$	$\times$	$\times$	$\times$	$\times$	$\hat{\boldsymbol{E}}$	$\hat{\boldsymbol{E}}$	$\hat{\boldsymbol{E}}$	$\times$	$\times$
$(0, 0, +, -)$	$\frac{1}{\hat{E}^2}$	$\times$	$\times$	$\hat{E}^0$	$\times$	$\times$	$\hat{E}^0$	$\times$	$\times$	$\times$	$\hat{\boldsymbol{E}}$	$\times$	$\times$	$\hat{\boldsymbol{E}}$	$\times$
$(0, 0, \mp, \mp)$	$\frac{1}{\hat{E}^4}$	$\frac{1}{\hat{E}^2}$	$\times$	$\frac{1}{\hat{E}^2}$	$\times$	$\frac{1}{\hat{E}^2}$	$\frac{1}{\hat{E}^2}$	$\times$	$\hat{E}^0$	$\times$	$\hat{E}^0$	$\times$	$\hat{E}^0$	$\hat{E}^0$	$\times$
$(0, +, +, +)$	$\frac{1}{\hat{E}^2}$	$\times$	$\frac{1}{\hat{E}^2}$	$\frac{1}{\hat{E}^2}$	$\frac{1}{\hat{E}^2}$	$\frac{1}{\hat{E}^2}$	$\frac{1}{\hat{E}^2}$	$\frac{1}{\hat{E}^2}$	$\times$	$\frac{1}{\hat{E}}$	$\frac{1}{\hat{E}}$	$\frac{1}{\hat{E}}$	$\frac{1}{\hat{E}}$	$\frac{1}{\hat{E}}$	$\frac{1}{\hat{E}}$
$(-, 0, -, -)$															
$(0, +, -, -)$	$\frac{1}{\hat{E}^6}$	$\times$	$\frac{1}{\hat{E}^4}$	$\frac{1}{\hat{E}^4}$	$\frac{1}{\hat{E}^4}$	$\frac{1}{\hat{E}^4}$	$\frac{1}{\hat{E}^4}$	$\frac{1}{\hat{E}^4}$	$\times$	$\frac{1}{\hat{E}}$	$\frac{1}{\hat{E}}$	$\frac{1}{\hat{E}}$	$\frac{1}{\hat{E}}$	$\frac{1}{\hat{E}}$	$\frac{1}{\hat{E}}$
$(-, 0, +, +)$															
$(+, 0, -, -)$	$\frac{1}{\hat{E}^6}$	$\times$	$\frac{1}{\hat{E}^4}$	$\frac{1}{\hat{E}^4}$	$\frac{1}{\hat{E}^4}$	$\frac{1}{\hat{E}^4}$	$\frac{1}{\hat{E}^4}$	$\frac{1}{\hat{E}^4}$	$\times$	$\frac{1}{\hat{E}}$	$\frac{1}{\hat{E}}$	$\frac{1}{\hat{E}}$	$\frac{1}{\hat{E}}$	$\frac{1}{\hat{E}}$	$\frac{1}{\hat{E}}$
$(0, -, -, -)$															
$(0, -, +, +)$	$\frac{1}{\hat{E}^6}$	$\times$	$\frac{1}{\hat{E}^4}$	$\frac{1}{\hat{E}^4}$	$\frac{1}{\hat{E}^4}$	$\frac{1}{\hat{E}^4}$	$\frac{1}{\hat{E}^4}$	$\frac{1}{\hat{E}^4}$	$\times$	$\frac{1}{\hat{E}}$	$\frac{1}{\hat{E}}$	$\frac{1}{\hat{E}}$	$\frac{1}{\hat{E}}$	$\frac{1}{\hat{E}}$	$\frac{1}{\hat{E}}$
$(+, 0, +, +)$															
$(+, 0, -, +)$	$\frac{1}{\hat{E}^4}$	$\times$	$\frac{1}{\hat{E}^2}$	$\frac{1}{\hat{E}^2}$	$\frac{1}{\hat{E}^2}$	$\frac{1}{\hat{E}^2}$	$\times$	$\frac{1}{\hat{E}^2}$	$\times$	$\hat{E}^0$	$\hat{E}^0$	$\hat{E}^0$	$\hat{E}^0$	$\times$	$\hat{E}^0$
$(0, -, -, +)$															
$(-, 0, -, +)$	$\frac{1}{\hat{E}^4}$	$\times$	$\frac{1}{\hat{E}^2}$	$\frac{1}{\hat{E}^2}$	$\frac{1}{\hat{E}^2}$	$\frac{1}{\hat{E}^2}$	$\times$	$\frac{1}{\hat{E}^2}$	$\times$	$\hat{E}^0$	$\hat{E}^0$	$\hat{E}^0$	$\hat{E}^0$	$\times$	$\hat{E}^0$
$(0, +, -, +)$															
$(+, 0, +, -)$	$\frac{1}{\hat{E}^4}$	$\times$	$\frac{1}{\hat{E}^2}$	$\frac{1}{\hat{E}^2}$	$\times$	$\times$	$\frac{1}{\hat{E}^2}$	$\frac{1}{\hat{E}^2}$	$\times$	$\hat{E}^0$	$\hat{E}^0$	$\times$	$\times$	$\hat{E}^0$	$\hat{E}^0$
$(0, -, +, -)$															
$(-, 0, +, -)$	$\frac{1}{\hat{E}^4}$	$\times$	$\frac{1}{\hat{E}^2}$	$\frac{1}{\hat{E}^2}$	$\times$	$\times$	$\frac{1}{\hat{E}^2}$	$\frac{1}{\hat{E}^2}$	$\times$	$\hat{E}^0$	$\hat{E}^0$	$\times$	$\times$	$\hat{E}^0$	$\hat{E}^0$
$(0, +, +, -)$															
$(\pm, \mp, -, +)$	$\frac{1}{\hat{E}^2}$	$\times$	$\times$	$\times$	$\frac{1}{\hat{E}^2}$	$\times$	$\times$	$\times$	$\times$	$\times$	$\times$	$\frac{1}{\hat{E}}$	$\times$	$\times$	$\times$
$(+, +, -, -)$	$\frac{1}{\hat{E}^8}$	$\times$	$\frac{1}{\hat{E}^4}$	$\times$	$\times$	$\times$	$\times$	$\times$	$\times$	$\hat{E}^0$	$\times$	$\times$	$\times$	$\times$	$\times$
$(-, -, -, -)$	$\frac{1}{\hat{E}^4}$	$\times$	$\frac{1}{\hat{E}^2}$	$\times$	$\times$	$\times$	$\times$	$\times$	$\times$	$\hat{E}^0$	$\times$	$\times$	$\times$	$\times$	$\times$
$(\pm, \mp, -, -)$	$\frac{1}{\hat{E}^4}$	$\times$	$\times$	$\times$	$\frac{1}{\hat{E}^4}$	$\times$	$\times$	$\times$	$\times$	$\times$	$\times$	$\frac{1}{\hat{E}^2}$	$\times$	$\times$	$\times$
$(\pm, \mp, +, +)$	$\frac{1}{\hat{E}^4}$	$\times$	$\times$	$\times$	$\frac{1}{\hat{E}^4}$	$\times$	$\times$	$\times$	$\times$	$\times$	$\times$	$\frac{1}{\hat{E}^2}$	$\times$	$\times$	$\times$
$(+, +, +, +)$	$\frac{1}{\hat{E}^4}$	$\times$	$\frac{1}{\hat{E}^2}$	$\times$	$\times$	$\times$	$\times$	$\times$	$\times$	$\hat{E}^0$	$\times$	$\times$	$\times$	$\times$	$\times$
$(-, -, +, +)$	$\frac{1}{\hat{E}^8}$	$\times$	$\frac{1}{\hat{E}^4}$	$\times$	$\times$	$\times$	$\times$	$\times$	$\times$	$\hat{E}^0$	$\times$	$\times$	$\times$	$\times$	$\times$
$(\pm, \pm, -, +)$	$\frac{1}{\hat{E}^6}$	$\times$	$\frac{1}{\hat{E}^2}$	$\times$	$\times$	$\times$	$\times$	$\times$	$\times$	$\hat{\boldsymbol{E}}$	$\times$	$\times$	$\times$	$\times$	$\times$
$(\pm, \pm, +, -)$	$\frac{1}{\hat{E}^6}$	$\times$	$\frac{1}{\hat{E}^2}$	$\times$	$\times$	$\times$	$\times$	$\times$	$\times$	$\hat{\boldsymbol{E}}$	$\times$	$\times$	$\times$	$\times$	$\times$

Secondly, we can see from the Table 4.1 that for the anomalous triple gauge boson couplings $\delta\kappa_{Z,\gamma}$ in the $(\mp\frac{1}{2},\pm\frac{1}{2})$ top quark pair helicities and the anomalous top quark electroweak coupling $\delta_{Wtb},\delta_{Zt_L}(\delta_{Zt_R})$ in the $(-\frac{1}{2},\frac{1}{2})$ ($(\frac{1}{2},-\frac{1}{2})$) top quark pair helicities, the helicity amplitudes from longitudinal gauge bosons scale like $\hat{E}^2$, while the SM contributions stay constant in the high energy limit. As discussed above, this means that for both the exclusive channel with all the helicities of the particles fully measured and the inclusive channel where all the helicity configurations are included, the statistical significance scales like $\hat{E}$, which results in larger sensitivity for higher energy bins. However, for the modification of the top Yukawa coupling δ_{tth} in the high energy limit [3], the helicity amplitude only grows linearly as $\hat{E}$ in the $(0,0,\mp\frac{1}{2},\mp\frac{1}{2})$ helicity configuration and the SM contribution decreases like $1/\hat{E}$. This in turn leads to the constant behavior for the statistical significance in the exclusive channel and decreasing statistical significance as $\mathcal{O}(1/\hat{E})$ in the inclusive channel. This means that in the realistic case at the muon collider, the sensitivity on the top Yukawa coupling from the electroweak top pair production would mostly come from low energy bins. The high energy muon collider benefits us from the growth of the VBF cross sections, i.e. the enhancement of the vector boson parton luminosity. We finally note that for the case of systematical uncertainty dominance, the significance grows as energy increases for all anomalous couplings in the exclusive channel. For the fully inclusive channel, the significance grows as $\hat{E}^2$ for the anomalous couplings $\delta\kappa_{Z,\gamma},\delta_{Wtb},\delta_{Zt_L},\delta_{Zt_R}$, but stays constant for aTGC $\lambda_{Z,\gamma}$ and the anomalous top Yukawa coupling δ_{tth}.

Now we examine the threshold behavior of top quark electroweak pair production. We expand the helicity amplitudes in terms of the top quark velocity β_t around the $\sqrt{s}\sim 2m_t$. For simplicity, we also keep only the leading power of $m_{W,Z}^2/m_t^2$. The results are presented in Table 4.4 for the helicity configurations $(h_t,h_{\bar{t}})=(\mp\frac{1}{2},\pm\frac{1}{2})$ and listed in Table 4.5 for the helicity configurations $(h_t,h_{\bar{t}})=(\mp\frac{1}{2},\mp\frac{1}{2})$. We can see from the tables that all the SM helicity amplitudes arise at the zeroth order of top quark velocity β_t^0 except the helicity

[3] Likewise for the anomalous Higgs gauge boson coupling δ_{hWW}, as only the combination of $\delta_{tth}+\delta_{hWW}$ appears in the helicity amplitudes at linear order.

Table 4.4: Threshold behaviors of the Helicity amplitude for $W^+W^- \to t\bar{t}$ with $h_t - h_{\bar{t}} = \mp 1$. Here we keep the leading terms in the top velocity β_t expansion and $\frac{m_{W,Z}^2}{m_t^2}$ expansion.

$(h_t\, h_{\bar{t}})$	$(h_{W^+}\, h_{W^-})$	$\widetilde{\mathcal{M}}^{\rm SM}_{h_{W^+}h_{W^-};h_t h_{\bar{t}}}$	$\widetilde{\mathcal{M}}^{\rm BSM}_{h_{W^+}h_{W^-};h_t h_{\bar{t}}}$
$(\mp\frac{1}{2}\ \ \pm\frac{1}{2})$	(+1 -1),(-1 +1)	$\mathcal{O}(\beta_t)$	$\mathcal{O}(\beta_t \delta_{Wtb})$
	(+1 +1),(-1 -1)	$-i\frac{g^2}{2\sqrt{2}}$	$i\frac{g^2(3\lambda_Z+8s_W^2(\lambda_\gamma-\lambda_Z))m_t^2}{3\sqrt{2}m_W^2}$
	(+1 0),(0 -1)	$-i\frac{g^2 m_t}{\sqrt{2}m_W}$	$\mathcal{O}\left(\frac{m_t}{m_W}(\delta_{Wtb}, \lambda_{Z,\gamma}, \delta g_1^Z, \delta\kappa_{Z,\gamma}, \delta_{Zt_L}, \delta_{Zt_R})\right)$
	(-1 0),(0 +1)	$-i\frac{g^2 m_t}{\sqrt{2}m_W}$	$\mathcal{O}\left(\frac{m_t}{m_W}(\lambda_{Z,\gamma}, \delta g_1^Z, \delta\kappa_{Z,\gamma}, \delta_{Zt_L}, \delta_{Zt_R})\right)$
	(0 0)	$-i\frac{g^2 m_t^2}{\sqrt{2}m_W^2}$	$i\frac{g^2(-3(\delta\kappa_Z+\delta_{Zt_L})+4s_W^2(2\delta\kappa_Z-2\delta\kappa_\gamma+\delta_{Zt_L}+\delta_{Zt_R}))m_t^2}{3\sqrt{2}m_W^2}$

configurations for $(h_{W^+}, h_{W^-}) = (\pm 1, \mp 1)$ as they arise from the $J \geq 2$ partial waves. We also find that for the processes involving the longitudinal W bosons, there is an additional factor of m_t/m_W enhancement for each longitudinal mode. For the anomalous TGCs $\delta\kappa_{Z,\gamma}$ in the helicity configuration of the longitudinal $W^\pm$ bosons and $\lambda_{Z,\gamma}$ in the helicity configurations $(h_{W^+}, h_{W^-}) = (\pm 1, \pm 1))$, the amplitudes at threshold are enhanced by m_t^2/m_W^2 for all the helicity configurations of top quark pair. Since the SM contribution to amplitudes of $(h_{W^+}, h_{W^-}) = (\pm 1, \pm 1))$ at threshold are not suppressed, it provides an interesting possibility to measure aTGCs $\lambda_{Z,\gamma}$, which we leave for future studies. For the top Yukawa coupling modification δ_{tth}, its leading contribution to the longitudinal $W^\pm$ gauge boson arises at order β_t, which means that the linear BSM helicity cross sections arise at β_t^2 [4]. The statistical significance will scale like $\beta_t^{3/2}$ in the small β_t approximation and we need to have sizable top quark velocity to achieve maximal sensitivity.

We finally comment on the scattering angle θ distribution, where θ is the polar angle between the outgoing top quark and incoming W^+ boson. As is well-known, there is a $t-$channel singularity in the cross section of this process, which can seen from the high energy limit in Table 4.1 and appears in the helicity configuration $(h_{W^+}, h_{W^-}, h_t, h_{\bar{t}}) = (-1, +1, -\frac{1}{2}, \frac{1}{2})$. Note that to obtain the θ distribution for the helicity amplitudes, one needs

[4] The extra β_t comes in because the final two-body phase space has linear dependence on the velocity of the top quark.

Table 4.5: Threshold behaviors of the Helicity amplitude for $W^+W^- \to t\bar{t}$ with $h_t - h_{\bar{t}} = 0$. Here we keep the leading terms in the top velocity β_t expansion and $\frac{m_{W,Z}^2}{m_t^2}$ expansion.

$(h_t\, h_{\bar{t}})$	$(h_{W^+} h_{W^-})$	$\widetilde{\mathcal{M}}^{\rm SM}_{h_{W^+}h_{W^-};h_t h_{\bar{t}}}$	$\widetilde{\mathcal{M}}^{\rm BSM}_{h_{W^+}h_{W^-};h_t h_{\bar{t}}}$
$(-\frac{1}{2}\ \ -\frac{1}{2})$	(+1 -1),(-1 +1)	$\mathcal{O}(\beta_t)$	$\mathcal{O}(\beta_t \delta_{Wtb})$
	(+1 +1),(-1,-1)	$ig^2 \frac{\pm 2 - \cos\theta}{4}$	$i\frac{g^2(3\lambda_Z + 8s_W^2(\lambda_\gamma - \lambda_Z))m_t^2 \cos\theta}{6m_W^2}$
	(+1 0),(0 -1)	$-ig^2 \frac{m_t}{2m_W}$	$\mathcal{O}\left(\frac{m_t}{m_W}(\delta_{Wtb}, \lambda_{Z,\gamma}, \delta g_1^Z, \delta\kappa_{Z,\gamma}, \delta_{Zt_L}, \delta_{Zt_R})\right)$
	(-1 0),(0,+1)	$-ig^2 \frac{m_t}{2m_W}$	$\mathcal{O}\left(\frac{m_t}{m_W}(\lambda_{Z,\gamma}, \delta g_1^Z, \delta\kappa_{Z,\gamma}, \delta_{Zt_L}, \delta_{Zt_R})\right)$
	(0 0)	$-i\frac{g^2 m_t^2}{2m_W^2}\cos\theta$	$i\frac{g^2(-3\delta(\kappa_Z + \delta_{Zt_L}) + 4s_W^2(2\delta\kappa_Z - 2\delta\kappa_\gamma + \delta_{Zt_L} + \delta_{Zt_R}))m_t^2 \cos\theta}{6m_W^2}$ $+i\frac{2g^2 m_t^4 \beta_t(\delta_{tth} + \delta_{hWW})}{(m_h^2 - 4m_t^2)m_W^2}$

$(h_t\, h_{\bar{t}})$	$(h_{W^+} h_{W^-})$	$\widetilde{\mathcal{M}}^{\rm SM}_{h_{W^+}h_{W^-};h_t h_{\bar{t}}}$	$\widetilde{\mathcal{M}}^{\rm BSM}_{h_{W^+}h_{W^-};h_t h_{\bar{t}}}$
$(\frac{1}{2}\ \ \frac{1}{2})$	(+1 -1),(-1 +1)	$\mathcal{O}(\beta_t)$	$\mathcal{O}(\beta_t \delta_{Wtb})$
	(+1 +1),(-1,-1)	$ig^2 \frac{\pm 2 + \cos\theta}{4}$	$-i\frac{g^2(3\lambda_Z + 8s_W^2(\lambda_\gamma - \lambda_Z))m_t^2 \cos\theta}{6m_W^2}$
	(+1 0),(0 -1)	$ig^2 \frac{m_t}{2m_W}$	$\mathcal{O}\left(\frac{m_t}{m_W}(\delta_{Wtb}, \lambda_{Z,\gamma}, \delta g_1^Z, \delta\kappa_{Z,\gamma}, \delta_{Zt_L}, \delta_{Zt_R})\right)$
	(-1 0),(0,+1)	$ig^2 \frac{m_t}{2m_W}$	$\mathcal{O}\left(\frac{m_t}{m_W}(\lambda_{Z,\gamma}, \delta g_1^Z, \delta\kappa_{Z,\gamma}, \delta_{Zt_L}, \delta_{Zt_R})\right)$
	(0 0)	$i\frac{g^2 m_t^2}{2m_W^2}\cos\theta$	$-i\frac{g^2(-3\delta(\kappa_Z + \delta_{Zt_L}) + 4s_W^2(2\delta\kappa_Z - 2\delta\kappa_\gamma + \delta_{Zt_L} + \delta_{Zt_R}))m_t^2 \cos\theta}{6m_W^2}$ $-i\frac{2g^2 m_t^4 \beta_t(\delta_{tth} + \delta_{hWW})}{(m_h^2 - 4m_t^2)m_W^2}$

to bring back the Wigner d-functions. For the t-channel singularity, the relevant functions are as follows:

$$d^2_{-2,-1} = \frac{1}{2}\sin\theta(1+\cos\theta), \qquad d^2_{2,-1} = -\frac{1}{2}\sin\theta(1-\cos\theta) \tag{4.1.10}$$

We can see that for other helicity configuration $(h_{W^+}, h_{W^-}, h_t, h_{\bar{t}}) = (+1, -1, -\frac{1}{2}, \frac{1}{2})$, the t-channel pole is cancelled by the kinematical zero in the Wigner function $d^2_{2,-1}(\theta)$. The differential helicity cross section with respect to $\cos\theta$ for the t-channel singularity in the high energy limit scales like:

$$\frac{d\sigma^{(h_{W^+}, h_{W^-})=(+1,-1)}}{d\cos\theta} \sim \frac{\sin^2\theta(1+\cos\theta)^2}{(1-\cos\theta)^2} \sim \frac{(1+\cos\theta)^3}{1-\cos\theta} \tag{4.1.11}$$

which strongly peaks in the forward region with an enhanced factor of $s/4m_t^2$. On the other hand, the anomalous top Yukawa coupling δ_{tth} appears in the longitudinal gauge bosons helicity configuration and the differential cross section in the high energy limit reads:

$$\frac{d\sigma^{(h_{W^+},h_{W^-})=(0,0)}}{d\cos\theta} \sim \sin^2\theta \tag{4.1.12}$$

which has its maximum near the central region $\theta \sim \pi/2$. This means that at the high energy bin, the sensitivity on the top Yukawa coupling measurement will mostly come from the central region where the transverse W-PDFs are suppressed.

At the threshold, the top quark pair production from the longitudinal gauge bosons fusion is enhanced by a factor of m_t^4/m_W^4. By focusing on this helicity category, the statistical significance for the top Yukawa coupling behaves as:

$$\frac{S}{\sqrt{B}} \sim \sin\theta\cos\theta \tag{4.1.13}$$

where for the SM background, we only include the helicity conserving top quark pair production, i.e., $(h_t, h_{\bar{t}}) = (\mp\frac{1}{2}, \pm\frac{1}{2})$, which is a factor of 2 larger than the helicity violating ones. The significance peaks around $\theta \sim \pi/4$.

4.1.3 Weak Boson PDF and Energy Scaling Behavior

In this section, we analyze the energy scaling behavior of $\mu^+\mu^- \to X\bar{X}\nu\bar{\nu}$ processes by making use of the Effective W-boson Approximation (EWA) [115–117]. As illustrated in Fig. 4.2. EWA states that at sufficiently high energies and suitable kinematical regimes, the cross section for the process $\mu^+\mu^- \to X\bar{X}\nu\bar{\nu}$ can be factorized into the on-shell hard subprocess $V\bar{V} \to X\bar{X}$ convoluted with the W-boson parton distribution functions:

$$\sigma(\mu^+\mu^- \to X\bar{X}\nu\bar{\nu})(s) = \int_{\tau_0}^{1} d\tau \sum_{ij} \Phi_{ij}(\tau, \mu_f)\hat{\sigma}(ij \to X\bar{X})(\tau s) \tag{4.1.14}$$

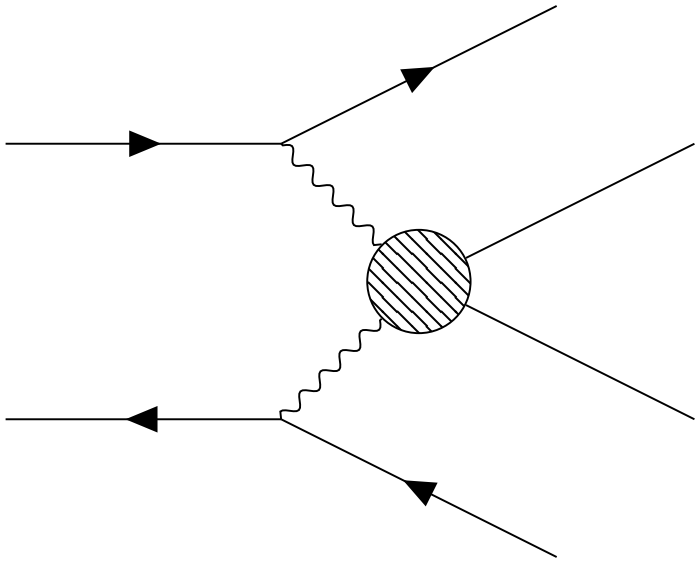

Fig. 4.2: Illustration of the EWA approximation at the muon collider.

where $\sqrt{s}$ is the center-of-mass energy of muons and $\sqrt{\hat{s}} = \sqrt{\tau s}$ is the center-of-mass energy of the $X\bar{X}$. Here $V = W^{\pm}, Z$ denotes any of the SM massive electroweak gauge bosons [5]. The parton luminosity $\Phi_{ij}(\tau, \mu_f)$ is given by [8]:

$$\Phi_{ij}(\tau, \mu_f) = \int_{\tau}^{1} \frac{d\xi}{\xi} f_i(\xi, \mu_f) f_j(\frac{\tau}{\xi}, \mu_f) \tag{4.1.15}$$

Here μ_f is the factorization scale in the process under study and the weak boson PDFs at muon collider read:

$$\begin{aligned} f_{V_\lambda}(\xi, \mu_f, \lambda = \pm 1) &= \frac{C}{16\pi^2} \frac{(g_V^\mu \mp g_A^\mu)^2 + (g_V^\mu \pm g_A^\mu)^2 (1-\xi)^2}{\xi} \log\left(\frac{\mu_f^2}{M_V^2}\right) \\ f_{V_0}(\xi, \mu_f, \lambda = 0) &= \frac{C}{4\pi^2} \left((g_V^\mu)^2 + (g_A^\mu)^2\right) \left(\frac{1-\xi}{\xi}\right) \end{aligned} \tag{4.1.16}$$

The coupling constants C, g_V^μ, g_A^μ denote the corresponding muon-weak-boson couplings and for the $W^{\pm}$-boson, it reads:

$$C = \frac{g^2}{2}, \qquad g_V^\mu = -g_A^\mu = 1 \tag{4.1.17}$$

[5] We will not discuss about the $\gamma\gamma$ PDF here.

while for the Z-boson, we have:

$$C = \frac{g^2}{\cos^2\theta_W}, \qquad g_V^\mu = \frac{1}{2}(T_L^3)^\mu + \sin^2\theta_W, \qquad g_A = -\frac{1}{2}(T_L^3)^\mu \tag{4.1.18}$$

where we have neglected the masses of the muons. Note that $(T_L^3)^{\mu_L} = -\frac{1}{2}, (T_L^3)^{\mu_R} = 0$. We will focus on the W^+W^- parton luminosity, since it is dominant compared with ZZ. To obtain the energy scaling behavior of the parton luminosity $\Phi_{W^+W^-}$, we first divide the allowed values of the parameter τ into four regions: [10^{-4}, 0.01], [0.01,0.2], [0.2,0.8],[0,8,0.95] and then approximate the dependence of $\Phi_{W^+W^-}$ on τ as τ^{-n} in each region. The results are shown in Table 4.6, where we neglected the scale-dependent logarithmic terms [6]. Recalling the relations $\tau = \frac{\hat{s}}{s}$ and $\sqrt{\hat{s}} = \hat{E}$, the dependence on τ can be translated into the dependence on the invariant mass of W^+W^- system $\hat{E}^{-2n}$ for constant invariant mass of $\mu^+\mu^-$ system. We can see that due to the absence of $(1-\xi)^2$ term in Eq. (4.1.16) for the plus helicity of the W boson, the parton luminosity $\Phi_{W^+W^-}(\tau)$ in the $(h_{W^+}, h_{W^-}) = (+,+)$ category has the most mildest decrease as τ increases.

Table 4.6: Best fit for $\Phi_{W^+W^-}$ for different ranges of τ without including the log terms.

h_{W^+}	h_{W^-}	$10^{-4} \leq \tau \leq 0.01$	$0.01 \leq \tau \leq 0.2$	$0.2 \leq \tau \leq 0.8$	$0.8 \leq \tau \leq 0.95$
-	-	$\frac{1}{\tau^{1.2}}$	$\frac{1}{\tau^{1.7}}$	$\frac{1}{\tau^{3.9}}$	$\frac{1}{\tau^{27}}$
0	0	$\frac{1}{\tau^{1.2}}$	$\frac{1}{\tau^{1.5}}$	$\frac{1}{\tau^{3.0}}$	$\frac{1}{\tau^{18}}$
+	+	$\frac{1}{\tau^{1.1}}$	$\frac{1}{\tau^{1.3}}$	$\frac{1}{\tau^{2.1}}$	$\frac{1}{\tau^{8.0}}$
-	+	$\frac{1}{\tau^{1.2}}$	$\frac{1}{\tau^{1.4}}$	$\frac{1}{\tau^{2.9}}$	$\frac{1}{\tau^{18}}$
+	-	$\frac{1}{\tau^{1.2}}$	$\frac{1}{\tau^{1.4}}$	$\frac{1}{\tau^{2.9}}$	$\frac{1}{\tau^{18}}$
-	0	$\frac{1}{\tau^{1.2}}$	$\frac{1}{\tau^{1.5}}$	$\frac{1}{\tau^{3.4}}$	$\frac{1}{\tau^{22}}$
0	-	$\frac{1}{\tau^{1.2}}$	$\frac{1}{\tau^{1.5}}$	$\frac{1}{\tau^{3.4}}$	$\frac{1}{\tau^{22}}$
+	0	$\frac{1}{\tau^{1.1}}$	$\frac{1}{\tau^{1.4}}$	$\frac{1}{\tau^{2.5}}$	$\frac{1}{\tau^{13}}$
0	+	$\frac{1}{\tau^{1.1}}$	$\frac{1}{\tau^{1.4}}$	$\frac{1}{\tau^{2.5}}$	$\frac{1}{\tau^{13}}$

Then from Eq. (4.1.14), we can see that the differential cross section in the invariant

[6] We have checked that the results won't be changed significantly by including the log terms.

mass of $X\bar{X}$ becomes

$$\frac{d\sigma}{d\hat{E}}(\mu^+\mu^- \to X\bar{X}\nu\bar{\nu}) = \frac{2\hat{E}}{s}\sum_{h_2,h_2}\Phi_{W^+_{h_1}W^-_{h_2}}(\hat{E})\hat{\sigma}(W^+_{h_1}W^-_{h_2} \to X\bar{X}). \tag{4.1.19}$$

Now for the most ideal scenario where the helicities of the initial and final particles can be measured and assuming that statistical error is dominant, the signal significance scales like:

$$\frac{S}{\sqrt{B}} \sim \frac{\frac{d\sigma_S}{d\hat{E}}}{\sqrt{\frac{d\sigma_B}{d\hat{E}}}} \sim \sqrt{\frac{\Phi_{W^+_{h_1}W^-_{h_2}}}{\hat{E}}}\mathcal{M}^{h_1h_2h_3h_4}_{\delta_i} \sim \frac{\mathcal{M}^{h_1h_2h_3h_4}_{\delta_i}}{\hat{E}^{n+\frac{1}{2}}} \tag{4.1.20}$$

where we have used the energy scaling of the parton luminosity $\Phi_{W^+W^-} \sim \hat{E}^{-2n}$ and keep the center-of-mass energy of the muons $\sqrt{s}$ as constant. From Table 4.6, we can see that the statistical significance decreases for the linear energy growth of BSM helicity amplitude in the whole considered regions and increases or stays constant for the quadratic energy growth for $\tau \in [10^{-4}, 0.2]$. For higher τ values ($\tau \gtrsim 0.2$), the statistical significance decreases at least as $\hat{E}^{-1}$ for the quadratic energy growth of the BSM helicity amplitude. Similar conclusion holds for the fully inclusive case if we replace $\mathcal{M}^{h_1\cdots h_4}_{\delta_i}$ with $\mathcal{M}^{h_1\cdots h_4}_{\delta_i}\mathcal{M}^{h_1\cdots h_4}_{\rm SM}$, as can be seen from the energy scaling of the statistical signal significance as follows:

$$\frac{S}{\sqrt{B}} \sim \frac{\frac{d\sigma_S}{d\hat{E}}}{\sqrt{\frac{d\sigma_B}{d\hat{E}}}} \sim \frac{1}{\sqrt{\hat{E}}}\frac{\sum_{h_1\cdots h_4}\Phi_{W^+_{h_1}W^-_{h_2}}\mathcal{M}^{h_1\cdots h_4}_{\rm SM}\mathcal{M}^{h_1\cdots h_4}_{\delta_i}}{\sqrt{\sum_{h_1\cdots h_4}\Phi_{W^+_{h_1}W^-_{h_2}}\left(\mathcal{M}^{h_1\cdots h_4}_{\rm SM}\right)^2}} \tag{4.1.21}$$

By using the energy scaling behavior of parton luminosity $\Phi_{W^+W^-}$ in Table 4.6 and partonic cross section in Table 4.3 for the process $\mu^+\mu^- \to t\bar{t}\nu\bar{\nu}$ in the presence of anomalous couplings, we can obtain the energy scaling for the statistical signal significance in the fully inclusive case. For the top Yukawa coupling δ_{tth} and the Higgs gauge boson coupling δ_{hWW}, the result reads :

$$\frac{S}{\sqrt{B}} \sim \hat{E}^{-1.8}, \quad \hat{E}^{-2.1}, \quad \hat{E}^{-4}, \qquad \text{for} \qquad \tau \in [10^{-4}, 0.01], \quad [0.01, 0.2], \quad [0.2, 0.8], \tag{4.1.22}$$

where we have omitted the highest τ region. As expected, the sensitivity on the top Yukawa coupling decreases as bin energy becomes larger. For the anomalous coupling $\delta\kappa_{Z,\gamma}, \delta_{Wtb}, \delta_{Zt_L}, \delta_{Zt_R}$, the sensitivity scales like:

$$\frac{S}{\sqrt{B}} \sim \hat{E}^{0.2}, \quad \hat{E}^{-0.1}, \quad \hat{E}^{-2}, \qquad \text{for} \qquad \tau \in [10^{-4}, 0.01], \quad [0.01, 0.2], \quad [0.2, 0.8]. \tag{4.1.23}$$

from which, we can see that there is a mild increase for the signal significance at low τ, a mild decrease for the intermediate τ and a decrease at high τ. Finally, we find that for the anomalous coupling $\lambda_{Z,\gamma}$, the energy scaling behaves as:

$$\frac{S}{\sqrt{B}} \sim \hat{E}^{-1.6}, \quad \hat{E}^{-1.7}, \quad \hat{E}^{-2.2}, \qquad \text{for} \qquad \tau \in [10^{-4}, 0.01], \quad [0.01, 0.2], \quad [0.2, 0.8]. \tag{4.1.24}$$

and for the coupling δg_1^Z, we have:

$$\frac{S}{\sqrt{B}} \sim \hat{E}^{-1.6}, \quad \hat{E}^{-1.9}, \quad \hat{E}^{-3}, \qquad \text{for} \qquad \tau \in [10^{-4}, 0.01], \quad [0.01, 0.2], \quad [0.2, 0.8]. \tag{4.1.25}$$

which decreases with the energy bins.

4.2 Top Yukawa couplings at the high energy muon collider

In this section, we study in detail the prospects of measuring the top Yukawa coupling at a high energy muon collider. To quantify the importance of the anomalous couplings, we parametrize the cross sections as

$$\sigma = \sigma_{\text{SM}} \left(1 + R_1 \delta + R_2 \delta^2\right), \tag{4.2.1}$$

where δ_i signifies some fractional deviation in a SM coupling. Throughout this chapter, we will be primarily considering the interference term which is linear in δ, but we also remark on the inclusion of the quadratic term. In terms of the kappa framework [1], δ_i and κ_i are

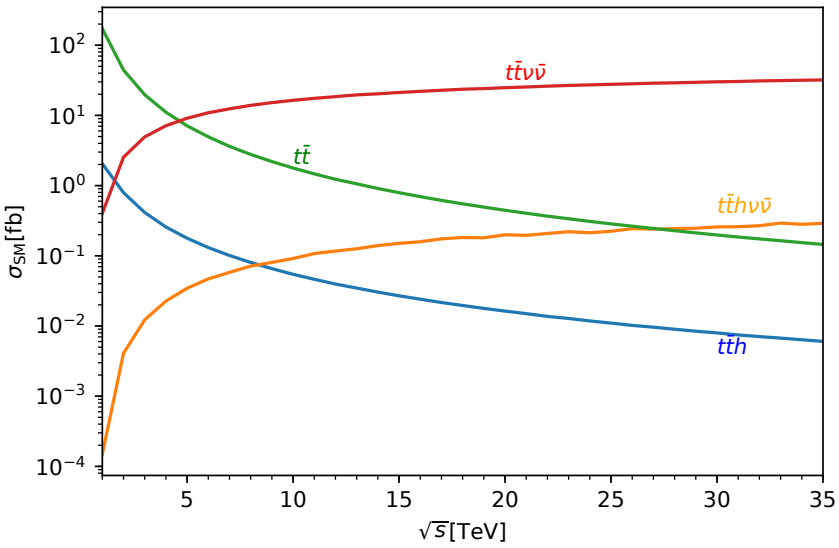

Fig. 4.3: Cross section of SM $\mu^+\mu^- \to t\bar{t}$, $\mu^+\mu^- \to t\bar{t}h$, and $\mu^+\mu^- \to t\bar{t}\nu\bar{\nu}$ with the onshell Z contribution removed.

related by $\kappa_i = 1 + \delta_i$.

Before we present the detailed analysis for the VBF production of top quark pair, we make some comments about the Drell-Yan processes which are also involving top Yukawa coupling. The relevant processes are:

$$\mu^+\mu^- \to t\bar{t}, t\bar{t}h \tag{4.2.2}$$

in which there is no energy growing behavior for the anomalous top Yukawa coupling δ_{tth}. In Fig. 4.3, we have plotted the SM cross sections as functions of center-of-mass energy of the muon collider for both DY and VBF productions of top quark pair and top quark pair plus a Higgs boson. We can see that due to the logarithmic growth of the VBF processes and the inverse of energy squared decrease of the DY processes, the VBF productions start to become dominant at 5 (8) TeV center-of-mass energy for the $t\bar{t}(t\bar{t}h)$. Besides the small cross sections at the high energy muon collider, the R-values defined in in Eq. (4.2.1) are also very small for the DY production of top quark pair. In order to have the $t\bar{t}$ process involve

the top Yukawa coupling, it is necessary to include the non-zero muon masses. In this case, the dependence of the cross section on δ_{tth} will be suppressed by the muon Yukawa coupling squared $m_\mu^2/v^2 \sim 2 \times 10^{-7}$. We have checked that for this process, the R-ratios defined in Eq. (4.2.1) for the anomalous coupling δ_{tth} are very small:

$$\begin{aligned} R_1 &= 2.337 \times 10^{-5}, \qquad R_2 = 1.169 \times 10^{-5} \qquad @10 \text{ TeV} \\ R_1 &= 2.343 \times 10^{-5}, \qquad R_2 = 1.172 \times 10^{-5} \qquad @30 \text{ TeV} \end{aligned} \tag{4.2.3}$$

and we will not consider it any further. For the DY process $\mu^+\mu^- \to t\bar{t}h$, the R-values are:

$$\begin{aligned} R_1 &= 1.62, \qquad R_2 = 0.797 \qquad \text{at 10 TeV} \\ R_1 &= 1.56 \qquad R_2 = 0.774 \qquad \text{at 30 TeV} \end{aligned} \tag{4.2.4}$$

We can see that the R-values stay almost constant as the center-of-mass energy of the muon collider increases. We expect that the sensitivity on the top Yukawa coupling from this process will come from the lower energy stages of the muon collider. Such analysis has been performed at CLIC in the baseline energy of 1.4 TeV [4].

4.2.1 Simulation and Cuts

We now turn to the simulation and analysis of the process $\mu^+\mu^- \to t\bar{t}\nu_\mu\bar{\nu}_\mu, t\bar{t}h\nu_\mu\bar{\nu}_\mu$ in the presence of the anomalous top Yukawa coupling δ_{tth}. We are using `Madgraph5` [121] to calculate the cross sections and generate the events at LO. The anomalous coupling δ_{tth} is implemented by using the BSMC model file [122]. We will work at the level of top quarks and no decaying of the top quarks will be simulated.

One advantage of the lepton colliders compared with hadron collider is that the initial energies of the colliding leptons are known very precisely [79], as a result, the invariant mass of the two outgoing neutrinos is indirectly determined by the momenta of the top quark pair or the top quark pair plus Higgs boson. This is defined as recoil mass and for the $t\bar{t}\nu_\mu\bar{\nu}_\mu$

Table 4.7: Cross sections for signal and background. For the VBF processes, the cut on the recoil mass in Eq. (4.2.7) has been imposed.

$\sqrt{s}$ **(TeV)** $\backslash\sigma_{\rm SM}$**(fb)**	3	6	10	14	30
$t\bar{t}\nu_\mu\bar{\nu}_\mu$	4.93	10.9	16.4	20.5	30.1
$t\bar{t}h\nu_\mu\bar{\nu}_\mu$	0.0121	0.0460	0.0914	0.141	0.269
$t\bar{t}$	19.7	4.95	1.78	0.909	0.198
$t\bar{t}h$	0.414	0.131	0.0547	0.0305	0.00793
$W^+W^-\nu_\mu\bar{\nu}_\mu$	120	259	399	515	815
$W^\pm Z\mu^\mp(\bar{\nu}_\mu/\nu_\mu)$ [7]	96.6	215	340	443	717

process,

$$M^2_{\rm recoil} = (p_{\mu^+} + p_{\mu^-} - p_t - p_{\bar{t}})^2, \tag{4.2.5}$$

For the $t\bar{t}h\nu_\mu\bar{\nu}_\mu$ process, it is given by:

$$M^2_{\rm recoil} = (p_{\mu^+} + p_{\mu^-} - p_t - p_{\bar{t}} - p_h)^2. \tag{4.2.6}$$

We will impose the following cut on the recoil mass at the generator level:

$$M_{\rm recoil} > 200{\rm GeV}, \tag{4.2.7}$$

which will remove the contribution from the process $t\bar{t}Z \to t\bar{t}(\nu\bar{\nu})$. In Table 4.7, we have presented the cross sections of the VBF $t\bar{t}$ production and the potential relevant backgrounds for some benchmark scenarios at the high energy muon collider. For all the VBF processes, the cross sections are presented after the cut in Eq. (4.2.7).

The decaying branching ratios for the top quark pair are respectively 45%, 28%, 4.4% in the fully hadronically decaying channel, semi-leptonically decaying channel and fully lep-

[7] Sum of the cross sections for $W^+Z\mu^-\bar{\nu}$ and $W^-Z\mu^+\nu$ with $p_T > 30$ GeV for charged leptons and the on-shell $W \to \mu\nu$ contribution removed.

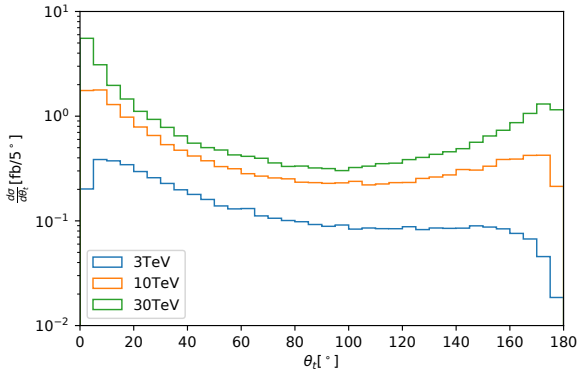

(a) Standard Model θ_t.

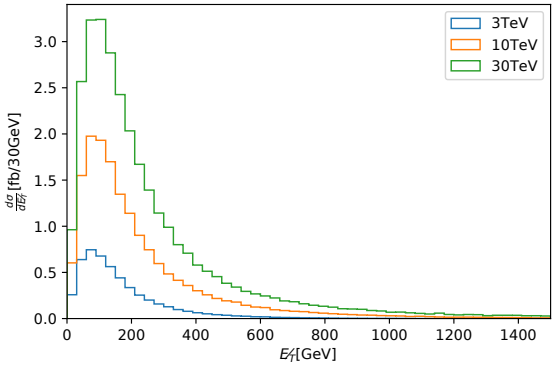

(b) Standard Model $\not{E}_T$ of the top

Fig. 4.4: Standard Model distribution of θ and p_T of the top quark at 3, 10, and 30 TeV muon colliders after the cut on the recoil mass in Eq. (4.2.7).

tonically decaying channel [123] [124] [8]. We will focus on the semi-leptonically decaying channel where the top quark and anti-top quark can be reconstructed and distinguished by the charges of the decayed leptons. To suppress the beam induced background, we put the following cuts on the polar angles of the top quark pair in the laboratory frame:

$$10^\circ < \theta_{t,\bar{t}} < 170^\circ \tag{4.2.8}$$

where in our convention, the z-axis align with the direction of the μ^+ beam. As shown in Fig. 4.4, the θ_t distribution peaks strongly in the forward region at 3, 10, 30 TeV muon collider and peaks also mildly in the backward region for 10, 30 TeV center-of-mass energy. The cut efficiencies for the $\theta_{t,\bar{t}}$ cuts at the 10 TeV and 30 TeV muon collider are 0.57 and 0.43, respectively. This reduces the cross sections of the SM $t\bar{t}v\bar{v}$ in the semi-leptonically decaying channel to 2.63 fb and 3.61 fb for 10 TeV and 30 TeV muon collider respectively. Here the numbers have also taken into account the branching ratios of the semi-leptonically decaying channel of top quark pair.

We expect that the signal manifests itself in the kinematical region where effective W

[8] In the estimation of the decaying branching ratios, we have neglected the $\tau\nu$ decay of the W bosons. Including it will have mild effects on the final results.

approximation applies as this is the hard scattering regime. To maximize the sensitivity and also to help to reconstruct the effective W boson partonic center-of-mass frame, we impose the following criterion:

$$\not{E}_T < 200\text{GeV} \tag{4.2.9}$$

where at the truth-level, the missing transverse energy $\not{E}_T$ is equal to the magnitude of the transverse momentum of the two neutrino system or top quark pair system:

$$\not{E}_T = |\boldsymbol{p}_{T,\nu} + \boldsymbol{p}_{T,\bar{\nu}}| = |\boldsymbol{p}_{t,t} + \boldsymbol{p}_{T,\bar{t}}|. \tag{4.2.10}$$

Note that we also require the missing transverse energy to be larger than 20 GeV

$$\not{E}_T > 20\text{GeV}, \tag{4.2.11}$$

which is used to reduce the background from DY production of $t\bar{t}$ with initial state radiation or bremsstrahlung effects [4]. The cut efficiencies we obtain from comparing the $\not{E}_T$ and $\theta_{t,\bar{t}}$ cuts to the $\theta_{t,\bar{t}}$ cuts alone are 0.50 and 0.44 for 10 TeV and 30 TeV, which further reduces the SM cross sections to 1.32 fb and 1.59 fb, where again we include the semi-leptonic branching ratio. This sizable suppression from $\not{E}_T$ cut is as expected as from Fig. 4.4. For illustration, in Table 4.8, we have listed the values of the SM cross sections in the semi-leptonically decaying channel and the $R_{1,2}$ in different bins of $m_{t\bar{t}}$ for the VBF production of top quark pair after all the preliminary cuts in Eq. (4.2.7), (4.2.8), (4.2.9),(4.2.11) at 30 TeV muon collider. We can see that there is no energy growing behavior for the interference term, as expected from the previous analytical study. On the other hand, we do see the R-value for the squared term possess larger values at higher energy bins. For comparison, we have also presented the SM cross sections R-values for the process $\mu^+\mu^- \to t\bar{t}h\nu\bar{\nu}$ with semi-leptonically decaying top quark pair and Higgs decaying to bottom quark pair at 30 TeV muon collider. We can see that there is indeed energy growing behavior for the linear term.

Table 4.8: The SM cross sections and the R-values for anomalous top Yukawa coupling in the process $\mu^+\mu^- \to t\bar{t}\nu\bar{\nu}, t\bar{t}h\nu\bar{\nu}$ after all the preliminary cuts in Eq. (4.2.7), (4.2.8), (4.2.9), (4.2.11) with semi-leptonic decay for $t\bar{t}$, and $b\bar{b}$ decay for the Higgs boson in different invariant mass bins at 30 TeV muon collider.

$m(\bar{t}t)$	$\sigma_{\rm SM}$ (fb)	R_1	R_2
0-1TeV	1.28	-0.0803	1.33
1-5TeV	0.325	-0.220	12.3
5-10TeV	0.00538	-0.155	157
10-15TeV	$4.17 \cdot 10^{-4}$	-0.152	468
15-20TeV	$5.21 \cdot 10^{-5}$	-0.163	886
20-25TeV	$6.36 \cdot 10^{-6}$	-0.0608	1199
25-30TeV	$1.06 \cdot 10^{-6}$	-0.00202	355

$m(\bar{t}th)$	$\sigma_{\rm SM}$ (fb)	R_1	R_2
0-1TeV	$1.10 \cdot 10^{-3}$	5.75	15.5
1-5TeV	$2.74 \cdot 10^{-3}$	7.73	320
5-10TeV	$1.72 \cdot 10^{-4}$	26.8	9090
10-15TeV	$2.14 \cdot 10^{-5}$	49.8	51400
15-20TeV	$3.48 \cdot 10^{-6}$	72.8	147000
20-25TeV	$7.44 \cdot 10^{-7}$	58.7	186000
25-30TeV	$1.16 \cdot 10^{-7}$	16.5	76500

As discussed in previous sections and also shown in Fig. 4.5, the scattering angle in the partonic center-of-mass frame θ^* can be used to enhance the sensitivity to the top Yukawa coupling. Here we have used an asterisk to distinguish between the polar angle of top quark in the W^+W^- frame and the polar angle in the $\mu^+\mu^-$ frame. Furthermore, in determining the scattering angle θ^* in the partonic frame, we assume that the neutrinos are collinear with the muon beams. To be explicit, the scattering angle θ^* can be obtained from the

kinematical variables in the lab frame as follows:

$$\tan\theta^* = \frac{\sqrt{p_{t,x}^2 + p_{t,y}^2}\, m_{t\bar{t}}}{-E_t\, \boldsymbol{p}_{t\bar{t}} + p_{t,z}\, E_{t\bar{t}}}. \tag{4.2.12}$$

where $p_{t,x}$ is the x-component of the momentum of the top quark and similarly for the $p_{t,y}, p_{t,z}$. $m_{t\bar{t}}$ is the invariant mass of the top quark pair and $(E_{t\bar{t}}, \boldsymbol{p}_{t\bar{t}})$ is the four-momentum of the top quark pair. Here we have used the fact that the transverse momentum of the top quark is the same in both frame and the z-component of the momentum of the top quark in the partonic frame is obtained by a boost.

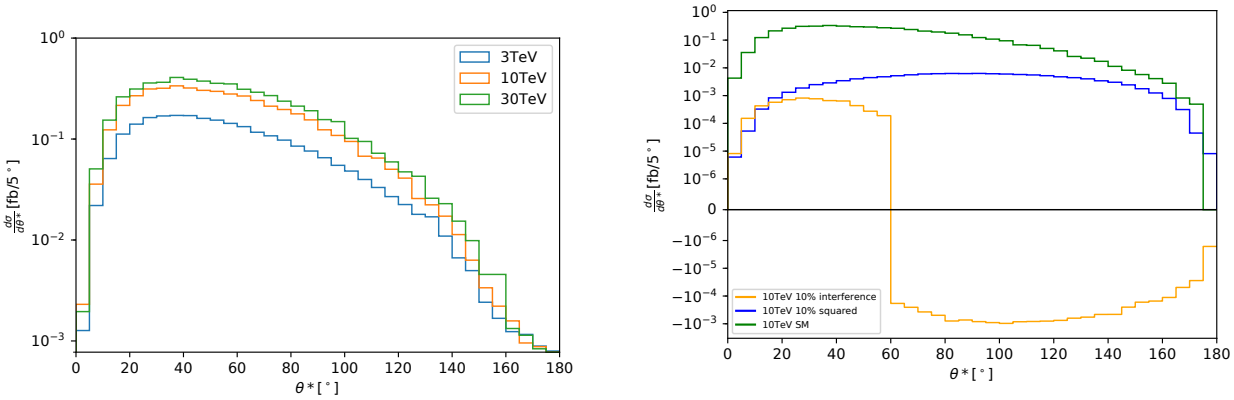

(a) θ^* (the angle between the top and the W^+ in the W^+W^- center of mass) distribution

(b) θ^* (the angle between the top and the W^+ in the W^+W^- center of mass) distribution.

Fig. 4.5: The distributions of θ^* for the SM (left panel) and $\delta_{tth} = 10\%$ (right panel) after the all the preliminary cuts in Eq. (4.2.7), (4.2.8), (4.2.9), (4.2.11).

Table 4.9: Efficiencies from CLIC analysis of the semi-leptonically decaying channel with $\mathrm{P}(e^-) = -80\%$ [4].

$\sqrt{s}$	380 GeV	1.4 TeV ($\sqrt{s'} \geq 1.2$ TeV)	3 TeV ($\sqrt{s'} \geq 2.6$ TeV)
$\epsilon_{\text{eff}}(e^+e^- \to t\bar{t} \to qqqql\nu)$	64%	37%	33%

In addition to the invariant mass bins of the top quark pair in Table 4.8, we also divide the scattering angle θ^* into six bins with bin width of 30°. The corresponding cross sections and R-values in each two-dimensional bin are shown in Table B.1, B.2 and Table B.3,

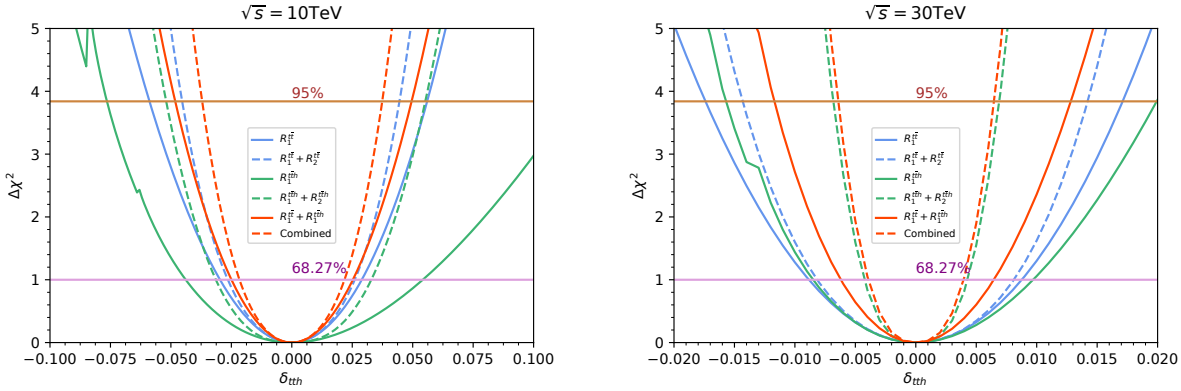

(a) $\mu^+\mu^- \to t\bar{t}\nu\bar{\nu}$ with $\sqrt{s} = 10$ TeV and $L = 10\,\text{ab}^{-1}$.

(b) $\mu^+\mu^- \to t\bar{t}\nu\bar{\nu}$ with $\sqrt{s} = 30$ TeV and $L = 90\,\text{ab}^{-1}$.

Fig. 4.6: $\Delta\chi^2$ plot as a function of anomalous top Yukawa coupling δ_{tth} for processes $\mu^+\mu^- \to t\bar{t}\nu\bar{\nu}$ and $\mu^+\mu^- \to t\bar{t}\nu\bar{\nu}h$ at 10 TeV (left panel) and 30 TeV (right panel) muon collider. Here $R_1(R_2)$ denotes the interference term and the squared term respectively.

B.4 respectively in Appendix B. In order to take into account the reconstruction efficiencies of the semi-leptonically decaying top quark pair, we have extracted the numbers from the analysis of top quark pair production at 380 GeV, 1.4 TeV and 3 TeV center-of-mass energy of CLIC [4]. The results are listed in Table 4.9. We will use the following values for the reconstruction efficiencies for different $m_{t\bar{t}}$ bins:

$$[0,1]\text{TeV}: \quad 64\%, \qquad \text{all other bins}: \quad 33\% \tag{4.2.13}$$

and assume that the SM reducible backgrounds has been reduced to a negligible level. Similar efficiencies apply to the bins of $m_{t\bar{t}h}$ for the process $\mu^+\mu^- \to t\bar{t}h\nu\bar{\nu}$ with the Higgs boson decaying into bottom quark pair $h \to b\bar{b}$ with a branching ratio of 58% [123] [124].

4.3 Results and Discussion

We follow the procedure in Appendix D to construct the likelihood functions by combing all the two dimensional bins defined in Table B.1 and Table B.2 for 10 TeV, 30 TeV muon collider correspondingly. The integrated luminosity is assumed to be 10 (90)ab^{-1} at 10

(30)TeV muon collider. The $\Delta\chi^2$ as functions of the anomalous top Yukawa coupling δ_{tth} for the semileptonically decaying channels of the $t\bar{t}\nu\bar{\nu}, t\bar{t}h\nu\bar{\nu}$ are presented in Fig. 4.6. For each process, we have considered two cases: with only the linear term R_1 and with both the linear term R_1 and the quadratic term R_2. The 95% C.L. interval for the δ_{tth} for different scenarios are shown in Table 4.10. We find that due to the lack of energy growing behaviors in the $t\bar{t}\nu\bar{\nu}$, the expected sensitivity on the anomalous top Yukawa coupling δ_{tth} is not majorly affected by the inclusion of the quadratic term at both 10 TeV and 30 TeV. In contrast, for the $t\bar{t}h\nu\bar{\nu}$, the quadratic terms can make a big difference (a factor of 2-3) on the top Yukawa coupling sensitivity, which is a reflection of the energy growing effects. For this process, a dedicated study should be provided to address the issue of the effective field theory breaking down, which we leave for future work. Here we are focusing on the results obtained by including the linear term R_1 only. At 10 (30) TeV muon collider, the 95% C.L. on the anomalous coupling δ_{tth} from $t\bar{t}\nu\bar{\nu}$ reads 5.6% (1.7%), which is generally in agreement with the results of [5]. These can be compared with 4% and 2 % projections at 95% C.L. for the HE-LHC under the base and optimal scenarios respectively [3] as well as the 2% projection at a 100TeV collider [125], which are also listed in Table 4.10. For the process $t\bar{t}h\nu\bar{\nu}$, without worrying about the issues of EFT mentioned earlier, we find that the result is comparable with $t\bar{t}\nu\bar{\nu}$, especially at 30 TeV muon collider. It deserves further detailed study, which we leave for future work.

Table 4.10: 95% C.L. on the anomalous top Yukawa coupling δ_{tth} for different scenarios at 10 TeV and 30 TeV muon collider.

$\sqrt{s_{\mu^+\mu^-}}$	Process	Sensitivity
10 TeV @ 10 ab^{-1}	$t\bar{t}\nu\bar{\nu}$ R_1	$[-5.9\%, 5.6\%]$
	$t\bar{t}\nu\bar{\nu}$ $R_1 + R_2$	$[-4.5\%, 4.5\%]$
	$t\bar{t}h\nu\bar{\nu}$ R_1	$[-7.6\%, 12\%]$
	$t\bar{t}h\nu\bar{\nu}$ $R_1 + R_2$	$[-5.2\%, 5.5\%]$
	$t\bar{t}\nu\bar{\nu} + t\bar{t}h\nu\bar{\nu}$ R_1	$[-4.8\%, 5.0\%]$
	$t\bar{t}\nu\bar{\nu} + t\bar{t}h\nu\bar{\nu}$ $R_1 + R_2$	$[-3.7\%, 3.7\%]$
30 TeV @ 90 ab^{-1}	$t\bar{t}\nu\bar{\nu}$ R_1	$[-1.7\%, 1.7\%]$
	$t\bar{t}\nu\bar{\nu}$ $R_1 + R_2$	$[-1.4\%, 1.4\%]$
	$t\bar{t}h\nu\bar{\nu}$ R_1	$[-1.6\%, 2.0\%]$
	$t\bar{t}h\nu\bar{\nu}$ $R_1 + R_2$	$[-0.68\%, 0.69\%]$
	$t\bar{t}\nu\bar{\nu} + t\bar{t}h\nu\bar{\nu}$ R_1	$[-1.2\%, 1.3\%]$
	$t\bar{t}\nu\bar{\nu} + t\bar{t}h\nu\bar{\nu}$ $R_1 + R_2$	$[-0.64\%, 0.65\%]$
Other Colliders		
14 TeV HL-LHC @ 3 ab^{-1}	$t\bar{t}h \to$ Multiple Leptons	6.9% [3]
1.4 TeV CLIC @ 1.5 ab^{-1}	$t\bar{t}h \to 6j + b\bar{b}, \ell\nu 4j + b\bar{b}$	7.4% [4]
100 TeV Collider @ 20 ab^{-1}	$t\bar{t}h \to \ell\nu 4j + b\bar{b}$	2% [125]

4.4 Conclusion

In this chapter, we have performed a detailed analysis about the measurement of the top Yukawa coupling at the high energy muon collider by studying the process $\mu^+\mu^- \to t\bar{t}\nu\bar{\nu}$. In particular, we have studied the energy scaling behavior of statistical signal significance $S/\sqrt{B}$ for the subprocess $W^+W^- \to t\bar{t}$ and for the full processes at the muon collider by employing the effective W-boson approximation. In addition, we have presented the explicit

formulae for the helicity amplitudes for the subprocess $W^+W^- \to t\bar{t}$ in the presence of anomalous couplings, where for completeness, we have also included anomalous triple gauge boson couplings and anomalous gauge-boson-fermions couplings. The high energy limits of the different helicity amplitudes are shown in Table 4.1, 4.2, whereas the threshold behaviors are given in Table 4.4, 4.5. We have found that the sensitivity on the anomalous top Yukawa coupling δ_{tth} decreases as the energy of the bin increases as shown in Eq. (4.1.22). This is partially due to the fact that the SM amplitude for the helicity configurations $(0, 0, \pm\frac{1}{2}, \pm\frac{1}{2})$ scales like $m_t/\hat{E}$. As a result, the interference between the SM and BSM amplitudes will stay constant instead of growing linearly with $\hat{E}$. Secondly, the suppression of the parton luminosity $\Phi_{W^+W^-}(\tau)$ at high τ also reduces the signal significance $S/\sqrt{B}$ at high energy bins. As a byproduct, we also found that in the case of triple-gauge- boson couplings $\delta\kappa_{Z,\gamma}$ and the gauge-boson-fermion couplings $\delta_{Wtb}, \delta_{Zu_L}, \delta_{Zu_R}$, the statistical signal significance mildly increases for small values of τ, mildly decreases for intermediate values of τ, and decreases at large τ values.

The semi-analytical analysis has been confirmed by our numerical simulation, where we studied the prospects on the top Yukawa coupling measurement at 10 TeV and 30 TeV muon colliders. We have imposed the basic selections cuts in Eq. (4.2.7), (4.2.8), (4.2.9), (4.2.11) and focused on the semi-leptonically decaying channel of the top quark pair. The reconstruction efficiencies in this channel have been extracted from the CLIC analysis for different stages. Similar efficiencies are also applied to the $t\bar{t}h\nu_\mu\bar{\nu}_\mu$ process, where the Higgs boson is assumed to decay into a bottom quark pair. Furthermore, we used the distribution of the scattering angle in the partonic center-of-mass frame for the $t\bar{t}\nu_\mu\bar{\nu}_\mu$ to enhance sensitivity. The precision on the anomalous top Yukawa coupling at the 95 % C.L. is projected to be 5.6% (1.7%) for VBF production of a top quark pair at a 10 (30) TeV muon collider. The precision from VBF production of $t\bar{t}h$ is comparable to the top quark pair, but is sensitive to contributions from the quadratic term. Therefore, it demands further detailed study, which we leave for future possible work.

Chapter 5

Conclusion

In this dissertation, we discussed BSM physics connected to the Higgs boson and its couplings to other SM particles.

In Chapter 2, we determined the energy scales at which new physics should emerge given some deviation in a Higgs coupling using arguments based on tree level unitarity. We showed energy scales for deviations in the top Yukawa and massive gauge boson couplings at both linear and quadratic order and compared the results to the ATLAS runs. We also examined the differences between the bottom up approach of adding operators with increasing powers of the Higgs boson and SMEFT.

In Chapter 3, we found the number of independent primary operators at each dimension for 3 and 4 point functions involving the Higgs boson and listed a set of them. In order to determine linear independence, we used a combination of the Hilbert series, analytic methods, and brute force numerical methods. We also used tree level unitarity to estimate the possible sizes of the coefficients of these operators in order to identify the more phenomenologically interesting ones. As mentioned in the chapter, some detailed phenomenological studies have already been conducted for a few of the operators listed in the tables and similar work can be done for the others.

In Chapter 4, we examined the possibility of measuring the top Yukawa coupling at a future muon collider by examing VBF processes. We used EWA to perform an analytic analysis on general couplings to the Higgs boson and then ran Madgraph simulations for $\mu_+\mu_- \to t\bar{t}\nu\bar{\nu}$ and $\mu_+\mu_- \to t\bar{t}h\nu\bar{\nu}$. Analysis of the results shows that measurements at a muon collider are competitive with those at a 100 TeV hadron collider.

In each chapter, we initially establish a general framework, then specialize to specific anomalous couplings and interactions, particularly those involving the Higgs. The results can serve as guides to searches for new physics. Future work can follow the steps we have outlined and produce similar results for other iteractions that can further inform searches at particle colliders.

Appendix A

Calculation Techniques and Results

In this appendix we define the multi-particle amplitudes we use to obtain the unitarity bounds, explain how they are computed, discuss potential infrared enhancements, and give the results of the calculations used in the main text. We extend the results of Ref. [29] to include fermions, momentum-dependent couplings, and tree-level diagrams with propagators.

A.1 Scalar Amplitudes

We first discuss amplitudes involving only scalar fields, which includes amplitudes with longitudinal W and Z bosons when we use the equivalence theorem. Given r species of scalars $\phi_1, \ldots, \phi_r$ we define the states

$$\begin{aligned} |P; k_1, \ldots, k_r\rangle &\equiv C_{k_1,\ldots,k_r} \int d^4x\, e^{-iP\cdot x}\, \phi_1^{(-)}(x)^{k_1} \cdots \phi_r^{(-)}(x)^{k_r} |0\rangle \\ &= C_{k_1,\ldots,k_r} \int d\Phi_k(P; p_1, \ldots, p_k)\, |\phi_1(p_1) \cdots \phi_r(p_k)\rangle. \end{aligned} \tag{A.1.1}$$

Here $k_1, \ldots, k_r$ are non-negative integers that give the number of each species of particle in the state, $\phi_i^{(-)}$ is the negative frequency (creation operator) part of the interaction picture

field ϕ_i, $|\phi_1(p_1)\cdots\phi_r(p_k)\rangle$ is an ordinary k-particle state with $k = k_1 + \cdots + k_r$, and

$$d\Phi_k(P; p_1, \ldots, p_k) = \frac{d^3p_1}{(2\pi)^3}\frac{1}{2E_1}\cdots\frac{d^3p_k}{(2\pi)^3}\frac{1}{2E_k}(2\pi)^4\delta^4(p_1 + \cdots + p_k - P) \tag{A.1.2}$$

is the Lorentz invariant k-body phase space. These states are s-wave states defined by integrating k-particle states over the full phase space. The normalization of the states is chosen to be

$$\langle P'; k'|P; k\rangle = (2\pi)^4\delta^4(P' - P)\,\delta_{k'k}, \tag{A.1.3}$$

where we use the abbreviations

$$|P; k\rangle = |P; k_1, \ldots, k_r\rangle, \qquad \delta_{k'k} = \delta_{k'_1k_1}\cdots\delta_{k'_rk_r}, \qquad C_k = C_{k_1,\ldots,k_r}. \tag{A.1.4}$$

The normalization constant is given by

$$\frac{1}{|C_k|^2} = k_1!\cdots k_r!\,\Phi_k(P), \tag{A.1.5}$$

where

$$\Phi_k(P) = \int d\Phi_k(P) = \frac{1}{8\pi(k-1)!(k-2)!}\left(\frac{E}{4\pi}\right)^{2k-4}, \tag{A.1.6}$$

is the total volume of phase space for massless particles with center of mass energy $E = \sqrt{P^2}$.

We then consider S-matrix elements between these states:

$$\langle P'; k'|T|P; k\rangle = (2\pi)^4\delta^4(P' - P)\hat{\mathcal{M}}(P; k_1, \ldots, k_r \to k'_1, \ldots, k'_r), \tag{A.1.7}$$

where $S = 1 + iT$. The amplitude $\hat{\mathcal{M}}$ is Lorentz invariant and depends only on P_μ, so it is a function of E only. With the normalization Eq. (A.1.3), unitarity of the S matrix implies

that these amplitudes satisfy

$$|\hat{\mathcal{M}}| \leq 1. \tag{A.1.8}$$

For non-forward amplitudes this follows directly from the unitarity of the S-matrix. For forward amplitudes ($k_i' = k_i$) a few additional steps are required to show that this holds for tree-level amplitudes, see Ref. [29]. This is the unitarity constraint we employ in this chapter.

The Feynman rules for these amplitudes follow straightforwardly from the standard rules. The result is that the amplitude $\hat{\mathcal{M}}$ are obtained from the standard Lorentz invariant amplitude $\mathcal{M}$ by averaging over the initial and final state phase space:

$$\hat{\mathcal{M}}_{fi}(P) = C_f^* C_i \int d\Phi_f(P)\, d\Phi_i(P)\, \mathcal{M}_{fi}, \tag{A.1.9}$$

where $\mathcal{M}_{fi}$ is the usual Lorentz-invariant amplitude.[1] Because we are averaging over final state momenta, these amplitudes have contributions from disconnected diagrams, with each disconnected component contributing a $\hat{\mathcal{M}}$ factor, leading to a form $\hat{\mathcal{M}} \propto \Pi_i \hat{\mathcal{M}}_i$. However, the leading contribution to high-energy amplitudes always comes from connected diagrams.

In simple cases, these amplitudes can be computed in terms of the total volume of phase space given in Eq. (A.1.6). For example, for a single insertion of a coupling with no derivatives

[1] In more detail, Eq. (A.1.9) is

$$\hat{\mathcal{M}}(P; k_1, \ldots, k_r \to k_1', \ldots, k_r') = C_{k'}^* C_k \int d\Phi_{k'}(P; p_1', \ldots, p_{k'}')\, d\Phi_k(P; p_1, \ldots, p_k) \times \mathcal{M}(\phi_1(p_1) \cdots \phi_r(p_k) \to \phi_1(p_1') \cdots \phi_r(p_{k'}')). \tag{A.1.10}$$

we have

$$\frac{\langle P';k'|\int d^4x\,\phi_1^{n_1}(x)\cdots\phi_r^{n_r}(x)|P;k\rangle}{(2\pi)^4\delta^4(P'-P)} = C^*_{k'}C_k\,n_1!\cdots n_r!\Phi_{k'}(P)\Phi_k(P) \tag{A.1.11}$$

$$= \frac{1}{C_{k'}C^*_k}\,\frac{n_1!\cdots n_r!}{k_1!\cdots k_r!k'_1!\cdots k'_r!}, \tag{A.1.12}$$

where we assume $n_i = k_i + k'_i$. For diagrams with a single insertion of a vertex containing derivatives, we use the identities

$$\int d\Phi_k(P;p_1,\ldots,p_k)\,p_1^\mu = \frac{P^\mu}{k}\Phi_k(P), \tag{A.1.13}$$

$$\int d\Phi_k(P;p_1,\ldots,p_k)\,p_1\cdot p_2 = \frac{P^2}{2\binom{k}{2}}\Phi_k(P), \tag{A.1.14}$$

which hold for the case where all particles are massless.

A.2 States with One Fermion

We consider a state containing a single fermion and k scalars

$$|P;k_1,\ldots,k_r,\alpha,a\rangle \equiv C'_k\int d^4x\,e^{-iP\cdot x}\,\phi_1^{(-)}(x)^{k_1}\cdots\phi_r^{(-)}(x)^{k_r}\psi_{L\alpha}^{a(-)}(x)|0\rangle$$

$$= C'_k\int d\Phi_{k+1}(P;p_1,\ldots,p_k,q)\,v_L^\alpha(q)|\phi_1(p_1)\cdots\phi_r(p_k)\bar{\psi}_R^a(q)\rangle, \tag{A.2.1}$$

where ψ_L is a left-handed Weyl spinor field, α is a spinor index, and a is a gauge index (*e.g.* a color index). Note that these states are given by phase space integrals of scattering states weighted by a spinor wavefunction, so Eq. (A.1.9) is modified for amplitudes involving these states. (In the example above, the state created by the left-handed spinor field is a

right-handed antifermion.) The normalization of these states is given by

$$\begin{aligned}\langle P';k,\beta,b|P;k,\alpha,a\rangle &= (2\pi)^4\delta^4(P'-P)\,k_1!\cdots k_r!|C_k'|^2\int d\Phi_{k+1}(P;p_1,\ldots,p_k,q)\,q^\mu\sigma_\mu^{\alpha\dot\beta}\delta_{ab}\\ &= (2\pi)^4\delta^4(P'-P)\,k_1!\cdots k_r!|C_k'|^2\delta_{ab}\frac{P\cdot\sigma^{\alpha\dot\beta}}{k+1}\Phi_{k+1},\end{aligned}\tag{A.2.2}$$

where we used Eq. (A.1.13). We choose the states Eq. (A.2.1) to have normalization

$$\langle P';k',\beta,b|P;k,\alpha,a\rangle = (2\pi)^4\delta^4(P'-P)\,\delta_{ab}\delta_{k'k}\frac{P\cdot\sigma^{\alpha\dot\beta}}{E}.\tag{A.2.3}$$

Note that in the P^μ rest frame we have $P\cdot\sigma^{\alpha\dot\beta}/E=\delta^{\alpha\dot\beta}$, so this is the natural generalization of the normalization condition Eq. (A.1.3). The normalization constants are therefore given by

$$\frac{1}{|C_k'|^2} = k_1!\cdots k_r!\frac{E}{k+1}\Phi_{k+1}(P).\tag{A.2.4}$$

A.3 States with Two Fermions

We now consider states with two fermions and k scalars of the form

$$\begin{aligned}|P;k_1,\ldots,k_r,L/R\rangle &\equiv C_k''\int d^4x\,e^{-iP\cdot x}\,\phi_1^{(-)}(x)^{k_1}\cdots\phi_r^{(-)}(x)^{k_r}\overline{\psi}^{a(-)}_{R/L}(x)\psi^{a(-)}_{L/R}(x)|0\rangle\\ &= C_k''\int d\Phi_{k+2}(P;p_1,\ldots,p_k,q,q')\,\overline{u}_{R/L}(q')v_{L/R}(q)\\ &\qquad\times\sum_a|\phi_1(p_1)\cdots\phi_r(p_k)\psi^a_{R/L}(q')\overline{\psi}^a_{R/L}(q)\rangle,\end{aligned}\tag{A.3.1}$$

where ψ_L (ψ_R) are left-handed (right-handed) Weyl spinors. In the massless limit the states $|\ldots L\rangle$ and $|\ldots R\rangle$ are orthogonal s-wave states, with the L (R) state containing a fermion-antifermion pair which are both right-handed (left-handed) in helicity. These states are

normalized as in Eq. (A.1.3) if we choose

$$\frac{1}{|C_k''|^2} = k_1! \cdots k_r! \frac{2NE^2}{(k+1)(k+2)} \Phi_{k+2}(P), \tag{A.3.2}$$

where $a = 1, \ldots, N$ and for a top quark, $N = N_c$. To compute amplitudes for these states, we use

$$\begin{aligned}
&\frac{\langle P'; k' | \int d^4x\, \phi_1(x)^{n_1} \cdots \phi_r(x)^{n_r} \overline{\psi}_{L/R}(x) \psi_{R/L}(x) | P; k, L/R \rangle}{(2\pi)^4 \delta^4(P' - P)} \\
&\qquad = C_{k'}^* C_k'' n_1! \cdots n_r! \frac{2NE^2}{(k+2)(k+1)} \Phi_{k'}(P) \Phi_{k+2}(P), \\
&\qquad = \frac{1}{C_{k'} (C_k'')^*} \frac{n_1! \cdots n_r!}{k_1! \cdots k_r! k_1'! \cdots k_r'!}, \qquad \text{(A.3.3)} \\
&\frac{\langle P'; k' | \int d^4x\, \phi_1(x)^{n_1} \cdots \phi_r(x)^{n_r} \overline{\psi}_{L/R}(x) \psi_{R/L}(x) | P; k, R/L \rangle}{(2\pi)^4 \delta^4(P' - P)} = 0. \qquad \text{(A.3.4)}
\end{aligned}$$

A.4 Example Calculations

We now give some examples of calculations involving these rules. The amplitudes involving a single insertion of a vertex without derivatives is straightforward using the formulas given above, and will not be discussed further. Diagrams with derivatives are less trivial because the derivatives may act on fields that are connected with either initial or final state particles. For example, consider

$$\begin{aligned}
\frac{\langle P'; 2 | \int d^4x\, \phi^2 (\partial\phi)^2 | P; 2 \rangle}{(2\pi)^4 \delta^4(P' - P)} &= \int d^4x \Big[\langle P'; 2 | \phi^2 | 0 \rangle \langle 0 | (\partial\phi)^2 | P; 2 \rangle \\
&\qquad + \langle P'; 2 | (\partial\phi)^2 | 0 \rangle \langle 0 | \phi^2 | P; 2 \rangle \\
&\qquad + 4 \langle P'; 2 | \phi \partial^\mu \phi | 0 \rangle \langle 0 | \phi \partial_\mu \phi | P; 2 \rangle \Big] \\
&= 4 |C_2|^2 \left(-2 \cdot \frac{1}{2} E^2 + 4 \cdot \frac{-iP^\mu}{2} \frac{iP_\mu}{2} \right) \Phi_2(P)^2 = 0. \qquad \text{(A.4.1)}
\end{aligned}$$

The cancellation can be understood at the level of the ordinary amplitude from the fact that crossing symmetry implies that the amplitude is proportional to $s + t + u = 4m_\phi^2$, which vanishes in the massless limit.

We now give an example of a diagram that contains a propagator:

$$\begin{aligned}\frac{\langle P';0,0,2|\int d^4x\,(\partial\phi_3)^2\phi_2\int d^4y\,\phi_2(\partial\phi_1)^2|P';2,0,0\rangle}{(2\pi)^4\delta^4(P'-P)} \\ &= |C_2|^2\int d\Phi_2(P';p_1',p_2')\,d\Phi_2(P;p_1,p_2)\,(2p_1'\cdot p_2')(2p_1\cdot p_2)\frac{i}{P^2} \\ &= |C_2|^2\frac{i}{E^2}\big[E^2\Phi_2(P)\big]^2. \end{aligned} \tag{A.4.2}$$

Diagrams with propagators are generally subleading at high energies compared to diagrams with a single insertion. There are a few relevant exceptions, which are discussed in the main chapter.

A.5 IR Enhancement

The amplitudes $\hat{\mathcal{M}}$ are dimensionless, and once coupling constants have been factored out, they depend on a single dimensionful variable E in the massless limit. The dependence on E is therefore determined by dimensional analysis, provided that there are no IR enhancements in the massless limit. Such IR enhancements can arise because the integration over initial and final state phase space can go over regions where internal propagators go on shell. We now present arguments that such IR enhancements do not invalidate the leading large E scaling for any of the processes used to set the unitarity bounds in this chapter. First, we show that many (but not all) possible IR enhancements can be ruled out by a simple parametric argument. Second, we give a diagrammatic argument that IR enhancements can modify the naïve power counting by at most corrections of order $\log(E/m)^n$ for some positive integer n, where m is the mass of a SM particle such as m_W or m_h. Finally, we point out that the gauge boson equivalence theorem itself is invalid in the phase space region of the potential

IR enhancements, since these are regions where some Lorentz invariants $p_i \cdot p_j \sim m_W^2$ rather than E^2. Therefore, phase space integration over these regions is suspect. (We note that this issue arises already for $2 \to 2$ partial wave amplitudes.) We argue that, because the singular phase space regions are parametrically small, they cannot give rise to additional $\log(E/m_W)$ enhancements, and therefore the Goldstone amplitudes correctly give the correct leading behavior at large E.

For the parametric argument, consider an amplitude with leading large-E behavior

$$\hat{\mathcal{M}} \sim C \left(\frac{E}{v}\right)^n \left(\frac{E}{m}\right)^r \log(E/m)^s, \tag{A.5.1}$$

where C is a BSM coupling, m is an IR mass (such as m_W or m_h), and n, r, s are non-negative integers. Observe that if $r + s > 0$ this becomes arbitrarily large for any fixed E in the limit $m \to 0$ with v and c fixed. But the amplitude cannot become arbitrarily large in this limit because the massless limit is equivalent to a weak-coupling limit where the SM couplings $g, \lambda, y_t \to 0$. The coupling C is held fixed in this limit, but can be chosen to be arbitrarily small. It is clear that we cannot have unitarity violation at arbitrary energy scales in this limit, so IR enhancements of the form Eq. (A.5.1) are ruled out.

Note that the combinations $\lambda\delta_3$, $\lambda\delta_4$, λc_n, $y_t\delta_{t1}$, and $y_t c_{tn}$ should be viewed as BSM couplings that are held fixed in the limit $\lambda, y_t \to 0$. On the other hand, the couplings δ_{V1}, δ_{V2}, and c_{Vn} for $n \geq 3$ should be held fixed in the $g \to 0$ limit, since these give Nambu-Goldstone interactions of finite strength in this limit. This limit rules out many possible IR enhancements, but it is not sufficient to justify the power counting of the amplitudes in Eqs. (2.2.5), (2.3.8), (2.4.5), (2.5.1), and (2.5.6). In particular, it does not rule out power IR enhancements proportional to additional powers of the SM couplings g, λ, y_t, for example

$$\lambda \frac{E^2}{m_h^2} \sim \frac{E^2}{v^2}, \qquad y_t \frac{E}{m_t} \sim \frac{E}{v}, \qquad g^2 \frac{E^2}{m_W^2} \sim \frac{E^2}{v^2}, \tag{A.5.2}$$

which have a finite weak-coupling limit as well as log terms such as

$$\lambda \ln(E^2/m_h^2), \qquad y_t \ln(E/m_t), \qquad g^2 \ln(E^2/m_W^2), \tag{A.5.3}$$

which go to zero as $\lambda, y_t, g \to 0$.

Next, by examining the structure of the exchange diagrams, we will now argue that the IR enhancement of tree diagrams is at most logarithmic. In all the amplitudes we computed, we find that such logs are absent, although they may well be present in more complicated diagrams that we have not computed. As we point out below, even though the equivalence theorem cannot be trusted in parts of the phase space where the IR enhancement occurs, it is valid for a parametrically large region that could contribute to a logarithmic enhancement. Therefore, the absence of logs in our calculations prove that the corresponding longitudinal gauge boson scattering amplitudes are free of logs. By excising the small untrustworthy regions, we will then argue that the Nambu-Goldstone amplitudes can be used to set a conservative limit on the unitarity violating scale. A better theoretical understanding of these log corrections is desirable, but we will leave this for future work.

We now consider possible IR enhancements from a general tree diagram contributing to the integrated amplitude $\hat{\mathcal{M}}$, whether computed in the full SM or using the equivalence theorem. An IR divergence can arise only from integrating over a region where an internal propagator becomes large. This can happen if the momentum flowing through an internal line goes on shell, or is soft. If only a single propagator goes on shell, it is easy to understand why the correction is at most logarithmic. Consider an internal line with momentum $q - q'$, where q (q') is the momentum of one of the initial (final) state particles. Then the relevant part of the phase space integral is (in the massless limit)

$$d^4q\,\delta(q^2)\,d^4q'\,\delta(q'^2)\,\frac{1}{(q-q')^2} \propto \frac{d|\boldsymbol{q}|\,d|\boldsymbol{q}'|d\cos\theta}{1-\cos\theta}, \tag{A.5.4}$$

where θ is the angle between $\boldsymbol{q}$ and $\boldsymbol{q}'$. This integral diverges at most logarithmically because the integral has a simple pole in $\cos\theta$, which is one of the integration variables. A general propagator with more legs attached can be analyzed by considering the following momenta structure $P_1 + P_2 \to K_1 + K_2$ where $P_1 = (p_1 + \cdots + p_r), P_2 = (p_{r+1} + \cdots + p_n), K_1 = (k_1 + \cdots + k_s), K_2 = (k_{s+1} + \cdots + k_m)$ and the momentum flowing through the propagator is $K_1 - P_1$. By factorizing the incoming $n-$body phase into $r + (n-r)$-body phase space and similarly for the outgoing, we also see this propagator gives a log when integrating over $\cos\theta = \boldsymbol{P_1} \cdot \boldsymbol{K_1}/(|\boldsymbol{P_1}||\boldsymbol{K_1}|)$.

Next, we have to consider regions of the phase space integration where more than one propagator gets large at the same time. In all the cases we studied, the denominator of each of the large propagators has a linear zero that depends on an independent parameter, either another angle or invariant mass of a set of particles, that is integrated over. That is, near the singularity the integral behaves like $\int dxdy/xy$ and not $\int dx/x^2$. We checked this for $2 \to 2$ and $2 \to 3$ topologies, but we do not have a general proof for all topologies. However, this makes intuitive sense given that a set of n internal propagators going onshell requires n independent conditions on the phase space. Integrating over each of these conditions, then gives at most a $\log^n(E/m)$ singularity.[2]

We now note that in cases where there is a log enhancement in an amplitude involving longitudinal gauge bosons, it is not obvious whether the corresponding Nambu-Goldstone amplitude correctly reproduces these logs. The gauge boson equivalence theorem guarantees that the Nambu-Goldstone amplitude correctly reproduces the full amplitude if $|p_i \cdot p_j| \gg m_V^2$ for all external 4-momenta p_i and more generally for all Mandelstam invariants. To see this, compare the exact dot products of longitudinal polarization vectors

$$\epsilon_L(p_1) \cdot \epsilon_L(p_2) = \frac{E_1 E_2}{m_V^2} \left(\frac{|\boldsymbol{p}_1||\boldsymbol{p}_2|}{E_1 E_2} - \cos\theta \right) \tag{A.5.5}$$

[2] In Ref. [12] it is stated without proof that the $2 \to n$ partial wave amplitudes have at most logarithmic singularities.

with the approximation $\epsilon_L^\mu(p) \simeq p^\mu/m_V$:

$$\frac{p_1}{m_V} \cdot \frac{p_2}{m_V} = \frac{E_1 E_2}{m_V^2}\left(1 - \frac{|\boldsymbol{p}_1||\boldsymbol{p}_2|}{E_1 E_2}\cos\theta\right), \tag{A.5.6}$$

where θ is the angle between $\boldsymbol{p}_1$ and $\boldsymbol{p}_2$. For $E_{1,2} \gg m_V^2$ and $\cos\theta \ll 1$, these are equal up to corrections suppressed by m_V^2/E^2. But for $\theta \sim m_V/E$, the dot products are completely different. (For $\theta = 0$, they even have opposite sign.) This means that we cannot expect the equivalence theorem to be correct in regions where some of the Mandelstam invariants are small.

This is relevant for the present discussion because these regions are precisely the ones where one or more internal propagators can go on shell in the massless limit, potentially giving an IR enhancement. However, we note that the regions where the gauge boson equivalence theorem does not apply are a parametrically small part of the phase space integral. Integrals over such regions cannot give rise to IR singularities of the form $\log(E/m)$, which instead arise from integrals of the form $\sim \int dx/x$ over a parametrically large range $\Delta x \sim E/m$. Thus, for example, when we obtain a Goldstone amplitude $\hat{M}$ that does not have a $\log(E/m)$ enhancement, we know that the corresponding gauge boson amplitude also does not have such an IR enhancement. Omitting the singular region from the phase space integral in a Goldstone amplitude without a log IR enhancement only changes the answer by a small correction suppressed by powers of m_W/E, and therefore gives a good approximation to the exact amplitude.

The discussion above has been less systematic than we would like. It would be nice to have a better understanding of the gauge boson equivalence theorem for partial wave amplitudes, including the IR enhancements and subleading contributions. We leave this for future work.

A.6 Results

We now give the results for the leading high-energy behavior for the processes used in the main text in tables A.1-A.10. All gauge bosons are understood to be longitudinally polarized. Also, note that since Z_L is CP-odd, amplitudes involving an odd number of Z_L's will be purely imaginary, however, these amplitudes can be made real by redefining the Z_L states. All other processes are related to the ones listed in the tables via charge conjugation and/or crossing symmetry. All of these amplitudes are calculated in the contact approximation. As Eqs. (2.3.8), (2.4.5), (2.5.1), and (2.5.6) show, the nonlinear terms are small due to constraints on δ_{V1}, δ_{t1}. However, there are linear terms proportional to δ_{V1}, δ_{V2} in the top processes Eqs. (2.4.5) and (2.5.6), so we've calculated the largest terms as shown in Eqs. (2.4.1) and (2.5.7).

Process	$\times \frac{\delta_{V1} E^2}{8\pi v^2}$	**Process**	$\times \frac{(\delta_{V1} - \frac{1}{2}\delta_{V2}) E^2}{8\pi v^2}$
$ZZ \to W^+W^-$	$-\sqrt{2}$	$hZ \to hZ$	-1
$W^+W^+ \to W^+W^+$	1	$ZZ \to hh$	1
$ZW^+ \to ZW^+$	1	$hW^+ \to hW^+$	-1
$W^+W^- \to W^+W^-$	-1	$hh \to W^+W^-$	$\sqrt{2}$

Table A.1: 4-body model-independent unitarity-violating process from modifications to the Higgs coupling to W/Z bosons. The left-hand side amplitudes are model-independent since they only depend on δ_{V1} while the ones on right-hand side depend on δ_{V2} as well.

Process	$\times \frac{(\delta_{V2} - 4\delta_{V1}) E^3}{96\pi^2 v^3}$	**Process**	$\times \frac{(\delta_{V2} - 4\delta_{V1}) E^3}{96\pi^2 v^3}$
$hW^+W^+ \to W^+W^+$	$\sqrt{2}$	$hW^-W^+ \to ZZ$	-2
$hW^+W^- \to W^+W^-$	$-\sqrt{2}$	$ZW^-W^+ \to hZ$	0
$W^-W^+W^+ \to hW^+$	0	$Z^3 \to hZ$	0
$ZZW^+ \to hW^+$	0	$Z^2h \to Z^2$	0
$hZW^+ \to ZW^+$	$\sqrt{2}$	$Z^2h \to W^+W^-$	-2

Table A.2: 5-body unitarity-violating processes that depend on δ_{V2} and δ_{V1}. One can see that the dim-6 SMEFT prediction $\delta_{V2} = 4\delta_{V1}$ gives vanishing amplitudes for all processes.

Process	$\times \frac{\delta_{Z1} E^2}{8\pi v^2}$	**Process**	$\times \frac{\delta_{Z1} E^3}{24\pi^2 v^3}$
$ZZ \to ZZ$	0	$W^+W^- \to Z^3$	0
$ZZ \to W^+W^-$	$-\frac{1}{\sqrt{2}}\Big(1+\lambda_{WZ}\Big)$	$ZW^+ \to Z^2W^+$	0
$ZW^+ \to ZW^+$	$\frac{1}{2}\Big(1+\lambda_{WZ}\Big)$	$Z^2 \to ZW^+W^-$	0
$W^+W^- \to W^+W^-$	$-\lambda_{WZ}$	$W^+W^- \to ZW^+W^-$	0
$W^+W^+ \to W^+W^+$	λ_{WZ}	$W^+W^+ \to ZW^+W^+$	0
$hW^+ \to ZW^+$	$\frac{3i}{2}\Big(1-\lambda_{WZ}\Big)$	$ZW^+ \to W^+W^-W^+$	$i\Big(1-\lambda_{WZ}\Big)$
$W^+W^- \to hZ$	0		

Table A.3: 4-body and some 5-body unitarity-violating processes without assuming custodial symmetry. Here $\lambda_{WZ} = \frac{\delta_{W1}}{\delta_{Z1}} = 1$ in the custodial-preserving limit.

Process	$\times \frac{(\delta_{V2}-4\delta_{V1})E^4}{384\pi^3 v^4}$
$ZZZ \to ZZZ$	0
$W^+W^+W^+ \to W^+W^+W^+$	1
$ZW^+W^+ \to ZW^+W^+$	1
$ZW^+W^- \to ZZZ$	$-\sqrt{\frac{2}{3}}$
$ZZW^+ \to W^+W^+W^-$	$-\frac{2}{3}$
$ZZW^+ \to ZZW^+$	$\frac{2}{3}$
$ZW^+W^- \to ZW^+W^-$	$\frac{1}{3}$
$W^+W^+W^- \to W^+W^+W^-$	$-\frac{1}{3}$

Table A.4: 6-body unitarity-violating processes that depend on δ_{V2} and δ_{V1}. One can see that the dim-6 SMEFT prediction $\delta_{V2} = 4\delta_{V1}$ gives vanishing amplitudes for all processes.

Process	$\times \frac{E^4}{1152\pi^3 v^4}$
$hZ^2 \to hZ^2$	$[4\delta_{V1} - 2\delta_{V2} + \frac{1}{2}c_{V3}]$
$h^2Z \to Z^3$	$-\frac{\sqrt{3}}{2}[4\delta_{V1} - 2\delta_{V2} + \frac{1}{2}c_{V3}]$
$h^2W^+ \to Z^2W^+$	$-\frac{1}{2}[4\delta_{V1} - 2\delta_{V2} + \frac{1}{2}c_{V3}]$
$h^2Z \to ZW^+W^-$	$-\frac{1}{\sqrt{2}}[4\delta_{V1} - 2\delta_{V2} + \frac{1}{2}c_{V3}]$
$h^2W^+ \to W^+W^-W^+$	$-[4\delta_{V1} - 2\delta_{V2} + \frac{1}{2}c_{V3}]$
$hZW^+ \to hZW^+$	$[36\delta_{V1} - 13\delta_{V2} + 2c_{Vc}]$
$hW^+W^+ \to hW^+W^+$	$[36\delta_{V1} - 13\delta_{V2} + 2c_{V3}]$
$hW^+W^- \to hW^+W^-$	$-[28\delta_{V1} - 9\delta_{V2} + c_{V3}]$
$hZ^2 \to hW^+W^-$	$-\sqrt{2}[32\delta_{V1} - 11\delta_{V2} + \frac{3}{2}c_{V3}]$

Table A.5: 6-body unitarity-violating processes that depend on δ_{V1}, δ_{V2}, and c_{V3}. One can see that the dim-6 SMEFT prediction $\delta_{V2} = 4\delta_{V1}$ and $c_{V3} = 8\delta_{V1}$ gives vanishing amplitudes for all processes.

Process	$\times \frac{m_t \delta_{t1} E}{8\pi v^2}$	**Process**	$\times \frac{m_t \delta_{t1} E}{8\pi v^2}$
$\bar{t}_R t_R \to Zh$	$i\sqrt{N_c}$	$t_R W^+ \to t_L W^+$	$-\frac{1}{2}$
$\bar{t}_R t_R \to ZZ$	$-\sqrt{\frac{N_c}{2}}$	$\bar{b}_R t_R \to hW^+$	$\sqrt{2N_c}$
$\bar{t}_R t_R \to W^-W^+$	$-\sqrt{N_c}$	$t_R h \to b_L W^+$	$\frac{1}{\sqrt{2}}$
$t_R Z \to t_L h$	$\frac{i}{2}$	$t_R W^- \to b_L h$	$\frac{1}{\sqrt{2}}$
$t_R Z \to t_L Z$	$-\frac{1}{2}$		
Process	$\times \frac{m_t c_{t2} E}{8\pi v^2}$	**Process**	$\times \frac{m_t c_{t2} E}{8\pi v^2}$
$\bar{t}_R t_R \to hh$	$-\sqrt{\frac{N_c}{2}}$	$t_R h \to t_L h$	$-\frac{1}{2}$

Table A.6: 4-body model-independent unitarity-violating processes from the top sector.

Process	$\times \frac{m_t \delta_{t1} E^2}{64\pi^2 v^3}$	**Process**	$\times \frac{m_t \delta_{t1} E^2}{64\pi^2 v^3}$
$\bar{t}_R t_R \to ZZZ$	$i\sqrt{3N_c}$	$Z^2 \to \bar{t}_L b_L W^+$	$\sqrt{\frac{2N_c}{3}}$
$\bar{t}_R t_R \to ZW^+W^-$	$i\sqrt{2N_c}$	$ZW^- \to Zb_L\bar{t}_L$	$2\sqrt{\frac{N_c}{3}}$
$t_R Z \to t_L W^- W^+$	$\frac{i}{\sqrt{3}}$	$t_R Z \to b_L Z W^+$	$\sqrt{\frac{2}{3}}$
$t_R Z \to t_L ZZ$	$i\sqrt{\frac{3}{2}}$	$t_R W^- \to b_L Z^2$	$\frac{1}{\sqrt{3}}$
$t_R W^+ \to t_L Z W^+$	$\frac{i}{\sqrt{3}}$	$\bar{b}_R t_R \to W^+W^+W^-$	$2\sqrt{2N_c}$
$W^+W^- \to \bar{t}_L t_L Z$	$i\sqrt{\frac{2N_c}{3}}$	$W^-W^- \to b_L\bar{t}_L W^-$	$2\sqrt{\frac{2N_c}{3}}$
$W^+Z \to \bar{t}_L t_L W^+$	$i\sqrt{\frac{2N_c}{3}}$	$W^+W^- \to b_L\bar{t}_L W^+$	$4\sqrt{\frac{N_c}{3}}$
$ZZ \to \bar{t}_L t_L Z$	$i\sqrt{3N_c}$	$t_R W^+ \to b_L W^+W^+$	$2\sqrt{\frac{N_c}{3}}$
$\bar{b}_R t_R \to Z^2 W^+$	$\sqrt{2N_c}$	$t_R W^- \to b_L W^-W^+$	$2\sqrt{\frac{2N_c}{3}}$

Table A.7: 5-body model-independent unitarity-violating processes from the top sector.

Process	$\times \frac{\left(\frac{1}{2}c_{t2} - \delta_{t1}\right) m_t E^2}{32\pi^2 v^3}$	**Process**	$\times \frac{\left(\frac{1}{2}c_{t2} - \delta_{t1}\right) m_t E^2}{32\pi^2 v^3}$
$\bar{t}_R t_R \to Zh^2$	$i\sqrt{N_c}$	$\bar{t}_R t_R \to W^+W^-h$	$-\sqrt{2N_c}$
$h^2 \to Z\bar{t}_L t_L$	$i\sqrt{\frac{N_c}{3}}$	$W^+W^- \to \bar{t}_L t_L h$	$-\sqrt{\frac{2N_c}{3}}$
$Zh \to h\bar{t}_L t_L$	$i\sqrt{\frac{2N_c}{3}}$	$W^+h \to \bar{t}_L t_L W^+$	$-\sqrt{\frac{2N_c}{3}}$
$t_R Z \to t_L h^2$	$\frac{i}{\sqrt{6}}$	$t_R W^+ \to t_L W^+ h$	$-\frac{1}{\sqrt{3}}$
$t_R h \to t_L Zh$	$\frac{i}{\sqrt{3}}$	$t_R h \to t_L W^+W^-$	$-\frac{1}{\sqrt{3}}$
$\bar{t}_R t_R \to Z^2 h$	$-\sqrt{N_c}$	$\bar{b}_R t_R \to W^+h^2$	$\sqrt{2N_c}$
$Z^2 \to \bar{t}_L t_L h$	$-\sqrt{\frac{N_c}{3}}$	$W^-h \to b_L\bar{t}_L h$	$2\sqrt{\frac{N_c}{3}}$
$Zh \to \bar{t}_L t_L Z$	$-\sqrt{\frac{2N_c}{3}}$	$h^2 \to b_L\bar{t}_L W^+$	$\sqrt{\frac{2N_c}{3}}$
$t_R h \to t_L Z^2$	$-\frac{1}{\sqrt{6}}$	$t_R W^- \to b_L h^2$	$\frac{1}{\sqrt{3}}$
$t_R Z \to t_L Zh$	$-\frac{1}{\sqrt{3}}$	$t_R h \to b_L W^+h$	$\sqrt{\frac{2}{3}}$

Table A.8: 5-body unitarity-violating processes that depend on c_{t2} and δ_{t1}.

Process	$\times \frac{(3\delta_{t1}-c_{t2})m_t E^3}{256\pi^3 v^4}$	**Process**	$\times \frac{(3\delta_{t1}-c_{t2})m_t E^3}{256\pi^3 v^4}$
$\bar{t}_R t_R Z \to Z^3$	$\sqrt{\frac{N_c}{2}}$	$t_R Z^2 \to t_L Z h$	$-\frac{i}{\sqrt{2}}$
$t_R Z^2 \to t_L Z^2$	$\frac{1}{2}$	$\bar{t}_R t_R Z \to h W^+ W^-$	$-i\sqrt{\frac{N_c}{3}}$
$\bar{t}_R t_R W^+ \to Z^2 W^+$	$\sqrt{\frac{N_c}{6}}$	$t_R Z h \to t_L W^+ W^-$	$-\frac{i}{3}$
$\bar{t}_R t_R Z \to Z W^+ W^-$	$\sqrt{\frac{N_c}{3}}$	$\bar{b}_R t_R W^- \to h Z^2$	$-\sqrt{\frac{N_c}{3}}$
$t_R Z^2 \to t_L W^+ W^-$	$\frac{1}{3\sqrt{2}}$	$\bar{b}_R t_R Z \to h Z W^+$	$-\sqrt{\frac{2N_c}{3}}$
$t_R Z W^+ \to t_L Z W^+$	$\frac{1}{3}$	$t_R Z^2 \to b_L W^+ h$	$-\frac{1}{3}$
$\bar{t}_R t_R W^+ \to W^+ W^+ W^-$	$\sqrt{\frac{2N_c}{3}}$	$t_R Z h \to b_L Z W^+$	$-\frac{\sqrt{2}}{3}$
$t_R W^+ W^+ \to t_L W^+ W^+$	$\frac{1}{3}$	$\bar{b}_R t_R h \to W^+ W^+ W^-$	$-2\sqrt{\frac{N_c}{3}}$
$t_R W^+ W^- \to t_L W^+ W^-$	$\frac{2}{3}$	$\bar{b}_R t_R W^- \to h W^+ W^-$	$-2\sqrt{\frac{2N_c}{3}}$
$\bar{t}_R t_R h \to Z^3$	$-i\sqrt{\frac{N_c}{2}}$	$t_R W^- W^- \to b_L W^- h$	$-\frac{2}{3}$
$\bar{t}_R t_R Z \to Z^2 h$	$-i\sqrt{\frac{3N_c}{2}}$	$t_R W^- h \to b_L W^+ W^-$	$-\frac{2\sqrt{2}}{3}$
$\bar{b}_R t_R W^+ \to h W^+ W^+$	$-2\sqrt{\frac{N_c}{3}}$		

Table A.9: 6-body unitarity-violating processes that depend on c_{t2} and δ_{t1}. One can see that the dim-6 SMEFT prediction $c_{t2} = 3\delta_{t1}$ gives vanishing amplitudes for all processes.

Process	$\times \frac{(c_{t2}-3\delta_{t1})m_t E^4}{1024\pi^4 v^5}$	**Process**	$\times \frac{(c_{t2}-3\delta_{t1})m_t E^4}{1024\pi^4 v^5}$
$\bar{t}_R t_R Z \to Z^4$	$\frac{5i}{4}\sqrt{\frac{N_c}{3}}$	$ZW^+W^+ \to \bar{t}_L t_L W^+W^+$	$\frac{i\sqrt{N_c}}{6}$
$\bar{t}_R t_R W^+ \to W^+Z^3$	$\frac{i}{2}\sqrt{\frac{N_c}{3}}$	$ZW^+W^- \to \bar{t}_L t_L Z^2$	$\frac{i}{2}\sqrt{\frac{N_c}{2}}$
$\bar{t}_R t_R W^+ \to ZW^-W^+W^+$	$\frac{i\sqrt{N_c}}{3}$	$ZW^+W^- \to \bar{t}_L t_L W^+W^-$	$\frac{i\sqrt{N_c}}{3}$
$\bar{t}_R t_R Z \to W^+W^+W^-W^-$	$\frac{i}{3}\sqrt{\frac{N_c}{2}}$	$W^+W^+W^- \to \bar{t}_L t_L ZW^+$	$\frac{i}{3}\sqrt{\frac{N_c}{2}}$
$t_R Z^2 \to t_L ZW^-W^+$	$\frac{i}{4}$	$\bar{b}_R t_R W^- \to Z^4$	$\frac{1}{4}\sqrt{\frac{2N_c}{3}}$
$t_R Z^2 \to t_L Z^3$	$\frac{5i}{4\sqrt{6}}$	$\bar{b}_R t_R Z \to W^+Z^3$	$\frac{1}{2}\sqrt{\frac{2N_c}{3}}$
$t_R W^+W^+ \to t_L ZW^+W^+$	$\frac{i}{6\sqrt{2}}$	$Z^3 \to b_L \bar{t}_L ZW^+$	$\frac{1}{2}\sqrt{\frac{N_c}{3}}$
$t_R W^-W^+ \to t_L Z^3$	$\frac{i}{4\sqrt{3}}$	$Z^2W^- \to b_L \bar{t}_L Z^2$	$\frac{1}{2}\sqrt{\frac{N_c}{2}}$
$t_R W^-W^+ \to t_L ZW^+W^-$	$\frac{i}{3\sqrt{2}}$	$t_R Z^2 \to b_L W^+Z^2$	$\frac{1}{4}$
$t_R ZW^+ \to t_L Z^2W^+$	$\frac{i}{4}$	$t_R ZW^- \to b_L Z^3$	$\frac{\sqrt{2}}{4\sqrt{3}}$
$t_R ZW^+ \to t_L W^+W^+W^-$	$\frac{i}{6}$	$\bar{b}_R t_R W^+ \to W^+W^+Z^2$	$\frac{\sqrt{N_c}}{3}$
$Z^3 \to \bar{t}_L t_L Z^2$	$\frac{5i}{4}\sqrt{\frac{N_c}{3}}$	$\bar{b}_R t_R W^- \to Z^2W^+W^-$	$\frac{\sqrt{2N_c}}{3}$
$Z^3 \to \bar{t}_L t_L W^+W^-$	$\frac{i}{2}\sqrt{\frac{N_c}{6}}$	$W^+W^-W^- \to b_L \bar{t}_L Z^2$	$\frac{1}{3}\sqrt{\frac{N_c}{2}}$
$Z^2W^+ \to \bar{t}_L t_L ZW^+$	$\frac{i}{2}\sqrt{\frac{N_c}{2}}$	$ZW^-W^- \to b_L \bar{t}_L ZW^-$	$\frac{\sqrt{N_c}}{3}$
$t_R W^-W^- \to b_L W^-Z^2$	$\frac{1}{6}$	$W^+W^-W^- \to b_L \bar{t}_L W^-W^+$	$\sqrt{N_c}$
$t_R W^+W^- \to b_L Z^2W^+$	$\frac{\sqrt{2}}{6}$	$W^+W^+W^- \to b_L \bar{t}_L W^+W^+$	$\sqrt{\frac{N_c}{2}}$
$t_R ZW^- \to b_L ZW^-W^+$	$\frac{1}{3}$	$t_R W^+W^+ \to b_L W^+W^+W^+$	$\frac{1}{2\sqrt{3}}$
$\bar{b}_R t_R W^+ \to W^+W^+W^+W^-$	$\sqrt{\frac{2N_c}{3}}$	$t_R W^-W^- \to b_L W^+W^-W^-$	$\frac{1}{2}$
$\bar{b}_R t_R W^- \to W^-W^-W^+W^+$	$\sqrt{N_c}$	$t_R W^+W^- \to b_L W^-W^+W^+$	$\frac{1}{\sqrt{2}}$
$W^-W^-W^- \to b_L \bar{t}_L W^-W^-$	$\sqrt{\frac{N_c}{6}}$	$t_R Z^2 \to b_R W^+W^-W^+$	$\frac{1}{6}$
$\bar{t}_R t_R Z \to W^+W^-Z^2$	$\frac{i\sqrt{N_c}}{2}$	$\bar{b}_R t_R ZW^- \to W^+W^-Z$	$\frac{\sqrt{2N_c}}{3}$
$\bar{b}_R t_R W^+W^- \to Z^2W^+$	$\frac{\sqrt{N_c}}{3}$	$\bar{b}_R t_R Z \to W^+W^-W^+Z$	$\frac{\sqrt{2N_c}}{3}$

Table A.10: 7-body unitarity-violating processes that depend on c_{t2} and δ_{t1}. One can see that the dim-6 SMEFT prediction $c_{t2} = 3\delta_{t1}$ gives vanishing amplitudes for all processes.

Appendix B

Cross sections, the R-values and errors

In this appendix, we list the cross sections and the R-values for the two-dimensional bins in terms of $m_{t\bar{t}}, \theta^*$. The cross sections are presented in Table B.1 for 10 TeV muon collider and in Table B.2 for 30 TeV muon collider. The R-values are given in Table B.3 for 10 TeV muon collider and in Table B.4 for 30 TeV muon collider. The errors in the tables are associated with the limited number of events generated by `Madgraph5` [126] and we describe about how to obtain them in the following. Note that we do not take into account the errors when we make the projections for the top Yukawa coupling measurement.

The cross section of a given process for some set of cuts is

$$\sigma = \frac{\sum_i w_i}{N} \tag{B.0.1}$$

where the w_i are the weights of events that remain after the cuts and N is the total amount of events in the run [1]. In the case where all events have positive weight, the error is the familiar $\frac{1}{\sqrt{N}}$. However, the error increases when roughly half of the events have negative

[1] In order to find cross sections across multiple LHE files with different cuts, we simply sum the individual over cross sections.

weight.

To determine the error in the cross section, we begin by writing the cross section of each individual run as

$$\sigma = \sigma_+ + \sigma_- = \frac{wm_1}{N} - \frac{wm_2}{N}, \tag{B.0.2}$$

where N denotes the total number of events in the LHE file, m_1 is the total number of positive weight events, m_2 the number of negative weights, and w is absolute value of the weight. For the case where no cuts are imposed, we have that $m_1 + m_2 = N$, but this is not the case in general. Taking $\frac{\delta\sigma_+}{\sigma_+} = \frac{1}{\sqrt{m_1}}$ and similar for σ_-, we have that

$$\begin{aligned} \delta\sigma^2 = \delta\sigma_+^2 + \delta\sigma_-^2 &= \frac{w^2(m_1+m_2)}{N^2} \\ \delta\sigma &= \sigma\frac{\sqrt{m_1+m_2}}{m_1-m_2} \end{aligned} \tag{B.0.3}$$

which is the error for each LHE file. The second line of Eq. (B.0.3) assumes that $m_1 \neq m_2$. Since the total cross section of a given bin is found by summing up the individual cross sections of the LHE files, we have that

$$\delta\sigma_{bin}^2 = \sum_i \delta\sigma_i^2 \tag{B.0.4}$$

Table B.1: The SM cross sections in [fb] in the two dimensional bins $m_{t\bar{t}}, \theta^*$ for the process $\mu^+\mu^- \to t\bar{t}\nu\bar{\nu}$ after all the preliminary cuts in Eq. (4.2.7), (4.2.8), (4.2.9), (4.2.11).

$m_{t\bar{t}}$[TeV] / θ^* [°] [fb]	**[0,30]**	**[30,60]**	**[60,90]**	**[90,120]**	**[120,150]**	**[150,180]**
[0, 1]	0.670 ± 0.00025	1.22 ± 0.00039	1.48 ± 0.00049	0.503 ± 0.00038	0.0933 ± 0.00022	0.0145 ± 0.00011
[1, 2]	0.234 ± 8.5×10^{-5}	0.233 ± 0.00012	0.142 ± 0.00012	0.0403 ± 8.3×10^{-5}	0.0122 ± 5.8×10^{-5}	0.00270 ± 3.5×10^{-5}
[2, 4]	0.0449 ± 2.3×10^{-5}	0.0322 ± 2.6×10^{-5}	0.0141 ± 2.3×10^{-5}	4.61×10^{-3} ± 1.6×10^{-5}	1.95×10^{-3} ± 1.3×10^{-5}	6.52×10^{-4} ± 9.0×10^{-6}
[4, 6]	3.08×10^{-3} ± 2.2×10^{-6}	1.76×10^{-3} ± 2.3×10^{-6}	6.49×10^{-4} ± 1.8×10^{-6}	2.78×10^{-4} ± 1.4×10^{-6}	1.40×10^{-4} ± 1.1×10^{-6}	8.01×10^{-5} ± 8.2×10^{-7}
[6, 8]	2.46×10^{-4} ± 1.9×10^{-7}	1.23×10^{-4} ± 1.9×10^{-7}	5.56×10^{-5} ± 1.5×10^{-7}	3.16×10^{-5} ± 1.1×10^{-7}	2.43×10^{-5} ± 8.8×10^{-8}	1.73×10^{-5} ± 6.9×10^{-8}
[8, 10]	8.33×10^{-6} ± 5.2×10^{-9}	6.71×10^{-6} ± 5.2×10^{-9}	6.47×10^{-6} ± 3.9×10^{-9}	6.21×10^{-6} ± 3.0×10^{-9}	7.13×10^{-6} ± 2.4×10^{-9}	9.54×10^{-6} ± 1.9×10^{-9}

Table B.2: The SM cross sections in the two dimensional bins $m_{t\bar{t}}, \theta^*$ for the process $\mu^+\mu^- \to t\bar{t}\nu\bar{\nu}$ at 30 TeV muon collider after all the preliminary cuts in Eq. (4.2.7), (4.2.8), (4.2.9), (4.2.11).

$m_{t\bar{t}}$[TeV] / θ^* [°] [fb]	**[0,30]**	**[30,60]**	**[60,90]**	**[90,120]**	**[120,150]**	**[150,180]**
[0, 1]	0.641 ± 0.00033	1.28 ± 0.00055	1.95 ± 0.00080	0.61 ± 0.00060	0.085 ± 0.00031	0.0119 ± 0.00014
[1, 5]	0.368 ± 0.00021	0.376 ± 0.00026	0.314 ± 0.00031	0.0821 ± 0.00022	0.0174 ± 0.00013	0.00375 ± 0.000083
[5, 10]	$8.33 \times 10^{-3} \pm 1.2 \times 10^{-5}$	$6.40 \times 10^{-3} \pm 1.4 \times 10^{-5}$	$3.03 \times 10^{-3} \pm 1.3 \times 10^{-5}$	$9.68 \times 10^{-4} \pm 9.0 \times 10^{-6}$	$3.90 \times 10^{-4} \pm 6.6 \times 10^{-6}$	$1.27 \times 10^{-4} \pm 4.8 \times 10^{-6}$
[10, 15]	$7.52 \times 10^{-4} \pm 1.5 \times 10^{-6}$	$4.55 \times 10^{-4} \pm 1.7 \times 10^{-6}$	$1.73 \times 10^{-4} \pm 1.3 \times 10^{-6}$	$6.71 \times 10^{-5} \pm 9.8 \times 10^{-7}$	$3.22 \times 10^{-5} \pm 7.7 \times 10^{-7}$	$1.41 \times 10^{-5} \pm 5.8 \times 10^{-7}$
[15, 20]	$9.77 \times 10^{-5} \pm 2.2 \times 10^{-7}$	$5.02 \times 10^{-5} \pm 2.3 \times 10^{-7}$	$1.97 \times 10^{-5} \pm 1.8 \times 10^{-7}$	$9.15 \times 10^{-6} \pm 1.3 \times 10^{-7}$	$5.65 \times 10^{-6} \pm 1.1 \times 10^{-7}$	$3.17 \times 10^{-6} \pm 8.3 \times 10^{-8}$
[20, 25]	$1.02 \times 10^{-5} \pm 2.4 \times 10^{-8}$	$5.29 \times 10^{-6} \pm 2.4 \times 10^{-8}$	$2.80 \times 10^{-6} \pm 1.8 \times 10^{-8}$	$1.83 \times 10^{-6} \pm 1.4 \times 10^{-8}$	$1.46 \times 10^{-6} \pm 1.1 \times 10^{-8}$	$1.12 \times 10^{-6} \pm 8.5 \times 10^{-9}$
[25, 30]	$4.47 \times 10^{-7} \pm 7.2 \times 10^{-10}$	$4.81 \times 10^{-7} \pm 7.2 \times 10^{-10}$	$5.44 \times 10^{-7} \pm 5.4 \times 10^{-10}$	$5.93 \times 10^{-7} \pm 4.1 \times 10^{-10}$	$7.04 \times 10^{-7} \pm 3.3 \times 10^{-10}$	$1.02 \times 10^{-6} \pm 2.6 \times 10^{-10}$

Table B.3: R-values in the two dimensional bins $m_{t\bar{t}}, \theta^*$ for the process $\mu^+\mu^- \to t\bar{t}\nu\bar{\nu}$ after all the preliminary cuts in Eq. (4.2.7), (4.2.8), (4.2.9), (4.2.11).

$m_{t\bar{t}}$[TeV] / θ^*[°]	**[0,30]**	**[30,60]**	**[60,90]**	**[90,120]**	**[120,150]**	**[150,180]**
[0, 1]						
R_1	0.209 ± 0.070	0.143 ± 0.052	-0.0484 ± 0.047	-0.647 ± 0.081	-1.54 ± 0.19	-2.60 ± 0.48
R_2	0.279 ± 0.67	0.563 ± 0.51	1.16 ± 0.48	3.40 ± 0.82	7.20 ± 1.7	12.8 ± 4.1
[1, 2]						
R_1	-0.0314 ± 0.055	-0.0778 ± 0.055	-0.266 ± 0.071	-0.827 ± 0.13	-1.79 ± 0.24	-3.81 ± 0.51
R_2	1.29 ± 0.57	3.06 ± 0.54	8.43 ± 0.70	29.9 ± 1.4	58.3 ± 2.3	110 ± 4.5
[2, 4]						
R_1	-0.0124 ± 0.052	-0.116 ± 0.061	-0.313 ± 0.092	-0.790 ± 0.16	-1.33 ± 0.25	-2.68 ± 0.43
R_2	5.28 ± 0.54	12.8 ± 0.57	36.2 ± 0.89	110 ± 1.7	212 ± 2.7	362 ± 6.2
[4, 6]						
R_1	-0.0109 ± 0.050	-0.127 ± 0.066	-0.331 ± 0.11	-0.481 ± 0.17	-0.842 ± 0.23	-1.25 ± 0.31
R_2	17.1 ± 0.53	44.7 ± 0.60	128 ± 1.1	297 ± 2.2	556 ± 4.9	649 ± 7.1
[6, 8]						
R_1	-0.0171 ± 0.049	-0.0997 ± 0.069	-0.205 ± 0.10	0.211 ± 0.14	-0.252 ± 0.16	-0.218 ± 0.18
R_2	33.7 ± 0.52	95.5 ± 0.65	207 ± 1.1	365 ± 1.9	478 ± 2.4	479 ± 2.5
[8, 10]						
R_1	0.0116 ± 0.073	-0.0316 ± 0.082	-0.0188 ± 0.083	-0.0103 ± 0.085	0.00346 ± 0.079	0.00128 ± 0.068
R_2	47.9 ± 0.79	81.3 ± 0.77	82.1 ± 0.80	85.2 ± 0.88	76.7 ± 0.86	41.7 ± 0.62

Table B.4: R-values in the two dimensional bins $m_{t\bar{t}}, \theta^*$ for the process $\mu^+\mu^- \to t\bar{t}\nu\bar{\nu}$ after all the preliminary cuts in Eq. (4.2.7), (4.2.8), (4.2.9), (4.2.11).

$m_{t\bar{t}}$[TeV] / $\theta^*[^\circ]$	**[0,30]**	**[30,60]**	**[60,90]**	**[90,120]**	**[120,150]**	**[150,180]**
[0, 1]						
R_1	0.197 ± 0.0056	0.137 ± 0.0044	-0.0365 ± 0.0041	-0.694 ± 0.012	-1.66 ± 0.057	-2.88 ± 0.24
R_2	0.286 ± 0.0078	0.508 ± 0.0072	1.08 ± 0.0091	3.55 ± 0.042	9.70 ± 0.32	22.3 ± 2.1
[1, 5]						
R_1	-0.00399 ± 0.0057	-0.0849 ± 0.0071	-0.287 ± 0.0099	-0.956 ± 0.030	-2.05 ± 0.10	-4.76 ± 0.39
R_2	2.66 ± 0.028	5.50 ± 0.049	12.8 ± 0.11	48.0 ± 0.71	145 ± 5.2	368 ± 30
[5, 10]						
R_1	-0.0171 ± 0.015	-0.101 ± 0.022	-0.236 ± 0.041	-0.824 ± 0.095	-0.882 ± 0.17	-2.59 ± 0.41
R_2	32.4 ± 0.30	92.4 ± 0.94	242 ± 3.3	654 ± 14	1459 ± 54	3465 ± 259
[10, 15]						
R_1	-0.00494 ± 0.020	-0.131 ± 0.037	-0.346 ± 0.077	-0.732 ± 0.15	-1.09 ± 0.24	-1.35 ± 0.42
R_2	99.5 ± 0.84	335 ± 3.6	890 ± 14	1946 ± 45	4012 ± 138	7773 ± 460
[15, 20]						
R_1	-0.0605 ± 0.023	-0.129 ± 0.046	-0.351 ± 0.092	0.406 ± 0.15	-0.914 ± 0.19	-0.639 ± 0.26
R_2	195 ± 1.5	738 ± 7.8	1770 ± 28	3159 ± 65	5080 ± 133	9193 ± 386
[20, 25]						
R_1	-0.0195 ± 0.023	-0.0786 ± 0.045	-0.0399 ± 0.064	-0.0314 ± 0.074	-0.201 ± 0.075	-0.268 ± 0.076
R_2	321 ± 2.5	1166 ± 13	1942 ± 27	2519 ± 40	3201 ± 56	4070 ± 95
[25, 30]						
R_1	0.0111 ± 0.016	-0.00137 ± 0.015	-0.0253 ± 0.010	-0.00295± 0.0069	0.00193 ± 0.0047	0.00218 ± 0.0026
R_2	339 ± 4.3	568 ± 7.7	488 ± 6.3	373 ± 4.3	303 ± 3.1	214 ± 2.2

Appendix C

Helicity Amplitudes for $W^+W^- \to t\bar{t}$

In this appendix, we present the full helicity amplitudes for the subprocess $W^+W^- \to t\bar{t}$:

$$\mathcal{M}(W^+(p_1)W^-(p_2) \to t(p_3)\bar{t}(p_4)) = \mathcal{M}^\gamma + \mathcal{M}^Z + \mathcal{M}^h + \mathcal{M}^t \tag{C.0.1}$$

where $\mathcal{M}^{\gamma,Z,h}$ denotes the $s-$channel contribution with γ, Z, h particles as internal lines and $\mathcal{M}^t$ corresponds to the $t-$channel contribution. Since the initial particles have the same masses as well as the final particles, the energies of the top quarks are equal to that of the W bosons in the partonic center-of-mass frame:

$$\hat{E}_t = \hat{E}_W = \frac{\sqrt{\hat{s}}}{2} \tag{C.0.2}$$

The other Mandelstam variables $\hat{t}, \hat{u}$ can be written as functions of $\hat{s}$:

$$\hat{t} = \frac{\hat{s}}{4}\left(-\beta_t^2 - \beta_W^2 + 2\beta_t\beta_W\cos\theta\right), \qquad \hat{u} = \frac{\hat{s}}{4}\left(-\beta_t^2 - \beta_W^2 - 2\beta_t\beta_W\cos\theta\right), \tag{C.0.3}$$

where the velocities of the W-bosons and the top quarks are given by:

$$\beta_{W,t} = \sqrt{1 - \frac{4m_{W,t}^2}{\hat{s}}} \tag{C.0.4}$$

Here the scattering angle θ in the partonic center-of-mass frame is the polar angle between the out-going top quark and the incoming W^+ gauge boson. The z-axis in chosen the direction of the W^+ spatial momentum. The azimuthal angles of the top quark and the anti-top quark are chosen as:

$$\varphi_t = 0, \qquad \varphi_{\bar{t}} = \pi \tag{C.0.5}$$

which will fix the possible i factors in the polarization functions of the anti-top quarks. We will present the helicity amplitudes in terms of the Wigner d functions [77]:

$$\mathcal{M}_{h_1h_2;h_3h_4} = \widetilde{\mathcal{M}}_{h_1h_2;h_3h_4}(\theta)(h_3 - h_4 + \delta_{h_3h_4})(-1)^{h_2} d^{J_0}_{\Delta h_{12},\Delta h_{34}}(\theta) \tag{C.0.6}$$

with

$$\Delta h_{12} = h_1 - h_2, \qquad \Delta h_{34} = h_3 - h_4, \qquad J_0 = \max(|\Delta h_{12}|, |\Delta h_{34}|) \tag{C.0.7}$$

and to make results more compact, we have also extracted some sign factors for convenience. The relevant d functions are listed as follows [124]:

$$\begin{aligned}
&d^1_{1,1} = d^1_{-1,-1} = \frac{1}{2}(1+\cos\theta), \qquad d^1_{1,-1} = d^1_{-1,1} = \frac{1}{2}(1-\cos\theta), \\
&d^1_{1,0} = -d^1_{-1,0} = -\frac{\sin\theta}{\sqrt{2}} \\
&d^2_{1,2} = -d^2_{-1,-2} = \frac{1}{2}\sin\theta(1+\cos\theta), \qquad d^2_{1,-2} = -d^2_{-1,2} = -\frac{1}{2}\sin\theta(1-\cos\theta)
\end{aligned} \tag{C.0.8}$$

which satisfy the following identities:

$$d^j_{m',m} = (-1)^{m-m'} d^j_{m,m'} = d^j_{-m,-m'} \tag{C.0.9}$$

The top Yukawa coupling modification is parametrized as:

$$\mathcal{L}_{ht\bar{t}} = -\frac{m_t}{v}(1+\delta_{tth}) h t\bar{t} \tag{C.0.10}$$

For future studies, we have also included the CP-even anomalous triple gauge boson couplings (aTGC), which are parametrized as follows [77]:

$$\mathcal{L}_{WWV}/g^{\rm SM}_{WWV} = ig_1^V\left(W^+_{\mu\nu}W^{-\mu}V^\nu - W^-_{\mu\nu}W^{+\mu}V^\nu\right) + i\kappa_V W^+_\mu W^-_\nu V^{\mu\nu} + i\frac{\lambda_V}{m_W^2}W^+_{\lambda\mu}W^{-\mu}{}_\nu V^{\nu\lambda} \tag{C.0.11}$$

where $W^\pm_{\mu\nu} = \partial_\mu W^\pm_\nu - \partial_\nu W^\pm_\mu$ and V = γ, Z. The SM values of the TGCs read:

$$g^{\rm SM}_{WW\gamma} = e, \qquad g^{\rm SM}_{WWZ} = g\cos\theta_W. \tag{C.0.12}$$

where θ_W is the weak mixing angle. The unbroken electromagnetism fixes g_1^γ to be 1. So we are left with 5 anomalous TGC couplings: $\delta g_1^Z, \delta\kappa_Z, \delta\kappa_\gamma, \lambda_Z, \lambda_\gamma$ defined as $\delta g_1^Z = g_1^Z - 1, \delta\kappa_V = \kappa_V - 1$. At dimension-six SMEFT, they are further related by the following identities [54]:

$$\delta\kappa_Z = \delta g_1^Z - \tan^2\theta_W\delta\kappa_\gamma, \qquad \lambda_Z = \lambda_\gamma. \tag{C.0.13}$$

but here we will take them as independent couplings. We also take into account the contributions from the possible modifications of the top electroweak couplings and the Higgs gauge boson coupling:

$$\delta_{Wtb} = \frac{g_{Wtb}}{g^{\rm SM}_{Wtb}} - 1, \qquad \delta_{Zt_L} = \frac{g_{Zt_L}}{g^{\rm SM}_{Zt_L}} - 1, \qquad \delta_{Zt_R} = \frac{g_{Zt_R}}{g^{\rm SM}_{Zt_R}} - 1, \qquad \delta_{hWW} = \frac{g_{hWW}}{g^{\rm SM}_{hWW}} - 1 \tag{C.0.14}$$

with their SM values as follows:

$$g^{\rm SM}_{Wt} = \frac{g}{\sqrt{2}}, \quad g^{\rm SM}_{Zt_L} = \frac{g}{\cos\theta_W}\left(\frac{1}{2} - \frac{2}{3}\sin^2\theta_W\right), \quad g^{\rm SM}_{Zt_R} = -\frac{2}{3}\frac{g\sin^2\theta_W}{\cos\theta_W}, \quad g^{\rm SM}_{hWW} = \frac{2m_W^2}{v} \tag{C.0.15}$$

Now, we turn to the formulae for the helicity amplitudes. In order to list them compactly in tables, we further take some pre-factors out of $\widetilde{\mathcal{M}}$:

$$\begin{aligned}
\widetilde{\mathcal{M}}^{\gamma} &= i\frac{2\sqrt{2}g^2 s_W^2 \beta_W}{3} A^{\gamma}_{h_1 h_2; h_3 h_4} \\
\widetilde{\mathcal{M}}^{Z} &= i\sqrt{2}g^2\beta_W \left(\frac{1-\Delta h_{34}\,\beta_t}{4}(1+\delta_{Zt_L}) - \frac{2}{3}s_W^2 \left(1 + \frac{1-\Delta h_{34}\,\beta_t}{2}\delta_{Zt_L} + \frac{1+\Delta h_{34}\,\beta_t}{2}\delta_{Zt_R} \right) \right) \times \\
&\quad \frac{\hat{s}}{\hat{s}-m_Z^2} A^{Z}_{h_1 h_2; h_3 h_4} \\
\widetilde{\mathcal{M}}^{h} &= i\frac{g^2}{2\sqrt{2}}(1+\delta_{tth})(1+\delta_{hWW})\beta_t \frac{\hat{s}}{\hat{s}-m_h^2} A^{h}_{h_1 h_2; h_3 h_4} \\
\widetilde{\mathcal{M}}^{t} &= -i\frac{g^2(1-\Delta h_{34}\,\beta_t)}{2\sqrt{2}\beta_W}(1+\delta_{Wtb})^2 \left(B_{h_1 h_2; h_3 h_4} - \frac{1}{\beta_t^2+\beta_W^2-2\beta_t\beta_W\cos\theta} C_{h_1 h_2; h_3 h_4} \right)
\end{aligned} \tag{C.0.16}$$

where we have abbreviated $\sin\theta_W$ as s_W. Note that the kinematical function in front of $C_{h_1,h_2;h_3,h_4}$ is simply $\frac{\hat{s}}{4\hat{t}}$ and we have omitted the small bottom quark mass. The results for the helicity configurations $(\mp\frac{1}{2},\pm\frac{1}{2})$ of final top and anti-top quarks are presented in Table C.1 and for other helicity configurations $(\mp\frac{1}{2},\mp\frac{1}{2})$, they are shown in Table C.2.

Table C.1: Helicity amplitude factors for $W^+_{h_1}W^-_{h_2} \to t_{h_3}\bar{t}_{h_4}$ for $\Delta h_{34} = \mp 1$. Here $V = \gamma, Z$ and note that $\delta g_1^\gamma = 0$.

$(h_3 h_4)$	$(h_1 h_2)$	$A^V_{h_1h_2;h_3h_4}$	$A^h_{h_1h_2;h_3h_4}$	$B_{h_1h_2;h_3h_4}$	$C_{h_1h_2;h_3h_4}$
	(+1 -1),(-1 +1)	0	0	0	$-2\sqrt{2}\beta_t\beta_W$
	(+1 +1),(-1 -1)	$1+\delta g_1^V+\frac{s}{2m_W^2}\lambda_V$	0	1	$\beta_t^2-\beta_W^2$
$(-\frac{1}{2}\ \frac{1}{2})$	(+1 0),(0 -1)	$\frac{\sqrt{s}}{m_W}\left(1+\frac{\delta g_1^V+\delta\kappa_V+\lambda_V}{2}\right)$	0	$\frac{\sqrt{s}}{m_W}$	$\frac{\sqrt{s}(\beta_t+\beta_W)(\beta_t-\beta_W^2)}{m_W}$
	(-1 0),(0 +1)	$-\frac{\sqrt{s}}{m_W}\left(1+\frac{\delta g_1^V+\delta\kappa_V+\lambda_V}{2}\right)$	0	$-\frac{\sqrt{s}}{m_W}$	$-\frac{\sqrt{s}(\beta_t-\beta_W)(\beta_t-\beta_W^2)}{m_W}$
	(0 0)	$-1-\delta g_1^V-\frac{s}{2m_W^2}(1+\delta\kappa_V)$	0	$-\frac{s}{2m_W^2}$	$-\frac{s\left(\beta_t-\beta_W^2\right)^2}{2m_W^2}$
	(+1 -1),(-1 +1)	0	0	0	$-2\sqrt{2}\beta_t\beta_W$
	(+1 +1),(-1 -1)	$1+\delta g_1^V+\frac{s}{2m_W^2}\lambda_V$	0	1	$\beta_t^2-\beta_W^2$
$(\frac{1}{2}\ -\frac{1}{2})$	(+1 0),(0 -1)	$\frac{\sqrt{s}}{m_W}\left(1+\frac{\delta g_1^V+\delta\kappa_V+\lambda_V}{2}\right)$	0	$\frac{\sqrt{s}}{m_W}$	$\frac{\sqrt{s}(\beta_t-\beta_W)(\beta_t+\beta_W^2)}{m_W}$
	(-1 0),(0 +1)	$-\frac{\sqrt{s}}{m_W}\left(1+\frac{\delta g_1^V+\delta\kappa_V+\lambda_V}{2}\right)$	0	$-\frac{\sqrt{s}}{m_W}$	$-\frac{\sqrt{s}(\beta_t+\beta_W)(\beta_t+\beta_W^2)}{m_W}$
	(0 0)	$-1-\delta g_1^V-\frac{s}{2m_W^2}(1+\delta\kappa_V)$	0	$-\frac{s}{2m_W^2}$	$-\frac{s\left(\beta_t+\beta_W^2\right)^2}{2m_W^2}$

Table C.2: Helicity amplitude factors for $W^+_{h_1}W^-_{h_2} \to t_{h_3}\bar{t}_{h_4}$ for $\Delta h_{34} = 0$. Here $V = \gamma, Z$ and note that $\delta g_1^\gamma = 0$.

$(h_3 h_4)$	$(h_1 h_2)$	$A^V_{h_1h_2;h_3h_4}$	$A^h_{h_1h_2;h_3h_4}$
$(-\frac{1}{2}\ -\frac{1}{2})$	(+1 -1),(-1 +1)	0	0
	(+1 +1),(-1 -1)	$\frac{\sqrt{2}m_t}{\sqrt{s}}\left(1+\delta g_1^V+\frac{s}{2m_W^2}\lambda_V\right)\cos\theta$	$-\frac{\sqrt{2}m_t}{\sqrt{s}}$
	(+1 0),(0 -1)	$\frac{\sqrt{2}m_t}{m_W}\left(1+\frac{\delta g_1^V+\delta\kappa_V+\lambda_V}{2}\right)$	0
	(-1 0),(0 +1)	$-\frac{\sqrt{2}m_t}{m_W}\left(1+\frac{\delta g_1^V+\delta\kappa_V+\lambda_V}{2}\right)$	0
	(0 0)	$-\frac{\sqrt{2}m_t}{\sqrt{s}}\left(1+\delta g_1^V+\frac{s(1+\delta\kappa_V)}{2m_W^2}\right)\cos\theta$	$-\frac{\sqrt{2}m_t\sqrt{s}(1+\beta_W^2)}{4m_W^2}$
$(\frac{1}{2}\ \frac{1}{2})$	(+1 -1),(-1 +1)	0	0
	(+1 +1),(-1 -1)	$-\frac{\sqrt{2}m_t}{\sqrt{s}}\left(1+\delta g_1^V+\frac{s}{2m_W^2}\lambda_V\right)\cos\theta$	$\frac{\sqrt{2}m_t}{\sqrt{s}}$
	(+1 0),(0 -1)	$-\frac{\sqrt{2}m_t}{m_W}\left(1+\frac{\delta g_1^V+\delta\kappa_V+\lambda_V}{2}\right)$	0
	(-1 0),(0 +1)	$\frac{\sqrt{2}m_t}{m_W}\left(1+\frac{\delta g_1^V+\delta\kappa_V+\lambda_V}{2}\right)$	0
	(0 0)	$\frac{\sqrt{2}m_t}{\sqrt{s}}\left(1+\delta g_1^V+\frac{s(1+\delta\kappa_V)}{2m_W^2}\right)\cos\theta$	$\frac{\sqrt{2}m_t\sqrt{s}(1+\beta_W^2)}{4m_W^2}$

$(h_3 h_4)$	$(h_1 h_2)$	$B_{h_1h_2;h_3h_4}$	$C_{h_1h_2;h_3h_4}$
$(-\frac{1}{2}\ -\frac{1}{2})$	(+1 -1),(-1 +1)	0	$-\frac{8m_t\beta_t\beta_W}{\sqrt{3}\sqrt{s}}$
	(+1 +1),(-1 -1)	$\frac{m_t(\beta_t^2-\beta_W^2\mp 2\beta_t\beta_W+2\beta_t\beta_W\cos\theta)}{\sqrt{2}\sqrt{s}\beta_t\beta_W}$	$\frac{m_t(\beta_t\mp\beta_W)^2(\beta_t^2-\beta_W^2)}{\sqrt{2}\sqrt{s}\beta_t\beta_W}$
	(+1 0),(0 -1)	$\frac{\sqrt{2}m_t}{m_W}$	$\frac{\sqrt{2}m_t(\beta_t\mp\beta_W)(\beta_t\pm\beta_W^2)}{m_W}$
	(-1 0),(0 +1)	$-\frac{\sqrt{2}m_t}{m_W}$	$-\frac{\sqrt{2}m_t(\beta_t\pm\beta_W)(\beta_t\pm\beta_W^2)}{m_W}$
	(0 0)	$-\frac{\sqrt{s}m_t(\beta_t^2+\beta_W^4+2\beta_t\beta_W\cos\theta)}{2\sqrt{2}m_W^2\beta_t\beta_W}$	$-\frac{\sqrt{s}m_t(\beta_t^4+\beta_W^6-\beta_t^2(\beta_W^2+\beta_W^4))}{2\sqrt{2}m_W^2\beta_t\beta_W}$
$(\frac{1}{2}\ \frac{1}{2})$	(+1 -1),(-1 +1)	0	$\frac{8m_t\beta_t\beta_W}{\sqrt{3}\sqrt{s}}$
	(+1 +1),(-1 -1)	$-\frac{m_t(\beta_t^2-\beta_W^2\pm 2\beta_t\beta_W+2\beta_t\beta_W\cos\theta)}{\sqrt{2}\sqrt{s}\beta_t\beta_W}$	$-\frac{m_t(\beta_t\pm\beta_W)^2(\beta_t^2-\beta_W^2)}{\sqrt{2}\sqrt{s}\beta_t\beta_W}$
	(+1 0),(0 -1)	$-\frac{\sqrt{2}m_t}{m_W}$	$-\frac{\sqrt{2}m_t(\beta_t\pm\beta_W)(\beta_t\mp\beta_W^2)}{m_W}$
	(-1 0),(0 +1)	$\frac{\sqrt{2}m_t}{m_W}$	$\frac{\sqrt{2}m_t(\beta_t\mp\beta_W)(\beta_t\mp\beta_W^2)}{m_W}$
	(0 0)	$\frac{\sqrt{s}m_t(\beta_t^2+\beta_W^4+2\beta_t\beta_W\cos\theta)}{2\sqrt{2}m_W^2\beta_t\beta_W}$	$\frac{\sqrt{s}m_t(\beta_t^4+\beta_W^6-\beta_t^2(\beta_W^2+\beta_W^4))}{2\sqrt{2}m_W^2\beta_t\beta_W}$

Appendix D

Statistics

In order to constrain the top Yukawa coupling as shown in Fig. 4.6, we follow the frequentist statistics procedure outlined in [123]. We first construct the likelihood function $L(\delta_{tth})$:

$$L(\delta_{tth}) = P(n|\delta_{tth}) \tag{D.0.1}$$

where n is the observed number of events and $P(n|\delta_{tth})$ is the probability under the hypothesis of δ_{tth}. Here we have used the Poisson distribution:

$$P(n|\delta_{tth}) = \frac{(s(\delta_{tth}) + b)^n}{n!} e^{-(s(\delta_{tth})+b)}. \tag{D.0.2}$$

where s is the number of signal events, which is a function of δ_{tth} and b is the number of SM background events. For multi-bin analysis, as is the case in this chapter, the total probability function is given by the product of the probability function in each bin, i.e.:

$$P(\boldsymbol{n}|\delta_{tth}) = \prod_i \frac{(s_i(\delta_{tth}) + b_i)^{n_i}}{n_i!} e^{-(s_i(\delta_{tth})+b_i)}. \tag{D.0.3}$$

The χ^2 function is defined as:

$$\chi^2 = -2 \ln L \tag{D.0.4}$$

and we will use the method of maximum likelihood to estimate the confidence interval. The $\Delta\chi^2$ as plotted in Fig. 4.6 is defined as:

$$\Delta\chi^2 = \chi^2 - \chi^2_{\rm min} = 2\ln L_{\rm max} - 2\ln L \tag{D.0.5}$$

where $L_{\rm max}$ is the maximal value of the likelihood function with given date $\boldsymbol{n}$. The expected sensitivity is obtained by setting the observed number of events to the SM background values $\boldsymbol{n} = \boldsymbol{b}$. The confidence interval at m-standard deviation is obtained by solving the following equation:

$$\Delta\chi^2 = m^2 \tag{D.0.6}$$

Bibliography

[1] **LHC Higgs Cross Section Working Group** Collaboration, J. R. Andersen *et al.*, "Handbook of LHC Higgs Cross Sections: 3. Higgs Properties," arXiv:1307.1347 [hep-ph].

[2] **ATLAS** Collaboration, G. A. et al, "Combined measurements of Higgs boson production and decay using up to 80 fb^{-1} of proton-proton collision data at $\sqrt{s} = 13$ TeV collected with the ATLAS experiment," *Phys. Rev. D* **101** no. 1, (2020) 012002, arXiv:1909.02845 [hep-ex].

[3] M. Cepeda *et al.*, "Report from Working Group 2: Higgs Physics at the HL-LHC and HE-LHC," *CERN Yellow Rep. Monogr.* **7** (2019) 221–584, arXiv:1902.00134 [hep-ph].

[4] **CLICdp** Collaboration, H. Abramowicz *et al.*, "Top-Quark Physics at the CLIC Electron-Positron Linear Collider," *JHEP* **11** (2019) 003, arXiv:1807.02441 [hep-ex].

[5] H. Al Ali *et al.*, "The muon Smasher's guide," *Rept. Prog. Phys.* **85** no. 8, (2022) 084201, arXiv:2103.14043 [hep-ph].

[6] M. Chen and D. Liu, "Top Yukawa Coupling at the Muon Collider," arXiv:2212.11067 [hep-ph].

[7] B. Henning, D. Lombardo, M. Riembau, and F. Riva, "Measuring Higgs Couplings without Higgs Bosons," *Phys. Rev. Lett.* **123** no. 18, (2019) 181801, arXiv:1812.09299 [hep-ph].

[8] A. Costantini, F. De Lillo, F. Maltoni, L. Mantani, O. Mattelaer, R. Ruiz, and X. Zhao, "Vector boson fusion at multi-TeV muon colliders," *JHEP* **09** (2020) 080, arXiv:2005.10289 [hep-ph].

[9] F. Abu-Ajamieh, S. Chang, M. Chen, and M. A. Luty, "Higgs coupling measurements and the scale of new physics," *JHEP* **07** (2021) 056, arXiv:2009.11293 [hep-ph].

[10] S. Chang, M. Chen, D. Liu, and M. A. Luty, "Primary Observables for Indirect Searches at Colliders," arXiv:2212.06215 [hep-ph].

[11] C. Llewellyn Smith, "High-Energy Behavior and Gauge Symmetry," *Phys. Lett. B* **46** (1973) 233–236.

[12] J. M. Cornwall, D. N. Levin, and G. Tiktopoulos, "Uniqueness of spontaneously broken gauge theories," *Phys. Rev. Lett.* **30** (1973) 1268–1270. [Erratum: Phys.Rev.Lett. 31, 572 (1973)].

[13] S. D. Joglekar, "S matrix derivation of the Weinberg model," *Annals Phys.* **83** (1974) 427.

[14] J. M. Cornwall, D. N. Levin, and G. Tiktopoulos, "Derivation of Gauge Invariance from High-Energy Unitarity Bounds on the s Matrix," *Phys. Rev. D* **10** (1974) 1145. [Erratum: Phys.Rev.D 11, 972 (1975)].

[15] R. Aoude and C. S. Machado, "The Rise of SMEFT On-shell Amplitudes," *JHEP* **12** (2019) 058, arXiv:1905.11433 [hep-ph].

[16] G. Durieux, T. Kitahara, Y. Shadmi, and Y. Weiss, "The electroweak effective field theory from on-shell amplitudes," *JHEP* **01** (2020) 119, arXiv:1909.10551 [hep-ph].

[17] B. Bachu and A. Yelleshpur, "On-Shell Electroweak Sector and the Higgs Mechanism," arXiv:1912.04334 [hep-th].

[18] B. W. Lee, C. Quigg, and H. Thacker, "The Strength of Weak Interactions at Very High-Energies and the Higgs Boson Mass," *Phys. Rev. Lett.* **38** (1977) 883–885.

[19] B. W. Lee, C. Quigg, and H. Thacker, "Weak Interactions at Very High-Energies: The Role of the Higgs Boson Mass," *Phys. Rev. D* **16** (1977) 1519.

[20] T. Appelquist and M. S. Chanowitz, "Unitarity Bound on the Scale of Fermion Mass Generation," *Phys. Rev. Lett.* **59** (1987) 2405. [Erratum: Phys.Rev.Lett. 60, 1589 (1988)].

[21] M. S. Chanowitz and M. K. Gaillard, "The TeV Physics of Strongly Interacting W's and Z's," *Nucl. Phys. B* **261** (1985) 379–431.

[22] F. Maltoni, J. Niczyporuk, and S. Willenbrock, "The Scale of fermion mass generation," *Phys. Rev. D* **65** (2002) 033004, arXiv:hep-ph/0106281.

[23] D. A. Dicus and H.-J. He, "Scales of fermion mass generation and electroweak symmetry breaking," *Phys. Rev. D* **71** (2005) 093009, arXiv:hep-ph/0409131.

[24] T. Corbett, O. J. P. Eboli, and M. C. Gonzalez-Garcia, "Unitarity Constraints on Dimension-Six Operators," *Phys. Rev. D* **91** no. 3, (2015) 035014, arXiv:1411.5026 [hep-ph].

[25] T. Corbett, O. Eboli, and M. Gonzalez-Garcia, "Unitarity Constraints on Dimension-six Operators II: Including Fermionic Operators," *Phys. Rev. D* **96** no. 3, (2017) 035006, arXiv:1705.09294 [hep-ph].

[26] M. S. Chanowitz and M. K. Gaillard, "Multiple Production of W and Z as a Signal of New Strong Interactions," *Phys. Lett. B* **142** (1984) 85–90.

[27] A. Belyaev, A. Oliveira, R. Rosenfeld, and M. C. Thomas, "Multi Higgs and Vector boson production beyond the Standard Model," *JHEP* **05** (2013) 005, arXiv:1212.3860 [hep-ph].

[28] A. Falkowski and R. Rattazzi, "Which EFT," *JHEP* **10** (2019) 255, arXiv:1902.05936 [hep-ph].

[29] S. Chang and M. A. Luty, "The Higgs Trilinear Coupling and the Scale of New Physics," *JHEP* **03** (2020) 140, arXiv:1902.05556 [hep-ph].

[30] C. E. Vayonakis, "Born Helicity Amplitudes and Cross-Sections in Nonabelian Gauge Theories," *Lett. Nuovo Cim.* **17** (1976) 383.

[31] T. Ma, J. Shu, and M.-L. Xiao, "Standard Model Effective Field Theory from On-shell Amplitudes," arXiv:1902.06752 [hep-ph].

[32] A. Papaefstathiou and K. Sakurai, "Triple Higgs boson production at a 100 TeV proton-proton collider," *JHEP* **02** (2016) 006, arXiv:1508.06524 [hep-ph].

[33] C.-Y. Chen, Q.-S. Yan, X. Zhao, Y.-M. Zhong, and Z. Zhao, "Probing triple-Higgs productions via $4b2\gamma$ decay channel at a 100 TeV hadron collider," *Phys. Rev.* **D93** no. 1, (2016) 013007, arXiv:1510.04013 [hep-ph].

[34] A. S. Belyaev, P. B. Schaefers, and M. C. Thomas, "Precise test of Higgs boson properties via triple Higgs boson production in vector boson fusion at future colliders," *Phys. Rev.* **D99** no. 1, (2019) 015030, arXiv:1801.10157 [hep-ph].

[35] W. Kilian, S. Sun, Q.-S. Yan, X. Zhao, and Z. Zhao, "Multi-Higgs boson production and unitarity in vector-boson fusion at future hadron colliders," *Phys. Rev. D* **101** no. 7, (2020) 076012, arXiv:1808.05534 [hep-ph].

[36] D. Stolarski and Y. Wu, "Tree-level Interference in VBF production of Vh," arXiv:2006.09374 [hep-ph].

[37] J. A. Dror, M. Farina, E. Salvioni, and J. Serra, "Strong tW Scattering at the LHC," *JHEP* **01** (2016) 071, arXiv:1511.03674 [hep-ph].

[38] F. Maltoni, L. Mantani, and K. Mimasu, "Top-quark electroweak interactions at high energy," *JHEP* **10** (2019) 004, arXiv:1904.05637 [hep-ph].

[39] **ATLAS** Collaboration, "Projections for measurements of Higgs boson cross sections, branching ratios, coupling parameters and mass with the ATLAS detector at the HL-LHC,". https://cds.cern.ch/record/2652762.

[40] F. Bishara, R. Contino, and J. Rojo, "Higgs pair production in vector-boson fusion at the LHC and beyond," *Eur. Phys. J. C* **77** no. 7, (2017) 481, arXiv:1611.03860 [hep-ph].

[41] **ATLAS** Collaboration, G. A. et al, "Search for the $HH \to b\bar{b}b\bar{b}$ process via vector-boson fusion production using proton-proton collisions at $\sqrt{s} = 13$ TeV with the ATLAS detector," *JHEP* **07** (2020) 108, arXiv:2001.05178 [hep-ex].

[42] A. Azatov, R. Contino, G. Panico, and M. Son, "Effective field theory analysis of double Higgs boson production via gluon fusion," *Phys. Rev. D* **92** no. 3, (2015) 035001, arXiv:1502.00539 [hep-ph].

[43] C. Englert, F. Krauss, M. Spannowsky, and J. Thompson, "Di-Higgs phenomenology in $t\bar{t}hh$: The forgotten channel," *Phys. Lett. B* **743** (2015) 93–97, arXiv:1409.8074 [hep-ph].

[44] G. Li, L.-X. Xu, B. Yan, and C.-P. Yuan, "Resolving the degeneracy in top quark Yukawa coupling with Higgs pair production," *Phys. Lett. B* **800** (2020) 135070, arXiv:1904.12006 [hep-ph].

[45] L. Li, Y.-Y. Li, and T. Liu, "Anatomy of the *tthh* Physics at HL-LHC," *Phys. Rev. D* **101** no. 5, (2020) 055043, arXiv:1905.03772 [hep-ph].

[46] R. S. Gupta, A. Pomarol, and F. Riva, "BSM Primary Effects," *Phys. Rev. D* **91** no. 3, (2015) 035001, arXiv:1405.0181 [hep-ph].

[47] L. Lehman and A. Martin, "Hilbert Series for Constructing Lagrangians: expanding the phenomenologist's toolbox," *Phys. Rev. D* **91** (2015) 105014, arXiv:1503.07537 [hep-ph].

[48] B. Henning, X. Lu, T. Melia, and H. Murayama, "Hilbert series and operator bases with derivatives in effective field theories," *Commun. Math. Phys.* **347** no. 2, (2016) 363–388, arXiv:1507.07240 [hep-th].

[49] L. Lehman and A. Martin, "Low-derivative operators of the Standard Model effective field theory via Hilbert series methods," *JHEP* **02** (2016) 081, arXiv:1510.00372 [hep-ph].

[50] B. Henning, X. Lu, T. Melia, and H. Murayama, "2, 84, 30, 993, 560, 15456, 11962, 261485, ...: Higher dimension operators in the SM EFT," *JHEP* **08** (2017) 016, arXiv:1512.03433 [hep-ph]. [Erratum: JHEP 09, 019 (2019)].

[51] B. Henning, X. Lu, T. Melia, and H. Murayama, "Operator bases, S-matrices, and their partition functions," *JHEP* **10** (2017) 199, arXiv:1706.08520 [hep-th].

[52] L. Graf, B. Henning, X. Lu, T. Melia, and H. Murayama, "2, 12, 117, 1959, 45171, 1170086, ...: a Hilbert series for the QCD chiral Lagrangian," *JHEP* **01** (2021) 142, arXiv:2009.01239 [hep-ph].

[53] L. Gráf, B. Henning, X. Lu, T. Melia, and H. Murayama, "Hilbert Series, the Higgs Mechanism, and HEFT," arXiv:2211.06275 [hep-ph].

[54] G. F. Giudice, C. Grojean, A. Pomarol, and R. Rattazzi, "The Strongly-Interacting Light Higgs," *JHEP* **06** (2007) 045, arXiv:hep-ph/0703164.

[55] D. Liu, A. Pomarol, R. Rattazzi, and F. Riva, "Patterns of Strong Coupling for LHC Searches," *JHEP* **11** (2016) 141, arXiv:1603.03064 [hep-ph].

[56] S. R. Coleman, J. Wess, and B. Zumino, "Structure of phenomenological Lagrangians. 1.," *Phys. Rev.* **177** (1969) 2239–2247.

[57] S. Coleman, *Aspects of Symmetry: Selected Erice Lectures*. Cambridge University Press, Cambridge, U.K., 1985.

[58] H. Georgi, "On-shell effective field theory," *Nucl. Phys. B* **361** (1991) 339–350.

[59] C. Arzt, "Reduced effective Lagrangians," *Phys. Lett. B* **342** (1995) 189–195, arXiv:hep-ph/9304230.

[60] H. Elvang, D. Z. Freedman, and M. Kiermaier, "A simple approach to counterterms in N=8 supergravity," *JHEP* **11** (2010) 016, arXiv:1003.5018 [hep-th].

[61] Y. Shadmi and Y. Weiss, "Effective Field Theory Amplitudes the On-Shell Way: Scalar and Vector Couplings to Gluons," *JHEP* **02** (2019) 165, arXiv:1809.09644 [hep-ph].

[62] G. Durieux and C. S. Machado, "Enumerating higher-dimensional operators with on-shell amplitudes," *Phys. Rev. D* **101** no. 9, (2020) 095021, arXiv:1912.08827 [hep-ph].

[63] G. Durieux, T. Kitahara, C. S. Machado, Y. Shadmi, and Y. Weiss, "Constructing massive on-shell contact terms," *JHEP* **12** (2020) 175, arXiv:2008.09652 [hep-ph].

[64] M. Accettulli Huber and S. De Angelis, "Standard Model EFTs via on-shell methods," *JHEP* **11** (2021) 221, arXiv:2108.03669 [hep-th].

[65] A. Falkowski, "Higgs Basis: Proposal for an EFT basis choice for LHC HXSWG,". https://cds.cern.ch/record/2001958.

[66] A. Helset, A. Martin, and M. Trott, "The Geometric Standard Model Effective Field Theory," *JHEP* **03** (2020) 163, arXiv:2001.01453 [hep-ph].

[67] J. Galloway, M. A. Luty, Y. Tsai, and Y. Zhao, "Induced Electroweak Symmetry Breaking and Supersymmetric Naturalness," *Phys. Rev. D* **89** no. 7, (2014) 075003, arXiv:1306.6354 [hep-ph].

[68] S. Chang, J. Galloway, M. Luty, E. Salvioni, and Y. Tsai, "Phenomenology of Induced Electroweak Symmetry Breaking," *JHEP* **03** (2015) 017, arXiv:1411.6023 [hep-ph].

[69] T. Cohen, N. Craig, X. Lu, and D. Sutherland, "Is SMEFT Enough?," *JHEP* **03** (2021) 237, arXiv:2008.08597 [hep-ph].

[70] I. Banta, T. Cohen, N. Craig, X. Lu, and D. Sutherland, "Non-decoupling new particles," *JHEP* **02** (2022) 029, arXiv:2110.02967 [hep-ph].

[71] W. R. Inc., "Mathematica, Version 13.1." https://www.wolfram.com/mathematica. Champaign, IL, 2022.

[72] S. De Angelis, "Amplitude bases in generic EFTs," *JHEP* **08** (2022) 299, arXiv:2202.02681 [hep-th].

[73] D. Liu and Z. Yin, "Gauge invariance from on-shell massive amplitudes and tree-level unitarity," *Phys. Rev. D* **106** no. 7, (2022) 076003, arXiv:2204.13119 [hep-th].

[74] G. D. Kribs, X. Lu, A. Martin, and T. Tong, "Custodial symmetry violation in the SMEFT," *Phys. Rev. D* **104** no. 5, (2021) 056006, arXiv:2009.10725 [hep-ph].

[75] R. Escribano and E. Masso, "Constraints on fermion magnetic and electric moments from LEP-1," *Nucl. Phys. B* **429** (1994) 19–32, arXiv:hep-ph/9403304.

[76] **LHC Higgs Cross Section Working Group** Collaboration, A. David, A. Denner, M. Duehrssen, M. Grazzini, C. Grojean, G. Passarino, M. Schumacher, M. Spira, G. Weiglein, and M. Zanetti, "LHC HXSWG interim recommendations to explore the coupling structure of a Higgs-like particle," arXiv:1209.0040 [hep-ph].

[77] K. Hagiwara, R. D. Peccei, D. Zeppenfeld, and K. Hikasa, "Probing the Weak Boson Sector in e+ e- → W+ W-," *Nucl. Phys. B* **282** (1987) 253–307.

[78] S. Boselli, C. M. Carloni Calame, G. Montagna, O. Nicrosini, F. Piccinini, and A. Shivaji, "Higgs decay into four charged leptons in the presence of dimension-six operators," *JHEP* **01** (2018) 096, arXiv:1703.06667 [hep-ph].

[79] **ALEPH, DELPHI, L3, OPAL, SLD, LEP Electroweak Working Group, SLD Electroweak Group, SLD Heavy Flavour Group** Collaboration, S. Schael *et al.*, "Precision electroweak measurements on the Z resonance," *Phys. Rept.* **427** (2006) 257–454, arXiv:hep-ex/0509008.

[80] **LHC Higgs Cross Section Working Group** Collaboration, S. Dittmaier *et al.*, "Handbook of LHC Higgs Cross Sections: 1. Inclusive Observables," arXiv:1101.0593 [hep-ph].

[81] M. Farina, G. Panico, D. Pappadopulo, J. T. Ruderman, R. Torre, and A. Wulzer, "Energy helps accuracy: electroweak precision tests at hadron colliders," *Phys. Lett. B* **772** (2017) 210–215, arXiv:1609.08157 [hep-ph].

[82] R. Franceschini, G. Panico, A. Pomarol, F. Riva, and A. Wulzer, "Electroweak Precision Tests in High-Energy Diboson Processes," *JHEP* **02** (2018) 111, arXiv:1712.01310 [hep-ph].

[83] D. Liu and L.-T. Wang, "Prospects for precision measurement of diboson processes in the semileptonic decay channel in future LHC runs," *Phys. Rev. D* **99** no. 5, (2019) 055001, arXiv:1804.08688 [hep-ph].

[84] G. Panico, L. Ricci, and A. Wulzer, "High-energy EFT probes with fully differential Drell-Yan measurements," *JHEP* **07** (2021) 086, arXiv:2103.10532 [hep-ph].

[85] J. P. Delahaye, M. Diemoz, K. Long, B. Mansoulié, N. Pastrone, L. Rivkin, D. Schulte, A. Skrinsky, and A. Wulzer, "Muon Colliders," arXiv:1901.06150 [physics.acc-ph].

[86] **Muon Collider** Collaboration, D. Stratakis *et al.*, "A Muon Collider Facility for Physics Discovery," arXiv:2203.08033 [physics.acc-ph].

[87] M. Chiesa, F. Maltoni, L. Mantani, B. Mele, F. Piccinini, and X. Zhao, "Measuring the quartic Higgs self-coupling at a multi-TeV muon collider," *JHEP* **09** (2020) 098, arXiv:2003.13628 [hep-ph].

[88] R. Capdevilla, D. Curtin, Y. Kahn, and G. Krnjaic, "Discovering the physics of $(g-2)_\mu$ at future muon colliders," *Phys. Rev. D* **103** no. 7, (2021) 075028, arXiv:2006.16277 [hep-ph].

[89] T. Han, Y. Ma, and K. Xie, "High energy leptonic collisions and electroweak parton distribution functions," *Phys. Rev. D* **103** no. 3, (2021) L031301, arXiv:2007.14300 [hep-ph].

[90] T. Han, D. Liu, I. Low, and X. Wang, "Electroweak couplings of the Higgs boson at a multi-TeV muon collider," *Phys. Rev. D* **103** no. 1, (2021) 013002, arXiv:2008.12204 [hep-ph].

[91] T. Han, Z. Liu, L.-T. Wang, and X. Wang, "WIMPs at High Energy Muon Colliders," *Phys. Rev. D* **103** no. 7, (2021) 075004, arXiv:2009.11287 [hep-ph].

[92] D. Buttazzo and P. Paradisi, "Probing the muon $g-2$ anomaly with the Higgs boson at a muon collider," *Phys. Rev. D* **104** no. 7, (2021) 075021, arXiv:2012.02769 [hep-ph].

[93] W. Yin and M. Yamaguchi, "Muon g-2 at a multi-TeV muon collider," *Phys. Rev. D* **106** no. 3, (2022) 033007, arXiv:2012.03928 [hep-ph].

[94] D. Buttazzo, R. Franceschini, and A. Wulzer, "Two Paths Towards Precision at a Very High Energy Lepton Collider," *JHEP* **05** (2021) 219, arXiv:2012.11555 [hep-ph].

[95] G.-y. Huang, F. S. Queiroz, and W. Rodejohann, "Gauged $L_\mu - L_\tau$ at a muon collider," *Phys. Rev. D* **103** no. 9, (2021) 095005, arXiv:2101.04956 [hep-ph].

[96] W. Liu and K.-P. Xie, "Probing electroweak phase transition with multi-TeV muon colliders and gravitational waves," *JHEP* **04** (2021) 015, arXiv:2101.10469 [hep-ph].

[97] R. Capdevilla, D. Curtin, Y. Kahn, and G. Krnjaic, "No-lose theorem for discovering the new physics of (g-2) μ at muon colliders," *Phys. Rev. D* **105** no. 1, (2022) 015028, arXiv:2101.10334 [hep-ph].

[98] T. Han, S. Li, S. Su, W. Su, and Y. Wu, "Heavy Higgs bosons in 2HDM at a muon collider," *Phys. Rev. D* **104** no. 5, (2021) 055029, arXiv:2102.08386 [hep-ph].

[99] R. Capdevilla, F. Meloni, R. Simoniello, and J. Zurita, "Hunting wino and higgsino dark matter at the muon collider with disappearing tracks," *JHEP* **06** (2021) 133, arXiv:2102.11292 [hep-ph].

[100] T. Han, Y. Ma, and K. Xie, "Quark and gluon contents of a lepton at high energies," *JHEP* **02** (2022) 154, arXiv:2103.09844 [hep-ph].

[101] P. Asadi, R. Capdevilla, C. Cesarotti, and S. Homiller, "Searching for leptoquarks at future muon colliders," *JHEP* **10** (2021) 182, arXiv:2104.05720 [hep-ph].

[102] S. Bottaro, D. Buttazzo, M. Costa, R. Franceschini, P. Panci, D. Redigolo, and L. Vittorio, "Closing the window on WIMP Dark Matter," *Eur. Phys. J. C* **82** no. 1, (2022) 31, arXiv:2107.09688 [hep-ph].

[103] S. Qian, C. Li, Q. Li, F. Meng, J. Xiao, T. Yang, M. Lu, and Z. You, "Searching for heavy leptoquarks at a muon collider," *JHEP* **12** (2021) 047, arXiv:2109.01265 [hep-ph].

[104] M. Chiesa, B. Mele, and F. Piccinini, "Multi Higgs production via photon fusion at future multi-TeV muon colliders," arXiv:2109.10109 [hep-ph].

[105] W. Liu, K.-P. Xie, and Z. Yi, "Testing leptogenesis at the LHC and future muon colliders: A Z' scenario," *Phys. Rev. D* **105** no. 9, (2022) 095034, arXiv:2109.15087 [hep-ph].

[106] J. Chen, T. Li, C.-T. Lu, Y. Wu, and C.-Y. Yao, "Measurement of Higgs boson self-couplings through 2→3 vector bosons scattering in future muon colliders," *Phys. Rev. D* **105** no. 5, (2022) 053009, arXiv:2112.12507 [hep-ph].

[107] S. Chen, A. Glioti, R. Rattazzi, L. Ricci, and A. Wulzer, "Learning from Radiation at a Very High Energy Lepton Collider," arXiv:2202.10509 [hep-ph].

[108] C. Cesarotti, S. Homiller, R. K. Mishra, and M. Reece, "Probing New Gauge Forces with a High-Energy Muon Beam Dump," arXiv:2202.12302 [hep-ph].

[109] J. de Blas, J. Gu, and Z. Liu, "Higgs boson precision measurements at a 125 GeV muon collider," *Phys. Rev. D* **106** no. 7, (2022) 073007, arXiv:2203.04324 [hep-ph].

[110] Y. Bao, J. Fan, and L. Li, "Electroweak ALP searches at a muon collider," *JHEP* **08** (2022) 276, arXiv:2203.04328 [hep-ph].

[111] S. Homiller, Q. Lu, and M. Reece, "Complementary signals of lepton flavor violation at a high-energy muon collider," *JHEP* **07** (2022) 036, arXiv:2203.08825 [hep-ph].

[112] M. Forslund and P. Meade, "High precision higgs from high energy muon colliders," *JHEP* **08** (2022) 185, arXiv:2203.09425 [hep-ph].

[113] C. Csaki, A. Falkowski, and A. Weiler, "The Flavor of the Composite Pseudo-Goldstone Higgs," *JHEP* **09** (2008) 008, arXiv:0804.1954 [hep-ph].

[114] B. Keren-Zur, P. Lodone, M. Nardecchia, D. Pappadopulo, R. Rattazzi, and L. Vecchi, "On Partial Compositeness and the CP asymmetry in charm decays," *Nucl. Phys. B* **867** (2013) 394–428, arXiv:1205.5803 [hep-ph].

[115] S. Dawson, "The Effective W Approximation," *Nucl. Phys. B* **249** (1985) 42–60.

[116] Z. Kunszt and D. E. Soper, "On the Validity of the Effective W Approximation," *Nucl. Phys. B* **296** (1988) 253–289.

[117] P. Borel, R. Franceschini, R. Rattazzi, and A. Wulzer, "Probing the Scattering of Equivalent Electroweak Bosons," *JHEP* **06** (2012) 122, arXiv:1202.1904 [hep-ph].

[118] A. Azatov, J. Elias-Miro, Y. Reyimuaji, and E. Venturini, "Novel measurements of anomalous triple gauge couplings for the LHC," *JHEP* **10** (2017) 027, arXiv:1707.08060 [hep-ph].

[119] G. Panico, F. Riva, and A. Wulzer, "Diboson interference resurrection," *Phys. Lett. B* **776** (2018) 473–480, arXiv:1708.07823 [hep-ph].

[120] F. Maltoni, L. Mantani, and K. Mimasu, "Top-quark electroweak interactions at high energy," *JHEP* **10** (2019) 004, arXiv:1904.05637 [hep-ph].

[121] J. Alwall, R. Frederix, S. Frixione, V. Hirschi, F. Maltoni, O. Mattelaer, H. S. Shao, T. Stelzer, P. Torrielli, and M. Zaro, "The automated computation of tree-level and

next-to-leading order differential cross sections, and their matching to parton shower simulations," *JHEP* **07** (2014) 079, arXiv:1405.0301 [hep-ph].

[122] A. Falkowski, B. Fuks, K. Mawatari, K. Mimasu, F. Riva, and V. Sanz, "Rosetta: an operator basis translator for Standard Model effective field theory," *Eur. Phys. J. C* **75** no. 12, (2015) 583, arXiv:1508.05895 [hep-ph].

[123] **Particle Data Group** Collaboration, P. A. Zyla *et al.*, "Review of Particle Physics," *PTEP* **2020** no. 8, (2020) 083C01.

[124] **Particle Data Group** Collaboration, R. L. Workman and Others, "Review of Particle Physics," *PTEP* **2022** (2022) 083C01.

[125] M. L. Mangano, T. Plehn, P. Reimitz, T. Schell, and H.-S. Shao, "Measuring the Top Yukawa Coupling at 100 TeV," *J. Phys. G* **43** no. 3, (2016) 035001, arXiv:1507.08169 [hep-ph].

[126] J. Alwall, R. Frederix, S. Frixione, V. Hirschi, F. Maltoni, O. Mattelaer, H. S. Shao, T. Stelzer, P. Torrielli, and M. Zaro, "The automated computation of tree-level and next-to-leading order differential cross sections, and their matching to parton shower simulations," *JHEP* **07** (2014) 079, arXiv:1405.0301 [hep-ph].